# ON THE UNSTEADY BOUNDARY LAYER AND WAKE OF A FLAT PLATE, AND MODELING WATER FLOW NEAR A SHIP-SIDE

by

**Dimitrios P. Papadopoulos**

A thesis submitted for the degree of
Doctor of Philosophy
in the University of London

University College London
Department of Mathematics

**June 2000**

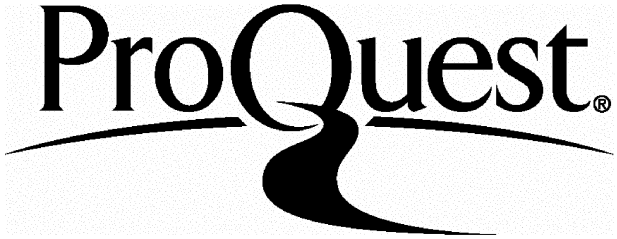

# ABSTRACT

The work in the thesis is concerned with the unsteady laminar two-dimensional flow of an incompressible fluid, at high Reynolds numbers, in the presence of a moving solid surface which is usually taken to be flat. There are two main aspects, one a numerical and analytical study, and the other on modeling. The unsteady flow past a flat plate is examined first, for the case of an impulsively started aligned plate in a free stream. Numerical solutions are obtained by an apparently novel and simple semi-implicit method, both for the plate boundary layer flow solution, which is found to agree with that based on the Blasius and Rayleigh forms, and for the wake solution beyond the trailing edge including the Goldstein near-wake form. Analysis is also performed to check the method in some detail, the numerical accuracy of the method is investigated, and the method is applied to other types of starting motion of the flat plate.

The method is subsequently extended to configurations modeling (in an apparently novel way) water flow induced by a flat vertical ship-side which is undergoing upward and/or downward motions partly submerged in a body of water under air. The model of the water flow in the downward case is based on the thin, inner, unsteady boundary layer produced on the ship-side, which is moving in its own plane, and a thick outer region of potential flow that responds to the small efflux or influx due to the ship-side boundary layer. The air-water interface is treated as a free surface, nearly horizontal at the top of the bulk of the water but nearly vertical beside the ship. The latter part of the free surface adjoins the wake of the ship-side boundary layer, this wake being found to be identical with that for which flow solutions are given earlier in the thesis. The junction between the boundary layer and wake, that is the contact point, typically exhibits no relative slip, while at the junction between the two parts of the free surface a tiny passive region forms. Similar modeling applies to upward motions in principle. The Froude number is taken to be large. The numerical work yields the efflux or displacement function for all finite scaled times and analysis is performed for both small and large times. The potential-flow analysis is with the aim of predicting the behaviour with time of the air-water interfaces both at the top

and at the side. The effect of reducing the Froude number is also examined. Further applications are considered, including those of a more general case of an inclined ship-side surface undergoing motion and a rotating, partly submerged, circular cylinder.

**Acknowledgements**

I would like to fully thank Professor Frank T. Smith for his guidance, support and help throughout the course of this research. I am eternally indebted to him for all that he has taught me during the period that I have had the honour to work with him.

Thanks are also extended to Dr. Linzhong Li for helpful discussions and to my best friend Dr. Rajat B. Nath for suggestions and guidance on the numerical analysis. I would like to thank with all my heart my parents, Professors Takis and Fofi Papadopoulos, for all their support and encouragement over the years.

---

"In the middle of difficulty lies opportunity."

*Albert Einstein*

"My father has given me life, and my teacher how to live."

*Alexander the Great*

---

# Table of Contents

# List of Tables

## List of Programs

# List of Figures

# CHAPTER 1

# Introduction

## 1.1 Prologue

The concern in this thesis is with certain viscous fluid flow problems which involve the high Reynolds number solution of the Navier-Stokes equations for assumed laminar flow. The Reynolds number is defined in the usual way, as a characteristic velocity scale multiplied by a characteristic length scale and divided by the kinematic viscosity of the fluid, and it provides a measure of the inertial forces relative to the viscous forces in the majority of the fluid motion.

One central part of this effort is to investigate the unsteady flow past a flat plate numerically employing a semi-implicit method. This approach is then extended to a class of problems associated with the unsteady motion of fluid adjacent to a moving partially immersed body such as a ship-side in which there exists a two phase air-water system. These include the consideration of inclined geometries and the incorporation of gravity effects into the flow problem. For the ship-side analyses, major consideration will also be given to the development of the upper free and side free surfaces as well as the associated moving contact point.

Thus the present investigation is based on combining three areas of research, in effect, namely the theory of high Reynolds number flows (especially unsteady boundary layers and wakes), predictions for free surface flows, and modeling of a moving contact point.

The flow problems studied here are inherently nonlinear. The constitutive equations of the laminar boundary layer in particular are nonlinear coupled partial differential equations, for which there exist only numerical or approximate solutions in general. There are families of relatively simple flows which can reduce the boundary layer equations to forms which are amenable to analysis which does not involve the solution of partial differential equations. These are the similarity flows of which the most famous is the Blasius solution (1908). The conditions on the validity of these

solutions are still debated, but it can be said that they have been very useful in a wide number of boundary layer studies. In the cases of present interest, however, computation is almost unavoidable.

The flow problems here are also unsteady. A classical problem of fluid mechanics is the determination of the unsteady viscous flow over a flat plate of finite length, which is aligned with the uniform stream of fluid far from the plate and is impulsively started from rest (Prandtl 1963, Landau & Lifshitz 1987, Dimitriou 1993). The unsteadiness in the problem may exist through the varying nature of the constituent boundary conditions with time or through the unsteadiness of the flow itself (Schlichting 1970, Telionis 1981, White 1991). The resultant formation of the boundary layer and the wake region are inherently unsteady in their nature and thus difficult to model. Consequently, there have been to date relatively few quantitative investigations of the problem.

The three areas of research referred to above are considered in turn in the following sections.

## 1.2 Literature survey

A review of relevant theoretical and numerical investigations that have been performed is given in the following sections for both the finite flat plate problem and free surface problems involving motion adjacent to a partially immersed body.

### 1.2.1 The flat plate problem

The unsteady problem of a flat plate of finite length that is aligned to the mainstream flow, in which the mainstream velocity is impulsively raised from zero to a constant velocity $U_\infty$, has been considered by Blasius (1908), Rayleigh (1911), in order to ascertain the nature of the growth of the boundary layer. The classical Rayleigh solution (which ignores the leading and trailing edges of the plate and treats the flow as if on a plate of semi-infinite length) is independent of the streamwise direction and gives a square-root temporal growth in the boundary layer thickness.

In his ground-breaking analysis, Stewartson (1951) used the fact that disturbances travel downstream in the boundary layer at a finite speed of propagation, and then

diffuse instantaneously across the layer, to suggest that the presence of the leading edge is known to only a finite portion of the flow; that is, the solution at a distance $x$ from the leading edge is independent of the streamwise coordinate until a time $x/U_\infty$. For suitable early times or further downstream, the flow behaves as though the plate is fully infinite, this giving the Rayleigh solution on the plate. (The trailing edge effect is discussed in sub-section 1.2.2 below). Lam & Crocco (1959), Hall (1969) and Dennis (1972) confirmed this theory numerically and Watson (in Hall's (1969) appendix) showed that for large values of time the solution approaches the steady-state Blasius form. Stewartson (1973) in a continuation paper developed the structure of the eigenfunctions which describe the manner in which the dependence on $x$ enters the flow solution. For finite bodies, the dual effect of leading and trailing edges has also been considered; for example in Williams (1982) and Williams & Stewartson (1983) it was shown that under some conditions the effect of the trailing edge can dominate the initial stages of the motion. This is distinct from the situation discussed in the next sub-section. Also, an investigation for the small time analytical solution by Elliott and Smith (1998) addressed the effect of a smooth deceleration of the external stream on an aligned flat plate boundary layer.

Reviews of other basic unsteady boundary layer flows are given by Elliott and Smith (1998) and Degani et al. (1998), including flow past an impulsively started circular cylinder for example and issues of unsteady separation.

### 1.2.2 Wake solution

The steady basic flow immediately downstream of the sharp trailing edge of a flat plate can be divided into the flow in a thin viscous wake, within which is contained a near wake region, and outside the wake region the uniform incompressible main stream, which continues only slightly disturbed. The flow in the thin wake is governed by the boundary-layer equations again and in the near wake is described by means of the asymptotic expansion of Goldstein (1930). (The same structure applies to the unsteady setting below.)

The typical laminar wake is very unstable in reality. Yet owing to the complex nature of the unperturbed steady flow, there have been very few theoretical investigations of

wake instability that employ correct wake features. Most investigators have only modeled basic flow properties in a rather ad hoc fashion and, for example, have computed growth rates at a position where the resultant basic profile roughly corresponds to the physical flow (see in Sato & Kuriki 1961, Mattingly & Criminale 1972, Papageorgiou & Smith 1989). Stability calculations have been performed however for basic flow profiles which are solutions of the boundary-layer equations with the appropriate boundary conditions that hold in the thin viscous wake, by Papageorgiou & Smith (1989). Another aspect, the linear stability of parallel shear flow to long-wavelength perturbations, has been the subject of a paper by Drazin and Howard (1966). The paper focused on jet and shear-layer-type profiles, and the results can be extended to wakes. It was found that the detailed properties of the velocity near the wake centreline are insignificant then, and that the dependence on the undisturbed velocity far away from the centreline is more important for such perturbations. Again, the issue of absolute instability in the wake is a significant one, as reviewed recently by Smith et al. (2000). Their paper, which contains many references on the subject, also points to the importance of using realistic velocity profiles rather than ad hoc ones in the wake.

The study by Elliott & Smith (1998) was one of the first investigations to solve both the unsteady boundary layer and the unsteady wake flows, in their case in response to unsteady disturbances in the mainstream flow. This setting, with fully nonlinear unsteadiness being present in the thin wake, is the one of most current concern.

### 1.2.3 Free surface analyses, and moving contact points

In order to analyse basic features of the free-surface effects that influence the frictional resistance on a ship-side, Chang et al. (1994) have investigated the unsteady boundary layer using finite element analysis. The laminar boundary layer equations are expanded with the assumption of small amplitude waves, and the second order equations, which describe the effect of the free-surface, are solved by a simplified integral method. The ship frictional resistance is found to decrease due to the free surface wave. The results explicitly indicate that the ship viscous resistance is dependent on the Froude number, which is defined here as the ratio of the square of the characteristic velocity scale to the product of the gravitational acceleration ($g$) and the characteristic length scale, although some authors adopt instead the square root of

this quantity to define the Froude number. The present Froude number yields a measure of the typical inertial forces relative to the gravity effects.

In this thesis we will be applying a simple no-slip condition at the moving contact point or line, which is the common interface between the air-water and the solid boundary. As the solid boundary moves downwards into the water, say, it is expected that in reality the contact point will move relative to the solid boundary, but here we keep to the no-slip case as a prime one to be explored. It is worth mentioning some of the many other aspects of moving contact points nevertheless. Some general problems relevant to the ship side analysis and the behaviour of the air-water interface near the contact line may be found in Foda & Cox (1980), King (1991), Vanden-Broeck & Tuck (1994), Billingham & King (1995), King et al. (1998), and more recently in Somalinga & Bose (2000). The study of Foda & Cox examines the spreading on a water-air interface of a thin liquid film for the situation in which surface tension gradients drive the motion. (Such capillary effects are excluded from consideration in the work of the present thesis but are still of much interest, for example see the recent paper of Kang & Vanden-Broeck 2000). King investigates the moving contact lines in slender fluid wedges. He finds the asymptotic and numerical solutions for a novel two-point boundary-value problem and the displacement of the contact point. Vanden-Broeck & Tuck investigate the flow near the intersection of the free surface with a vertical wall. The free surface here typically makes an angle of $120^{\circ}$ with the wall and it is assumed that the velocity close to separation is small. A nontrivial local solution with $90^{\circ}$ and $180^{\circ}$ contact angles is also computed here by a series truncation. Billingham and King (1995) analyse computationally and analytically the problem of a flat plate penetrating an air-water interface for both small and large times using the boundary integral method. It is found that far-field capillary waves are generated when the contact angle is close to $90^{\circ}$ and, as time increases, the interface becomes more non-linearly deformed. King et al. (1998) perform an extension of the same method to the case of an inclined plate/interface system. Similar profiles are again found. Somalinga and Bose (2000) investigate, using finite elements, the development of the free surface located between a static wall and a rod entering the fluid in a dynamic wetting process. General profiles are predicted for displacement and velocity fields for a numerical mesh which appears to be relatively coarse.

A similar problem is that of the development of the free surface flow past the bow of a ship in water of finite depth (Vanden-Broeck 1989). The problem is solved numerically using series truncation for various values of the Froude number. The development of the free surface for this geometry is briefly investigated. Concerning the above and subsequent works, we remark that in the current study the influence of gravity will be taken to be relatively small (corresponding to the Froude number being large), but it is interesting also to note some of the properties found in the literature for non-small gravity effects (for example Vanden-Broeck & Dias 1996, Daboussy et al. 1998).

For the moving ship-side analysis in which the effect of gravity is included, there exist comparatively few studies, one of which is Fraenkel and McLeod (1997). Their analytical study is concerned with the entry of a blunt wedge into a horizontal free surface. The behaviour of the contact angle and point is investigated. Another analysis is that by Daboussy et al. (1997). Here the series truncation method is applied to standard geometry flows under the influence of gravity and predicts the shape of the free surfaces.

For completeness, we may also mention Howison et al.'s (1991) work in which the impact response of a wedge entering a free surface is considered in the absence of gravity. The free surfaces are predicted analytically for various geometries of the penetrating body.

Finally here, it is interesting to consider numerical values of the Reynolds number and Froude number that might be encountered in practice. For a ship oscillating in water where approximately $\nu$=0.01 c.g.s. and gravity is 981 cm/s$^2$, the vertical length scale could be in the range 10 cm to 500 cm and the vertical velocities concerned could be in the range 50 cm/s to 200 cm/s, say. Thus values of *Re* are calculated in the range $5\times10^4$ to $10^7$. The range of values of Froude number is 0.005 to 4 for these types of flow. These numbers are also quoted in chapter 7 later in the thesis.

## 1.3 Numerical investigations

A quite common feature of unsteady boundary layer motions is that they often involve rather problem-specific singular behaviour, either at early times or at specific locations, for example near a leading edge or a trailing edge, in addition to being inherently nonlinear. The specific computational approach used in this thesis has been applied previously to study steady two- and three-dimensional boundary layer flows involving singular behavior, such as Smith and Timoshin (1996 a,b), and is advocated also for unsteady flows of the type concerned in this thesis. The other published numerical methods of most accuracy, applied to unsteady boundary layer flows different from the ones of current interest, appear to be the Lagrangian approach of Van Dommelen (1981), Peridier et al. (1991 a,b), Degani et al. (1998) and the adaptive gridding approach of Adams et al. (1995), although Li (2000) has recently developed an equally accurate compact differencing approach.

All numerical investigations described in the present study are performed using the programming languages Fortran 77 and 90. Flow charts for the various programs included in the thesis are given in the text and the complete program listings at the end of the relevant chapters. Specific numerical procedures for integration and differentiation, such as Simpson's rule and the solution of systems of equations, have been adapted from Roache (1976), James et al. (1985) and Gerald & Wheatley (1989).

The rates of convergence of the numerical solutions with grid resolution were investigated by varying the interval sizes of the computational runs for both spatial coordinates and time. Thus convergence of the various solutions that were found was established in a manner similar to that in Markatos & Assimacopoulos (1995).

## 1.4 Structure of the thesis

The thesis is partitioned into two major sections, which reflect the present combining of the three areas of research mentioned earlier in the introduction, a combination which appears to be novel. Part A considers the unsteady flat plate problem including the leading and trailing edge phenomena. Part B then considers the application of the work of Part A to the case of a downward moving ship-side. The problem is further generalised to that of an inclined ship-side and also to include the effects of gravity.

In Part A, a semi-implicit method is applied to allow for the leading and trailing edges of the flat plate. Chapter 2 considers the unsteady flat plate problem, for which the velocity profiles in the boundary layer are ascertained with respect to both spatial coordinates and with respect to time. A numerical grid is defined for finite differencing. The well-known Blasius and Rayleigh forms of solution hold on the plate sufficiently near the leading edge and sufficiently far downstream of it, respectively. In between them a similarity form (Stewartson, Hall) applies in which the streamwise and normal distances $x, y$ scale with positive powers of the time $t$. As grid refinement is increased, the solution is found to converge. We choose to tackle the whole solution by means of a parabolic time-marching technique for a number of reasons including the desire for a flexible treatment applicable to many different unsteady flows. Chapter 3 investigates the nature of the unsteady wake. Additionally, the scaled displacement and skin friction responses along the plate are predicted, and an investigation incorporating modified boundary conditions for the far-field flow is made. In the wake there is again a similarity solution for sufficiently small times and distances, whereas we seek the solution computationally for all times and distances. As far as we are aware this is the first calculation to include the unsteady wake as part of the total computation for such an impulsively started motion. In fact the word "is" should perhaps be replaced by "was at the time of its being done, in about 1997", because Li (2000) has since performed a numerical study of the flow problem involved.

Part B considers the problem of the ship-side motion, mainly downwards in an initially stationary fluid. In the investigation Chapter 4 takes the depth of the partially submerged ship-side within the stationary fluid (water) to set a definite length scale for the ensuing motion, which rules out the possibility of a global similarity solution. The problem is developed from the full governing equations employing suitable boundary conditions, and the Froude number is taken to be large. Various transformations are employed in order to develop the analysis and build into the problem realistic phenomena, with a view to obtaining the influence of the viscous displacement on the inviscid majority of the water flow. The area of investigation is divided into three regions which are analysed separately. For each of the regions, the initial and boundary conditions are developed and incorporated. In Chapter 5, the various regions are further considered in the complex plane. To aid the investigation,

a displacement derivative function is developed from the Cauchy-Hilbert relationship. Modeling of the problem is then undertaken for both small and large times, in which the displacement derivative function is evaluated. Chapter 6 subsequently uses the viscous displacement derivative function and mixed boundary conditions for the development of the solution for the shapes of the upper and side free surfaces. Direct relationships are found between the upper free and side free surface shapes and the displacement derivative function.

Chapter 7 contains more advanced considerations of the ship-side flow including the effect of gravity on the side free surface behaviour. The gravity effect is built into the problem by re-considering the original boundary conditions and incorporating the gravity contribution together with the viscous displacement derivative function of the earlier chapters. The development of the problem is in a similar manner as with chapter 5. An alternative method is also investigated to find the side free surface equation including the gravity effect. In Chapter 8, the analysis is then extended to the general case of an inclined ship-side moving downwards. For this case, the conformal transformation used is for a general angle of inclination to the horizontal, with the earlier studied vertical motion being a special case. A general transformation in the complex plane is developed valid for a range of inclinations to the horizontal, and consequently a general displacement derivative function is developed. The solution is then evaluated numerically for a range of angles, and comparison is made with the vertical case (90°) of chapter 5.

The thesis concludes with a short discussion on other types of configuration and on upward ship-side motion, along with a summary.

# PART A:

# THE FLAT PLATE PROBLEM

# CHAPTER 2

## The flow past an impulsively started finite flat plate, and its computation

### 2.1 Introduction

The subject of this chapter is the incompressible boundary layer over a flat plate that is started impulsively from rest with uniform velocity. The fundamental problem of the flat plate of finite length is of most interest to us, including its wake properties, but we start here with the semi-infinite case in effect. The two cases are identical between the leading and trailing edge of the finite-length plate anyway, because of the parabolic nature of the governing equations below. The development of the flow in time has two simple features, for a given position $x$ along the plate. In the beginning of the analysis, the flow is identical almost everywhere to that given by Rayleigh for an infinite plate; but the flow transforms, for large times (i.e. $t>>1$), to that given by Blasius for a semi-infinite plate in a steady uniform stream. Stewartson (1951), Hall (1969), Dennis (1972) and others have studied the problem in terms of similarity variables. For the current, mainly numerical, study the plate considered was divided into multiple $x$-stations and time marching was used in order to obtain a more widely applicable analysis of the flat plate and related problems. An indication of the difficulties associated with the problem may be gained from an examination of the governing differential equations and boundary conditions.

We consider the problem in the rectangular coordinate system $x$, $y$, $t$ with lines $x=0$ and $y=0$ fixed at the leading edge of the plate, and with the $x$-axis and $y$-axis parallel and normal to the plate, respectively. At high Reynolds numbers $Re$ the unsteady boundary layer equations apply, at least for some finite time interval. These equations hold in a number of contexts, including the case of ship-side water motions as will be investigated in Part B of the thesis. Thus we concentrate (in Part A of the thesis) on a numerical method of solution of the unsteady boundary layer equations suitable for a variety of imposed free stream conditions (or imposed pressure gradients) and wall conditions.

We attempt to develop a fairly flexible computational solution approach. A quite common feature of unsteady boundary layer motions is that they often involve rather problem-specific singular behaviour, either at early times or at certain locations, for example near a leading edge or a trailing edge, in addition to being inherently nonlinear. The specific approach used in the thesis has been applied previously to study steady two- and three-dimensional boundary layer flows involving singular behavior, by Smith and Timoshin (1996 a,b), and is advocated also for unsteady flows of the type concerned in this thesis.

The governing equations are the unsteady two-dimensional boundary-layer equations, for a uniform free stream in the first instance. In non-dimensional variables these may be written

$$\frac{\partial u}{\partial x}+\frac{\partial v}{\partial y}=0, \tag{2.1}$$

$$\frac{\partial u}{\partial t}+u\frac{\partial u}{\partial x}+v\frac{\partial u}{\partial y}=\frac{\partial^2 u}{\partial y^2}, \tag{2.2}$$

where the variables are defined as:

$$\left.\begin{aligned} &x=\frac{x'}{L},\ u=\frac{u'}{U},\ t=\frac{Ut'}{L},\\ &R_e=\frac{UL}{\nu},\\ &y=\frac{R_e^{1/2}y'}{L},\ v=\frac{R_e^{1/2}v'}{U}. \end{aligned}\right\} \tag{2.3}$$

Here $x'$ and $y'$, $t'$, $u'$ and $v'$ are the usual dimensional measures of distance, time, and velocity, $\nu$ is the kinematic viscosity, and $L$ and $U$ are a reference length and a reference velocity, respectively. It is convenient to take $L$ to be a representative distance from the leading edge, in the case of a semi-infinite plate, and $U$ to be the velocity of the free stream relative to the plate.

The boundary conditions at the surface and at the outer edge of the boundary layer are

$$\text{at } y=0,\ u=v=0 \text{ (at the wall)}, \tag{2.4}$$

$$\text{as } y\to\infty,\ u\to 1 \text{ (outside the boundary layer)}, \tag{2.5}$$

in turn. Away from the leading edge, for large values of $x$ and/or for small times $t$, we observe that the flow is equivalent to an impulsively started infinite plate with no leading edge. Thus setting the derivatives with respect to $x$ in equations (2.1-2.2) equal to zero, we have there the Rayleigh solution, for

$$x/t \geq 1,\ u=u_R(\zeta)=\frac{2}{\sqrt{\pi}}\int_0^{\zeta} e^{-\zeta^2}\cdot d\zeta \tag{2.6}$$

where $\zeta=\dfrac{y}{2\sqrt{t}}=\dfrac{y'}{2\sqrt{(vt')}}$.

The explanation of why this is for $x/t \geq 1$, rather than $x/t\to\infty$, is given by Stewartson (1951) and revolves around the subtle matching (which takes place in a zone close to $x=t$) with the solution holding nearer the leading edge. In general this is $x \geq Ut$ where $U$ is the velocity of the external flow, and thus the Rayleigh solution holds for $x \geq t$. Now, for sufficiently large times at fixed $x$ and/or for sufficiently small $x$ values, setting the derivative with respect to $t$ in equation (2.2) equal to zero, we have the Blasius solution, for

$$x/t\to 0,\ u=u_B(y/\sqrt{x}), \tag{2.7}$$

where $\dfrac{y}{\sqrt{x}}=\dfrac{y'}{x'}\sqrt{\left(\dfrac{Ux'}{v}\right)}$.

There is no known analytical method for the direct solution of equations (2.1)-(2.2) subject to the boundary and limiting conditions (2.4)-(2.7). However, the number of independent variables may be reduced from three to two as in Stewartson (1951) and Hall (1969). We may consider the new independent variables

$$T=\frac{t}{x},\ S=\frac{y}{\sqrt{x}}, \tag{2.8}$$

with $$V = \frac{v}{\sqrt{x}}, \tag{2.9}$$

which yield a similarity solution.

Equations (2.1) and (2.2) then become

$$S\frac{\partial u}{\partial S} + T\frac{\partial u}{\partial T} - \frac{\partial V}{\partial S} = 0, \tag{2.10}$$

$$(1 - Tu)\frac{\partial u}{\partial T} - \left(\frac{Su}{2} - V\right)\frac{\partial u}{\partial S} = \frac{\partial^2 u}{\partial S^2}, \tag{2.11}$$

respectively. Here $S$ is the Blasius variable, while the Rayleigh variable is given by $\zeta = \frac{S}{2\sqrt{T}}$, and the boundary conditions can be expressed as functions of only $T$ and $S$. The equations (2.10) and (2.11) therefore may be solved numerically for $u$ and $V$ in terms of $T$ and $S$ alone, as has previously been addressed by Hall (1969). A difficulty with the numerical task in the above $S$-$T$ formulation should be noted, however. It is that the property of parabolic dependence (in the original system (2.1)-(2.2)) is observed in a sense, because of the expanding coordinates associated with the $S$-$T$ formulation; the problem (2.10)-(2.11) is parabolic in the positive $T$ direction if $u < T^{-1}$ but parabolic in the negative $T$ direction if $u > T^{-1}$, due to the coefficient (1-$Tu$) in (2.11). Hence the overall problem in (2.10)-(2.11) is elliptic in effect, and this requires multiple sweeping in $T$ for instance.

## 2.2 Entire flat-plate problem

In contrast with Hall's (1969) approach for the semi-infinite plate, an outline is given in this section of the numerical method used for directly solving equations (2.1) and (2.2) subject to the boundary conditions (2.4) to (2.5) and the initial state $u = 1$, $v = 0$ everywhere, rather than the similarity form of (2.8)-(2.11).

The flow problem (2.1)-(2.2) is parabolic in the positive $x$ direction provided that $u$ is positive or zero, as well as being parabolic in time $t$. We assume the general linear approximation $u\frac{\partial u}{\partial x} \approx \frac{\overline{u}(u - \overline{u})}{\Delta x}$ as the basis of the semi-implicit numerical method, as

suggested by Smith and Timoshin, along with a similar approximation for $v\frac{\partial u}{\partial y}$ and $\frac{\partial u}{\partial t}$, to determine the unknowns $u$, $v$ at the current station $x$ and time $t$. The velocity components are denoted by $\bar{u}$, $\bar{v}$ at the previous $x$-station, $x$-$\Delta x$, for the current time $t$, and by $\hat{u}$ at the current $x$-station, $x$, for the previous time, $t$-$\Delta t$. These values are assumed known, as represented in figure 2.1. Additionally, $\Delta x$ and $\Delta t$ are the small streamwise and time steps, respectively. The approximation is first order in $x$, requiring tiny $x$-steps $\Delta x$ for accuracy, but second-order accuracy in $y$ will be imposed subsequently. For now the differential form in terms of $y$ is retained.

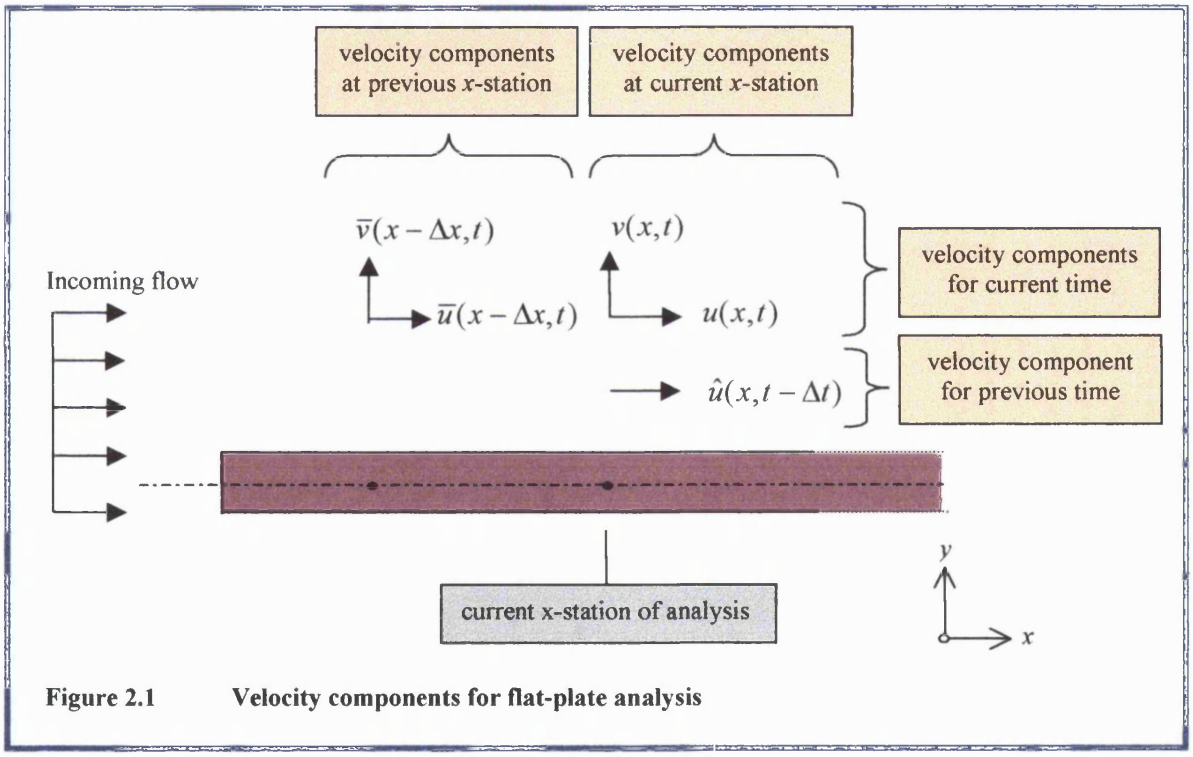


**Figure 2.1** **Velocity components for flat-plate analysis**

Thus equation (2.2) becomes

$$\left(\frac{u-\hat{u}}{\Delta t}\right)+\bar{u}\left(\frac{u-\bar{u}}{\Delta x}\right)+\bar{v}\frac{\partial u}{\partial y}=\frac{\partial^2 u}{\partial y^2}, \qquad (2.12)$$

essentially an equation for $u$ alone at a given $x$ station and given time $t$.

Next, the central differencing representations in $y$ are given by

$$\frac{\partial^2 u}{\partial y^2} = \frac{u(i,j,k) - 2u(i,j-1,k) + u(i,j-2,k)}{(\Delta y)^2}, \qquad (2.13)$$

and

$$\frac{\partial u}{\partial y} = \frac{u(i,j,k) - u(i,j-2,k)}{2\Delta y}, \qquad (2.14)$$

where $i,j,k$ are the step counters for the $x$ and $y$ coordinate directions and time, respectively.

Equations (2.13-2.14) are applied to equation (2.12), giving

$$\left(\frac{u(i,j-1,k) - u(i,j-1,k-1)}{\Delta t}\right) + u(i-1,j-1,k)\left(\frac{u(i,j-1,k) - u(i-1,j-1,k)}{\Delta x}\right)$$
$$+ v(i-1,j,k)\left(\frac{u(i,j,k) - u(i,j-2,k)}{2\Delta y}\right) = \frac{u(i,j,k) - 2\cdot u(i,j-1,k) + u(i,j-2,k)}{\Delta y^2}. \qquad (2.15)$$

This is regarded as an equation for the $u$ values at the $x$-station $i$. The velocity component $v$ may be obtained afterwards from equation (2.1) which is written as $\frac{\partial v}{\partial y} = \frac{-(u-\overline{u})}{\Delta x}$ or, using the values of $u$ and $\overline{u}$ averaged over $j$,

$$\left(\frac{v(i,j,k) - v(i,j-1,k)}{\Delta y}\right) =$$
$$-\frac{1}{2}\left(\left(\frac{u(i,j,k) - u(i-1,j,k)}{\Delta x}\right) + \left(\frac{u(i,j-1,k) - u(i-1,j-1,k)}{\Delta x}\right)\right). \qquad (2.16)$$

This implies that

$$v(i,j,k) = -\frac{1}{2}\left(\frac{\Delta y}{\Delta x}\right)\left(u(i,j,k) - u(i-1,j,k) + u(i,j-1,k) - u(i-1,j-1,k)\right)$$
$$+ v(i,j-1,k). \qquad (2.17)$$

The initial and boundary conditions for the system are as follows. At the first $t$-step, i.e. $t = \Delta t$, we have $u(i,j,k-1)$ equal to unity everywhere, corresponding to the

undisturbed uniform stream. Likewise at the first $x$-step, i.e. $x = \Delta x$, we have $\bar{u}$ equal to unity and $\bar{v}$ equal to zero. The conditions at the wall, $j$=1, are defined at each $x$-step as $u = v = 0$ at $y = 0$ (the no-slip wall condition), and $u$ is defined as unity, the velocity of the far-field flow, for $y$ at $j = j\max$, corresponding to the furthest value of $y$ in the far-field, in view of (2.4), (2.5).

The unknown variables in the tridiagonal system of equations (2.15) for $2 \le j \le (j\max - 1)$ are $u(i,j,k)$, $u(i,j\text{-}1,k)$, $u(i,j\text{-}2,k)$. The solution may be found as follows, with equation (2.15) expressed in the form

$$a \cdot u(i,j,k) + b \cdot u(i,j\text{-}1,k) + c \cdot u(i,j\text{-}2,k) = d\,. \qquad (2.18)$$

Thus, collecting the coefficients of the three unknowns, equation (2.15) becomes

$$u(i,j,k)\left(\frac{v(i-1,j,k)}{2\Delta y} - \frac{1}{\Delta y^2}\right) + u(i,j-1,k)\left(\frac{2}{\Delta y^2} + \frac{1}{\Delta t} + \frac{u(i-1,j,k)}{\Delta x}\right)$$
$$+ u(i,j-2,k)\left(-\frac{v(i-1,j,k)}{2\Delta y} - \frac{1}{\Delta y^2}\right) = \frac{u(i,j,k-1)}{\Delta t} + \frac{[u(i-1,j,k)]^2}{\Delta x}. \qquad (2.19)$$

### 2.2.1 Solution by Gaussian elimination for the flow velocities

To solve equation (2.18) or (2.19), for a given value of the $x$-station counter $i$ and time counter $k$, we use Gaussian elimination. The general form of the system of $n$-equations, which incorporate the boundary conditions for the far-field flow and the wall, is given as

$$\begin{bmatrix} 1 & 0 & 0 & 0 & \cdots & 0 \\ c_2 & b_2 & a_2 & 0 & \cdots & 0 \\ 0 & c_3 & b_3 & a_3 & \cdots & 0 \\ \vdots & \vdots & \vdots & \vdots & & \vdots \\ 0 & 0 & 0 & c_{n-1} & b_{n-1} & a_{n-1} \\ 0 & 0 & 0 & 0 & 0 & 1 \end{bmatrix} \begin{bmatrix} u_1 \\ u_2 \\ u_3 \\ \vdots \\ u_{n-1} \\ u_n \end{bmatrix} = \begin{bmatrix} 0 \\ d_2 \\ d_3 \\ \vdots \\ d_{n-1} \\ 1 \end{bmatrix}, \qquad (2.20)$$

with passive subscripts having been dropped.

Thus we have the augmented matrix formulation

$$\left[\begin{array}{cccccc|c} 1 & 0 & 0 & 0 & \cdots & 0 & 0 \\ c_2 & b_2 & a_2 & 0 & \cdots & 0 & d_2 \\ 0 & c_3 & b_3 & a_3 & \cdots & 0 & d_3 \\ \vdots & \vdots & \vdots & \vdots & & \vdots & \vdots \\ 0 & 0 & 0 & c_{n-1} & b_{n-1} & a_{n-1} & d_{n-1} \\ 0 & 0 & 0 & 0 & 0 & 1 & 1 \end{array}\right] \qquad (2.21)$$

$$\left[\begin{array}{cccccc|c} \mu_1 & a_1 & 0 & 0 & \cdots & 0 & \pi_1 \\ 0 & \mu_2 & a_2 & 0 & \cdots & 0 & \pi_2 \\ 0 & 0 & \mu_3 & a_3 & \cdots & 0 & \pi_3 \\ \vdots & \vdots & \vdots & \vdots & & \vdots & \vdots \\ 0 & 0 & 0 & 0 & \mu_{n-1} & a_{n-1} & \pi_{n-1} \\ 0 & 0 & 0 & 0 & 0 & 1 & 1 \end{array}\right] \qquad (2.22)$$

where $\mu_j = b_j - (a_{j-1}\, c_j / \mu_{j-1})$,

$\pi_j = d_j - (\pi_{j-1}\, c_j / \mu_{j-1})$.

Also we note that $\pi_1 = a_1 = 0$ and $\mu_1 = 1$.

Hence the velocity for a typical value of $j$ is given by $u_j = (\pi_j - a_j\, u_{j+1}) / \mu_j$.

## 2.3 Numerical solution

The flow chart for the structure of the computer program to evaluate the $u$ velocities at $i,j,k$ is given below.

The local system of equations for $u,v$ at the height counter $j$ above the flat plate is thereby solved at a given $x$-station for the time counter $k$. After the velocity components $u,v$ at $j$ have been evaluated the routine moves on to the next $x$-station. Once all the $x$-stations have been traversed, the procedure time-marches to the next value of the time counter $k$+1. This describes the overall semi-implicit marching numerical method. An investigation of how well the method performs (especially

concerning its accuracy) will be described below by comparing its results with the Hall similarity solution and observing the grid refinement effect on the rate of development of the solution, in order to estimate adequate grid sizes.

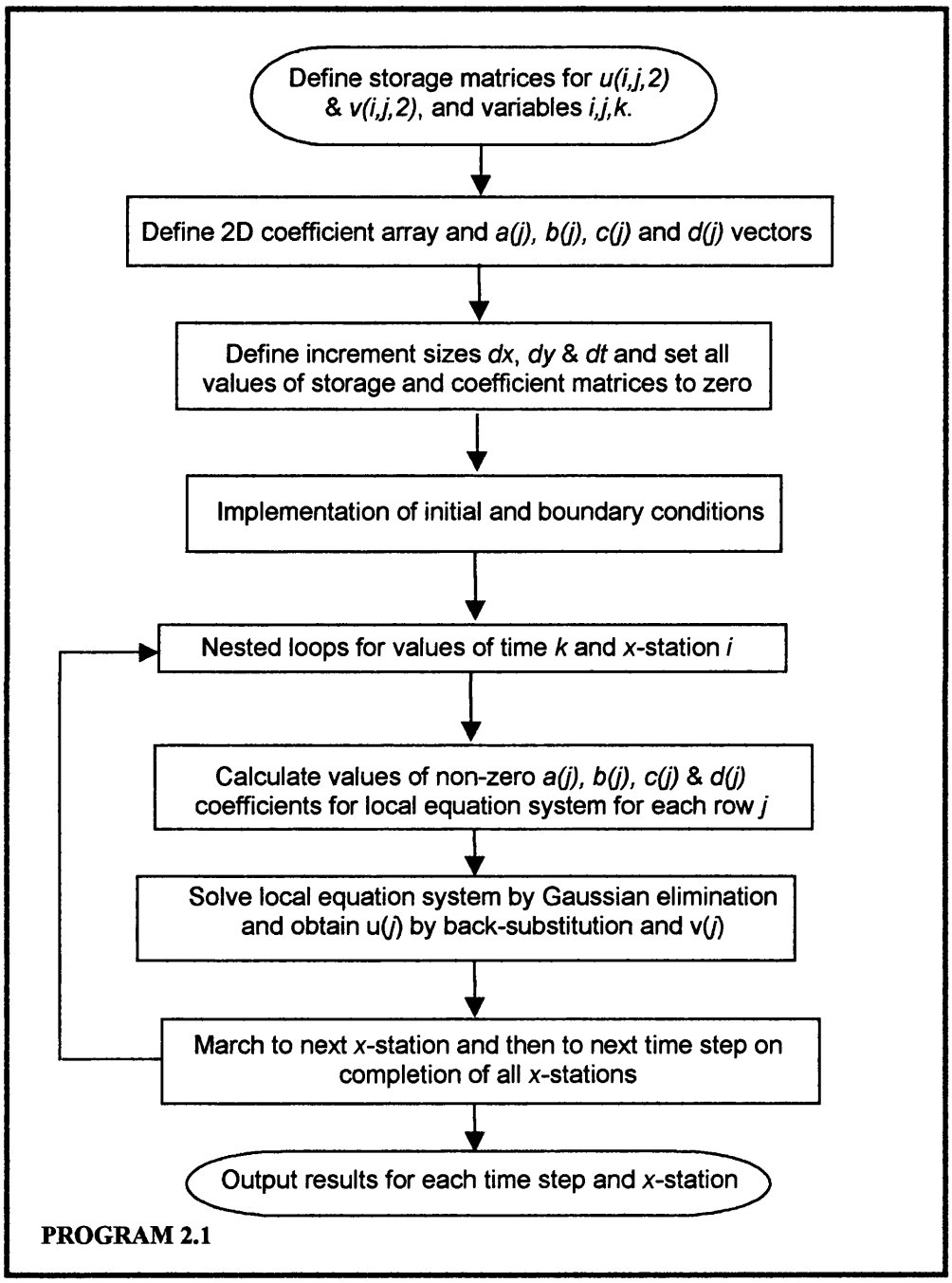


**PROGRAM 2.1**

Overall the advantages of the semi-implicit approach appear to be the following: it is relatively easy to program and to modify; it is fast in computer time for reasonable grid sizes; it can be made second order accurate in both $x$, $t$, through the double-stepping procedure of Smith and Timoshin (1996), through three-point backward differencing for the $x$-derivatives, or through iteration on the current $u$, $v$ values to

incorporate non-linearity; unusually for a numerical scheme for a partial differential equation, the approach can be checked in quite some detail by analytical means (see below in sections 2.4-2.7); and finally it is flexible in terms of alterations in the boundary conditions, for example in the free stream or at the wall or wake centre-line (see Chapter 3).

### 2.3.1 Results and discussion

Comparing the results with the predictions of Hall (1969), convergence to the similarity solution of Hall occurs after fewer time steps for a finer grid, i.e. for smaller values of the time and streamwise intervals, $\Delta t$ and $\Delta x$, respectively. The variation of the surface shear $\left(\frac{\partial u}{\partial S}\right)_{S=0}$ in particular with normalised time $T$ (equation 2.8) is shown in figures 2.2-5, together with Hall's predictions, for computational runs employing various levels of grading with respect to time. The numbers of time-steps thus chosen for examination of convergence of the solution were between one and thirty. The profiles are presented for runs performed for three values of $\Delta x$, to assess the level of grid refinement in the $x$-coordinate direction, in figures 2.3-5. Hall found that by $T$=4, the transition from Rayleigh to a steady-state Blasius flow regime was completed.

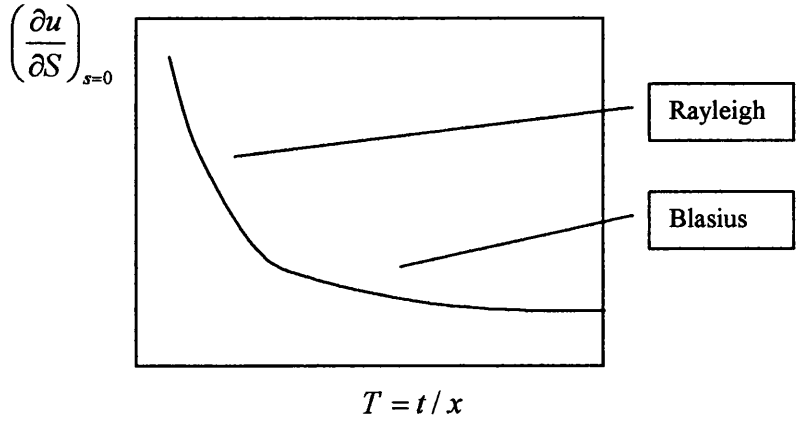


**Figure 2.6** **General form of the Hall solution**

As more time steps are employed in the runs, the solution converges more closely to the Hall solution, which is of the approximate form shown below in figure 2.6. As a general observation, the major part of the convergence to the Hall solution occurs over the first five time steps. By employing a larger number of time steps in the run,

the rate of convergence increases. By employing smaller values of $\Delta x$, the rate of convergence to the Hall solution, with respect to number of time steps, was faster and surprisingly attained with fewer-time steps. For example, when $\Delta x$ is 0.001, 30 time steps are required for fairly adequate convergence towards Hall's solution, whereas for $\Delta x$ equal to 0.0002 only 4 time steps are required for a similar level of convergence. It will also be observed that even for a single time step, the general two-part form of the solution curve is obtained. Thus the rate of convergence in terms of the number of time steps appears to be a function of the streamwise step. As $T$ tends to infinity, we notice that the profile is more or less constant.

The results altogether seem to capture the correct form of the solution qualitatively, and quantitative agreement also emerges if the grid taken is sufficiently refined. Grid refinement was performed in, for instance, the $x$-coordinate direction, while keeping the same level of grid refinement in the $y$-coordinate direction and with respect to time. Additionally, unequal steps were taken for the grid size refinement in order to check for convergence of solution more efficiently. The velocity computed was monitored at three given locations whose positions were fixed. Refinement with respect to $x$ and $t$ yielded negligible changes in the values of $u$, as shown in figures 2.7 and 2.8. Figure 2.9 shows grid refinement with respect to $y$, where the results show steady convergence for reducing $\Delta y$. This suggests that the solution is well converged with respect to the current sizes of $\Delta x$, $\Delta y$ and $\Delta t$.

## 2.4 Analytical properties at first x-station

### 2.4.1 The near-Blasius solution (initial time interval)

It is interesting to reconsider the general finite-difference equation (2.12) at the point $x=\Delta x$ and $t=\Delta t$. There, $\bar{u} = \hat{u} = 1$ and $\bar{v} = 0$ as stated earlier. So we have

$$\frac{u_{j+1} - 2u_j + u_{j-1}}{h^2} - Q^2 u_j = -Q^2, \qquad (2.23)$$

for $j$ = 1 to 100 to match with the computational program, where $Q^2 = \left(\frac{1}{\Delta t} + \frac{1}{\Delta x}\right)$ and $h = \Delta y$. This set of difference equations can be solved exactly.

The general solution is

$$u_j = A\lambda_1^j + B\lambda_2^j + 1, \tag{2.24}$$

where $\lambda_1$ and $\lambda_2$ are the roots of the characteristic equation

$$\lambda^2 - (2 + Q^2h^2)\lambda + 1 = 0. \tag{2.25}$$

One root, $\lambda_1$ say, is greater than 1 and the other, $\lambda_2$, is less than 1. In order to compare with the numerical results, we employ the boundary conditions at the wall and at infinity. In doing this, we obtain $A = 0$ and $B = -1$. The value of $Q^2$ is found to be 150 from $Q^2 = \left(\frac{1}{\Delta t} + \frac{1}{\Delta x}\right)$ with $\Delta t = 0.02$ and $\Delta x = 0.01$, and the value of $\Delta y$ taken is 0.1. So the two roots are $\lambda_1 = 3.186 > 1$ and $\lambda_2 = 0.314 < 1$. Then equation (2.24) yields $u_1 = 0.686$ which agrees exactly with the computed result at the first $x$-station $i$=1 and at $j$=1 in the numerical results. In addition, the implied dependence on $y/t^{1/2}$ and $y/x^{1/2}$ in (2.23)-(2.25) agrees with the known similarity form: see (2.8)-(2.11).

### 2.4.2 The Rayleigh solution for $x$>t

For $x$>t, we have from equation (2.12) the approximation

$$\frac{u-1}{\Delta t} = \frac{\partial^2 u}{\partial y^2}, \tag{2.26}$$

and the far-field and wall conditions apply, namely: $u$ tends to unity as $y$ tends to infinity, and $u$ is equal to zero when $y$ is equal to zero.

Equation (2.26) implies the second order differential equation

$$\frac{\partial^2 u}{\partial y^2} - uQ^2 = -Q^2, \tag{2.27}$$

where $Q^2 = \frac{1}{\Delta t}$ now.

The general solution is given as before by $u = A\lambda_1^j + B\lambda_2^j + 1$, and as before we find

$A = 0$, $B = -1$. Substituting in the numerical values we have $Q^2 = 50$ with $\Delta t = 0.02$, and $\Delta y = 0.1$ again, which gives the values $\lambda_1 = 2(>1)$ and $\lambda_2 = 0.5(<1)$. So the solution yields $u = 0.5$ at $j = 1$, which agrees with the numerical results for the Rayleigh range obtained by the above computations. The implied dependence on $y/t^{1/2}$ is also in agreement with the known exact form of solution noted just after (2.11).

### 2.5 Analysis at the second $x$-station ($x = 2\Delta x$)

Following the analytical solution obtained in section 2.4 for the first $x$-station of the plate at $x = \Delta x$, we see that the two computational programs above yield identical values. We now consider the possibility of an analytical based solution for the second $x$-station at the point $x = 2\Delta x$. This is done for two reasons: first, for the sake of comparing with and checking the numerical approach of sections 2.3, 2.4; second (in principle), for examining from an alternative viewpoint the double-stepping procedure of Smith and Timoshin (1996), which is advocated as a means of obtaining second-order accuracy in $x$. As before, we initialise the values of $\bar{u}$ and $\bar{v}$, for the previous $x$-station. For $\bar{u}$ we use the solution for $u$ derived already at the first $x$-station (section 2.4) and for $\bar{v}$ we then use the continuity equation. Hence $u = 1 - e^{-Qy}$, $\bar{u} = 1$ and $u_x = \dfrac{-e^{-Qy}}{\Delta x}$ over the first step. Thus continuity gives

$$v = \frac{-(e^{-Qy} - 1)}{Q\Delta x} \qquad (2.28a)$$

using $v = 0$ at $y = 0$, at the first $x$-station.

In addition, after some operations in equation (2.12), we obtain a differential equation of the apparently unusual form

$$\bar{v}\frac{\partial u}{\partial y} + (a - be^{-Qy})u = \frac{\partial^2 u}{\partial y^2}, \qquad (2.28b)$$

for u at the second $x$-station, where $a = Q^2$ and $b = 1/\Delta x$, while $\bar{v}$ is the right-hand side of (2.28a). We next transform equation (2.28b) into a form that is susceptible to solution.

Setting $s = e^{-Qy}$ we find again after various operations the form

$$s^2 u_{ss} + s(1 + K - Ks)u_s - (1 - Ks)u = 0, \qquad (2.29)$$

where the constant $K = b/Q^2$, which is a parameter dependent on the $\Delta x$ and $\Delta t$ intervals, and the homogeneous version of (2.28b) is addressed first seeking to obtain a form of the equation that is susceptible to solution, we perform the following series of manipulations. By further setting $u = AB$, we obtain the equation in the form

$$s^2(AB'' + 2A'B' + A''B) + s(1 + K - Ks)(AB' + A'B) - (1 - Ks)AB = 0. \qquad (2.30)$$

To solve equation (2.30), we choose B to eliminate the terms containing A, and we thus define B as

$$B = s^{-(1+K)/2} e^{Ks/2}. \qquad (2.31)$$

Inserting B into equation (2.30), we therefore obtain the standard form for A.

$$s^2 A'' + A\left(-\frac{K^2 s^2}{4} + (3+K)\frac{Ks}{2} - \frac{1}{4}(3+K^2)\right) = 0 \qquad (2.32)$$

Of more practical use subsequently (see sections 2.5.1, 2.6 below), however, is the non-homogeneous counterpart of (2.29), namely

$$s^2 u_{ss} + s u_s(1 + K - Ks) - (1 - Ks)u = -1 + 2Ks - Ks^2, \qquad (2.33)$$

which is subject to the conditions $u(1) = 0$ and $u(0) = 1$, for $u(s)$. The value of $K$ lies between 0 and 1. The homogeneous version then is the same as equation 22.6.17 of Abramowitz and Stegun (1972). Using their standard solution, we obtain

$$e^{-x/2} x^{(a+1)/2} Ln^{(a)}(x), \tag{2.34}$$

where $Ln^{(a)}(x)$ is the generalized Laguerre polynomial and $a$ is a known constant. On the other hand, we need a particular integral for the right hand side terms. For the $-1+2Ks$ terms, a particular integral is $u=1+s$, but there seems to be no straightforward particular integral for the $-Ks^2$ term. We return to (2.33) shortly.

So instead, for general values of $K$, we next solved equation (2.33) numerically using a tri-diagonal system as in section 2.2.1. The results are given in section 2.6 for various values of $K$.

### 2.5.1 Analytical solution for small $K$

An investigation of an analytical solution of (2.33) valid for small $K$ is useful here.

Equation (2.33) becomes, for small $K$,

$$s^2 u_{ss} + s u_s - u = -1, \tag{2.35}$$

subject to the conditions $u(1) = 0$ and $u(0) = 1$.

The solution is $u = As + Bs^{-1} + 1$. Then $u(0) = 1$ implies that $B = 0$ and $u(1) = 0$ implies that $A = -1$. Therefore we have the simple result $u = 1 - s$. This agrees with the trends of our numerical results in the figures below for decreasing $K$.

## 2.6 Computational results and discussion for $x = 2\Delta x$

The program used for the evaluation of $u$ at $2\Delta x$ is identical to Program 2.1. The only differences arise in the use of the height variable $s$ $(=(j-1)\Delta s)$ for the evaluation of the

coefficients of the velocities in (2.33), rather than as in equation (2.19). The results for the second $x$-station are then presented in figures 2.10-2.12.

For various values of *jmax* = *100*, 21, 41, 81, and interval parameter $K$, the results show that as $K$ is increased from 0.05 to 0.9, the non-linear nature of the velocity profile becomes gradually more emphasised. This is shown by the results for a given value of *jmax*, and varying $K$.

To add to this, we observe that the steady Blasius solution can be tackled similarly. Here $\Delta t \to \infty$ in effect. So $Q^2$ becomes $1/\Delta x$. By solving equation (2.24) and also employing (2.25) to evaluate $\lambda_2$ which was found to be 0.382, for $\Delta x = 0.01$ and $\Delta y = 0.1$. The calculated values of velocity $u_j$ are found to be $u_1 = 0.618$, $u_2 = 0.854$ and $u_3 = 0.944$ which agree exactly with those found computationally.

The computed value of the scaled wall shear with $x$, for the current grid spacing, is given in figure 2.13, together with the true Blasius values. Fair agreement is observed for values of $x \geq 0.03$.

## 2.7 The modified Blasius solution

For another analytical based comparison with the numerical work, we employ a Blasius 'modified' solution for the steady-state solution as $x \to 0$. This is defined as follows.

If $\bar{u} = f'(\zeta)$, where $\zeta = y/x^{1/2}$, then

$$f''' + \frac{ff''}{2} = 0, \tag{2.36}$$

together with the conditions

$$f(0) = f'(0) = 0 \tag{2.37a}$$

and

$$f'(\alpha) = 1. \tag{2.37b}$$

Here $\alpha$ is taken to be a finite positive constant, representing a modification of the classical Blasius case which has $\alpha$ being large in effect. Here, the parameter $a$ is the wavenumber of the disturbance when the wake thickness is scaled out (Papageorgiou & Smith 1989).

Numerical integration shows that $\lambda = f''(0) = 0.332...$ when $\alpha >> 1$ [see the Blasius case in Jones & Watson (1963)]. On the other hand, when we select $\alpha << 1$, we expect $f''' = 0$ from (2.36) to leading order since the range of $\zeta$ is then small. So we may anticipate that then

$$f = \hat{a}\zeta^2 + \hat{b}\zeta + \hat{c}, \tag{2.38}$$

with unknown constants $\hat{a},\hat{b},\hat{c}$. From equation (2.37a) we see that $\hat{c} = 0$ and $\hat{b} = 0$. Also equation (2.37b) requires $2\hat{a}\alpha = 1$ and thus $\hat{a}$ is determined as

$$\hat{a} = \frac{1}{2\alpha}. \tag{2.39}$$

So finally we obtain, using (2.39) in (2.36), in prediction that

$$f''(0) \sim \frac{1}{\alpha} \quad \text{as } \alpha \to 0. \tag{2.40}$$

Equation (2.40) gives the Blasius modified behaviour for small $\alpha$ and has been included in program 2.3 for comparison. Figure 2.14 shows the variation of $f''(0)$ with $\alpha$ for values of $\alpha$ up to five, from our numerical solution of (2.36)-(2.37b); the numerical solutions at these $\alpha$ values are joined together simply by straight lines. The Blasius value 0.332... for $f''(0)$ is closely approached for $\alpha$ near 5. For small $\alpha$ the asymptote (2.40) is remarkably close to the numerical results, due to the nature of the resultant series, thus providing an encouraging check on the latter. In fact (2.40) apparently works well for $\alpha$ as large as 2 or more. Figures 2.15-18 present the variation with $\zeta$, for a range of values of $\alpha$, of $f''$ (the shear function), $f'$ (the

velocity function) and $f$ (the stream function). The emergence of the simple forms implied in (2.38)-(2.40) for these profiles is evident for $\alpha$ values below about 3.

## 2.8 Fortran 77 and 90 programs and figures

```
C     ********************************************
C    PROGRAM TO SOLVE 2-D PROBLEM FOR FLAT PLATE
C      by      Dimitrios P. Papadopoulos
C      JULY 1998
C     ********************************************

C Define variables

        program plate
        INTEGER i,j,k,imax,jmax,kmax,ntmax,nt
        REAL  dy,dt,dx,f,x

C Define 3D storage arrays for computed values of u(i,j,k) & v(i,j,k)

        REAL  u(102,102,2),v(102,102,2),ss(102)

C Define 2D coefficient array and u(j) & d(j) vectors which form the"local"
C   system of equations for solution at each x-station

        REAL  coefficient(1051,1051),dvector(1051)
        REAL  a(1051),b(1051),c(1051),d(1051),mi(1051),pi(1051)
        INTEGER col

C Define increment sizes and storage-matrix dimensions

        dx = 0.01
        dy = 0.1
        dt = 0.02
        imax = 20
        jmax = 20
        kmax = 2
        ntmax= 1950

C     ****************************************************
C    IMPLEMENTATION OF BOUNDARY CONDITIONS  *
C     ****************************************************

        DO 42 k = 1,kmax,1
        DO 41 j = 1,jmax,1
        DO 40 i = 1,imax,1

C         Un-influenced flow field (before introduction of plate)

          IF (k.EQ.1)    u(i,j,k) = 1.0

C       Flow field at first x-station (at leading edge of plate)

          IF (i.EQ.1)     THEN
            u(i,j,k) = 1.0
            v(i,j,k) = 0.0
          ENDIF

C        Flow field at the wall (non-slip condition)

          IF (j.EQ.1) THEN
            u(i,j,k) = 0.0
            v(i,j,k) = 0.0
          ENDIF

        u(1,1,k) = 1.0

C       Flow field outside boundary layer region

          IF (j.EQ.jmax)   u(i,j,k) = 1.0
```

2.1 Program to solve 2-D problem for flat plate.

```
40      CONTINUE
41      CONTINUE
42      CONTINUE

C     ***********************************************
C    ASSEMBLE LOCAL SYSTEM OF EQUATIONS  *
C     ***********************************************

C       nested loops for each value of time and x-station

        k=2
        DO 200  nt=1,ntmax,1
        DO 90   i = 2,imax,1

C       Set all terms of coefficient matrix equal to zero

        DO 69 j=1,jmax,1
         DO 68 col=1,jmax,1
          coefficient(j,col) = 0

68      CONTINUE
69      CONTINUE

C       calculate values of non-zero coefficients - row by row (j)

        DO 70  j = 1,jmax,1

          IF (j.EQ.1) THEN
             dvector(j) = 0
             coefficient(j,j) = 1.0
          ENDIF

          IF (j.EQ.jmax) THEN
             dvector(j) = 1.0
             coefficient(j,j) = 1.0
         ENDIF

        IF ((j.NE.1).AND.(j.NE.jmax)) THEN

        a(j) =  (v(i-1,j,k)/(2*dy)) - (1/(dy**2))
        b(j) =   (1/dt)+(u(i-1,j,k)/dx) + (2/(dy**2))
        c(j)= (- (1/(dy**2))) - (v(i-1,j,k)/(2*dy))
        d(j)=((1/dt) * u(i,j,k-1)) + ((u(i-1,j,k)**2) *(1/dx))

        coefficient(j,j-1) = c(j)
        coefficient(j,j) = b(j)
        coefficient(j,j+1) = a(j)
        dvector(j) = d(j)

        ENDIF

70      CONTINUE

C     ***********************************************************************
C    SOLVE SYSTEM OF EQUATIONS WITH GAUSSIAN ELIMINATION  *
C     ***********************************************************************

C       we define values of transformed coefficients row by row (j)
C       first, evaluate mi and pi for each row (j)

        mi(1)=1
        pi(1)=0
```

```
          DO 75   j=2,(jmax-1),1
          mi(j)=b(j)-((c(j)*a(j-1))/mi(j-1))
          pi(j)=d(j)-((c(j)*pi(j-1))/mi(j-1))

C          second,insert mi and pi for each row(j) and also c(j)=0

          coefficient(j,j-1)=0
          coefficient(j,j)=mi(j)
          dvector(j)=pi(j)
75        CONTINUE

C         solve for u(j) by back substitution

          u(i,1,k) = 0

          DO 80  j=(jmax-1),2,-1
          u(i,j,k)=(pi(j)-(a(j)*u(i,j+1,k)))/mi(j)

80        CONTINUE

C         calculate v(j)

          v(i,1,k) = 0

          DO 85  j=2,jmax,1
          f =-((dy / (2*dx)) * (u(i,j,k)-u(i-1,j,k)+u(i,j-1,k)-u(i-1,j-1,k)))

          v(i,j,k) = (v(i,j-1,k)) + f

85         CONTINUE
90         CONTINUE

C         Copy values from k=2 to k=1 and print for current time step nt.

          do 102  i=1,imax,1
          do 101  j=1,jmax,1
          u(i,j,1)=u(i,j,2)
          v(i,j,1)=v(i,j,2)
101       continue
102       continue

          if ((nt.eq.3).or.(nt.eq.20).or.(nt.eq.120).or.
(nt.eq.320).or.(nt.eq.520)) then

          do i=2,imax,1
          x=(i-1)*dx
          ss(i)=( ((4*u(i,2,2))-u(i,3,2)) ) / (2*dy)
C         *(x**0.5)

C         WRITE (6,*)' x=',x,' ; ss=',ss(i)  ,'  time',nt
C         WRITE (6,*)  x ,  ss(i)

          enddo
C         WRITE (6,*) ''
          endif

200       CONTINUE

C  Print out values for u(i,j,k) and v(i,j,k) at each time step & x-station

          DO 225 i=2,imax,1
          k=2

          DO 210 j=jmax,1,-1
```

```
      WRITE (6,*)' u ', j ,   u(i,j,k)
210   CONTINUE

      WRITE (6,*)' '

      DO 220 j=jmax,1,-1
      WRITE (6,*)' v ', j ,   v(i,j,k)
220   CONTINUE
      WRITE (6,*)' '

225   CONTINUE

240   end
```

```
C     ************************************************************
C     PROGRAM TO FIND RESULT AT THE SECOND X-STATION
C                       by  Dimitrios P. Papadopoulos
C     ************************************************************

C Define variables

        INTEGER i,j,k,imax,jmax,kmax
        REAL  dy,dt,dx,s,Q,kay

C Define 3D storage arrays for computed values of u(i,j,k) & v(i,j,k)

        REAL  u(701,701,2)

C Define 2D coefficient array and u(j) & d(j) vectors which form the"local"
C   system of equations for solution at each x-station

        REAL  coefficient(701,701),dvector(701)
        REAL  a(701),b(701),c(701),d(701),mi(701),pi(701)
        INTEGER col

C Define increment sizes and storage-matrix dimensions

        dx = 0.001
        dt = 0.002
        imax = 2
        jmax = 51
        kmax = 31
        dy = 1.0 / (jmax-1.0)
        kay = 0.9
        Q = 12.47

C    Set  all values of storage-matrix equal to zero

10      DO 32 k = 1,kmax,1
        DO 31 j = 1,jmax,1
        DO 30 i = 1,imax,1

          u(i,j,k) = 0.0

30      CONTINUE
31      CONTINUE
32      CONTINUE

C     ***************************************************
C    IMPLEMENTATION OF BOUNDARY CONDITIONS  *
C     ***************************************************

        DO 42 k = 1,kmax,1
        DO 41 j = 1,jmax,1
        DO 40 i = 1,imax,1

C  Un-influenced flow field (before introduction of plate)
          IF (k.EQ.1)    u(i,j,k) = 1.0

C Flow field at first x-stations (at front of plate)
          IF (i.EQ.1)     THEN
            u(i,j,k) = 1.0
          ENDIF

C Flow field at the wall (non-slip condition)
          IF (j.EQ.1) THEN
            u(i,j,k) = 1.0
          ENDIF
```

2.2 Program to find results at the second $x$-station.

```
C Flow field outside boundary layer region
          IF (j.EQ.jmax)   u(i,j,k) = 0.0

40       CONTINUE
41       CONTINUE
42       CONTINUE

C     ********************************************
C    ASSEMBLE LOCAL SYSTEM OF EQUATIONS  *
C     ********************************************

C nested loops for each value of time and x-station

        DO 100  k = 2,kmax,1
        DO 90    i = 2,imax,1

C Set all terms of coefficient matrix equal to zero

        DO 69 j=1,jmax,1
         DO 68 col=1,jmax,1
          coefficient(j,col) = 0

68       CONTINUE
69      CONTINUE

C calculate values of non-zero coefficients - row by row (j)

        DO 70  j = 2,jmax,1

          IF (j.EQ.1) THEN
             dvector(j) = 1.0
             coefficient(j,j) = 1.0

          ENDIF

          IF (j.EQ.jmax) THEN
              dvector(j) = 0
             coefficient(j,j) = 1.0

          ENDIF

        IF ((j.NE.1).AND.(j.NE.jmax)) THEN

        s = (j-1)*dy

        a(j) = ((s**2)/(dy**2)) - (s*(1 + kay -(kay*s))/(2*dy))
        b(j) = ((kay*s)-1-((2*(s**2))/(dy**2)))
        c(j) = ((s**2)/(dy**2)) + (s*(1 + kay -(kay*s))/(2*dy))
        d(j) = ((2*kay*s)-1-(kay*(s**2)))

        coefficient(j,j-1) = a(j)
        coefficient(j,j) = b(j)
        coefficient(j,j+1) = c(j)
        dvector(j) = d(j)

        ENDIF

70      CONTINUE

C     ********************************************************************
C    SOLVE SYSTEM OF EQUATIONS WITH GAUSSIAN ELIMINATION  *
C     ********************************************************************
```

```
C we define values of transformed coefficients row by row (j)
C first, evaluate mi and pi for each row (j)

        mi(1) = 1
        pi(1) = 1
        mi(2) = b(2)
        pi(2) = d(2) - a(2)

        DO 75   j=3,(jmax-1),1

        mi(j)=b(j)-((a(j)*c(j-1))/mi(j-1))
        pi(j)=d(j)-((a(j)*pi(j-1))/mi(j-1))

C second,insert mi and pi for each row(j) and also a(j)=0

        coefficient(j,j-1)=0
        coefficient(j,j)=mi(j)
        dvector(j)=pi(j)

75      CONTINUE

C solve for u(j) by back substitution

        DO 80  j=(jmax-1),2,-1

        u(i,j,k)=(pi(j)-(c(j)*u(i,j+1,k)))/mi(j)


80      CONTINUE
90       CONTINUE
100      CONTINUE

C  Print out values for u(i,j,k) and v(i,j,k) at each time step & x-station

        DO 130 k=2,kmax,1
        DO 125 i=2,imax,1

        WRITE (6,*) ' '
        WRITE (6,*)' x-station ', i ,'                          time  ', k

        DO 110 j=jmax,1,-1
        WRITE (6,*)'   u    ',      j    ,    u(i,j,k)
110     CONTINUE

        WRITE (6,*)' '

125     CONTINUE
130     CONTINUE

140     end
```

```
C*********************BLASIUS Program*********************************

MODULE kind

IMPLICIT NONE
INTEGER, PARAMETER      :: dp = SELECTED_REAL_KIND(8,30)

END MODULE kind

MODULE similarity_solution

USE kind
IMPLICIT NONE
INTEGER, PARAMETER      :: kbot = 0, ktop = 2048
REAL(KIND=dp), PARAMETER:: etabot = 0.0_dp, etatop = 5.0_dp
REAL(KIND=dp), PARAMETER:: ubot = 0.0_dp, utop = 3.0_dp, psibot = 0.0_dp
REAL(KIND=dp)           :: deta
REAL(KIND=dp), DIMENSION(:), ALLOCATABLE        :: eta
REAL(KIND=dp), DIMENSION(:), ALLOCATABLE        :: delta_eta
REAL(KIND=dp), DIMENSION(:,:), ALLOCATABLE      :: f, fv

END MODULE similarity_solution

PROGRAM main

        IMPLICIT NONE

        CALL allocate_similarity_solution
        CALL set_similarity_solution
        CALL write_data_files

        END PROGRAM main

        SUBROUTINE allocate_similarity_solution

        USE kind
        USE similarity_solution
        IMPLICIT NONE
        INTEGER                 :: k

                ALLOCATE( eta(kbot:ktop) )
                ALLOCATE( delta_eta(kbot+1:ktop) )
                ALLOCATE( f(kbot:ktop,1:3) )
                ALLOCATE( fv(kbot:ktop,1:3) )

                deta    = (etatop - etabot)/(REAL((ktop-kbot),dp))

                DO k = kbot, ktop
                        eta(k)          = etabot + REAL((k-kbot),dp)*deta
                END DO

                DO k = kbot+1, ktop
                        delta_eta(k)    = deta
                END DO

      END SUBROUTINE allocate_similarity_solution

      SUBROUTINE set_similarity_solution

              USE kind
              IMPLICIT NONE
```

2.3 Program to evaluate the Blasius modified behaviour for small $\alpha$.

```
                CALL newton(0.0_dp)

        END SUBROUTINE set_similarity_solution

        SUBROUTINE newton(wall_shear)

        USE kind
        USE similarity_solution
        IMPLICIT NONE
        REAL(KIND=dp)           :: wall_shear, phi, phi_dashed

                f(0,1)  = psibot
                f(0,2)  = ubot
                f(0,3)  = wall_shear

                fv(0,1)         = 0.0_dp
                fv(0,2)         = 0.0_dp
                fv(0,3)         = 1.0_dp

                phi = 1.0_dp

        DO WHILE( ABS(phi) > 1.0E-12_dp)
                CALL runge_kutta(kbot, ktop, eta, delta_eta, f, fv)
                phi                     = f(ktop,2) - utop
                phi_dashed              = fv(ktop,2)
                wall_shear              = wall_shear - (phi/phi_dashed)
                f(0,3)                  = wall_shear
                WRITE(6,*)phi, wall_shear
        END DO

END SUBROUTINE newton

SUBROUTINE runge_kutta(kbot, ktop, t, h, x, v)

        USE kind
        IMPLICIT NONE
        INTEGER, INTENT(IN)                                     :: kbot, ktop
        REAL(KIND=dp), DIMENSION(0:ktop), INTENT(IN)            :: t
        REAL(KIND=dp), DIMENSION(1:ktop), INTENT(IN)            :: h
        REAL(KIND=dp), DIMENSION(0:ktop,1:3), INTENT(INOUT)     :: x, v
        INTEGER                                                 :: k

DO k = kbot+1, ktop
CALL runge_kutta_step(t(k-1),h(k),x(k-1,1:3),v(k-1,1:3),x(k,1:3),v(k,1:3))
END DO

        END SUBROUTINE runge_kutta

        SUBROUTINE runge_kutta_step(t, h, x, v, xout, vout)

USE kind
IMPLICIT NONE
REAL(KIND=dp), INTENT(IN)       :: t, h
REAL(KIND=dp), DIMENSION(1:3), INTENT(IN)       :: x, v
REAL(KIND=dp), DIMENSION(1:3), INTENT(OUT)      :: xout, vout
REAL(KIND=dp), DIMENSION(1:3)   :: f1, f2, f3, f4, fv1, fv2, fv3, fv4

CALL evaluate_functions(t, x, v, f1, fv1)
f1 = h*f1
fv1 = h*fv1
CALL evaluate_functions(t+(0.5_dp*h), x+(0.5_dp*f1), v+(0.5_dp*fv1), f2, fv2)
f2 = h*f2
fv2 = h*fv2
CALL evaluate_functions(t+(0.5_dp*h), x+(0.5_dp*f2), v+(0.5_dp*fv2), f3, fv3)
```

```
f3 = h*f3
fv3 = h*fv3
CALL evaluate_functions(t+h, x+f3, v+fv3, f4, fv4)
f4 = h*f4
fv4 = h*fv4

        xout = x + ((f1 + (2.0_dp*f2) + (2.0_dp*f3) + f4)/6.0_dp)
        vout = v + ((fv1 + (2.0_dp*fv2) + (2.0_dp*fv3) + fv4)/6.0_dp)

        END SUBROUTINE runge_kutta_step

        SUBROUTINE evaluate_functions(t, x, v, f, fv)

        USE kind
        IMPLICIT NONE
        REAL(KIND=dp), INTENT(IN)                                   :: t
        REAL(KIND=dp), DIMENSION(1:3), INTENT(IN)                   :: x, v
        REAL(KIND=dp), DIMENSION(1:3), INTENT(OUT)                  :: f, fv

                f(1)    = x(2)
                f(2)    = x(3)
                f(3)    = -0.5_dp*x(1)*x(3)

                fv(1) = v(2)
                fv(2) = v(3)
                fv(3) = -0.5_dp*((x(3)*v(1)) + x(1)*v(3))

        END SUBROUTINE evaluate_functions

        SUBROUTINE write_data_files

        USE similarity_solution
        IMPLICIT NONE
        INTEGER                                                     :: k

                OPEN(10, FILE='profiles.dat')
                DO k = kbot, ktop
                        WRITE(10,FMT=30)eta(k), f(k,1), f(k,2), f(k,3)
                END DO
                CLOSE(10)

30              FORMAT(4F12.6)

        END SUBROUTINE write_data_files
```

Variation of surface shear with T.
(dx=.005 dy=.05 dt=.01)

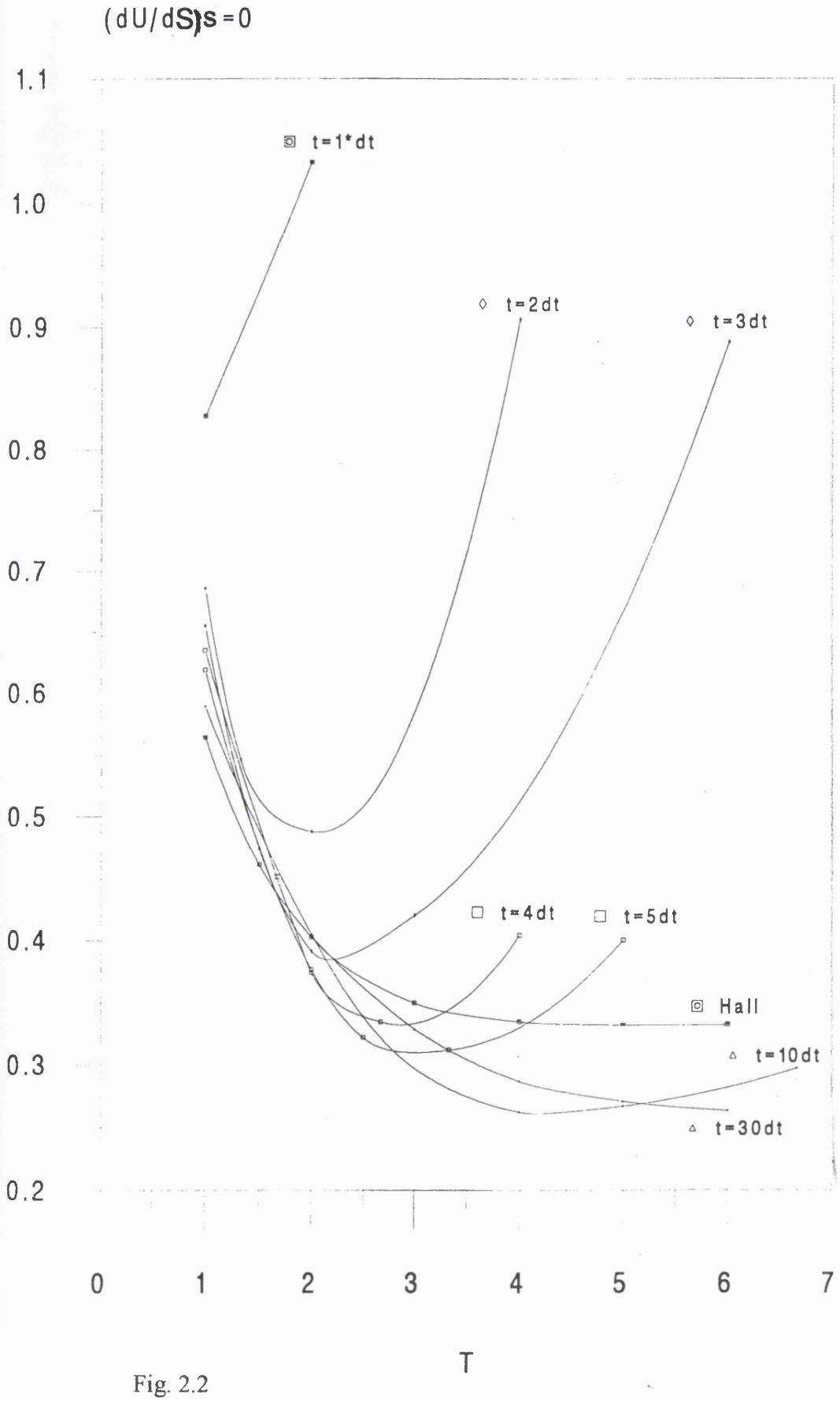


Fig. 2.2

Variation of surface shear with T.
(dx=.001 dy=.02 dt=.002)

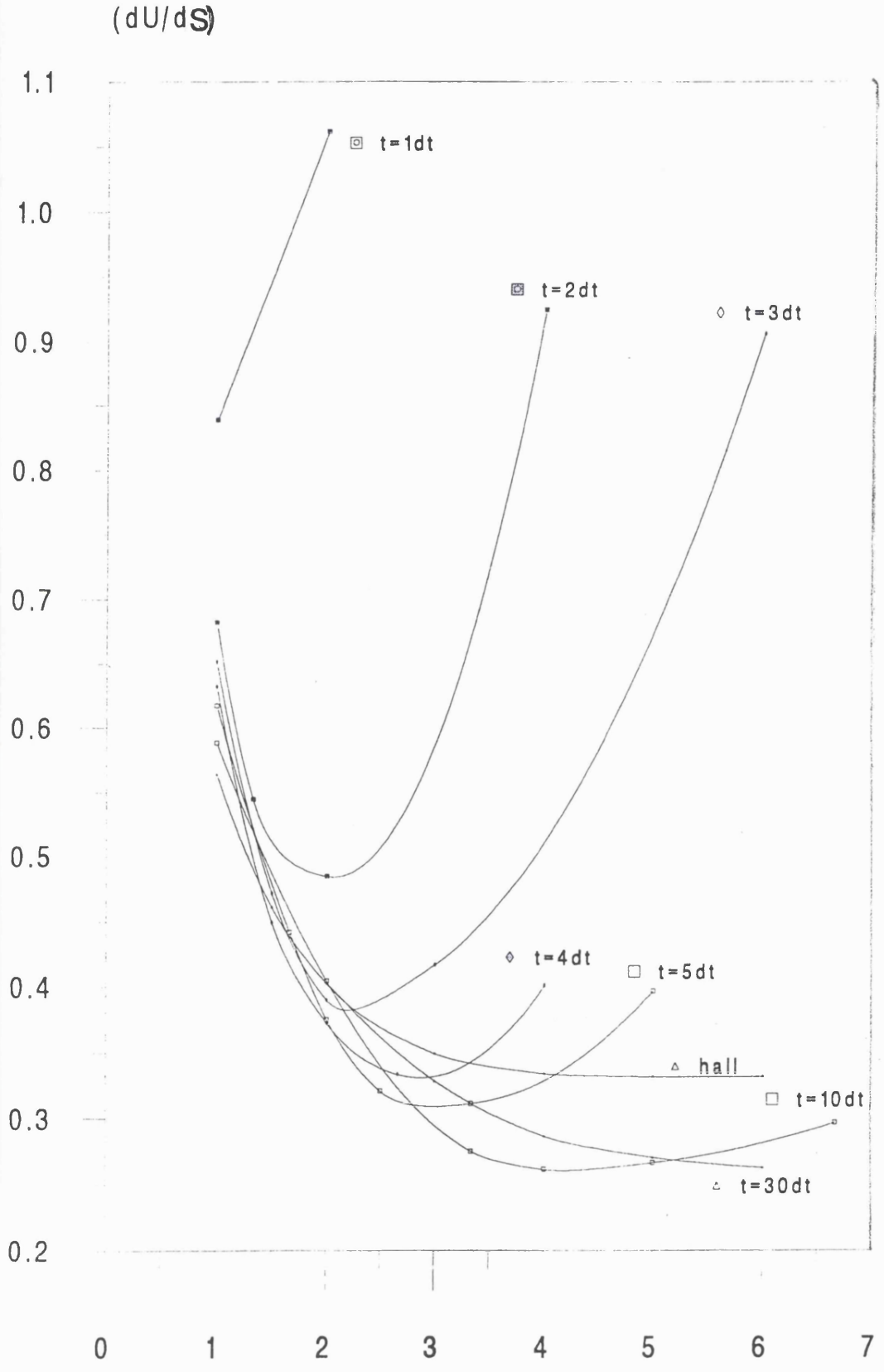


Fig. 2.3

Variation of surface shear with T.
(dx=.0005 dt=.002 dy=.02)

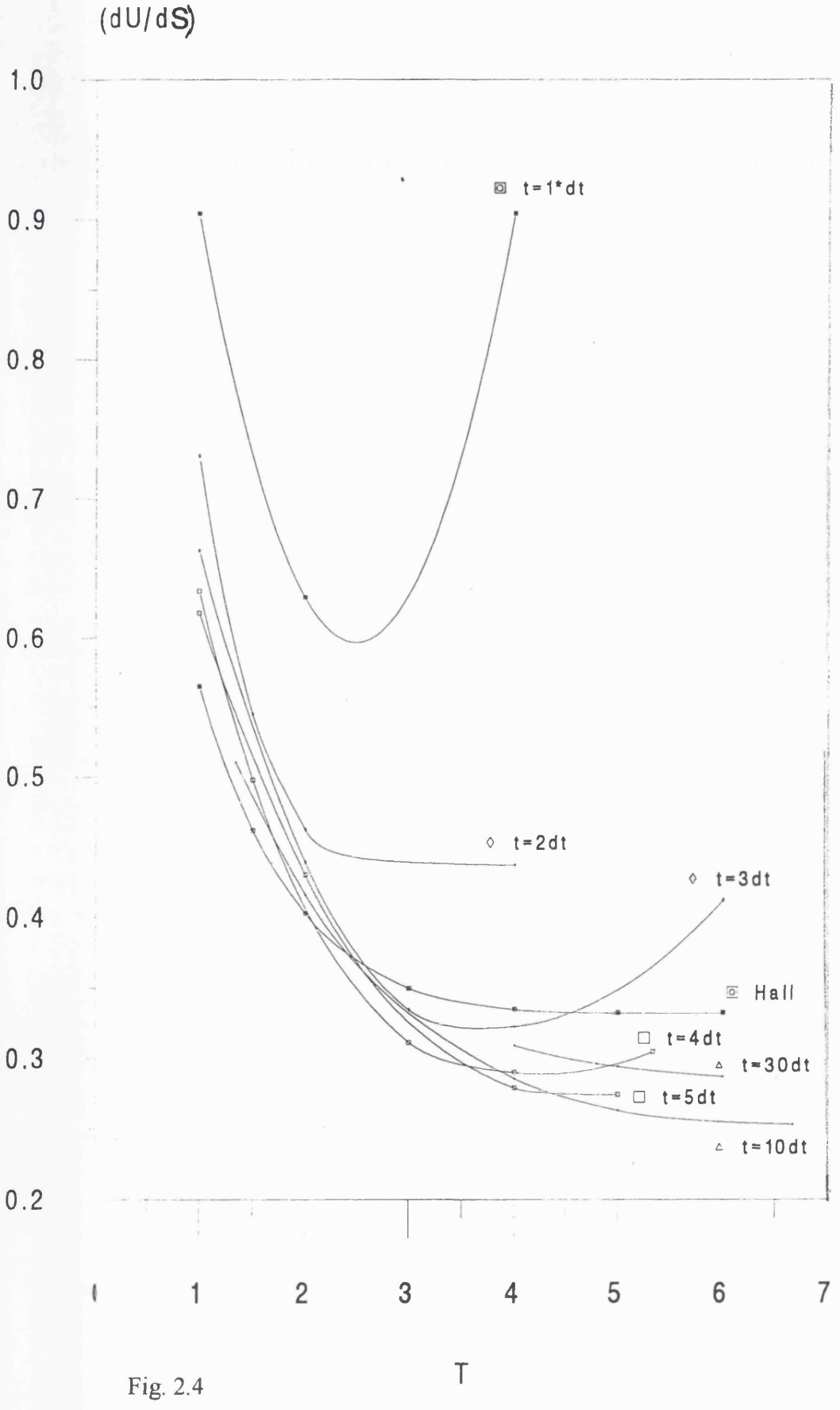


Fig. 2.4

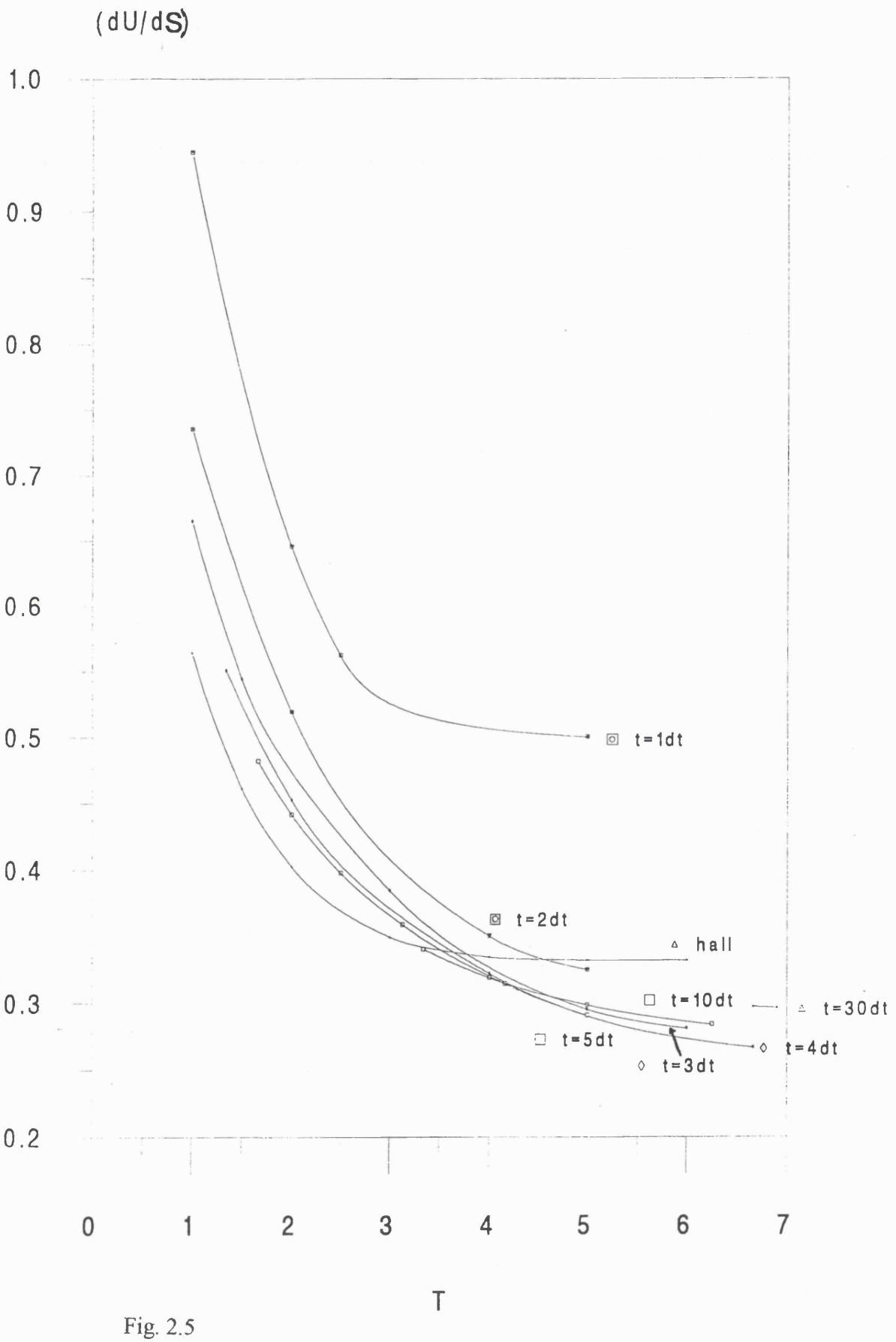
Variation of surface shear with T.
(dx=.0002 dt=.002 dy=.02)
(dU/dS)
1.0
0.9
0.8
0.7
0.6
0.5
0.4
0.3
0.2
0
1
2
3
4
5
6
7
T
t=1dt
t=2dt
hall
t=10dt
t=30dt
t=5dt
t=4dt
t=3dt

Fig. 2.5

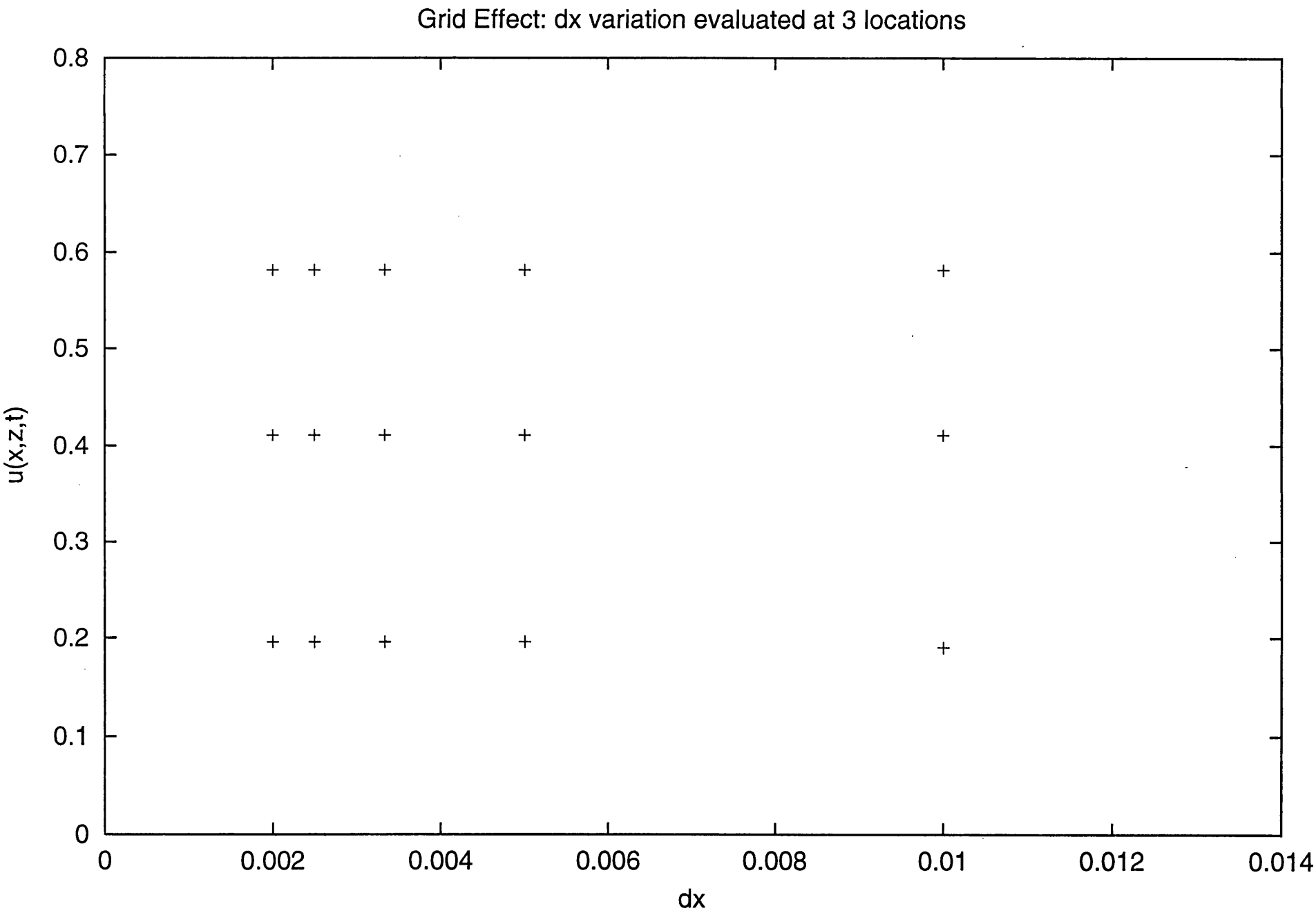
Grid Effect: dx variation evaluated at 3 locations
u(x,z,t)
dx
0.8
0.7
0.6
0.5
0.4
0.3
0.2
0.1
0
0
0.002
0.004
0.006
0.008
0.01
0.012
0.014

Fig. 2.7

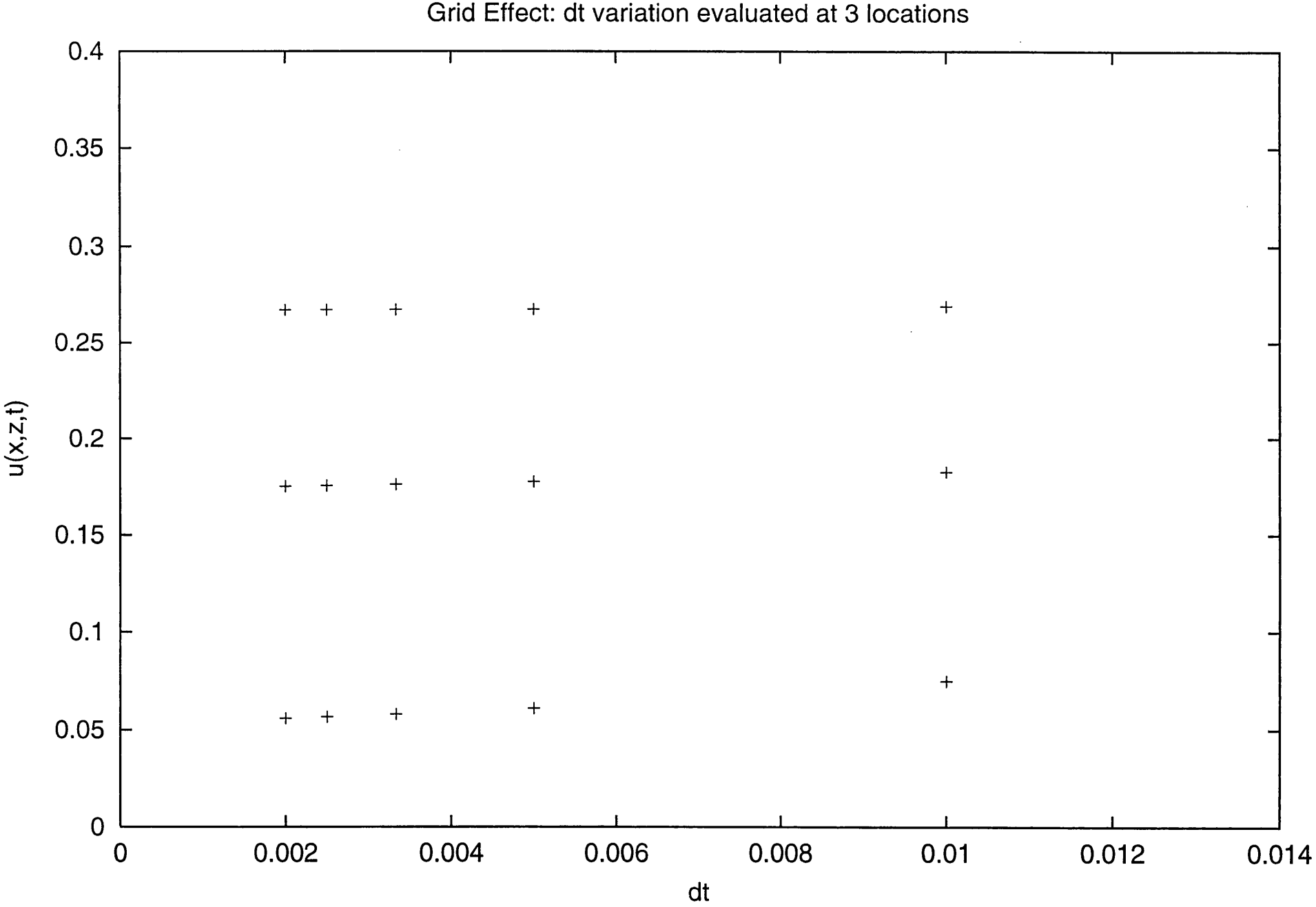
Grid Effect: dt variation evaluated at 3 locations
u(x,z,t)
dt
0.4
0.35
0.3
0.25
0.2
0.15
0.1
0.05
0
0
0.002
0.004
0.006
0.008
0.01
0.012
0.014

Fig. 2.8

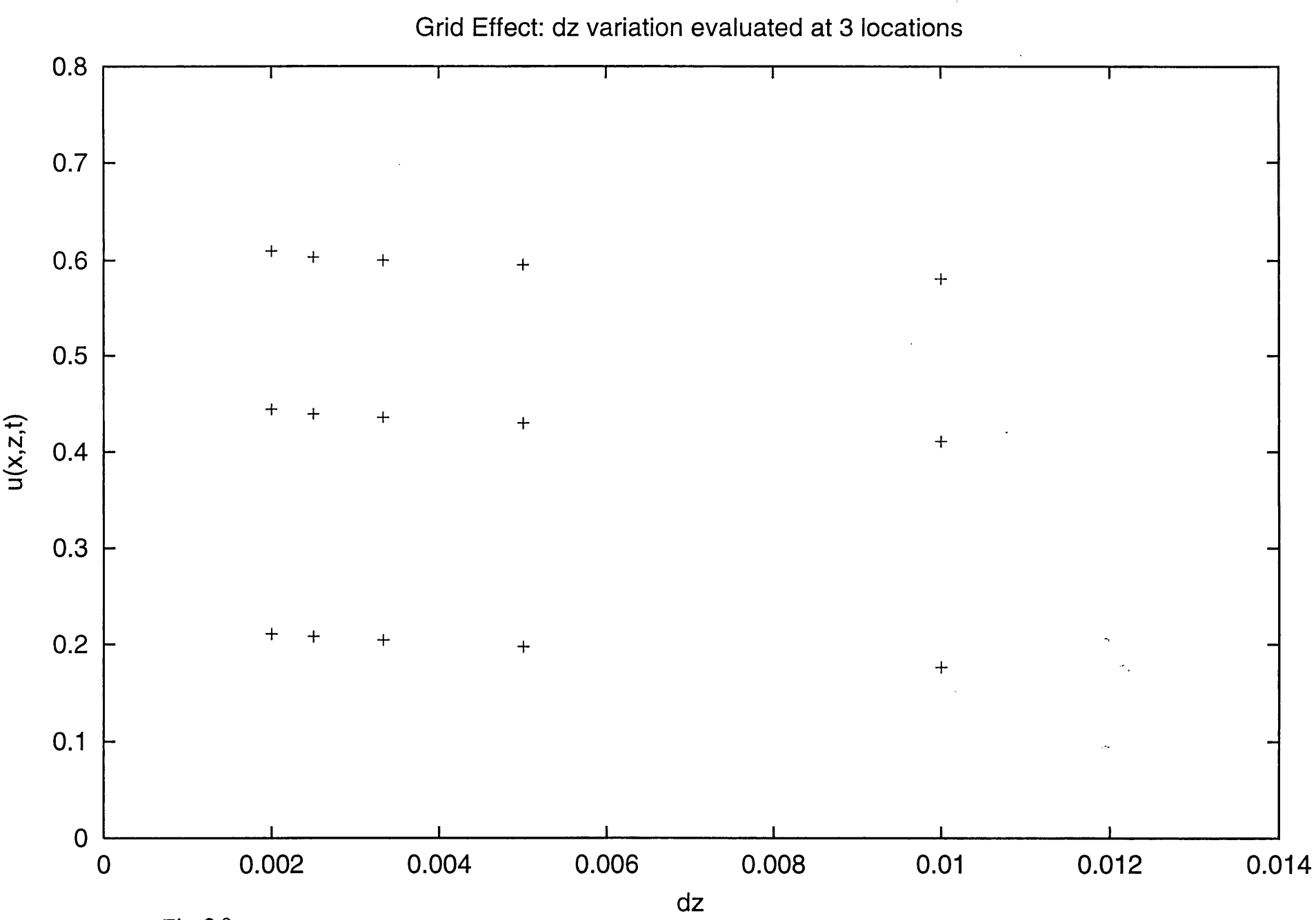
Grid Effect: dz variation evaluated at 3 locations
u(x,z,t)
dz
0
0.1
0.2
0.3
0.4
0.5
0.6
0.7
0.8
0
0.002
0.004
0.006
0.008
0.01
0.012
0.014

Fig. 2.9

# LEADING EDGE X=2DX FOR DIFFERENT VALUES OF K

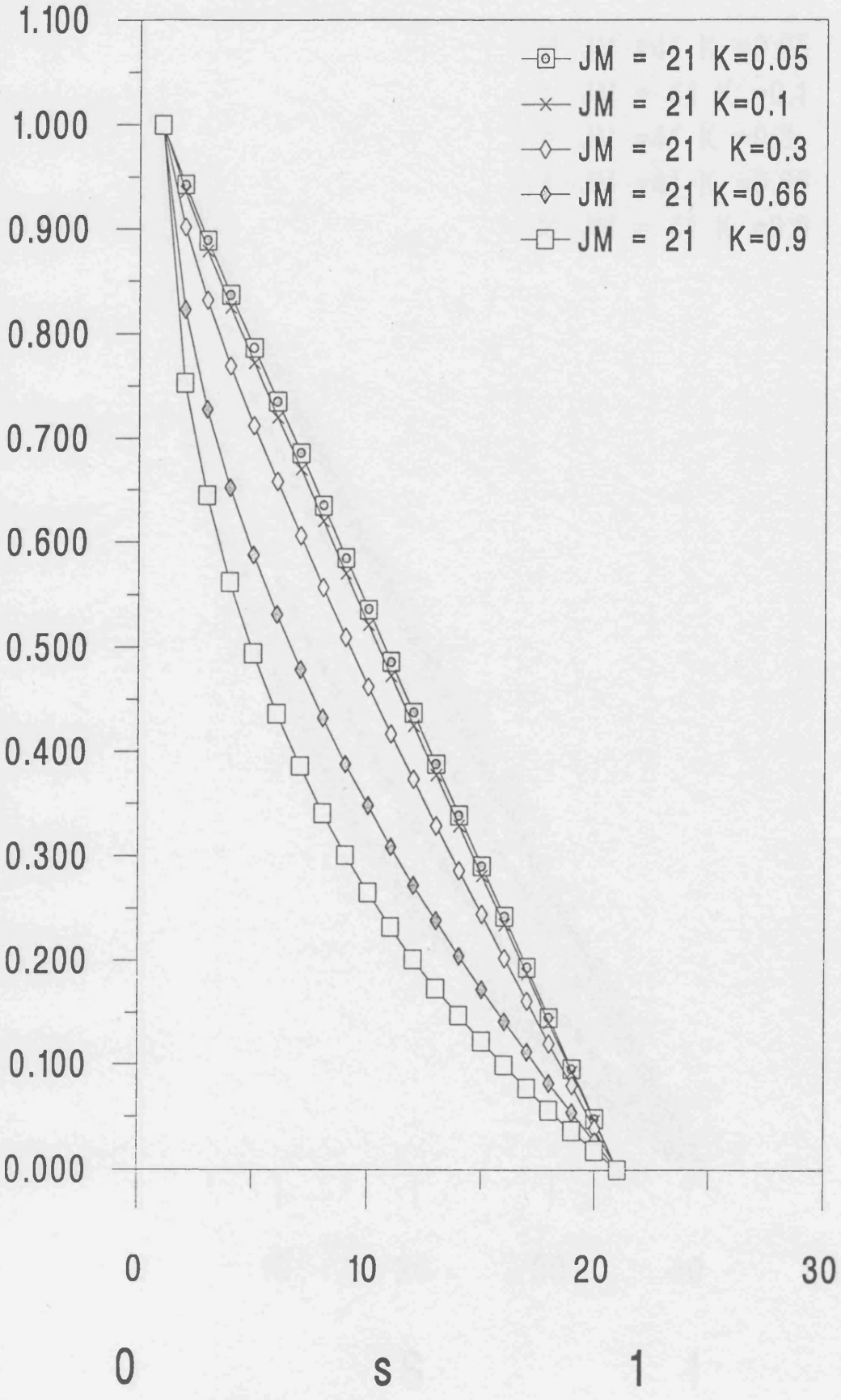


Fig. 2.10

14-1-1997

# LEADING EDGE X=2DX FOR DIFFERENT VALUES OF K

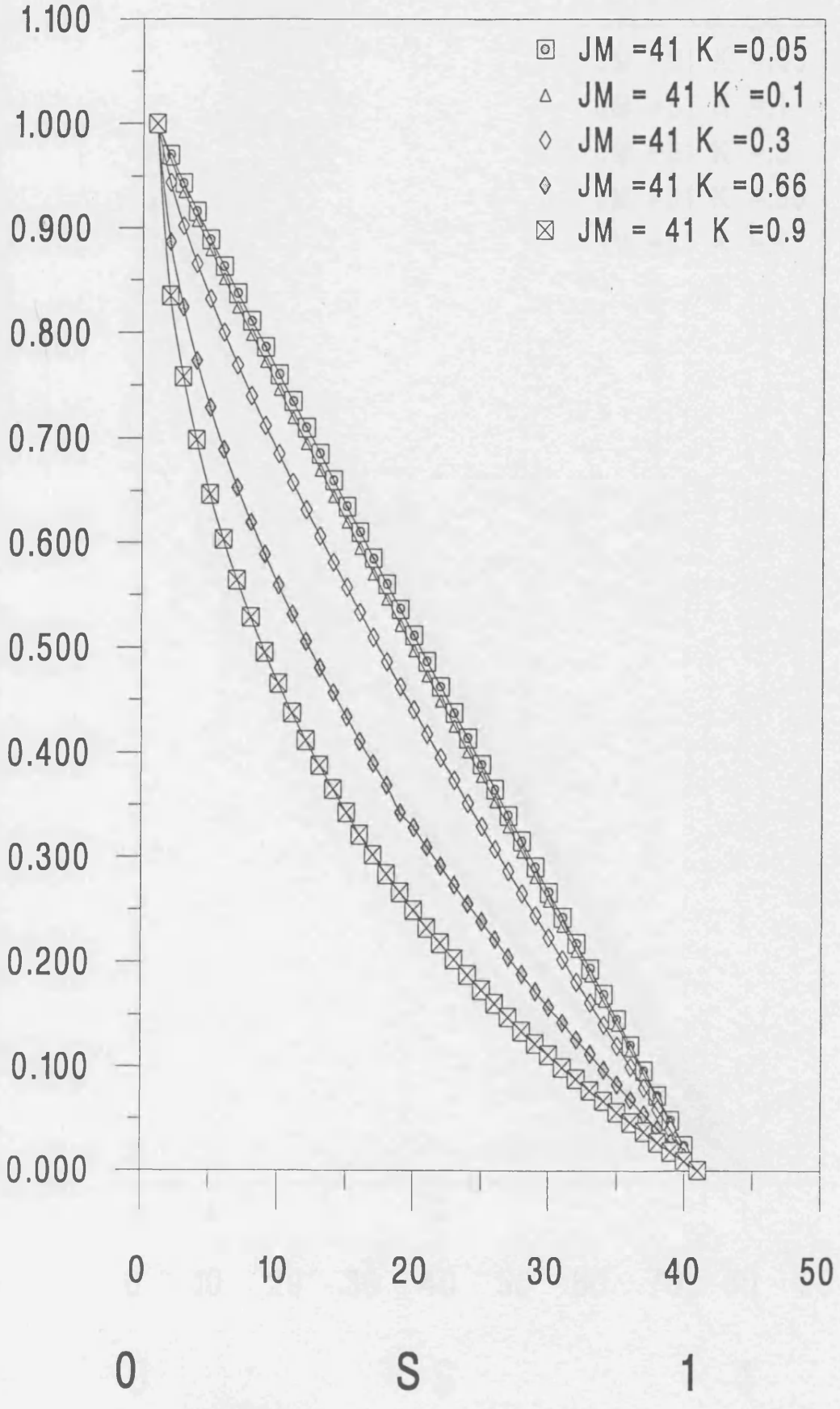


Fig. 2.11

14-1-1997

# LEADING EDGE X=2DX FOR DIFFERENT VALUES OF K

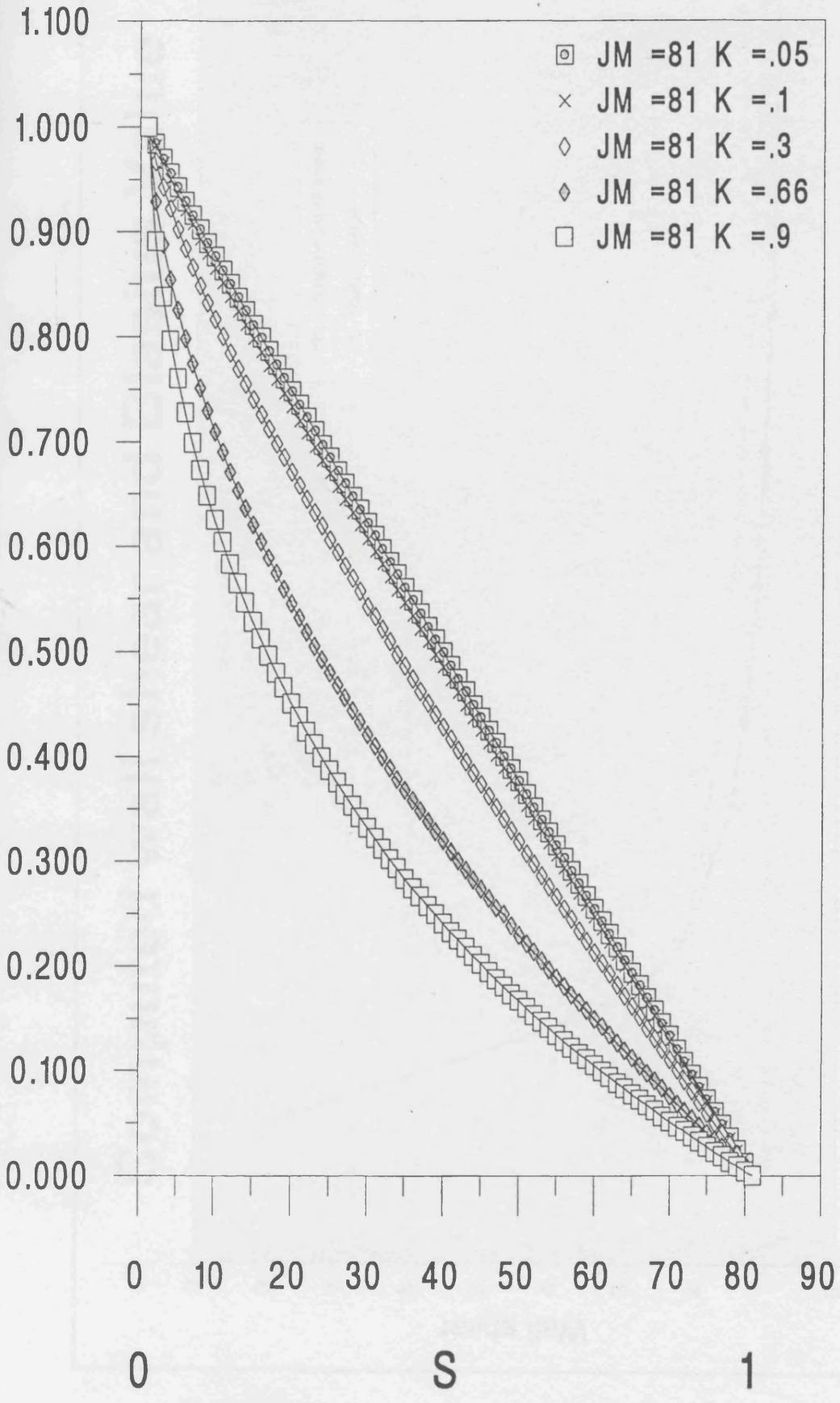


Fig. 2.12

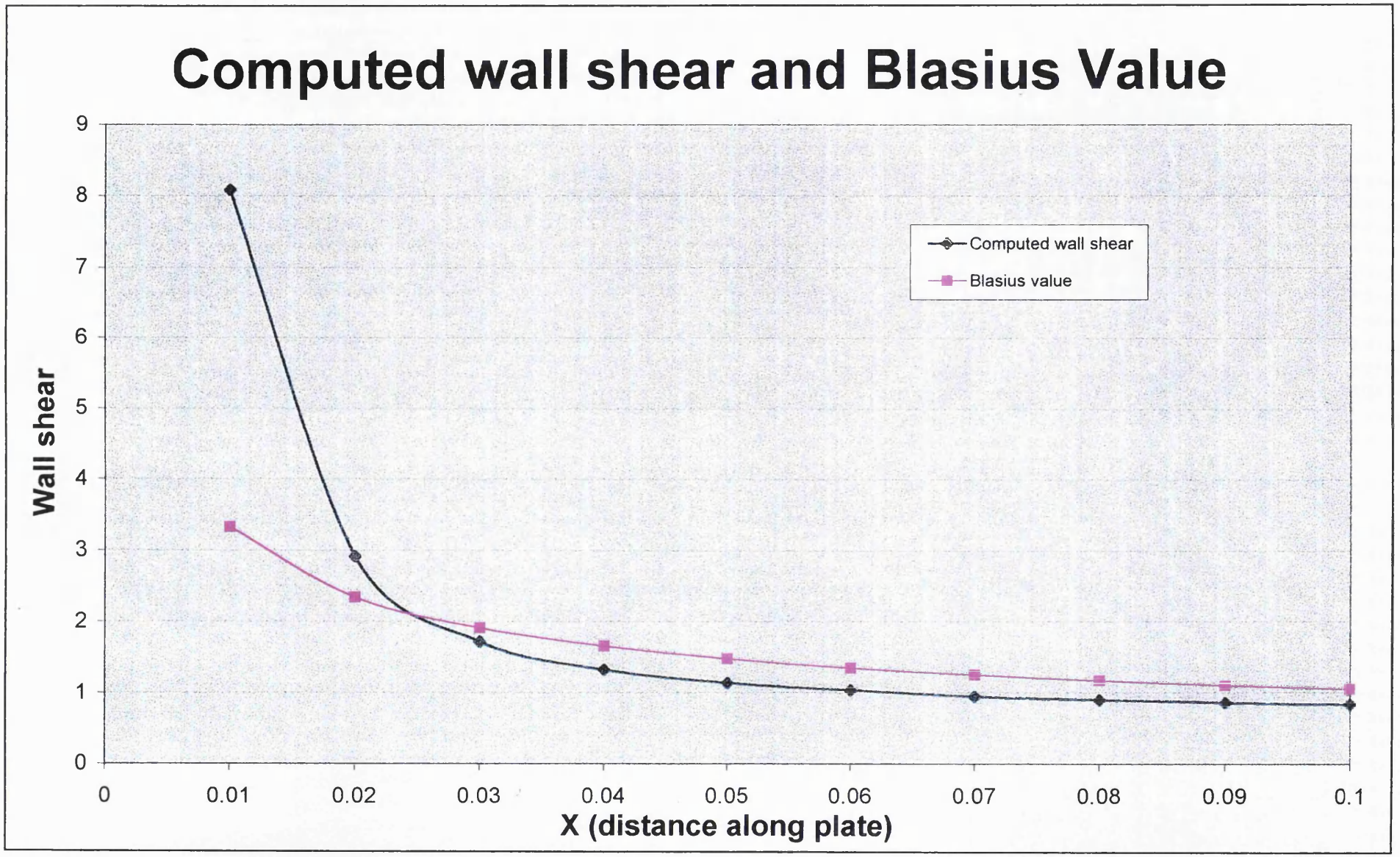
Computed wall shear and Blasius Value
Wall shear
X (distance along plate)
Computed wall shear
Blasius value
0
1
2
3
4
5
6
7
8
9
0
0.01
0.02
0.03
0.04
0.05
0.06
0.07
0.08
0.09
0.1

Fig. 2.13

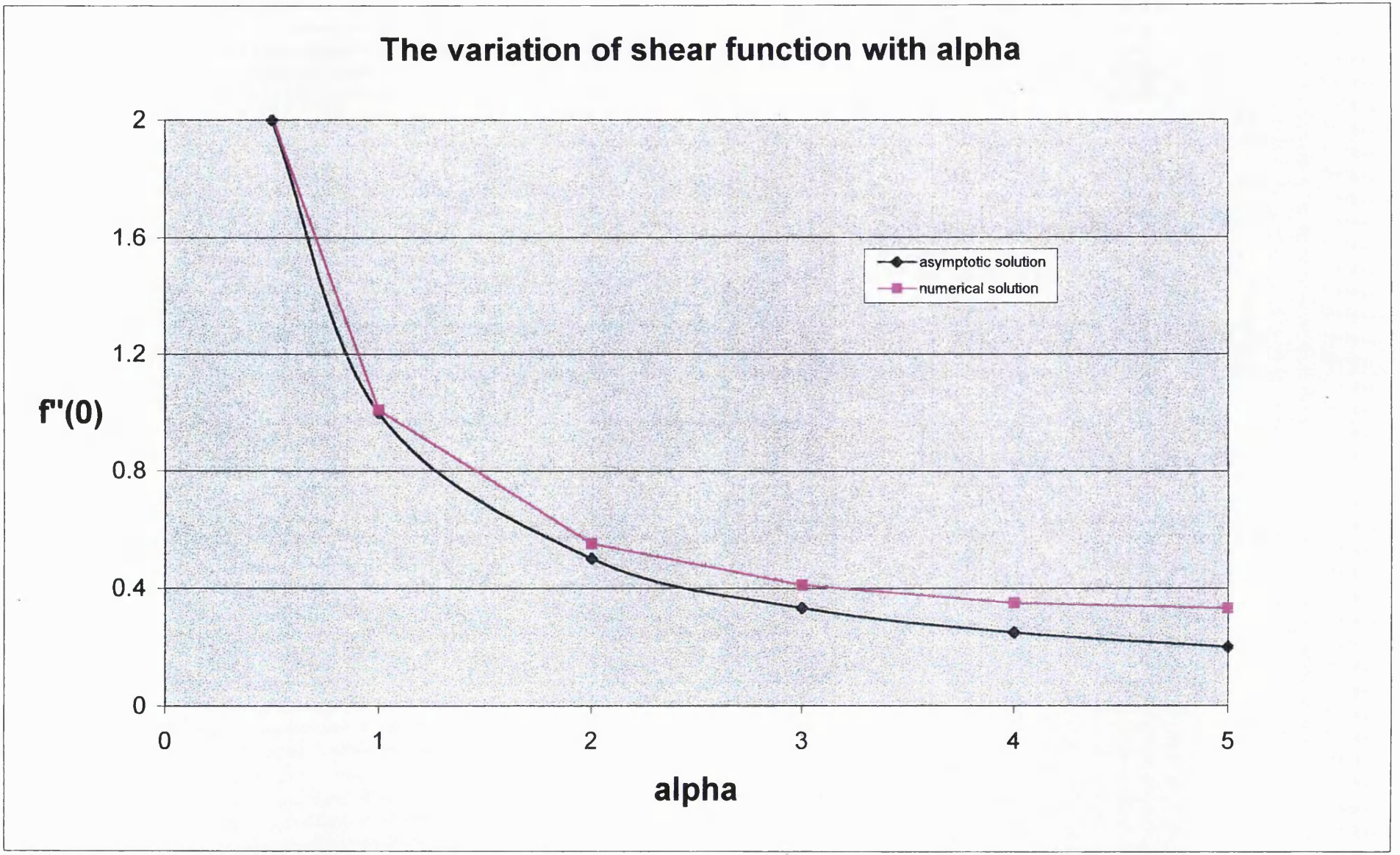
The variation of shear function with alpha
f''(0)
alpha
asymptotic solution
numerical solution
2
1.6
1.2
0.8
0.4
0
0
1
2
3
4
5

Fig. 2.14

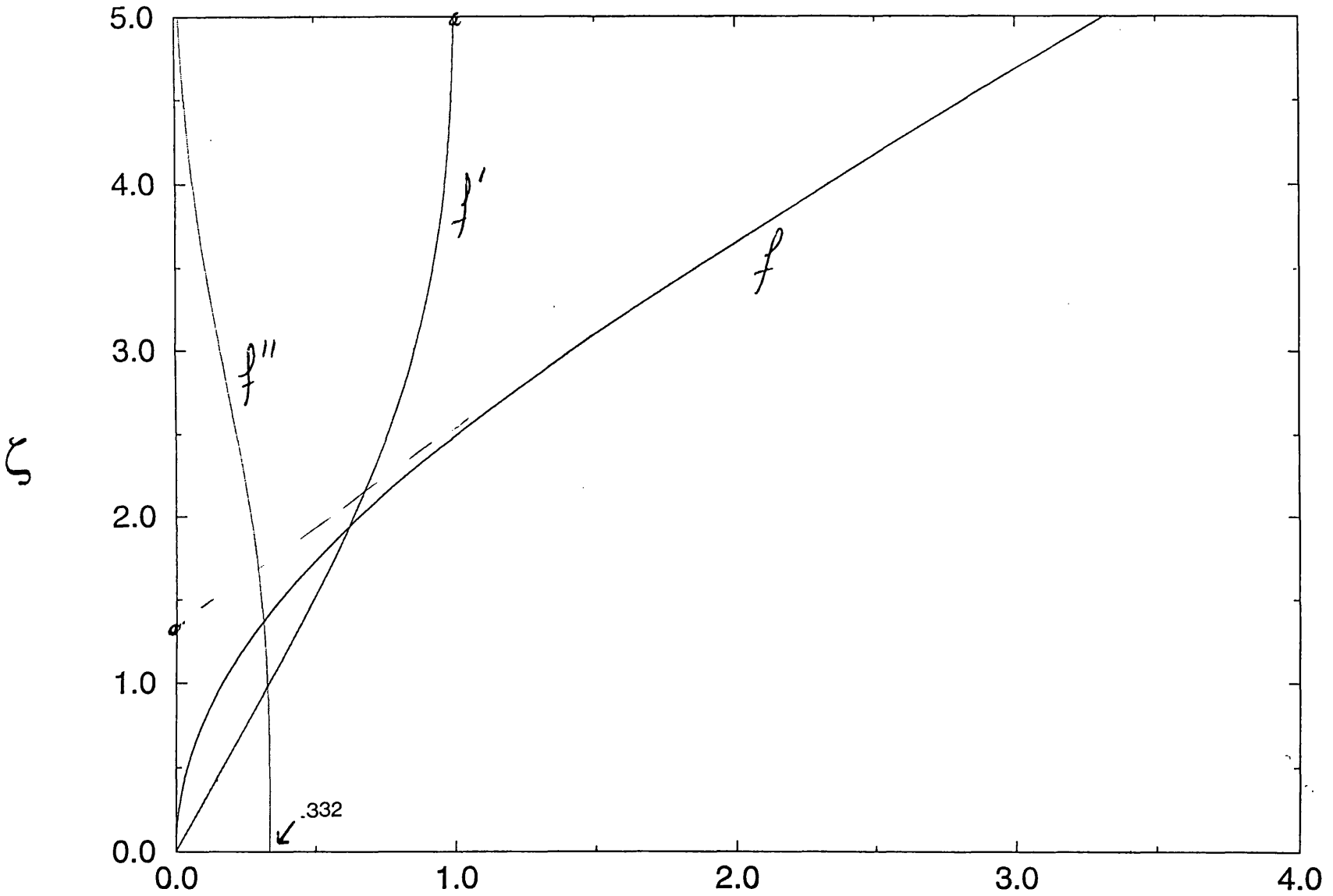


Fig. 2.15 Variation with $\zeta$, for a values of $\alpha$=5, of $f''$ (the shear function), $f'$ (the velocity function) and $f$ (the stream function).

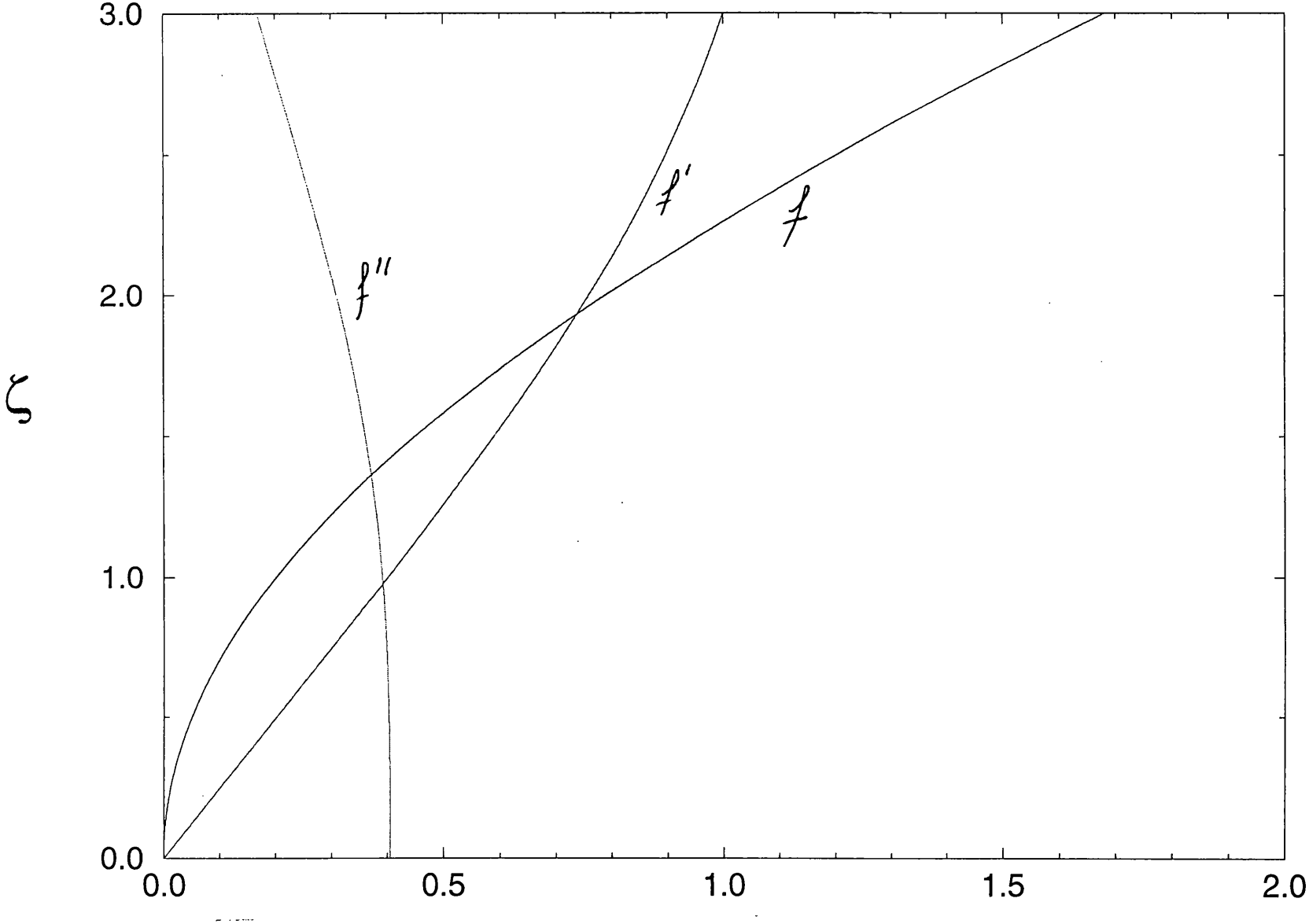


Fig. 2.16 Variation with $\zeta$, for a values of $\alpha$=3, of $f''$ (the shear function), $f'$ (the velocity function) and $f$ (the stream function).

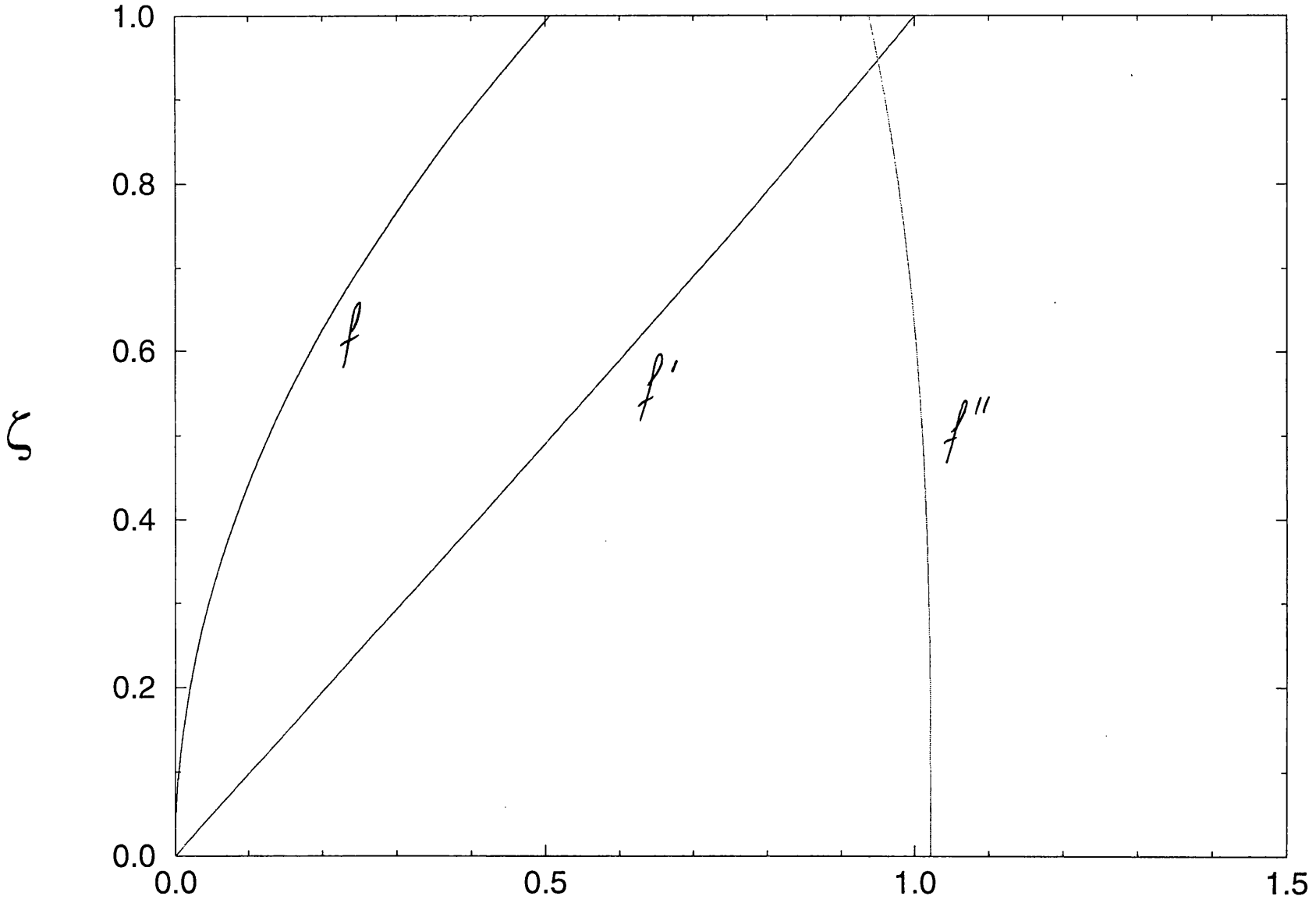


Fig. 2.17 Variation with $\zeta$, for a values of $\alpha$=1, of $f''$ (the shear function), $f'$ (the velocity function) and $f$ (the stream function).

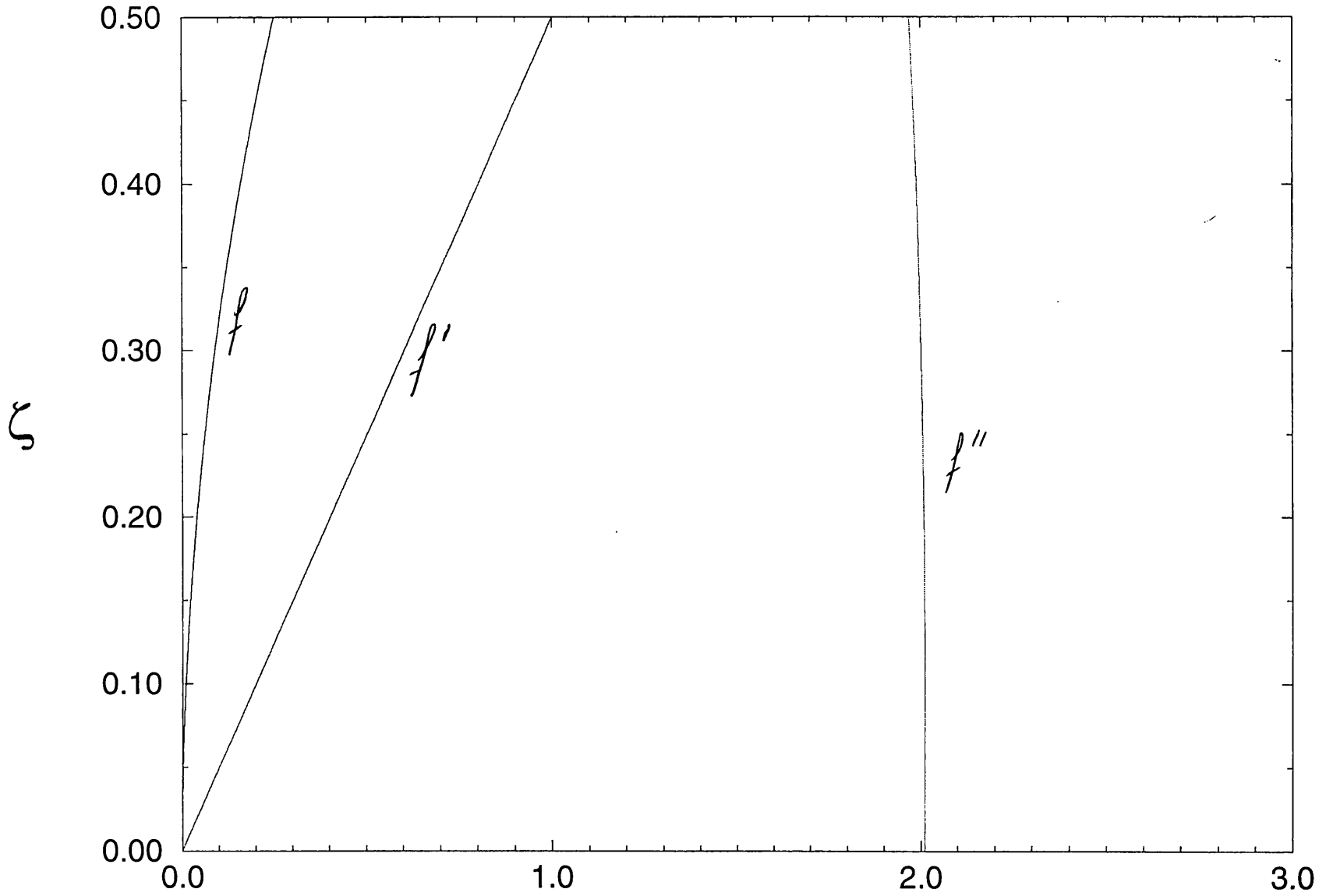


Fig. 2.18 Variation with $\zeta$, for a values of $\alpha$=0.5, of $f''$ (the shear function), $f'$ (the velocity function) and $f$ (the stream function).

# CHAPTER 3

## The trailing edge and the wake for the unsteady flat plate problem

### 3.1 Introduction

In this section, we study the flow field in the wake region at high Reynolds numbers *Re*. Wakes are common occurrences in flow around and adjacent to various geometric boundaries and are significant in many physical situations. Generally, these flows are unstable in reality and thus it is important to obtain a clear understanding of the mathematical nature of the flow field that constitutes the wake involved. The main problem considered is that of an infinitely thin aligned flat plate travelling with uniform speed in a viscous incompressible fluid, after an impulsive start at time $t = 0$. We then proceed to calculate the flow velocities at successive wake stations, which are obtained as solutions of the unsteady wake boundary-layer equations. The numerical results generated in earlier work on steady wakes indicate fairly good agreement with the asymptotic theory and some experimental work (see Papageorgiou and Smith 1989).

Due to the inherent scales, the wake region is ideally suited to numerical analysis based on the boundary-layer equations as in chapter 2, which is the approach that will be undertaken in the current chapter.

Throughout this chapter, the origin of the Cartesian coordinate system is again fixed at the leading edge and the Reynolds number is assumed to be asymptotically large. Also $u$, $v$, $p$ are the scaled component velocities in the $x$- and $y$- directions, and the scaled pressure, respectively, and $\Psi$ is taken to be the scaled stream function for the two-dimensional flow.

### 3.2 Trailing edge and wake solution

When the fluid leaves the trailing edge, the laminar boundary layers from either side of the plate merge and are accelerated to form a thin wake. The thickness of the wake

is of order $Re^{-1/2}$ and the motion is governed by the unsteady two-dimensional boundary–layer equations. The velocity $u$ in the $x$-direction is symmetric in profile about the wake centerline ($y = 0$) and thus has zero $y$-derivative at $y = 0$.

In chapter 2 we investigated the governing equations of the unsteady two-dimensional boundary layer for a uniform free stream. In non-dimensional variables these may be written as equations (2.1) and (2.2). The solution provided there was for every $x$-station in the domain of the flat plate.

In this section, we investigate the trailing edge and wake problem using equations (2.1) and (2.2). For times $t < 1$ (where the 'endplate' value of $x$ is unity), the $u$-profile entering the wake from the boundary layer is the Rayleigh solution, with zero $v$, both above and below the centreline $y = 0$. Hence in the wake, in numerical terms, we have

$$\left(\frac{u-1}{\Delta t}\right)+\overline{u}\left(\frac{u-\overline{u}}{\Delta x}\right)+0\cdot u_y = u_{yy}, \qquad (3.1)$$

where $\overline{u} = (1-e^{-Qy})$ is the numerical Rayleigh solution, in which $Q^2 = \left(\frac{1}{\Delta t}+\frac{1}{\Delta x}\right)$.

Here the partial differential equation (3.1) holds only in the immediate wake and is hyperbolic, since $u$ is a function of $x$, $y$ and $t$. The near-wake scaling for the original differential equations as well as the difference equations, at small times $t$, is $u \sim 1$, $\Psi \sim t^{1/2}$, $y \sim t^{1/2}$, $(x-1) \sim t$, (where the 'endplate' value of $x$ is 1), and strictly a similarity form applies similar to that in the unsteady upstream boundary layer (Stewartson, Hall) and to the Goldstein form for the near wake. The similarity form for this region of unsteady flow suffers from the same difficulty as that mentioned in chapter 2 for the unsteady flow on the plate, however, namely its effectively elliptic character due to the expanding coordinates locally. So we discard the (direct) similarity approach. Another reason for doing this is the question of flexibility, again as in chapter 2. Later in this section we describe the results obtained from marching forward in $x$ at all times $t > 0$ from the near wake to the $x$-station where the uniform stream $u = 1$ is attained. This is at $x = 1+t$.

If we introduce a new function $s$, which is equal to the exponential function $e^{-\tilde{Q}y}$, equation (3.1) implies the differential equation

$$\tilde{Q}^2 \frac{d^2u}{ds^2} s^2 + \tilde{Q}^2 \frac{du}{ds} s - (Q^2 - bs)u = 0, \qquad (3.2)$$

where $\tilde{Q} = \frac{1}{\Delta t}$ and $b = \frac{1}{\Delta x}$.

Given the complexity of equation (3.2), the problem is considered from a numerical point of view using Gaussian elimination for the flow velocities as described below.

### 3.2.1 Solution by Gaussian Elimination.

For every $x$-station in the wake, the flow below the plate influences the flow from above and vice versa, due to the absence of the solid boundary. Thus the two flows converge in a symmetric manner into a single flow as shown in figure 3.1, and (2.1), (2.2) have to be solved numerically again.

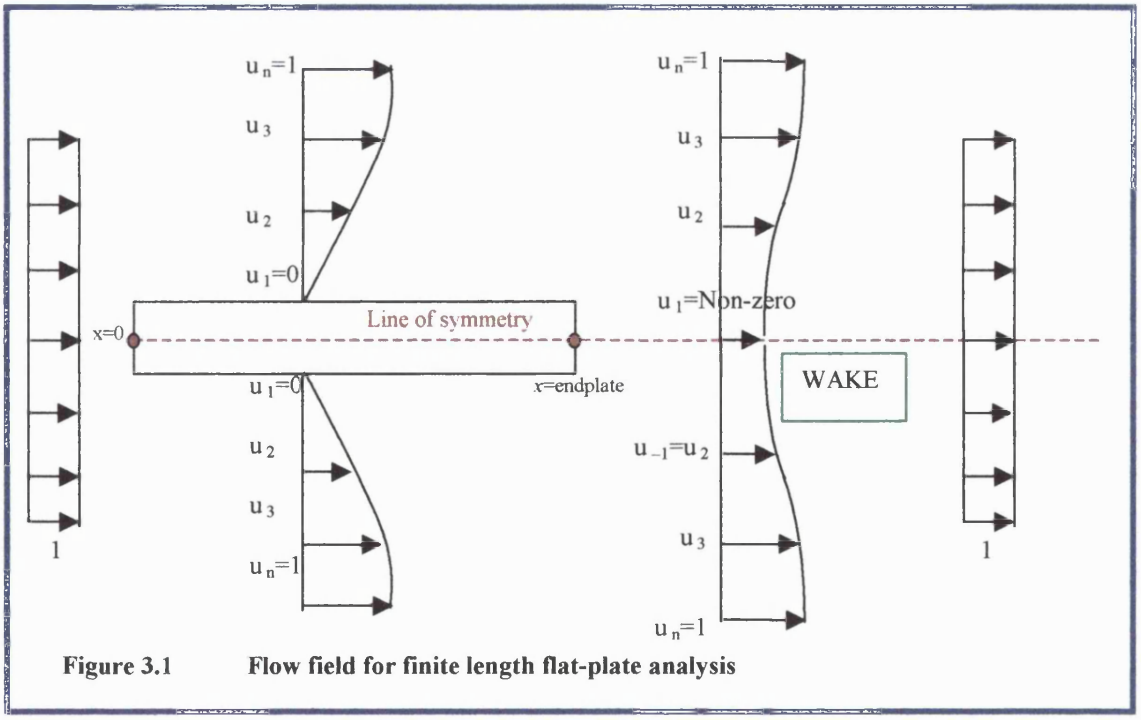


**Figure 3.1** **Flow field for finite length flat-plate analysis**

The flow problem remains symmetric and in the wake the centreline velocity, $u_1$, assumes a finite numerical value. The equation along the wake centreline is now different to that for the plate region in that it relates the $u_j$ velocities $u_2$, $u_1$ and $u_0$ to each other, where $u_0$ is the same as $u_2$ due to symmetry. Thus for the wake centreline where $j$=1, we have

$$(a_1 + c_1)\cdot u(i,j,k) + b_1 \cdot u(i,j-1,k) = d_1 \ . \qquad (3.3)$$

That is in terms of (2.18) and (2.19), for a given value of the $x$-station counter $i$ which is greater than the endplate value, and time counter $k$, we again apply Gaussian elimination. The general form of the system of $n$ equations, which incorporates the boundary condition for the far-field flow, is given as

$$\begin{bmatrix} b_1 & (a_1+c_1) & 0 & 0 & \cdots & 0 \\ c_2 & b_2 & a_2 & 0 & \cdots & 0 \\ 0 & c_3 & b_3 & a_3 & \cdots & 0 \\ \vdots & \vdots & \vdots & \vdots & & \vdots \\ 0 & 0 & 0 & c_{n-1} & b_{n-1} & a_{n-1} \\ 0 & 0 & 0 & 0 & 0 & 1 \end{bmatrix} \begin{bmatrix} u_1 \\ u_2 \\ u_3 \\ \vdots \\ u_{n-1} \\ u_n \end{bmatrix} = \begin{bmatrix} d_1 \\ d_2 \\ d_3 \\ \vdots \\ d_{n-1} \\ 1 \end{bmatrix} \qquad (3.4)$$

Thus we have the augmented matrix after the various row transformations as

$$\left[\begin{array}{cccccc|c} \mu_1 & a_1' & 0 & 0 & \cdots & 0 & \pi_1 \\ 0 & \mu_2 & a_2 & 0 & \cdots & 0 & \pi_2 \\ 0 & 0 & \mu_3 & a_3 & \cdots & 0 & \pi_3 \\ \vdots & \vdots & \vdots & \vdots & & \vdots & \vdots \\ 0 & 0 & 0 & 0 & \mu_{n-1} & a_{n-1} & \pi_{n-1} \\ 0 & 0 & 0 & 0 & 0 & 1 & 1 \end{array}\right] \qquad (3.5)$$

where $\mu_j = b_j - (a_{j-1}\, c_j / \mu_{j-1})$

$\pi_j = d_j - (\pi_{j-1}\, c_j / \mu_{j-1})$

We note that $\pi_1 = d_1$, $\mu_1 = b_1$ and also $a_1' = (a_1 + c_1)$.

Hence the velocity for a given value of $j$ is again given by $u_j = (\pi_j - a_j u_{j+1}) / \mu_j$.

### 3.3 Numerical solution and discussion

Program 3.1 to evaluate the $u$ component of velocity at stations $x$ downstream of the trailing edge as well as on the plate itself is almost identical to program 2.1. The only difference is that the step consisting of the evaluation of the coefficients for the local equation systems (for each row $j$) has two alternative sets of equations; one for the flat plate region and the other for the wake region. The program is given at the end of this chapter.

Figures 3.2-3.5 show the wake values of $u$ along the central axis of symmetry, $u_{CENTRELINE}$, plotted against $x$-station. Here the flat plate is of unit length (i.e. the value of the variable *endplate* in the program is 1). The profiles for $u_{CENTRELINE}$ are presented for selected values of time $t$, showing how they develop over time. In the figures, the profiles are labelled with the associated time step number. The initial profile is a step function, as required, since the wake has not started to develop then and the velocity virtually everywhere is unity. As time increases, the values of the wake velocity reduce in a nonlinear fashion with respect to time, converging towards a finite steady state variation for very large times. The grids employed in the analysis had values of $\Delta x = 0.016\text{-}0.008\text{-}0.004$, $\Delta y = 0.08\text{-}0.04\text{-}0.02$ and $\Delta t = 0.008\text{-}0.004\text{-}0.002$.

Close agreement is observed between our wake results at large $t$ and those predicted by the steady state solution of Papageorgiou and Smith (1989)'s figure 4. The streamwise variation of the centreline velocity in the wake is represented from their steady-flow calculation for comparison.

Figure 3.6 show the variation of $u_{CENTRELINE}$ with time $t$, at a given value of $x$=1.04 in the wake, a location immediately downstream of the trailing edge. The general trend is asymptotic to a steady-state value of approximately $u$=0.25. In figure 3.7, the $u$ values with time are given for various heights $y$ above the centreline, and convergence to the external far-field flow is observed for heights above the $y$=3 level which agrees

favourably with the conclusion of Papageorgiou & Smith (1989). The variation of $u$ with $y$ for the first $x$-station (at a distance of $x$=0.016) is given in figure 3.8, for various values of time. It was found that the results agreed with the Blasius solution.

Grid refinement was performed, as before, for each of the coordinate directions and time. The refinement was again performed using unequal interval sizes for efficiency. The velocity computed was monitored at three given locations in the region of the wake whose positions were fixed. Refinement with respect to $x$, $y$ and $t$ yielded negligible changes in the values of $u$, as shown in figures 3.9-3.11. This again tends to demonstrate numerically converged solutions.

### 3.4 The scaled displacement and skin friction

As far as we know, the present study provides the first computational solution for the unsteady flat plate problem including its wake. A subsequent study is made by Li (2000), however, and there is a perhaps mildly relevant paper by Phillips (1996) but in the unusual context of motion past a plate whose length varies in a specific way with time.

This similarity problem is itself quite difficult to solve numerically because of a reversal in direction of the parabolicity involved and its is quite problem-specific. We choose instead to use a flexible computational method based on time-marching using the form,

$$\delta(i) = \delta(i-1) + \left( \frac{\Delta x}{2} \left( v(i,j,k) + v(i-1,j,k) \right) \right). \qquad (3.6)$$

Thus program 3.1 was modified accordingly for the above case, investigates the numerical response for two grid sizes. The first one is for $\Delta x$=0.016, $\Delta t$=0.008 and $\Delta y$=0.08, and the second computation is for half these increment sizes. Profiles of $\delta$ against $x$ are given in figures 3.12-13 for times ranging between $t$=0.024 and $t$=4.16, and for a given value of $y$=6.4. For the displacement, agreement is found to be closer with the analytical solution for the computation performed using the finer grid. There is also observed to be a small kink in the Blasius solution for very small times, which

seems to be an anomaly of the approach. The boundary layer and wake displacement functions are given in figures 3.14-16 for values of time in the range 0.2-1 for use in part B of the thesis. These results are in good agreement with the numerical predictions according to the approach of Li (2000) (a quite different approach based on second order differencing as in the Crank-Nicholson method), which have been computed for the same values of time and are shown for comparison in figures 3.17 and 3.18. This provides an encouraging verification of our results which have been produced using the existing time-marching method.

The structure of the program to evaluate now, the skin friction quantity, *ss*, along the plate is the same as for program 3.1, but now with the evaluation of *ss* at the end. The relation for the skin friction is given by

$$ss = \left(\frac{\partial u}{\partial y}\right)_{y=0}. \tag{3.7}$$

From the profiles for skin friction against $x$, (figure 3.19), for various values of time, (figure 3.20), we observe that there is apparent convergence towards the steady-state Blasius solution, section 2.7, for larger values of time.

### 3.5 Numerical solution for modified boundary condition $u \to f(t)$

In order to make the current numerical analysis more widely applicable, program 3.1 was modified to accommodate a more general free stream condition, $u \to f(t)$ as $y \to \infty$, as given in program 3.2. This means employing new boundary conditions for the far-field and first $x$-station (the leading edge) which now incorporate the time variable implicitly. As a result, substitution of these modified boundary conditions into the local system of equations (2.20) yields modified coefficients d($j$) only. This demonstrates that the numerical approach is extremely flexible in its application to more general problems, since it may be used for any $f(t)$ in principle. For the current case, the function $f(t)$ is given by

$$f(t) = \frac{t}{1+t}. \tag{3.8}$$

The $u$ profiles against $x$ for a height $y$=0.16 close to the centreline, are given in figures 3.21-23, for the same three grid sizes as before. Following the classic Blasius-Rayleigh-like behaviour in the plate region, the wake profile function exhibits an initial increase with time followed by a movement downstream, resulting in a reduction of the function of (3.8) with increasing time. The apparent singularity at the leading edge of the plate is due to the nature of the boundary conditions defined in the program. Given the fact that virtually no noticeable difference in the solutions is observed between the three grids, it is concluded that there is probably sufficient convergence of the solutions here.

Figures 3.24-26 show the variation of $u$ versus height $y$ for the three grid sizes, with the corresponding Blasius solution also shown. For large values of time convergence with the Blasius solution (where $\eta = y/x^{1/2}$) is observed, e.g. for the $t$=8 profile. Figure 3.27 shows various $u$ profiles with time for the three grids. Closest agreement with the Blasius solution of 0.107 is observed for the finest grid.

## 3.6 Fortran 77 programs and figures

```
C     ************************************************
C     PROGRAM TO SOLVE 2-D PROBLEM FOR WAKE AREA
C        by      Dimitrios P. Papadopoulos
C
C        0CTOBER1997 - NOVEMBER 1998
C
C     ************************************************


C Define variables

        program endplate
        INTEGER i,j,k,imax,jmax,kmax,ntmax,nt
        REAL dy,dt,dx,x,f

C Define 3D storage arrays for computed values of u(i,j,k) & v(i,j,k)

        REAL  u(402,402,2),v(402,402,2)

C Define 2D coefficient array and u(j) & d(j) vectors which form the
C "local"system of equations for solution at each x-station

        REAL  coefficient(402,402),dvector(402)
        REAL  a(402),b(402),c(402),d(402),mi(402),pi(402)
        INTEGER col

C  Define end of plate variable and length of plate

        INTEGER endplate
        REAL length

C  Define increment sizes and storage-matrix dimensions

        length=1
        dx = 0.004
        dy = 0.02
        dt = 0.002
        imax = 400
        jmax = 400
        kmax = 2
        endplate =length/dx
        ntmax=1950
        nt=1

C    Set  all values of storage-matrix equal to zero

10      DO 32 k = 1,kmax,1
        DO 31 j = 1,jmax,1
        DO 30 i = 1,imax,1

          u(i,j,k) = 0.0
          v(i,j,k) = 0.0


30      CONTINUE
31      CONTINUE
32      CONTINUE

C     ************************************************
C     IMPLEMENTATION OF BOUNDARY CONDITIONS  *
C     ************************************************

35      DO 42 k = 1,kmax,1
```

3.1 Program to solve 2-D problem for wake area.

```
        DO 41 j = 1,jmax,1
        DO 40 i = 1,imax,1

C  Un-influenced flow field (before introduction of plate)
          IF (k.EQ.1)    u(i,j,k) = 1.0

C Flow field at first x-station (at leading edge of plate)
          IF (i.EQ.1)      THEN
            u(i,j,k) = 1.0
            v(i,j,k) = 0.0
          ENDIF

C Flow field at the wall (non-slip condition)
          IF ((j.EQ.1).AND.(i.LE.endplate)) THEN
            u(i,j,k) = 0.0
            v(i,j,k) = 0.0
          ENDIF
           u(1,1,k) =1.0

C  Flow field in the wake
          IF  ((j.EQ.1).AND.(i.GT.endplate))    v(i,j,k) = 0.0

C Flow field outside boundary layer region
          IF (j.EQ.jmax)   u(i,j,k) =1.0

40      CONTINUE
41      CONTINUE
42      CONTINUE


C   ***************************************************************************
C        EVALUATE U(I,J,K) + V(I,J,K) FOR EACH X-STATION (I),
C        FOR THE CURRENT TIME STEP (K).
C   ***************************************************************************

50      k = 2

        DO 90    i = 2,imax,1

C Set all terms of coefficient matrix equal to zero

        DO 69 j=1,jmax,1
         DO 68 col=1,jmax,1
          coefficient(j,col) = 0

68       CONTINUE
69      CONTINUE

C calculate values of non-zero coefficients - row by row (j)

        DO 70  j = 1,jmax,1

          IF  ((j.EQ.1).AND.(i.LE.endplate)) THEN
             dvector(j) = 0
             coefficient(j,j) = 1.0

          ENDIF

          IF (j.EQ.jmax) THEN
             dvector(j) = 1.0
             coefficient(j,j) = 1.0

          ENDIF
```

```
        IF ((j.NE.1).AND.(j.NE.jmax)) THEN

        a(j) =  (v(i-1,j,k)/(2*dy)) - (1/(dy**2))

        b(j) =   (1/dt) + (u(i-1,j,k)/dx) + (2/(dy**2))

        c(j) = (- (1/(dy**2))) - (v(i-1,j,k)/(2*dy))

        d(j) = ((1/dt) * u(i,j,k-1)) + ((u(i-1,j,k)**2) *(1/dx))

        coefficient(j,j-1) = c(j)
        coefficient(j,j) = b(j)
        coefficient(j,j+1) = a(j)
        dvector(j) = d(j)


        ENDIF

C       Calculation of U(i,j,k) on the zero-line of symmetry in the wake

        IF ((j.EQ.1).AND.(i.GT.endplate))  THEN

        a(1) = - (2/(dy**2))

        b(1) = (1/dt)+(u(i-1,1,k)/dx)+(2/(dy**2))

        d(1) = ((1/dt) * u(i,1,k-1))+((u(i-1,1,k)**2) *(1/dx))

        coefficient(1,1) = b(1)
        coefficient(1,2) = a(1)

        ENDIF

70      CONTINUE

C     ***********************************************************************
C      *  SOLVE SYSTEM OF EQUATIONS WITH GAUSSIAN ELIMINATION  *
C     ***********************************************************************

C we define values of transformed coefficients row by row (j)
C first, evaluate mi and pi for each row (j)

        IF (i.LT.endplate) THEN
        mi(1) = 1
        pi(1) = 0
        ENDIF

        IF (i.GT.endplate) THEN
        mi(1) = b(1)
        pi(1) = d(1)
        ENDIF

        DO 75   j = 2,(jmax-1),1

        mi(j) = b(j)-((c(j)*a(j-1))/mi(j-1))
        pi(j) = d(j)-((c(j)*pi(j-1))/mi(j-1))

C second,insert mi and pi for each row(j) and also c(j)=0

        coefficient(j,j-1) = 0
        coefficient(j,j) = mi(j)
        dvector(j) = pi(j)

75      CONTINUE
```

```
C solve for u(j) by back substitution

        DO 80  j = (jmax-1),2,-1

        u(i,j,k)= (pi(j)-(a(j)*u(i,j+1,k)))/mi(j)


80      CONTINUE

         u(i,1,k) = 0
        IF (i.GT.endplate) THEN
        u(i,1,k) = (pi(1) - (a(1)*u(i,2,k)))/mi(1)
        ENDIF

C    calculate v(j) not on centre line where it is zero

        v(i,1,k) = 0
        DO 85  j=2,jmax,1

        f =-((dy / (2*dx))*(u(i,j,k)-u(i-1,j,k)+u(i,j-1,k)-u(i-1,j-1,k)))

        v(i,j,k) = (v(i,j-1,k)) + f

85       CONTINUE

90       CONTINUE


C     ***********************************************************************
C     COPY RESULTS IN ARRAY FOR CURRENT TIME STEP AND OUTPUT RESULTS  *
C     ***********************************************************************

C       Copy results from current k value to previous k value

        do 1060 i=1,imax,1
        do 1050 j=1,jmax,1
        u(i,j,1)=u(i,j,2)
        v(i,j,1)=v(i,j,2)
1050    continue
1060    continue


C       Output u(i,j,k) results for all time (k) values for a given j height
C       above plate, at a fixed x-distance in the wake region.

        i=260
        j=31

        WRITE (6,*) nt, u(i,j,2)

C       Output u(i,j,k) & v(i,j,k)  results for symmetric y=0 line in wake
C       region, for a given value of k.

        if ((nt.eq.3).or.(nt.eq.20).or.(nt.eq.220).or.(nt.eq.520)) then

        WRITE (6,*) 'Wake profile results'
        WRITE (6,*) ''

        do i=200,imax,1
        x=dx*(i-1)
        WRITE (6,*) x, u(i,j,2)
        enddo
```

```
            WRITE (6,*) ''
            endif

C           Return to beginning for solution of next time step k

            nt=nt+1
            if (nt.le.ntmax) go to 50


2000        end
```

```
C     ***************************************************
C     PROGRAM TO SOLVE 2-D PROBLEM FOR PLATE & WAKE AREA
C        IN OTHER BOUNDARY CONDITIONS.
C
C        by      Dimitrios P. Papadopoulos
C
C         NOVEMBER 1998
C
C     ***************************************************


C Define variables

        program alteration
        INTEGER i,j,k,imax,jmax,kmax,ntmax,nt
        REAL  dy,dt,dx,x,f

C Define 3D storage arrays for computed values of u(i,j,k) & v(i,j,k)

        REAL  u(202,202,2),v(202,202,2)

C Define 2D coefficient array and u(j) & d(j) vectors which form the"local"
C   system of equations for solution at each x-station

        REAL  coefficient(202,202),dvector(202)
        REAL  a(202),b(202),c(202),d(202),mi(202),pi(202)
        INTEGER col

C  Define end of plate variable and length of plate

        INTEGER endplate
        REAL length

C - Define increment sizes and storage-matrix dimensions

        length=1
        dx = 0.016
        dy = 0.08
        dt = 0.008
        imax = 101
        jmax = 101
        kmax = 2
        endplate =length/dx
        ntmax=2101
        nt=1

C    Set  all values of storage-matrix equal to zero

10      k = 1
        DO 31 j = 1,jmax,1
        DO 30 i = 1,imax,1

          u(i,j,k) = 0.0
          v(i,j,k) = 0.0


30      CONTINUE
31      CONTINUE

C     ***************************************************
C     IMPLEMENTATION OF BOUNDARY CONDITIONS  *
C     ***************************************************
```

3.2 Program to solve 2-D problem for flat plate and wake area with modified boundary conditions.

```
35      k = 2
        DO 41 j = 1,jmax,1
        DO 40 i = 1,imax,1


C Flow field at first x-station (at leading edge of plate)

          IF (i.EQ.1)     THEN
            u(i,j,k) = (nt*dt)/((nt*dt)+1)
            v(i,j,k) = 0.0
          ENDIF

C Flow field at the wall (non-slip condition)

          IF ((j.EQ.1).AND.(i.LE.endplate)) THEN
            u(i,j,k) = 0.0
            v(i,j,k) = 0.0
          ENDIF

C  Flow field in the wake

          IF  ((j.EQ.1).AND.(i.GT.endplate))    v(i,j,k) = 0.0

C Flow field outside boundary layer region

          IF (j.EQ.jmax)   u(i,j,k) =(nt*dt)/((nt*dt)+1)
40      CONTINUE
41      CONTINUE


C   ***************************************************************************
C        EVALUATE U(I,J,K) + V(I,J,K) FOR EACH X-STATION (I),
C
C        FOR THE CURRENT TIME STEP (K).
C - ***************************************************************************

50      k = 2

        DO 90    i = 2,imax,1

C Set all terms of coefficient matrix equal to zero

        DO 69 j=1,jmax,1
         DO 68 col=1,jmax,1
          coefficient(j,col) = 0

68       CONTINUE
69      CONTINUE

C calculate values of non-zero coefficients - row by row (j)

        DO 70  j = 2,jmax,1

          IF  ((j.EQ.1).AND.(i.LE.endplate)) THEN
             dvector(j) = 0
             coefficient(j,j) = 1.0

          ENDIF

          IF (j.EQ.jmax) THEN
             dvector(j) = 1.0
             coefficient(j,j) = 1.0
```

```
          ENDIF

          IF ((j.NE.1).AND.(j.NE.jmax)) THEN

          a(j) =  (v(i-1,j,k)/(2*dy)) - (1/(d **2))

          b(j) =   (1/dt) + (u(i-1,j,k)/dx) + (2/(dy**2))

          c(j) = (- (1/(dy**2))) - (v(i-1,j,k)/(2*dy))

          d(j) = ((1/dt) * u(i,j,k-1)) + ((u(i-1,j,k)**2) *(1/dx))
                                  + ( 1.0/((1.0+(nt*dt))**2) )

          coefficient(j,j-1) = c(j)
          coefficient(j,j) = b(j)
          coefficient(j,j+1) = a(j)
          dvector(j) = d(j)


          ENDIF

C         Calculation of U(i,j,k) on the zero-line of symmetry in the wake

          IF ((j.EQ.1).AND.(i.GT.endplate))  THEN

          a(1) = - (2/(dy**2))

          b(1) = (1/dt)+(u(i-1,1,k)/dx)+(2/(dy**2))

          d(1) = ((1/dt) * u(i,1,k-1))+((u(i-1,1,k)**2) *(1/dx))
                                    + ( 1.0/((1.0+(nt*dt))**2) )

          coefficient(1,1) = b(1)
          coefficient(1,2) = a(1)

          ENDIF

70        CONTINUE

C     ***********************************************************************
C      *  SOLVE SYSTEM OF EQUATIONS WITH GAUSSIAN ELIMINATION  *
C     ***********************************************************************

C we define values of transformed coefficients row by row (j)
C first, evaluate mi and pi for each row (j)

          IF (i.LT.endplate) THEN
          mi(1) = 1
          pi(1) = 0
          ENDIF

          IF (i.GT.endplate) THEN
          mi(1) = b(1)
          pi(1) = d(1)
          ENDIF

          DO 75   j = 2,(jmax-1),1

          mi(j) = b(j)-((c(j)*a(j-1))/mi(j-1))
          pi(j) = d(j)-((c(j)*pi(j-1))/mi(j-1))

C second,insert mi and pi for each row(j) and also c(j)=0

          coefficient(j,j-1) = 0
```

```
          coefficient(j,j) = mi(j)
          dvector(j) = pi(j)

 75       CONTINUE

 C solve for u(j) by back substitution

          if (i.le.endplate)   u(i,1,k) = 0.0

          DO 80  j = (jmax-1),2,-1
          u(i,j,k)= (pi(j)-(a(j)*u(i,j+1,k)))/mi(j)
 80       CONTINUE

          IF (i.GT.endplate) THEN
          u(i,1,k) = (pi(1) - (a(1)*u(i,2,k)))/mi(1)
          ENDIF

 C    calculate v(j) not on centre line where it is zero

          v(i,1,k) = 0
          DO 85  j=2,jmax,1

          f =-((dy / (2*dx)) * (u(i,j,k)-u(i-1,j,k)+u(i,j-1,k)-u(i-1,j-1,k)))

          v(i,j,k) = (v(i,j-1,k)) + f

 85        CONTINUE

 90        CONTINUE


 C     ************************************************************************
 C     COPY RESULTS IN ARRAY FOR CURRENT TIME STEP AND OUTPUT RESULTS  *
 C     ************************************************************************

 C -     Copy results from current k value to previous k value

         do 1060 i=1,imax,1
         do 1050 j=1,jmax,1
         u(i,j,1)=u(i,j,2)
         v(i,j,1)=v(i,j,2)
 1050    continue
 1060    continue


 C       Output u(i,j,k) results for all time (k) values for a given j height
 C       above plate, at a fixed x-distance in the wake region.

         i=21
         j=4

         WRITE (6,*) nt, u(i,j,2)

 C       Output u(i,j,k) & v(i,j,k) & ss(i) results for symmetric y=0 line
 C       in wake region, for a given value of k.

                 if((nt.eq.3).or.(nt.eq.20).or.(nt.eq.100).or.(nt.eq.220).
                 or.(nt.eq.350).or.(nt.eq.520).or.(nt.eq.820).
                 or.(nt.eq.1000)) then

                 WRITE (6,*) 'Wake profile results'
                 WRITE (6,*) ''

 C               do i=2,imax,1
```

```
                do j=1,jmax,1
                x=dx*(i-1)
                y=dy*(j-1)

                WRITE (6,*) y, u(i,j,k)
                enddo
C               enddo
                WRITE (6,*) ''
                endif

C       Return to beginning for solution of next time step k

        nt=nt+1
        if (nt.le.ntmax) go to 35


2000    end
```

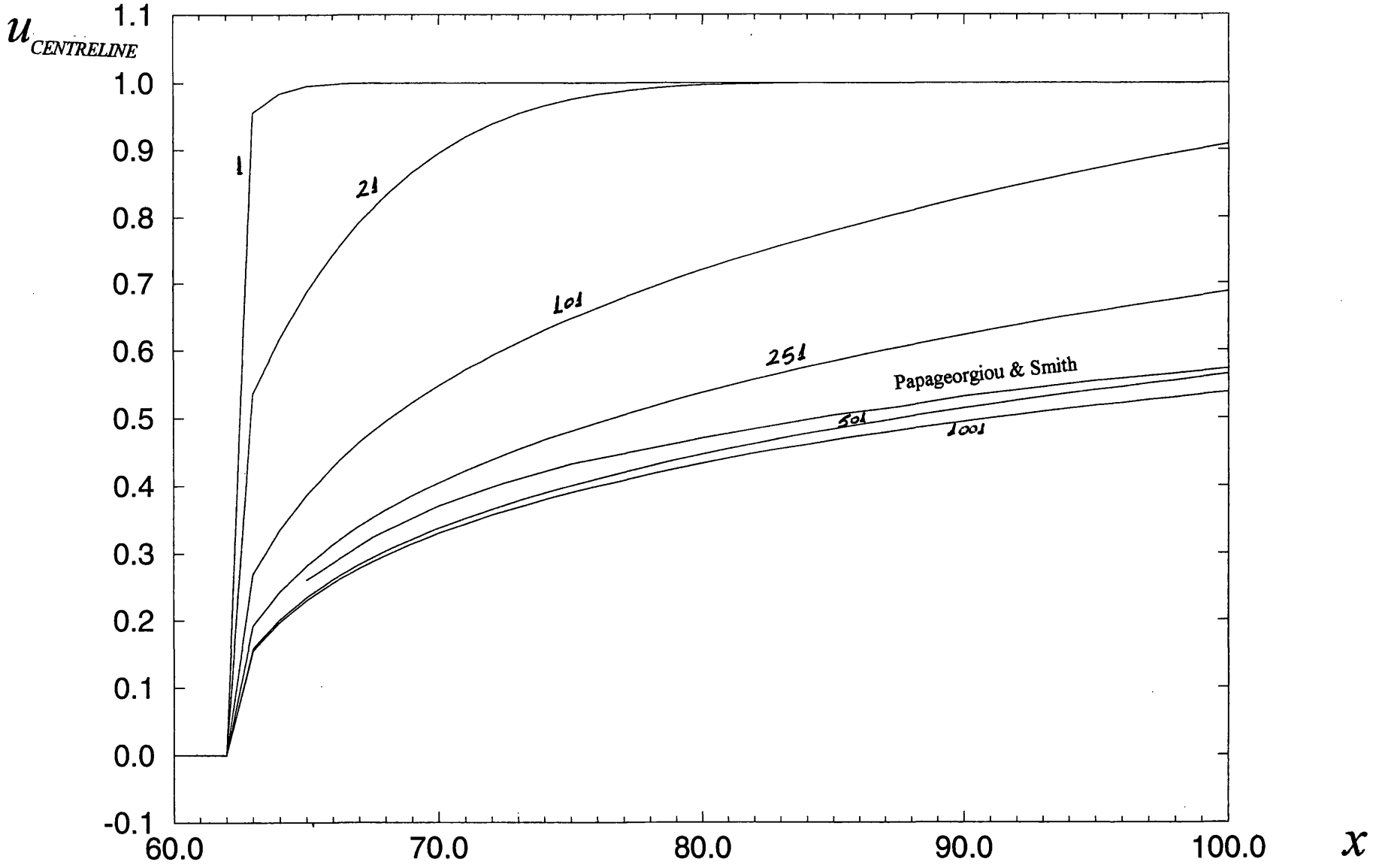


Fig. 3.2 Variation of $u_{CENTRELINE}$ along the central axis of symmetry, ($dx$=0.016, $dy$=0.08, $dt$=0.008).

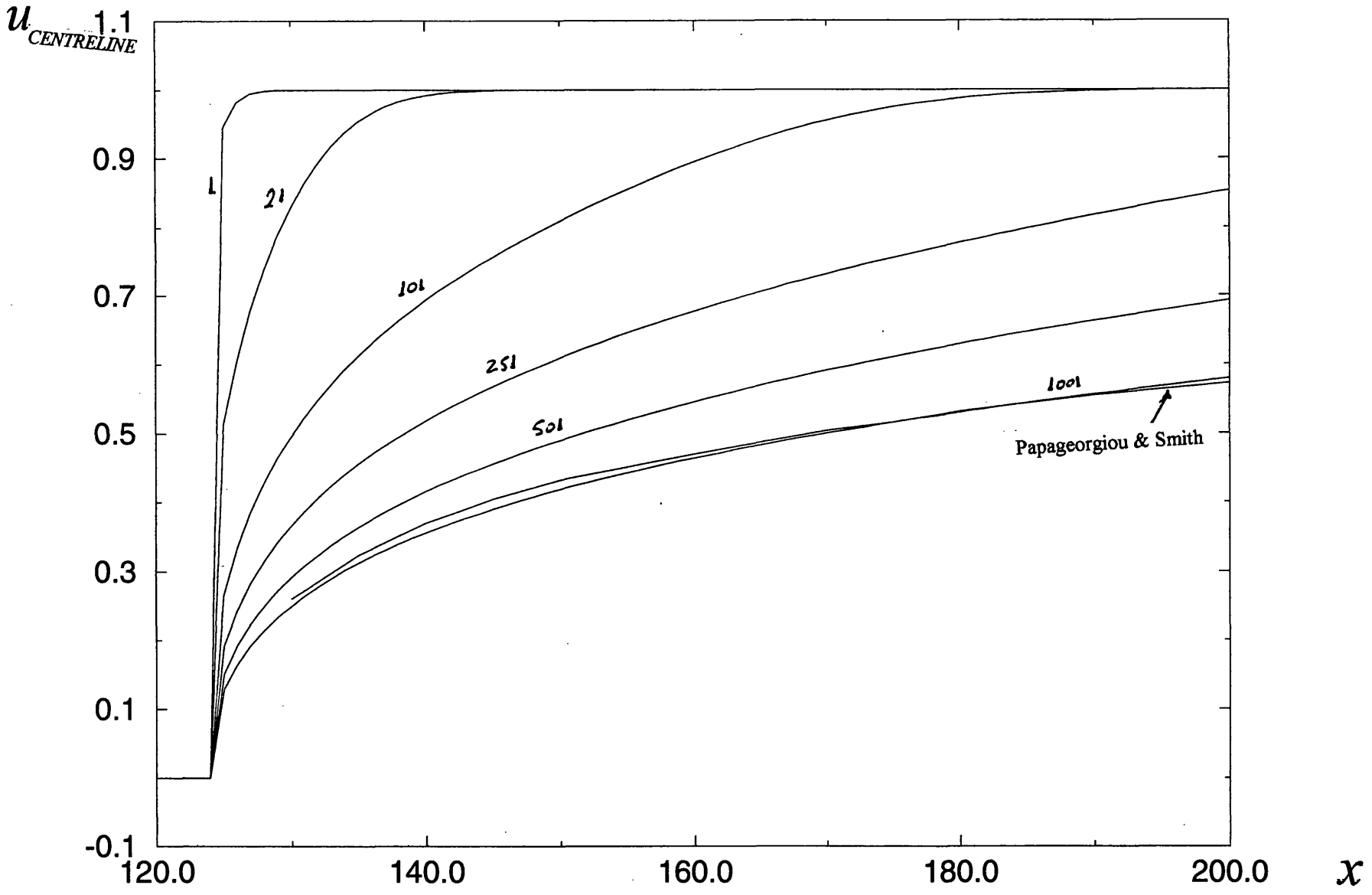


Fig. 3.3 Variation of $u_{CENTRELINE}$ along the central axis of symmetry, ($dx$=0.008, $dy$=0.04, $dt$=0.004).

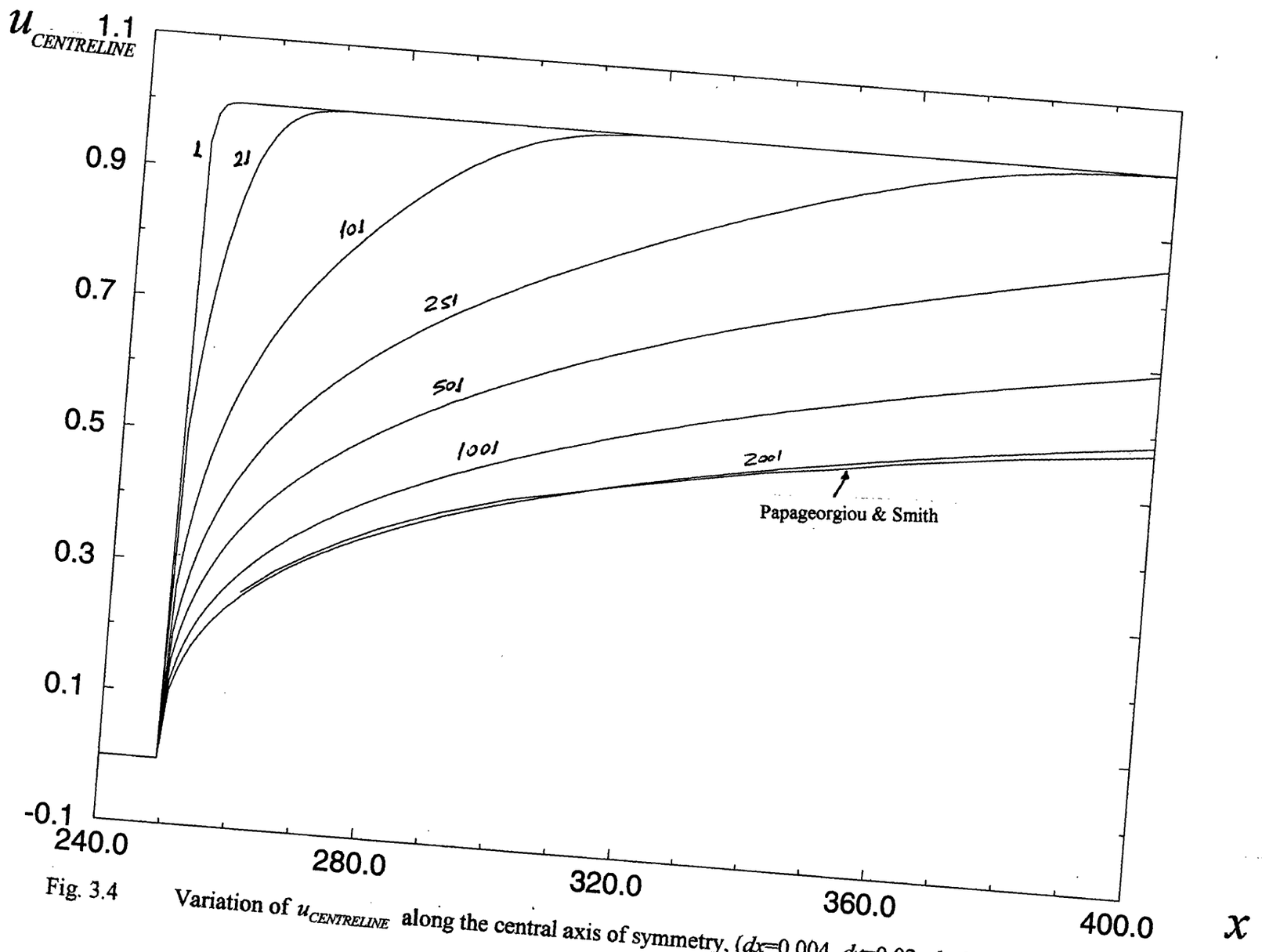


Fig. 3.4 Variation of $u_{CENTRELINE}$ along the central axis of symmetry, ($dx$=0.004, $dy$=0.02, $dt$=0.002).

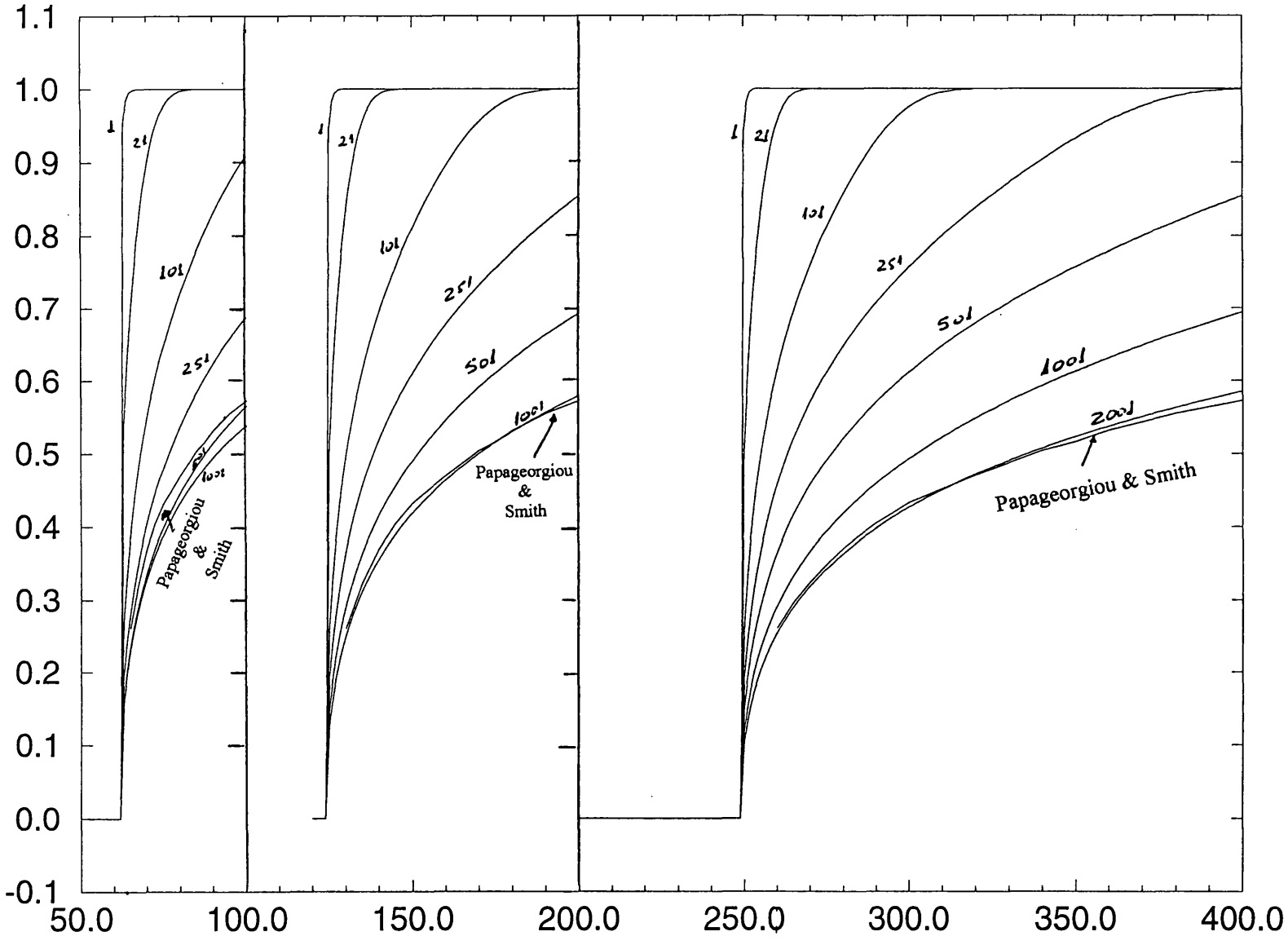


Fig. 3.5 Variation of $u_{CENTRELINE}$ along the central axis of symmetry, for the three grids.

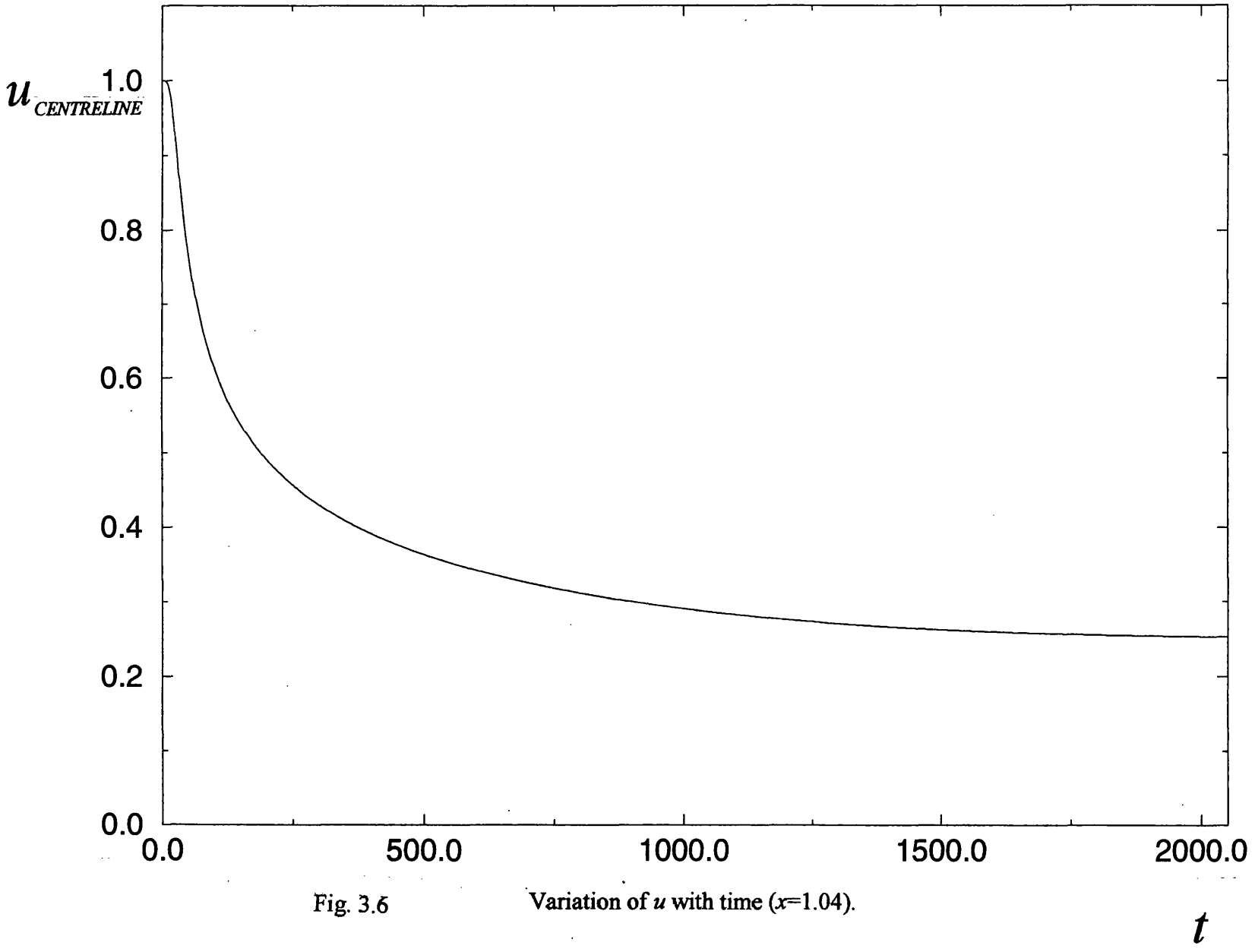


Fig. 3.6 Variation of $u$ with time ($x$=1.04).

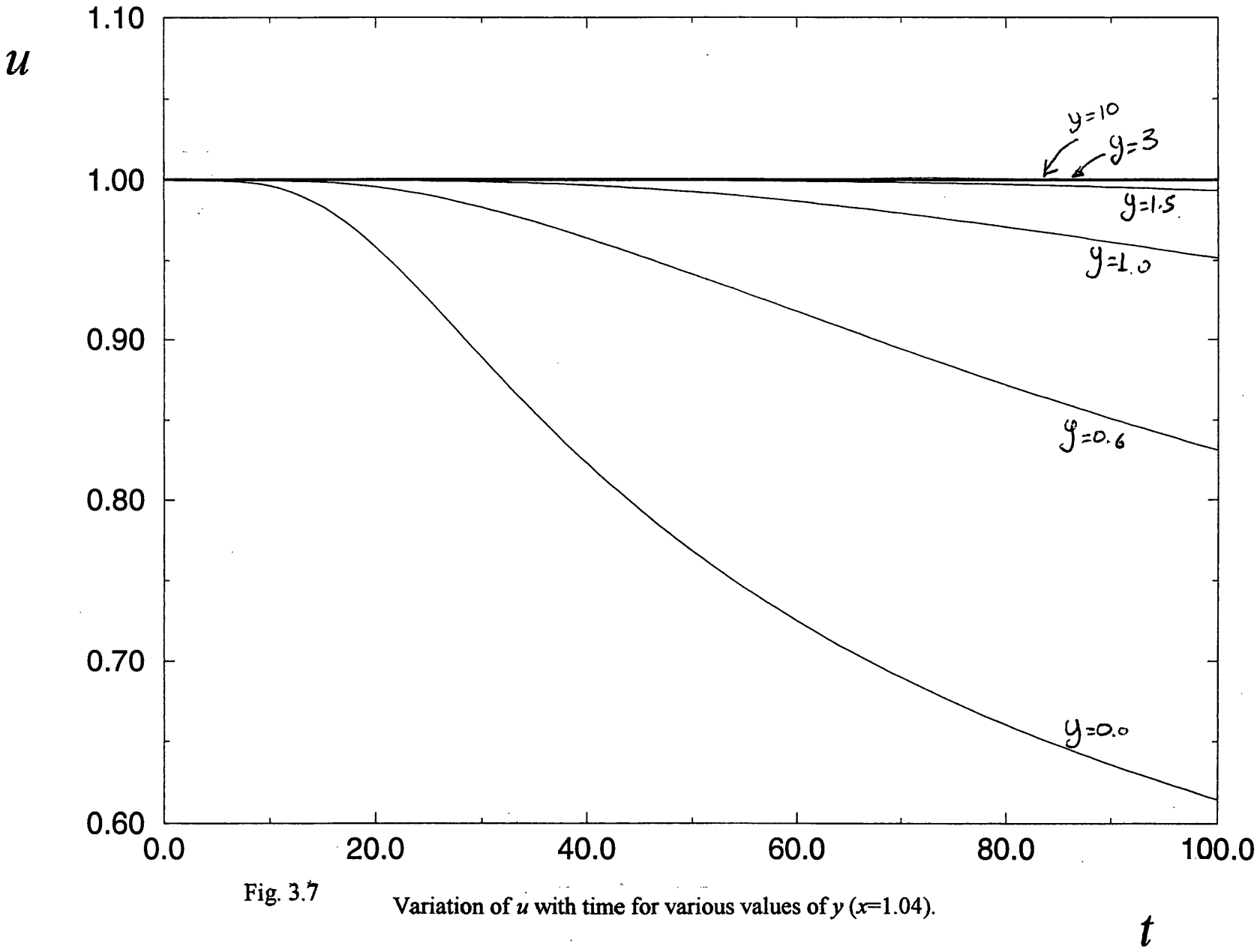


Fig. 3.7 Variation of $u$ with time for various values of $y$ ($x$=1.04).

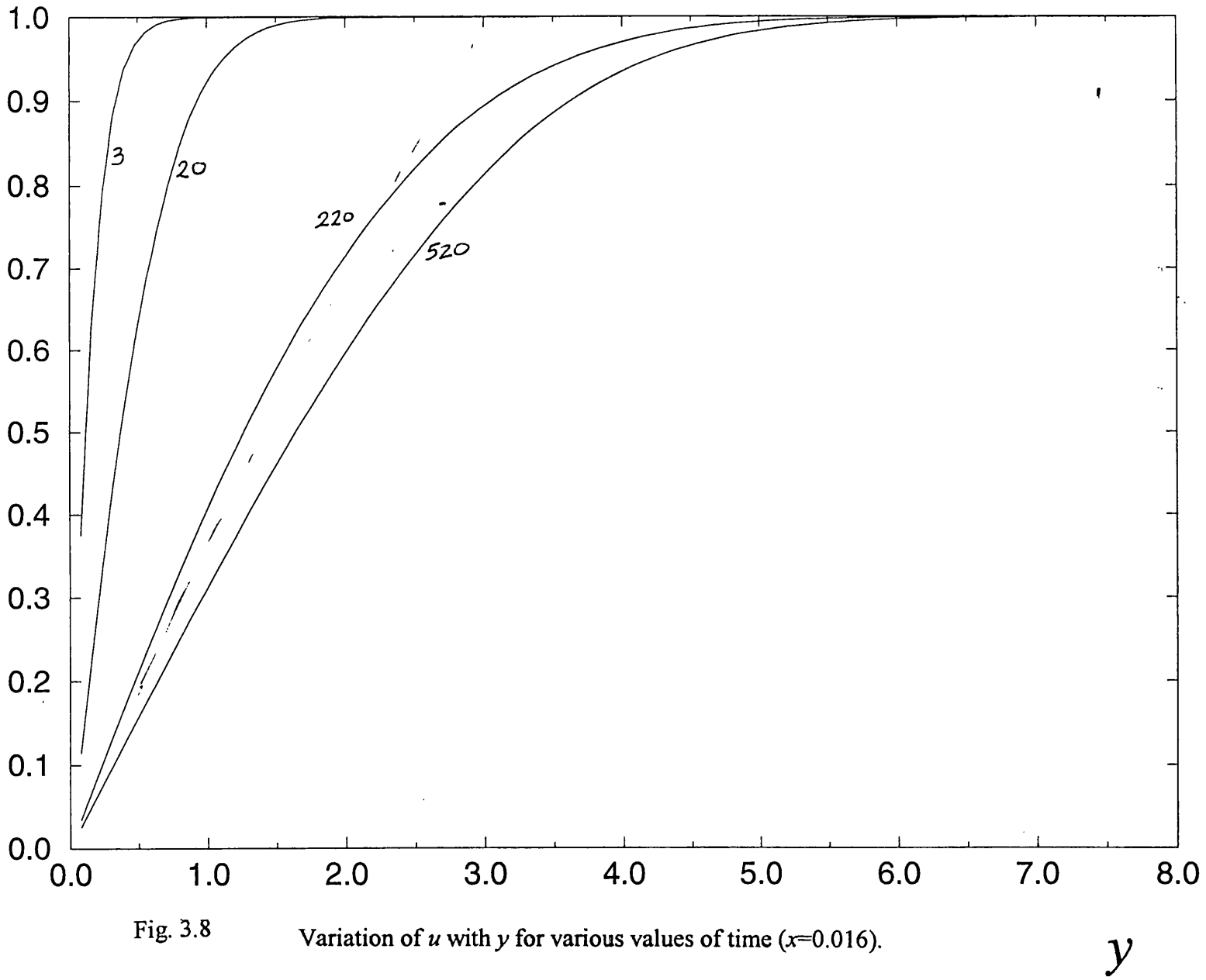


Fig. 3.8 Variation of $u$ with $y$ for various values of time ($x$=0.016).

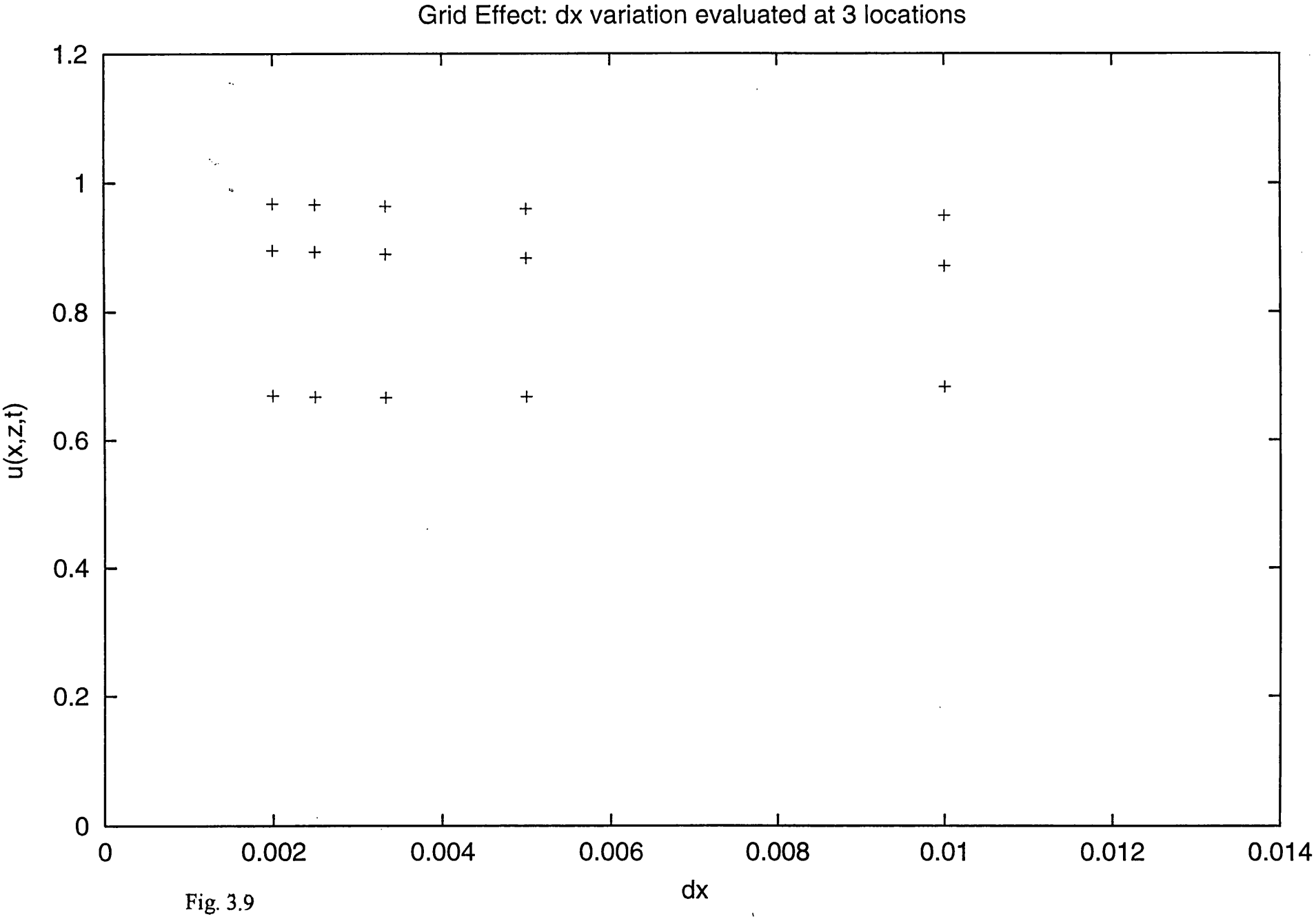
Grid Effect: dx variation evaluated at 3 locations
u(x,z,t)
dx
1.2
1
0.8
0.6
0.4
0.2
0
0
0.002
0.004
0.006
0.008
0.01
0.012
0.014

Fig. 3.9

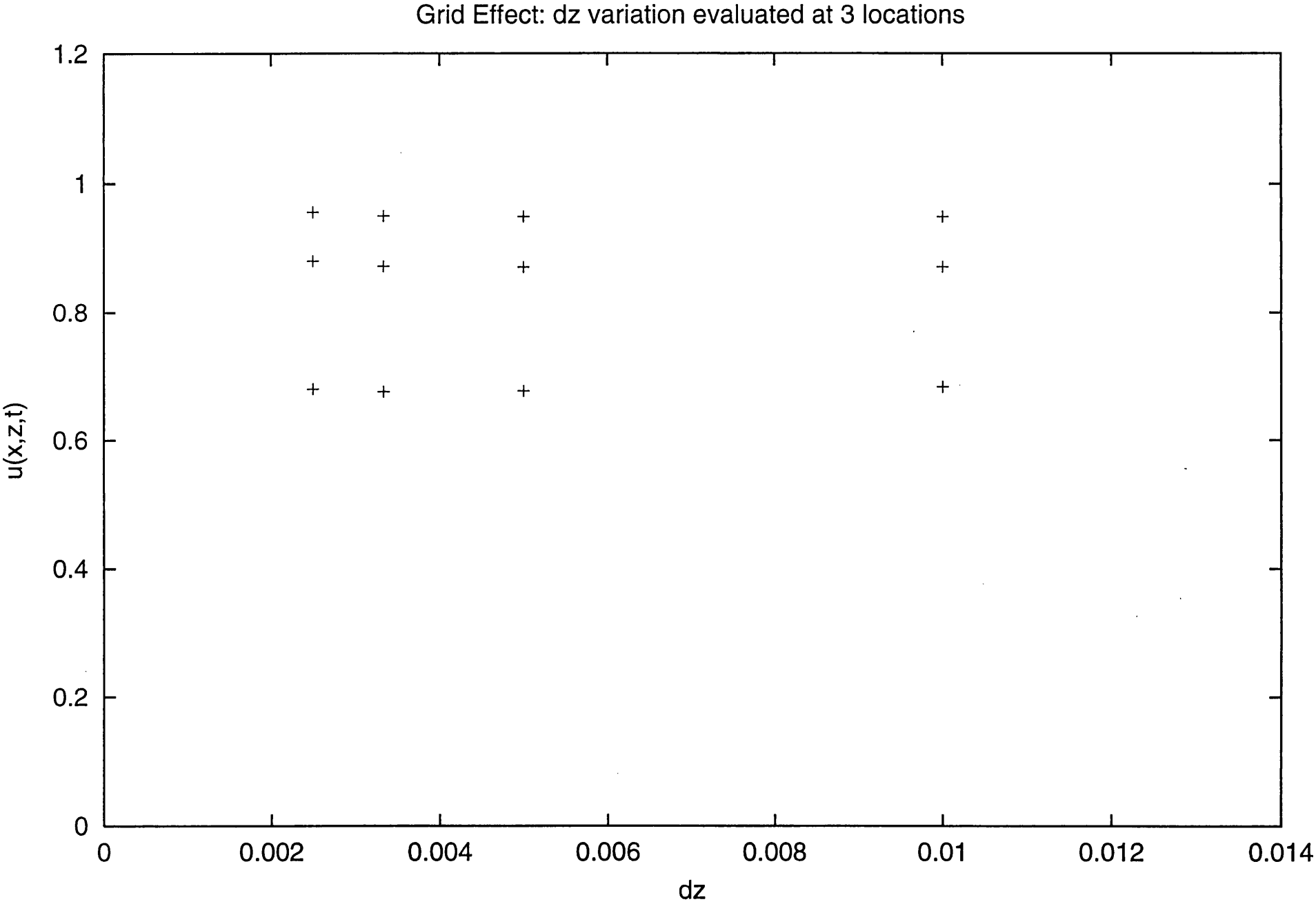
Grid Effect: dz variation evaluated at 3 locations
u(x,z,t)
dz
1.2
1
0.8
0.6
0.4
0.2
0
0
0.002
0.004
0.006
0.008
0.01
0.012
0.014

Fig. 3.10

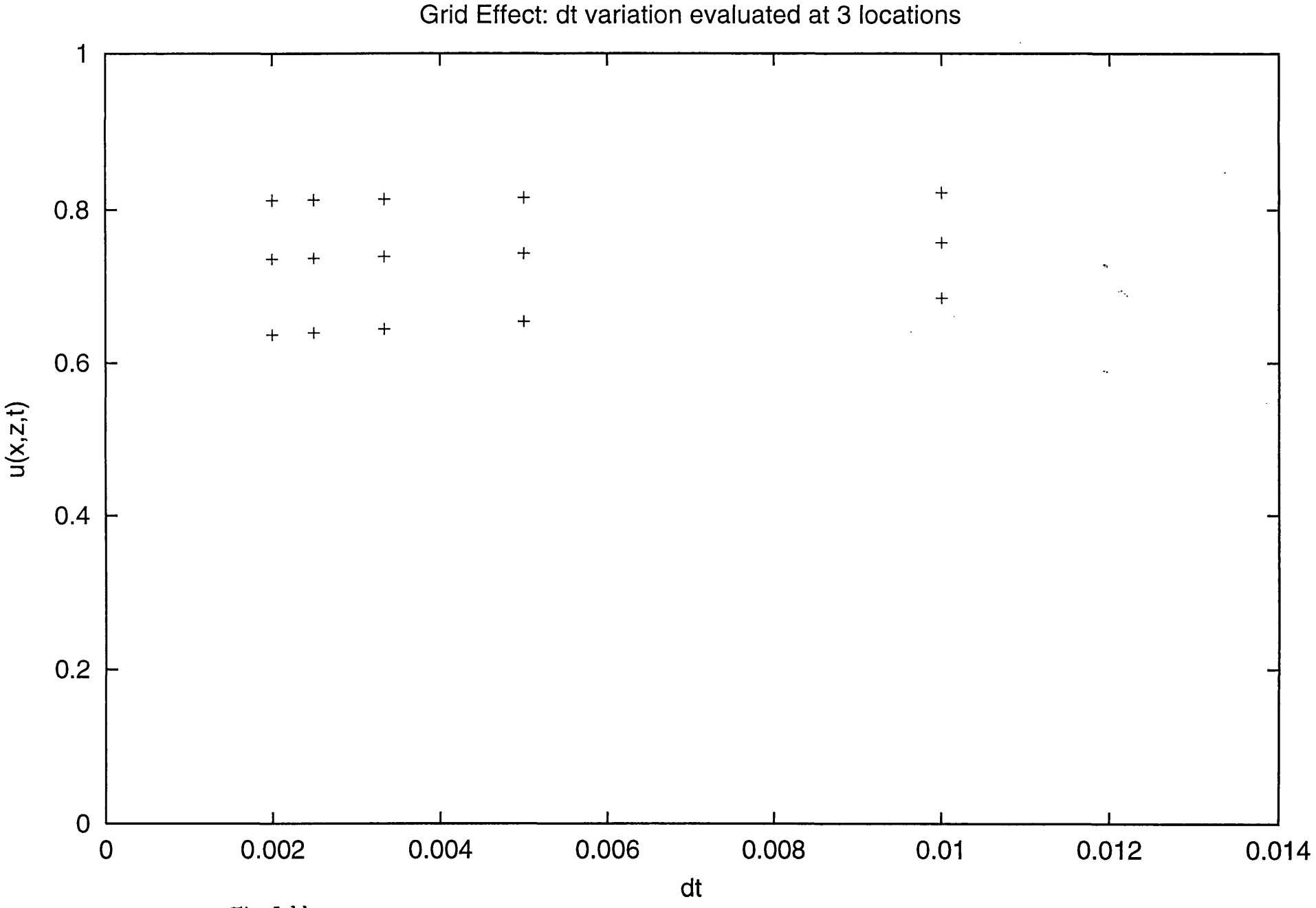
Grid Effect: dt variation evaluated at 3 locations
u(x,z,t)
dt
0
0.2
0.4
0.6
0.8
1
0
0.002
0.004
0.006
0.008
0.01
0.012
0.014

Fig. 3.11

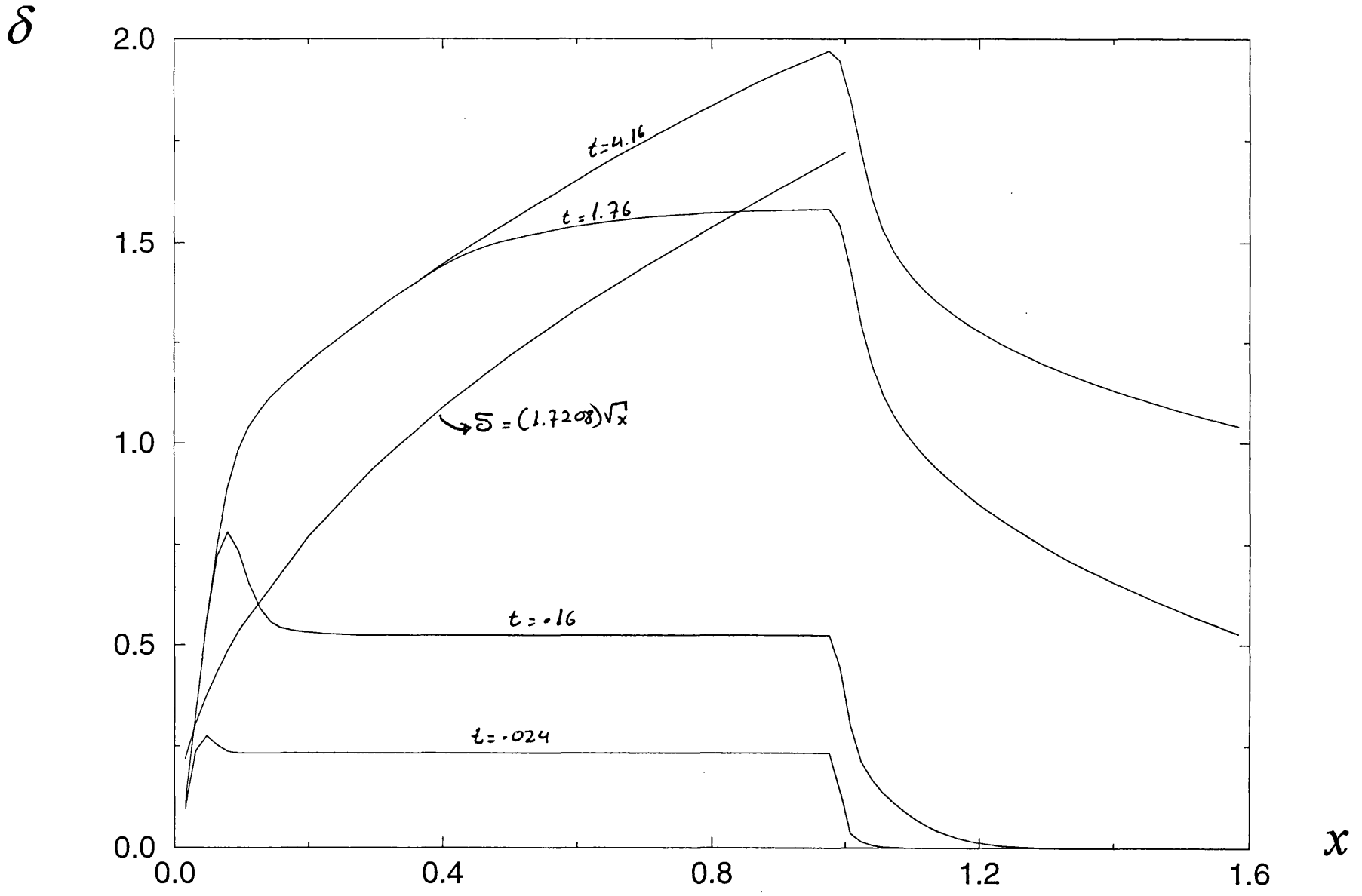


Fig. 3.12 Profiles of $\delta$ for times ranging between $t$=0.024 and $t$=4.16 ($dx$=0.016, $dy$=0.08, $dt$=0.008).

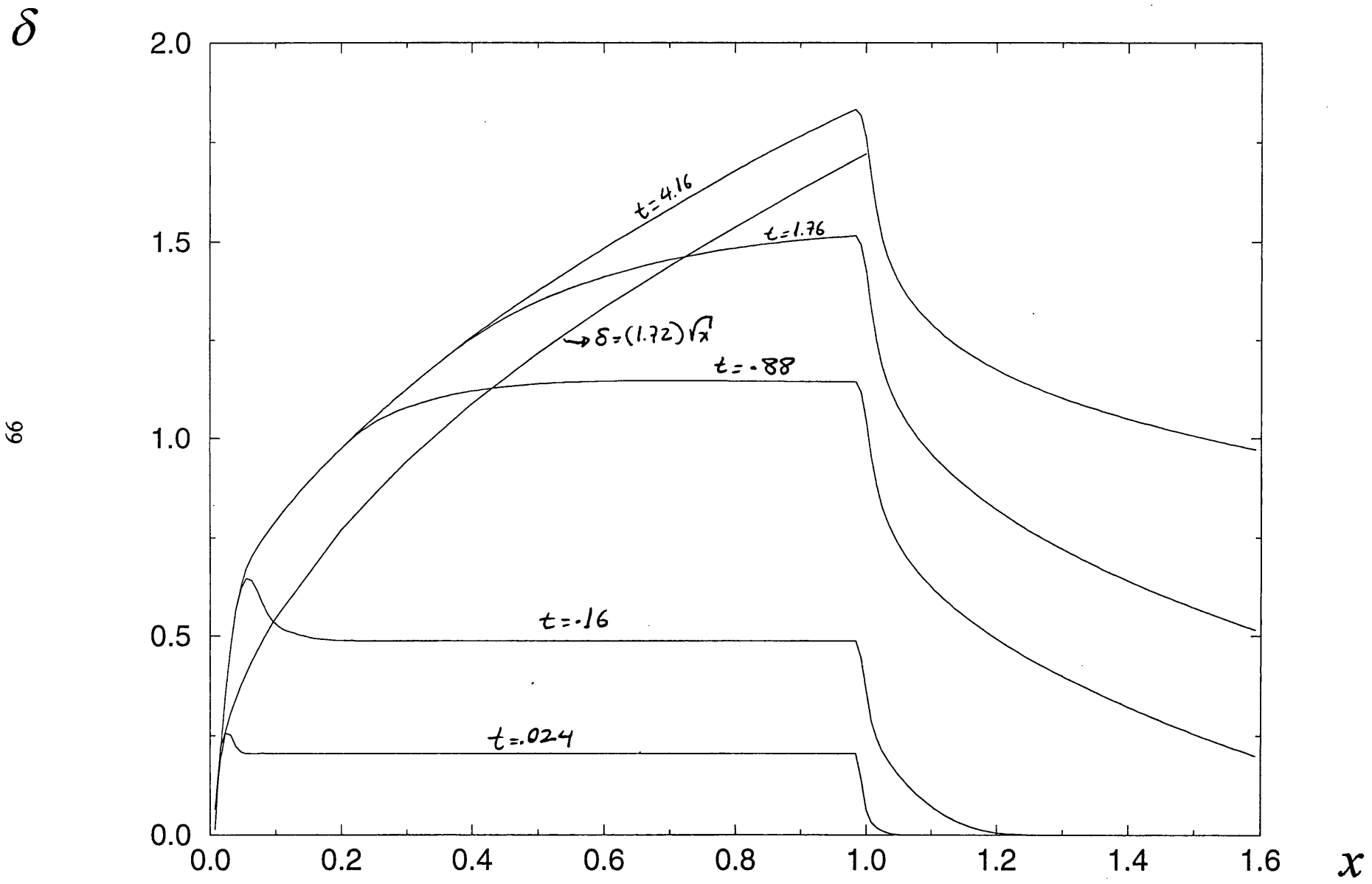


Fig. 3.13 Profiles of $\delta$ for times ranging between $t$=0.024 and $t$=4.16 ($dx$=0.008, $dy$=0.04, $dt$=0.004).

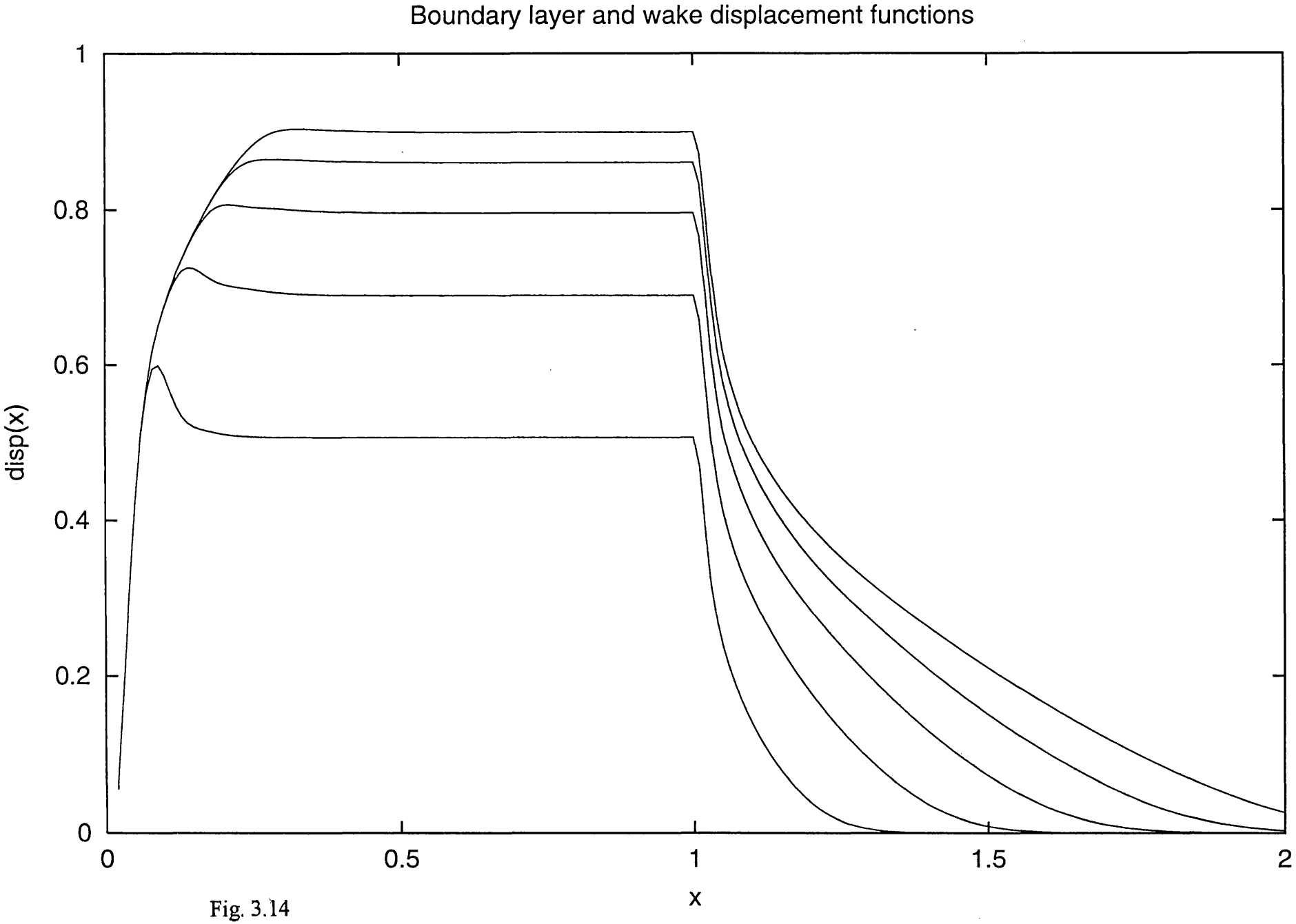
Boundary layer and wake displacement functions
disp(x)
x
0
0.2
0.4
0.6
0.8
1
0
0.5
1
1.5
2

Fig. 3.14

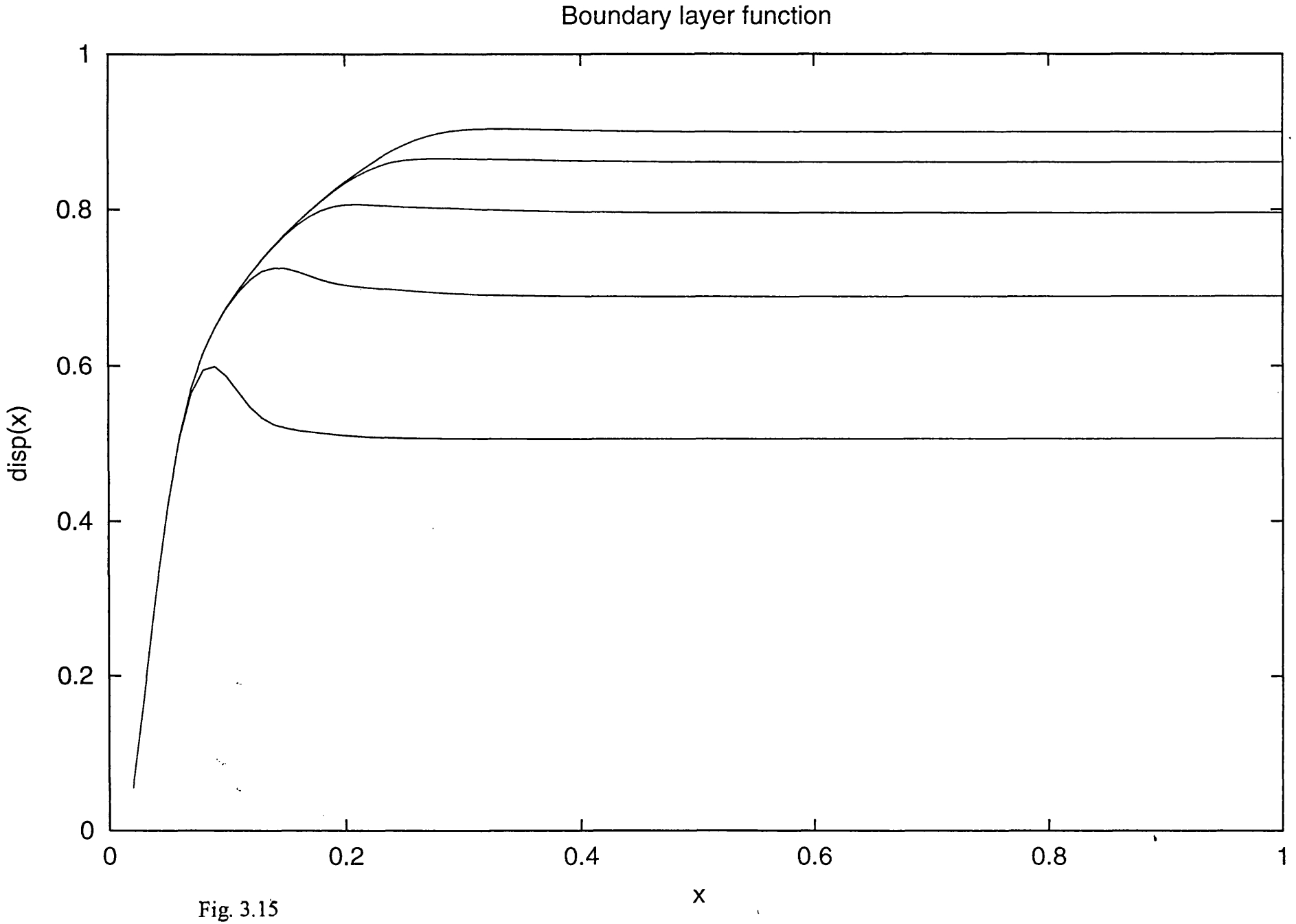


Fig. 3.15

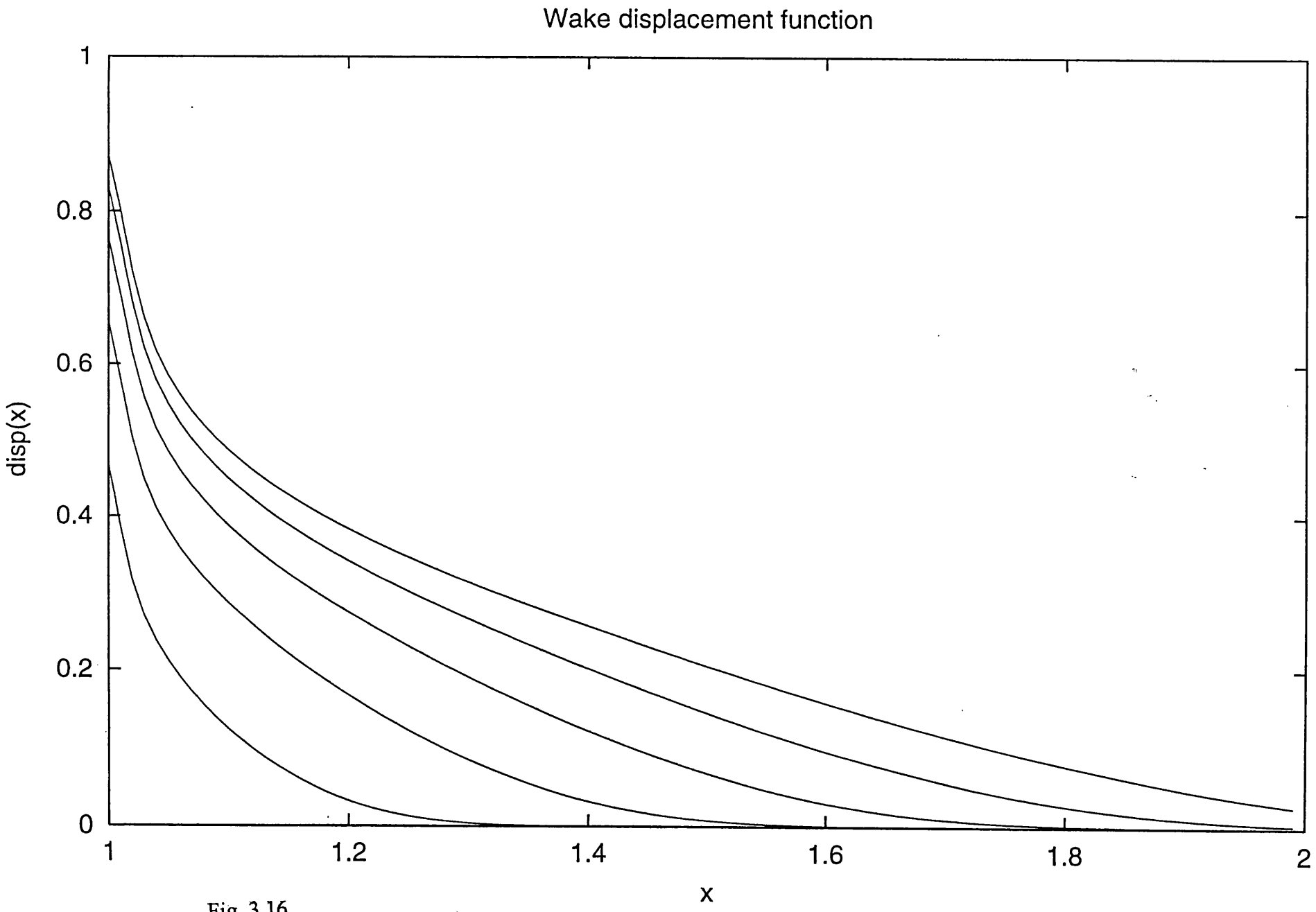
Wake displacement function
disp(x)
x
1
0.8
0.6
0.4
0.2
0
1
1.2
1.4
1.6
1.8
2

Fig. 3.16

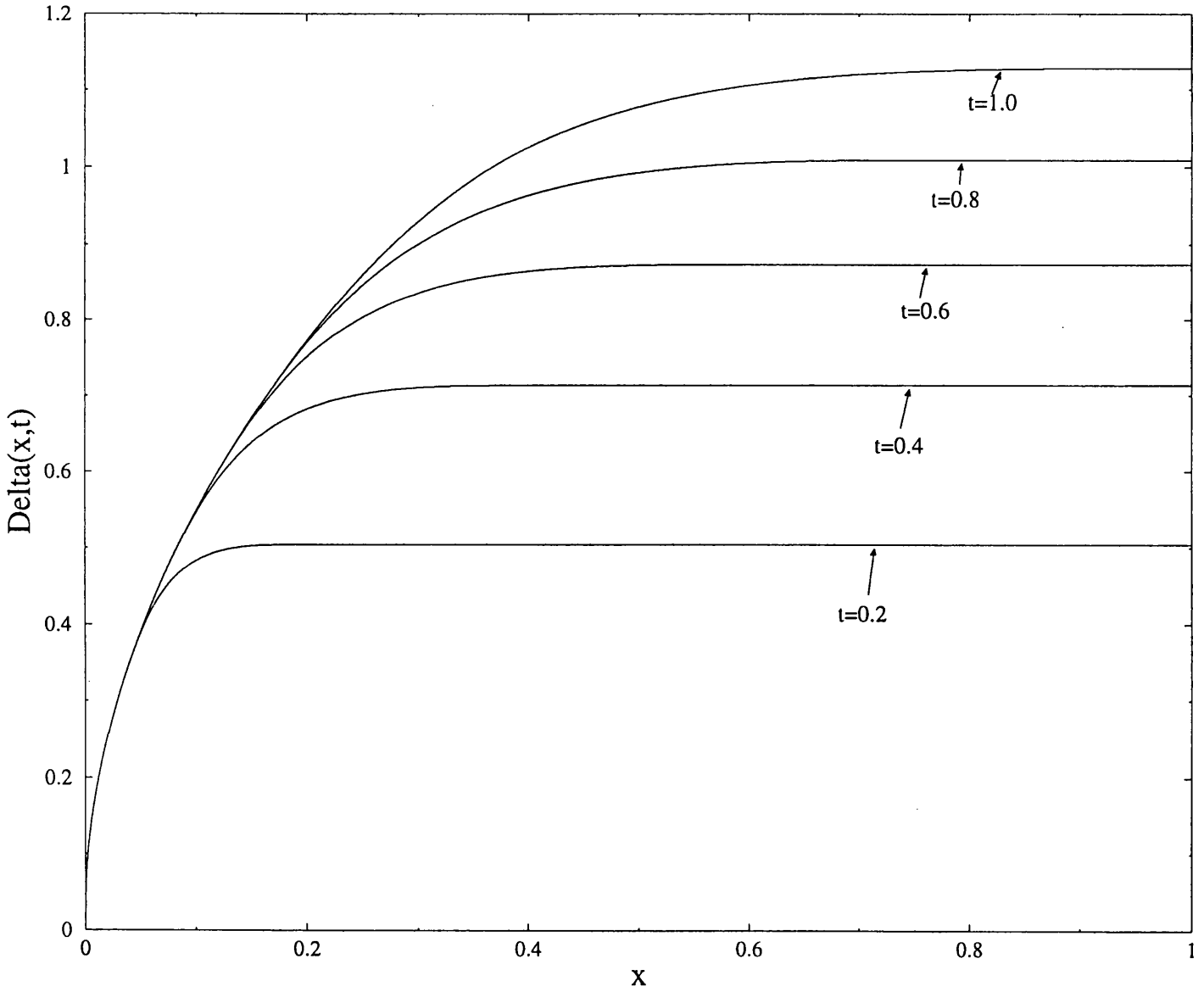
BL displacement thickness: Delta(x,t)
Delta(x,t)
x
t=1.0
t=0.8
t=0.6
t=0.4
t=0.2
0
0.2
0.4
0.6
0.8
1
1.2

Fig. 3.17

The displacement thickness of the wake: Delta(x,t)

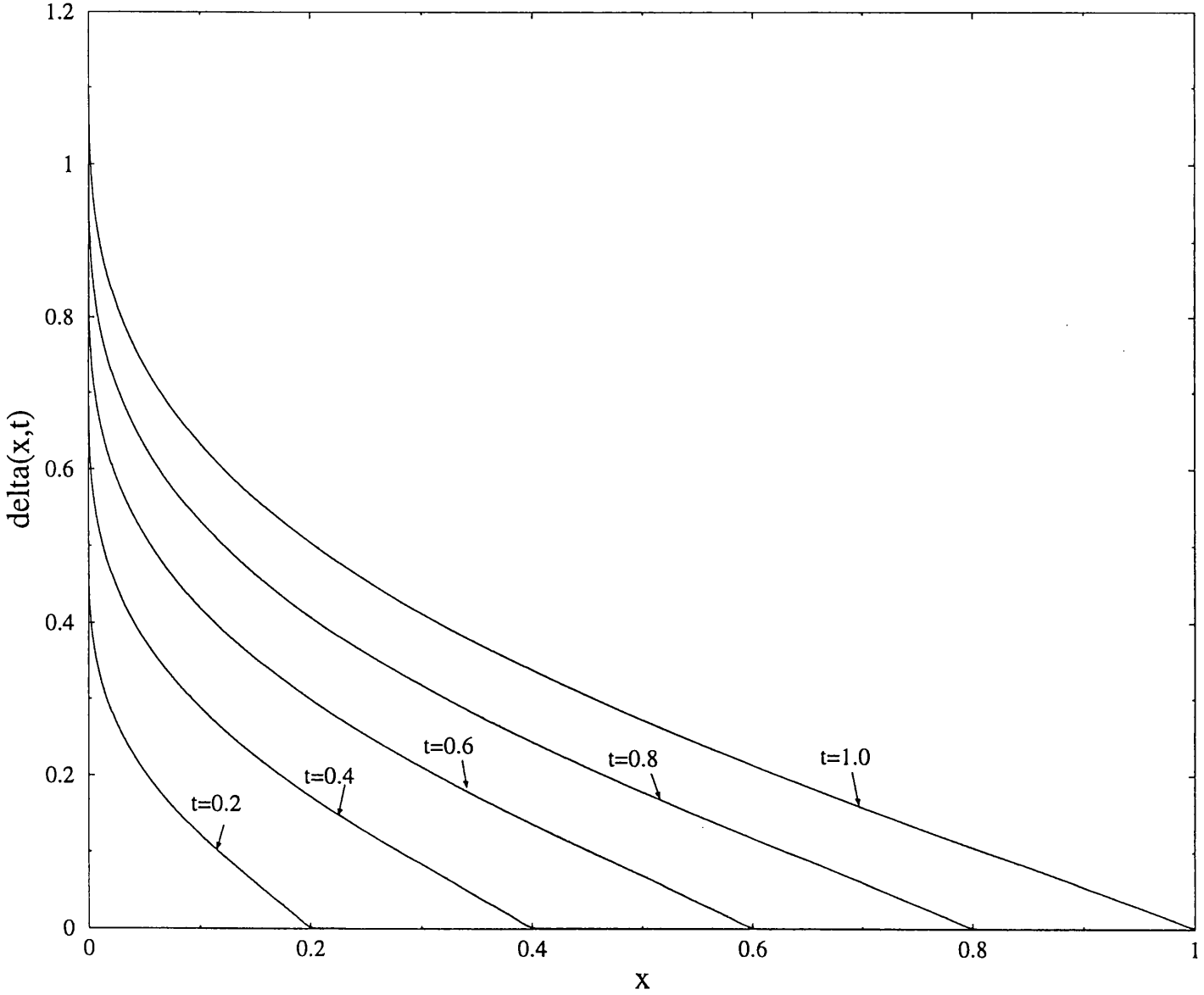


Fig. 3.18

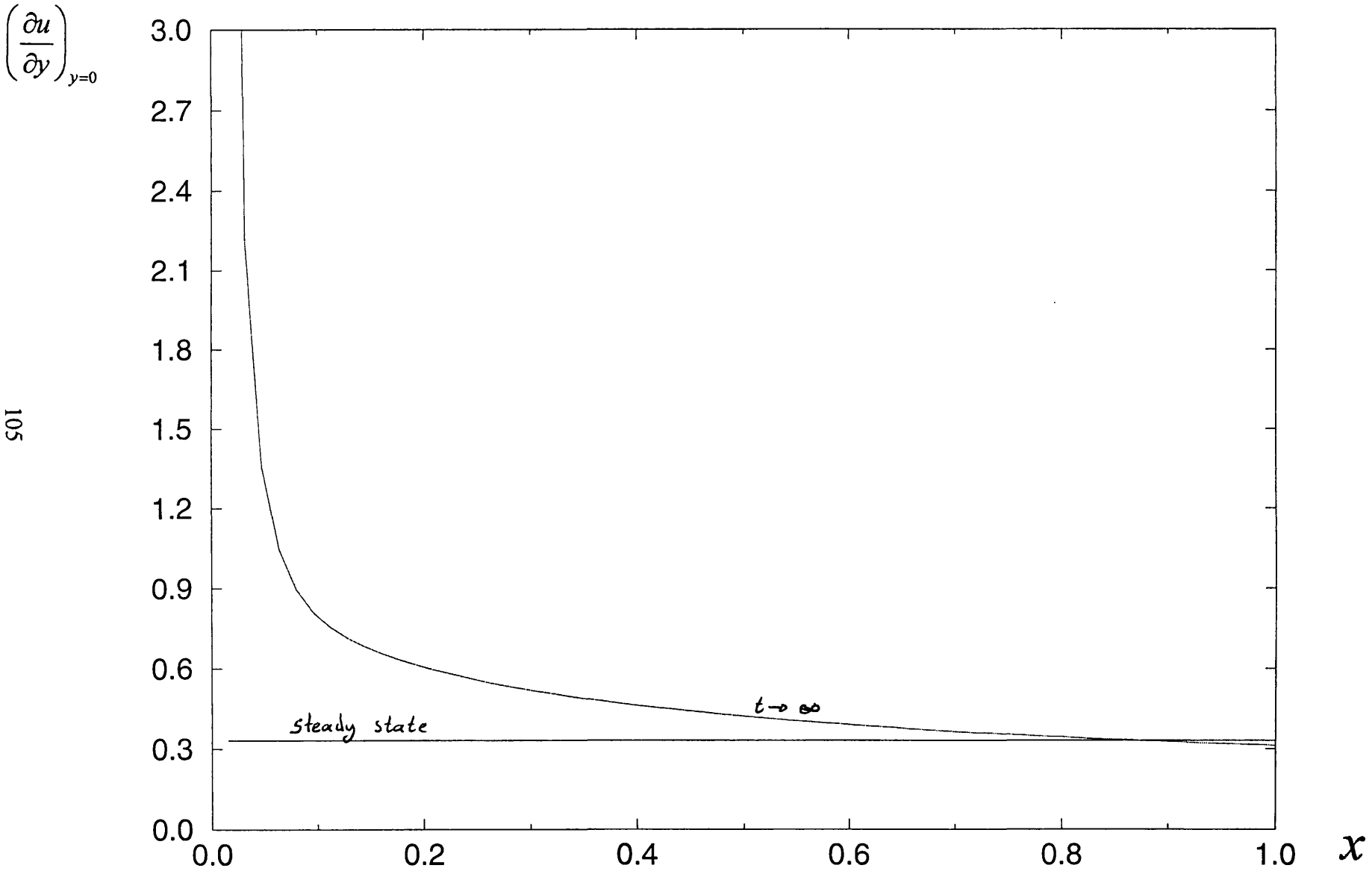


Variation of skin friction with $x$.

Fig. 3.19

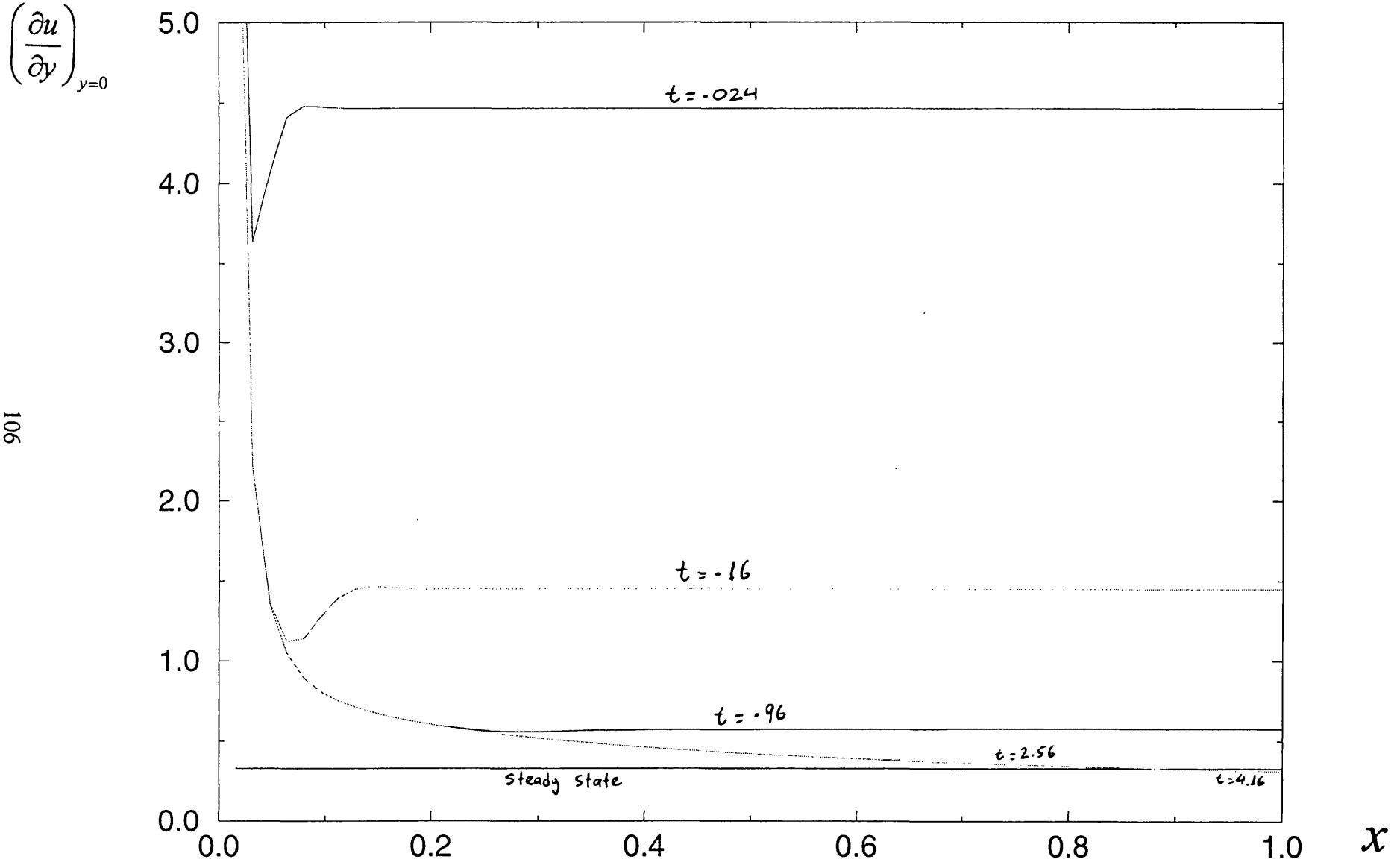


Fig. 3.20 Variation of skin friction with $x$ for various value of time.

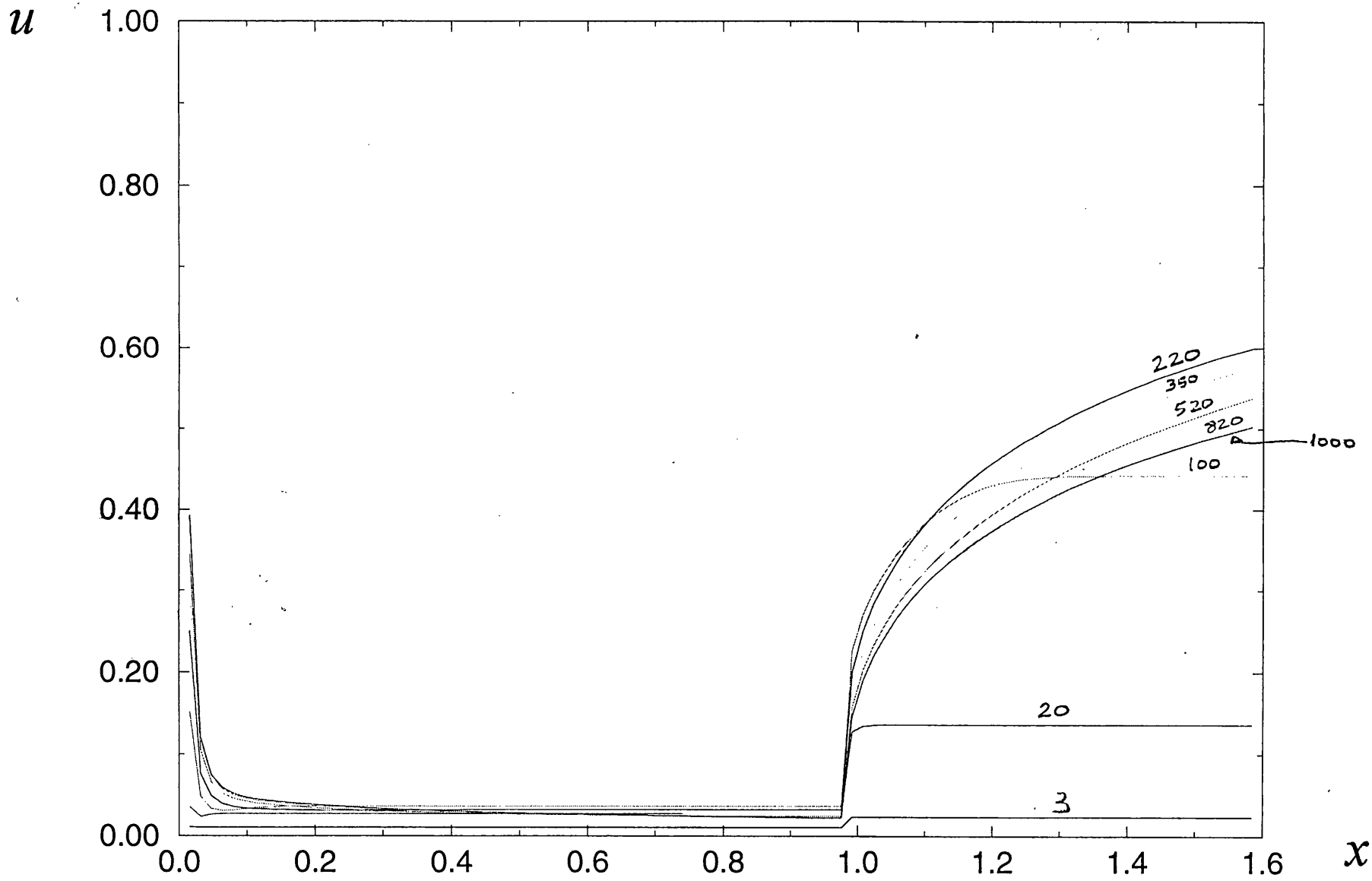


Fig. 3.21 Variation of the velocity $u$ with $x$ close to the centreline ($dx$=0.016, $dy$=0.08, $dt$=0.008).

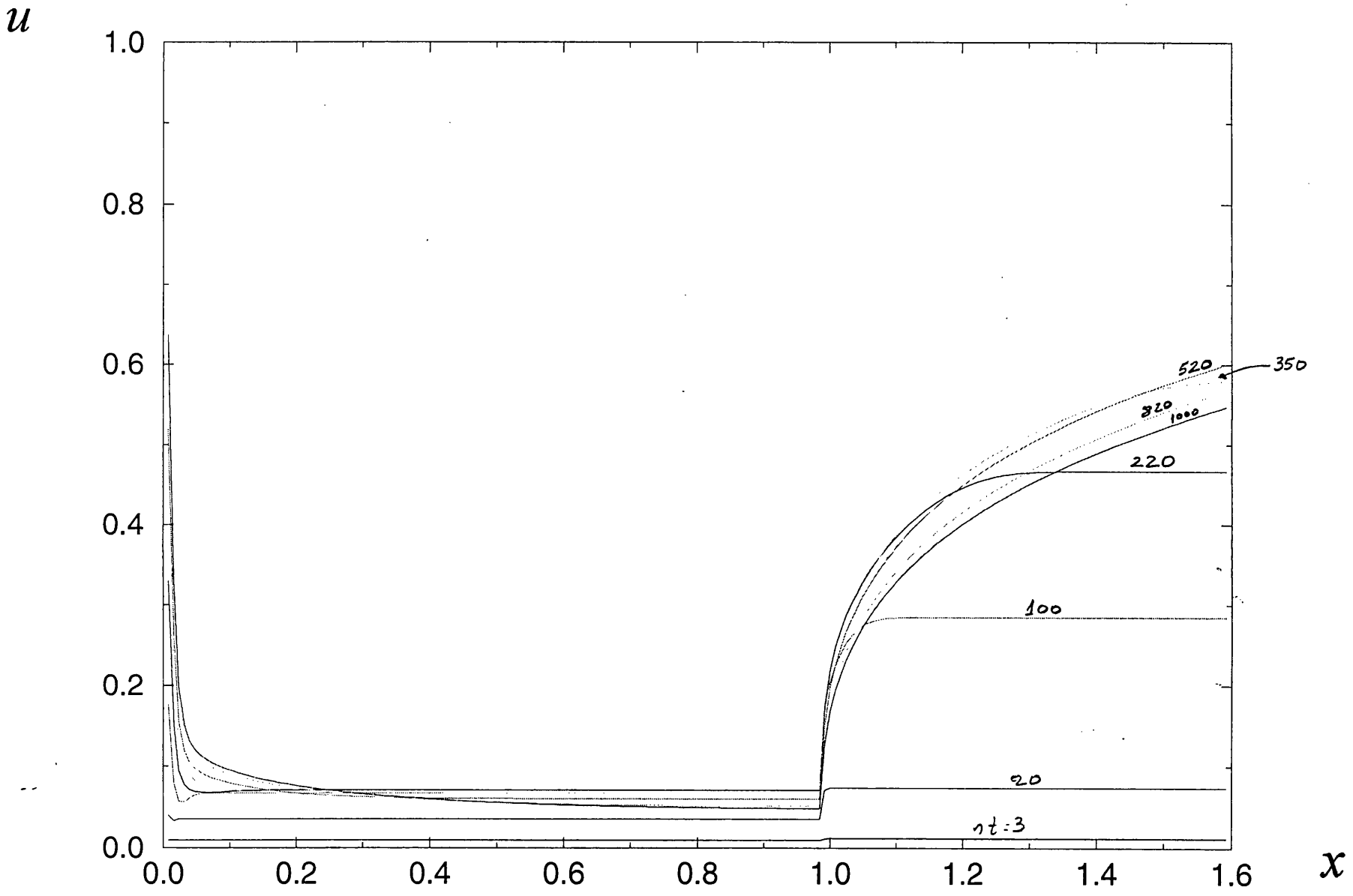


Fig. 3.22 Variation of the velocity $u$ with $x$ close to the centreline ($dx$=0.008, $dy$=0.04, $dt$=0.004).

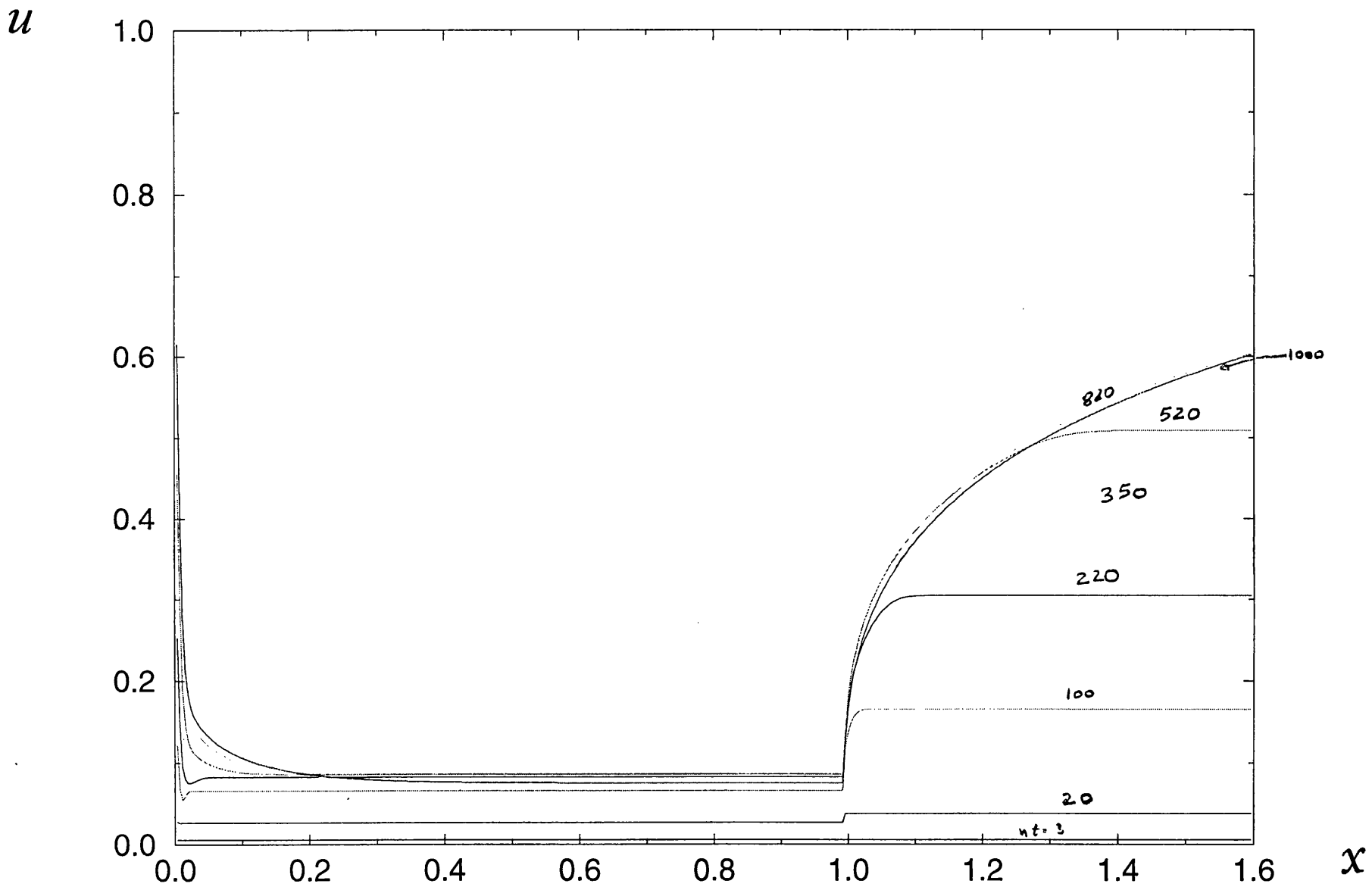


Fig. 3.23 Variation of the velocity $u$ with $x$ close to the centreline ($dx$=0.004, $dy$=0.02, $dt$=0.002).

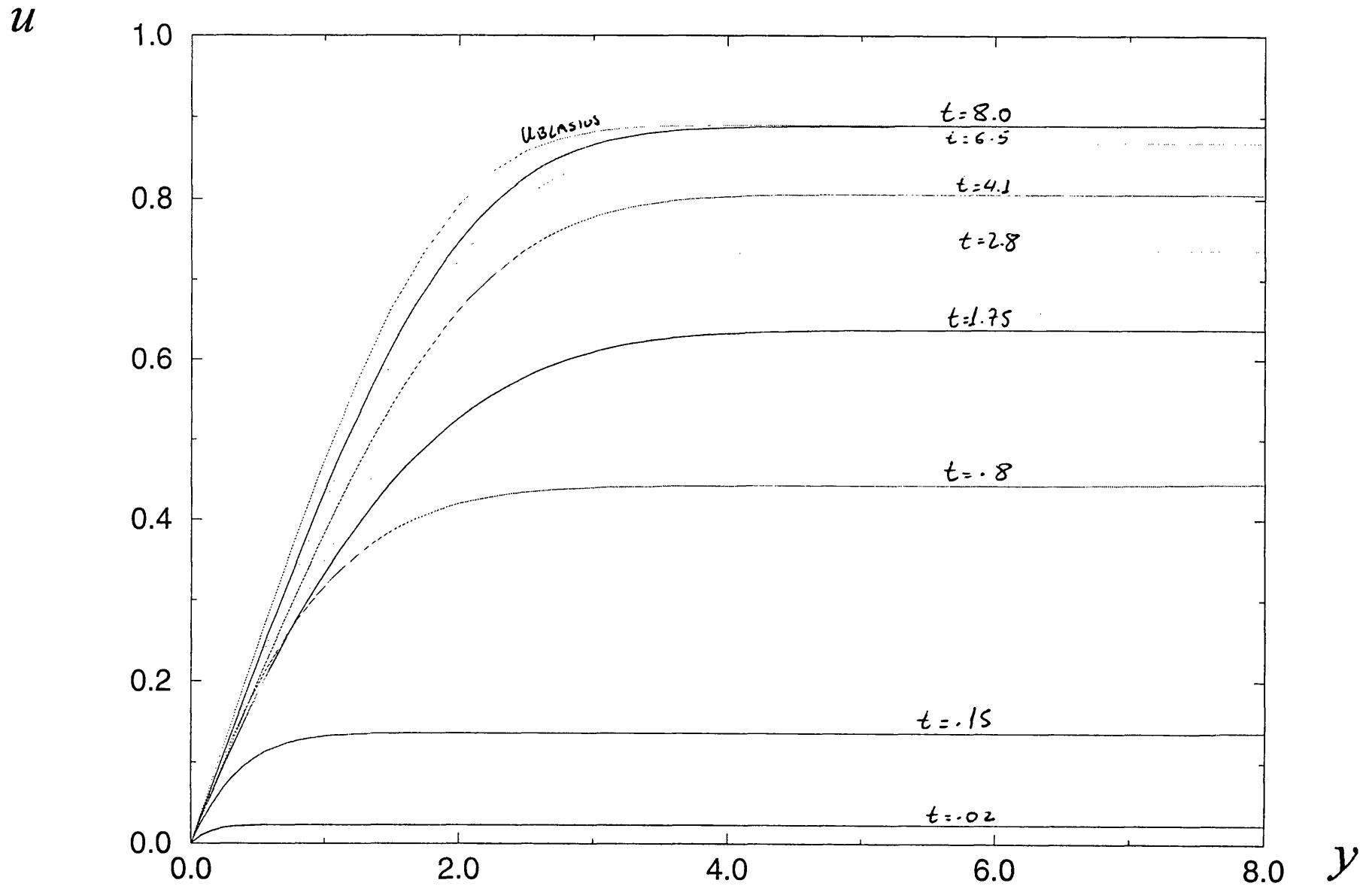


Fig. 3.24 Variation of $u$ with $y$, compared with the Blasius solution ($dx$=0.016, $dy$=0.08, $dt$=0.008).

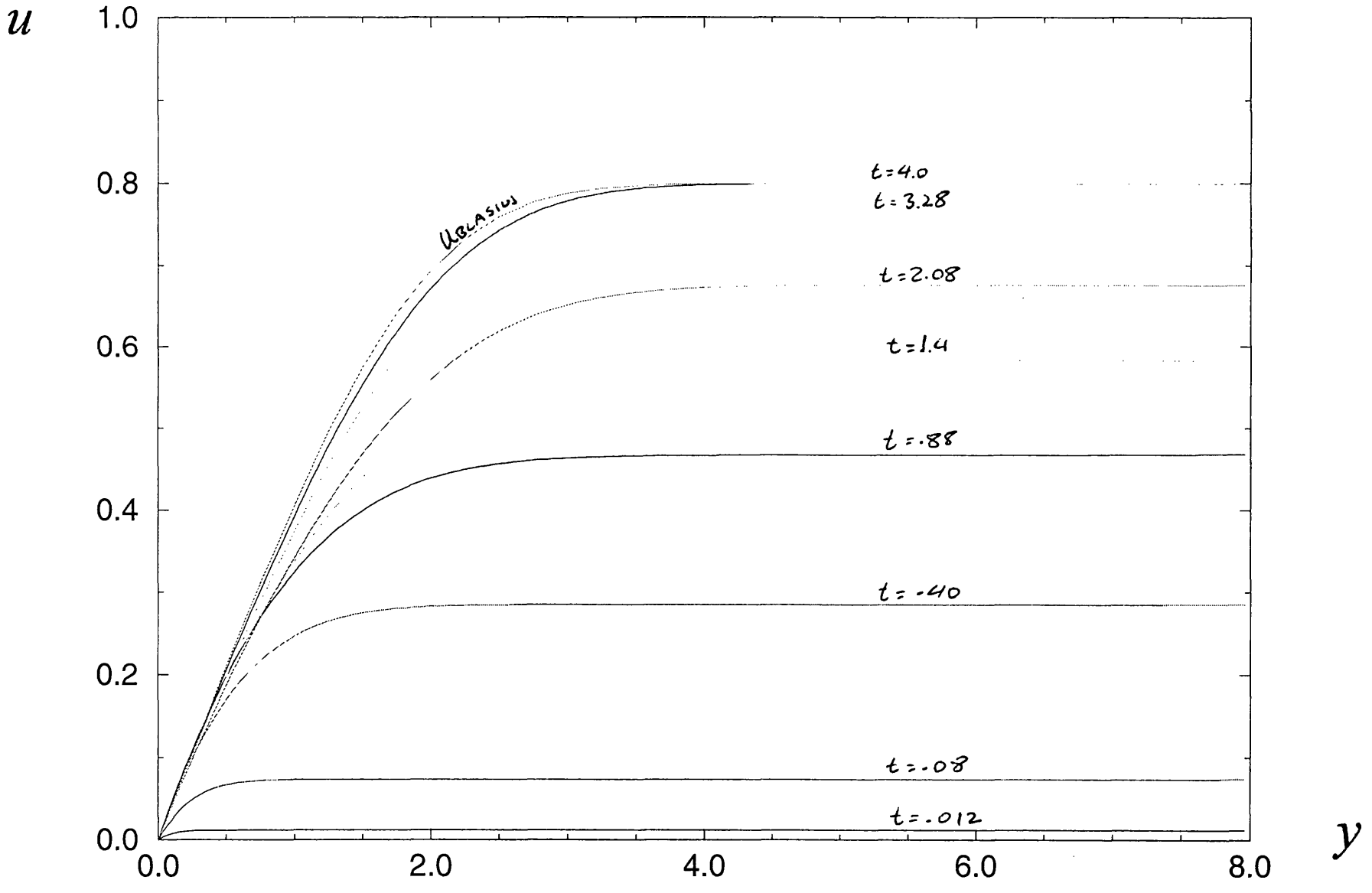


Fig. 3.25 Variation of $u$ with $y$, compared with the Blasius solution ($dx$=0.008, $dy$=0.04, $dt$=0.004).

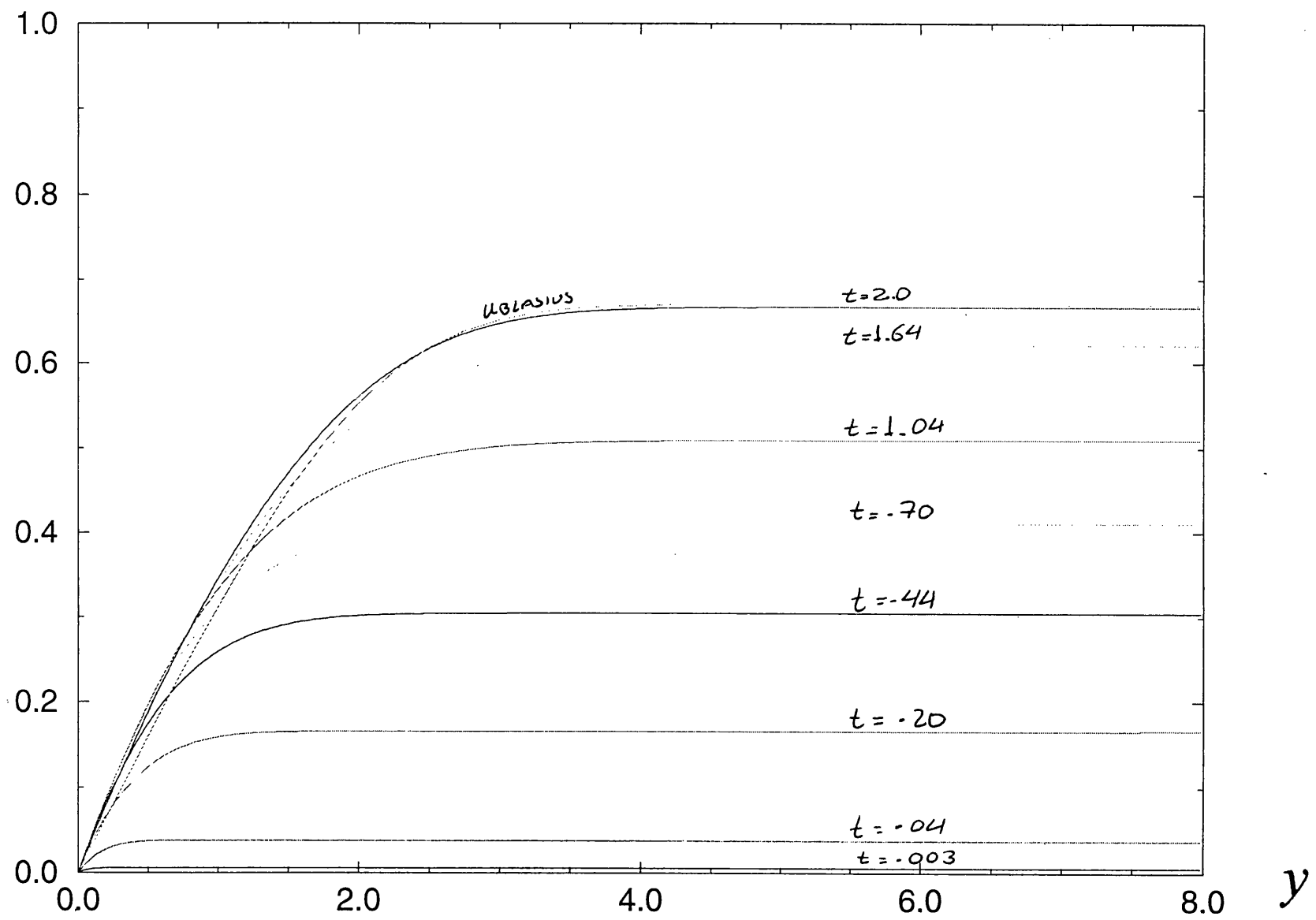


Fig. 3.26 Variation of $u$ with $y$, compared with the Blasius solution ($dx$=0.004, $dy$=0.02, $dt$=0.002).

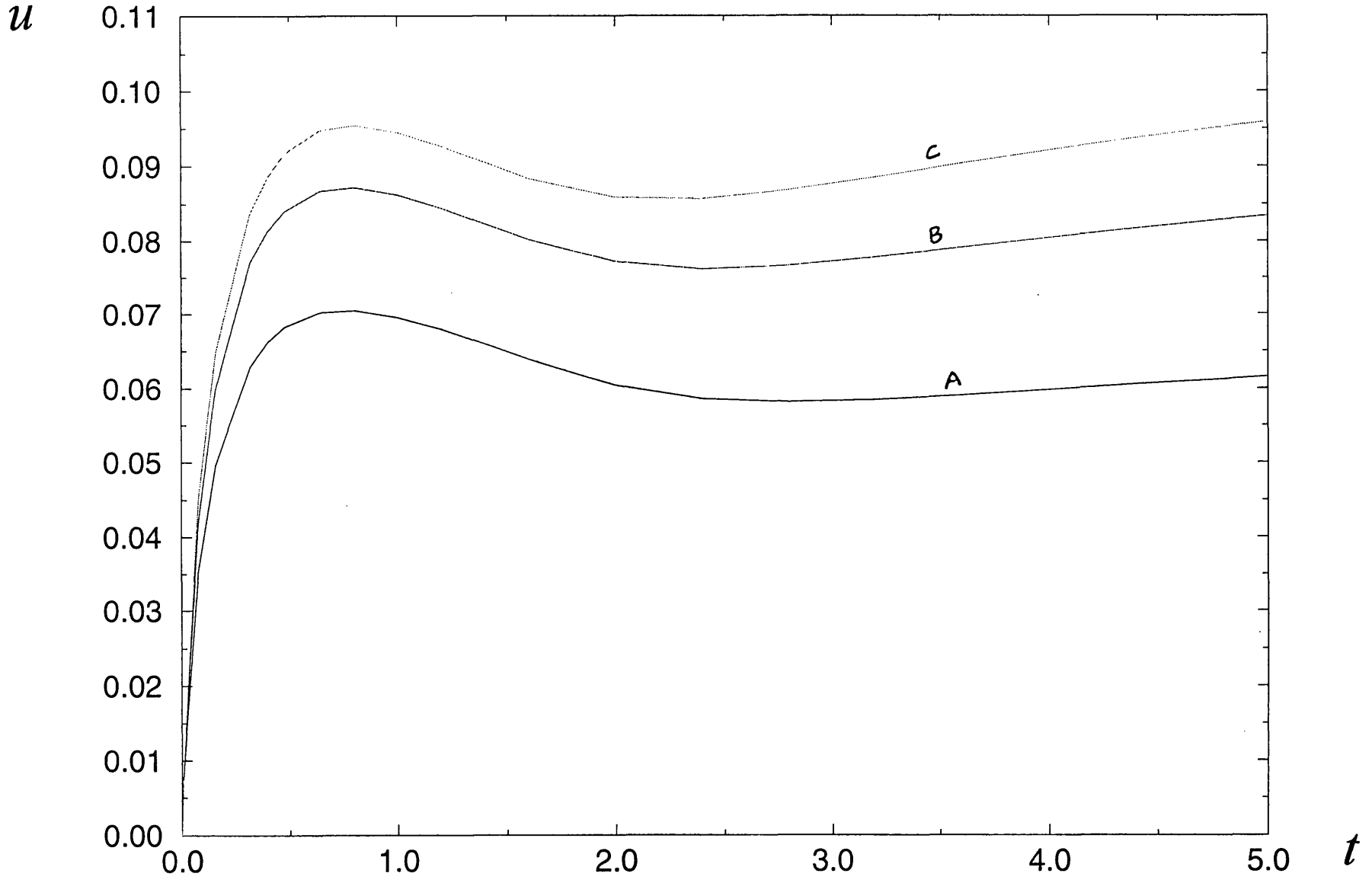


Fig. 3.27 Variation of $u$ with time for the three grids.

# PART B:

# THE SHIP-SIDE MOTION PROBLEM

# CHAPTER 4

## The downward vertical ship-side motion problem

### 4.1 Introduction

We now address a fairly fundamental application or applied problem, involving modelling. Our concern in the next few chapters is with the fluid (water) flow induced by the downward motion of a vertical flat solid surface, referred to herein as the ship-side. Initially, the ship-side and the water are at rest, at time $t=0$. The water then occupies the quarter plane $x>0$, $y<0$, as shown in figure 4.1.

Above the water, the fluid (air) motion is assumed to be dynamically negligible throughout, with the dominant stress forces there being only those due to uniform atmospheric pressure. The water surface acts as a free surface, with standard free surface conditions holding there (Batchelor 1967, Brotherton-Ratcliffe and Smith 1989, and see shortly below), and the evolution of this free surface for positive times $t$ is to be found.

The governing equations, in general, are the continuity and unsteady Navier-Stokes equations

$$\frac{\partial u}{\partial x}+\frac{\partial v}{\partial y}=0, \tag{4.1a}$$

$$\frac{\partial u}{\partial t}+u\frac{\partial u}{\partial x}+v\frac{\partial u}{\partial y}=\hat{g}-\frac{\partial p}{\partial x}+\mathrm{Re}^{-1}\nabla^2 u, \tag{4.1b}$$

$$\frac{\partial v}{\partial t}+u\frac{\partial v}{\partial x}+v\frac{\partial v}{\partial y}=-\frac{\partial p}{\partial y}+\mathrm{Re}^{-1}\nabla^2 v \tag{4.1c}$$

for the assumed two-dimensional flow of the water, which is taken to be incompressible. Here $\nabla^2$ denotes the Laplacian operator $\frac{\partial^2}{\partial x^2}+\frac{\partial^2}{\partial y^2}$, and $\hat{g}\equiv\frac{g\hat{L}}{\hat{U}^2}$ represents the normalized gravity force, related to the Froude number: see in chapter 1

and in (4.30) below. The Reynolds number is given by $\mathrm{Re} \equiv \frac{\hat{U}\hat{L}}{\nu}$, in terms of a characteristic dimensional velocity $\hat{U}$ and length $\hat{L}$ of the ship-side and the kinematic viscosity $\nu$ of the water [Lamb (1932)].

The appropriate boundary conditions are that, first, the velocity $(u,v)$ of the water at the (given) ship side is equal to that of the side itself (condition 1), i.e. there is no slip; second, at the unknown water surface (conditions 2a-c) there is zero tangential stress, the pressure $p$ is atmospheric wherever the radius of curvature of the free surface is relatively large (this is seen below to be almost everywhere, at high Reynolds numbers) and the kinematic condition on the velocity field is satisfied, i.e. no fluid particle can leave the free surface; and, third, the water is at rest ($u,v$ tend to zero) far from the ship side (condition 3). The precise free-surface conditions 2a-c read, respectively,

$$(u_y + v_x)(1-\eta_x{}^2) = 2(u_x - v_y)\eta_x,$$

$$p = \frac{2}{\mathrm{Re}(1+\eta_x{}^2)}\left(u_x\eta_x{}^2 - (u_y + v_x)\eta_x + v_y\right),$$

$$v = \eta_t + u\eta_x,$$

for a free surface at $y = \eta(x,t)$ say, with negligible surface tension. The contact point, where the water intersects the ship-side, is assumed here to have no movement relative to the ship side. In addition, there is a boundary condition to apply underneath the ship-side, if the side is to be treated as one of finite length, as considered subsequently (condition 4).

At high Reynolds numbers the controlling equations (4.1a-c) reduce to the boundary layer equations in a water layer near the ship side and to the potential flow equations in the water outside that layer, as examined below. An outer sub-region also occurs. The various layers or regions are considered in turn in this chapter, together with the matching conditions between them and the other appropriate boundary conditions. The upper free surface (the shape of the majority of the water surface, away from the

ship-side) and the side free surface (the shape of the water surface close to the ship side) of the water are thereby determined.

The unsteady viscous boundary layer equations are found to hold near the ship-side (for some finite time interval at least), then, whereas in the rest of the flow the inviscid Euler equations apply, leading to potential-flow properties. The application of the unsteady boundary layer equations in the present context of ship-side motions forms the anticipated connection with the work of chapters 2-3 on numerical solutions.

The aim of this part of the research is to predict, amongst other things, the resulting shape of the upper free surface of the water produced by the moving ship-side as the upper free surface evolves with the passage of time $t$. The initial state is shown below in Figure 4.1 before any motion of the ship-side occurs. The atmospheric pressure is taken to be zero without loss of generality, and in the water the pressure $p$ is $\hat{g}$ times $x$ initially since the density of the water has been normalized to unity in essence. The velocities $u,v$ are initially zero. The initial state is thus consistent with (4.1 a-c) and the boundary conditions described above.

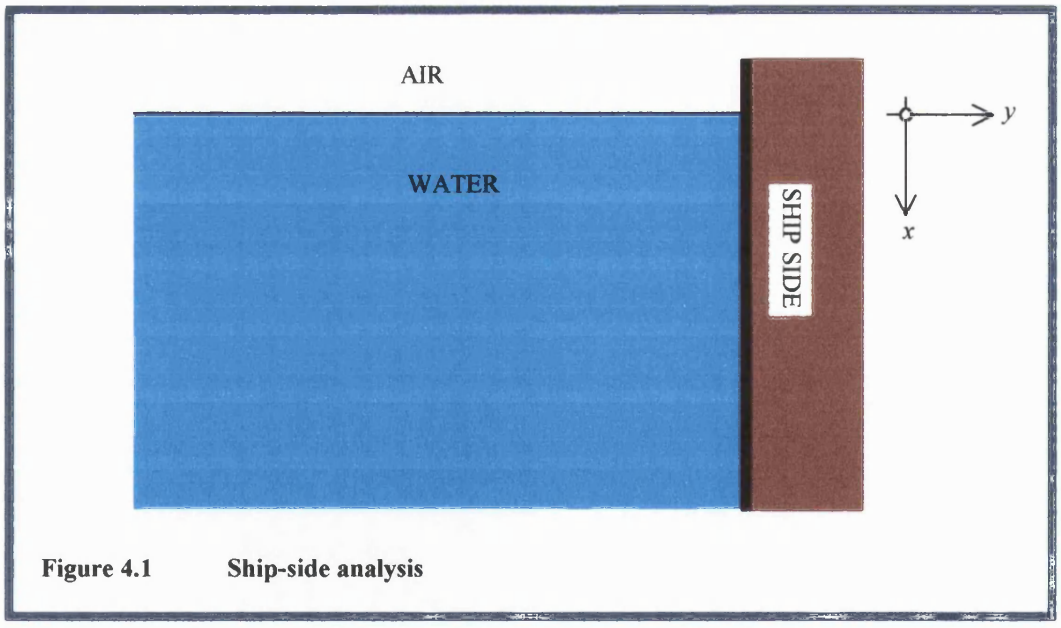


**Figure 4.1** **Ship-side analysis**

The motion of the vertical ship-side may be analysed first in the two central cases that are of interest here, which are the downward and upward motions, respectively. The

first case is considered in chapters 5 and 6, and the second case is briefly addressed in chapter 9.

## 4.2 The ship-side falls vertically

This case holds when the ship-side is moving vertically downwards, i.e. the relative velocity of the water corresponds to the adjacent fluid moving upwards. We will study this problem using the main regions, which are defined by figure 4.2, for high Reynolds numbers.

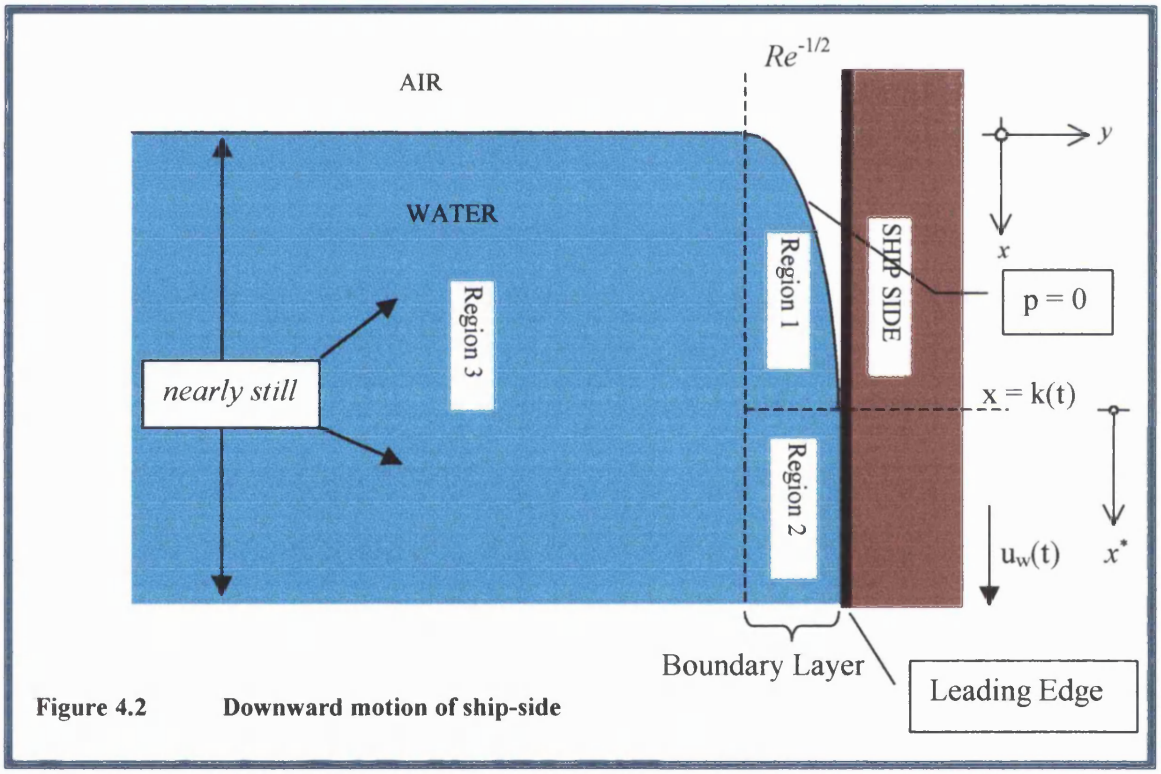


**Figure 4.2 Downward motion of ship-side**

The body of water flow next to the ship-side is divided into three regions labeled 1 to 3, respectively. Regions 1 and 2 constitute the boundary layer region, and region 3 the remainder of the body of water which is expected to be nearly still. The fixed spatial coordinate system $x$, $y$ has its origin at the geometric intersection of the water surface level and the ship-side wall at the initial time. Additionally, the $x^*$ coordinate direction is defined with its origin (at the ship side) corresponding to the region 1-region 2 interface, which is also known as the "contact point" by virtue of the fact that the water and air meet the ship-side wall at this point and which, as we have noted

already, is taken to move with the ship side velocity, so that there is no slip of the contact point relative to the ship side. This point is defined by a given function $k(t)$ say ($x=k(t)$) since the vertical position of the point is a prescribed function of time.
An important boundary condition (condition 2b) is that the pressure is equal to zero in the water at the side free surface in region 1, in view of the thin layer of air assumed to be immediately adjacent to the ship side in which the pressure is zero, by definition. The downward velocity of the ship-side $u_w(t)(=k'(t))$, given as a function of time, is also indicated. The lower edge of the ship-side corresponds, by analogy, to the leading edge of the flat plate. In essence we take here a symmetric-flow configuration, for convenience, corresponding to a thin vertical flat plate moving downwards in the water, so that on the x-axis underneath the leading edge where $y$ is zero $v$ must be zero for symmetry.

## 4.3 Investigation of the various regions

Regions 1 and 2 of the analysis are considered successively below, taking into account the various associated boundary conditions, while outer region 3 is considered in Chapter 5. Each region will be analysed separately using the unsteady two-dimensional boundary layer or potential flow equations suitably. Extensions of earlier analyses for external flow past a flat plate will be made in order to perform the overall analysis of the current ship-side problem.

For all the ship-side problems, the Reynolds number $Re$ is taken to be large. Further, in the analysis given below, the gravity force is included in part of the working for completeness, but in fact is later taken to be either negligible or small. Also, partly to clarify, the time is assumed to be positive, $t>0$, gravity $g$ is constant, and $u,v$ are the $x$-, $y$- velocity components.

### 4.3.1 Region 1

In this region, defined by $0 < x < k(t)$ and $y = O(\mathrm{Re}^{-1/2})$, we start with the flow equations and the boundary conditions, as well as the initial conditions. Thus $y = \mathrm{Re}^{-1/2} Y$ say, with $Y$ of $O(1)$, and we are seeking to determine the motion of the water near the ship-side.

The governing flow equations become

$$u_t + uu_x + Vu_Y = \hat{g} + u_{YY}, \tag{4.2a}$$

$$u_x + V_Y = 0, \tag{4.2b}$$

from a classical boundary-layer argument applied to (4.1a-c), with $v$ expressed as $\mathrm{Re}^{-1/2} V$ and with $V$ of order unity for the balance of continuity. In addition, the side free surface is assumed to be close to the ship side within a normal distance of order $\mathrm{Re}^{-1/2}$ at characteristic $O(1)$ values of $x$. The y-momentum equation (4.1c) yields $\partial p/\partial Y$ being zero, in effect, leaving $p$ independent of $Y$; but then the side-free-surface requirement of zero (atmospheric) pressure mentioned earlier (condition 2b) dictates that $p$ must be identically zero; hence only the $\hat{g}$ term remains on the right side of (4.2a), next to the dominant viscous term which is $\partial^2 u/\partial Y^2$. The boundary conditions are

$$u \to [u - edge] \text{ as } Y \to -\infty, \tag{4.3}$$

where $u$-edge is zero if $\hat{g}$ is negligible, for matching to the far-field flow.

In order to obtain the free surface condition, we require the function $q(x,y,t)$ to be constant. The condition then is $dq/dt = 0$, which implies

$$\frac{\partial q}{\partial t} + u\frac{\partial q}{\partial x} + v\frac{\partial q}{\partial y} = 0. \tag{4.4}$$

So, we may write $q = f - Y$ at $Y = f(x,t)$, to obtain

$$u_Y = 0,\ V = f_t + uf_x. \tag{4.4a}$$

In place of the latter condition, we may write, also, $q = F - x$ to obtain

$$u = F_t + VF_Y \text{ at } x = F(Y,t). \tag{4.4b}$$

Here $f(x,t)$ is an unknown scaled (shape) function of the vertical fixed spatial axis and time, and $F(Y,t)$ is an unknown scaled (shape) function of the horizontal fixed spatial axis and time. The first of the boundary conditions (equation 4.3) is, in the case of negligible gravity, the far-field condition (condition 3) that holds at a sufficiently large horizontal distance from the ship-side. The latter boundary conditions (equations 4.4a,b) describe conditions 2a,c, including the unknown shape $f$ of the side free surface, which is separated from the ship-side wall. We shall discuss (4.3) more later in the thesis but we note for now that $u$ = [$u$-edge] satisfies the nonlinear equation $\frac{\partial u}{\partial t} + u\frac{\partial u}{\partial x} = \hat{g}$ for general $\hat{g}$ values, in view of (4.2a).

The initial conditions are

$$u = V = 0 \text{ for } t = 0, \tag{4.5}$$

which correspond to the flow starting from a state of rest.

### 4.3.2 Region 2

In the adjacent region 2, defined by $x > k(t)$ above the leading edge, in accordance with the moving ship side, similarly we have $\partial p/\partial Y$ being negligible and so

$$p = \hat{g}(x - k(t)) \tag{4.6}$$

to match with the bulk of the water. As in the previous subsection the governing flow equations for this region become

$$u_t + uu_x + Vu_Y = \hat{g} - p_x + u_{YY}, \tag{4.7}$$

$$u_x + V_Y = 0, \tag{4.8}$$

from the orders of magnitude in (4.1a-c) again. Clearly however $\hat{g}$ and $-p_x$ cancel out in (4.7) due to the relation (4.6).

The associated boundary conditions are

$$u = u_w(t), V = 0 \tag{4.9}$$

at $Y = 0$ (no-slip wall conditions) and

$$u \to 0 \text{ as } Y \to -\infty \tag{4.10}$$

for matching to the far-field flow.

Boundary condition (4.9) stipulates that there is no slip at the ship-side wall (condition 1). This means that there the downward velocity of the water is equal to that of the ship-side, $u_w(t) = k'(t)$, and there is no transverse water velocity component. Boundary condition (4.10) stipulates that the water velocity tends to zero in the far-field, where there is virtually no motion (condition 3). In addition, the initial condition is

$$u = V = 0 \text{ for } t = 0, \tag{4.11}$$

corresponding to starting from rest.

Now we substitute into the flow equations (4.7) and (4.8) the coordinate shift

$$x = k(t) + x^*. \tag{4.12}$$

Then (4.7) and (4.8), with (4.6), become

$$u_t + uu_{x^*} + Vu_Y - k'u_{x^*} = 0 + u_{YY}, \tag{4.13}$$

$$u_{x^*} + V_Y = 0. \tag{4.14}$$

Also, we put

$$\overline{u} = u - k'(t), \tag{4.15a}$$

$$\overline{\Psi} = \Psi - k'(t)Y, \tag{4.15b}$$

and

$$\overline{F} = F - k(t), \tag{4.15c}$$

which yield the final equations

$$\overline{u}_t + \overline{u}\overline{u}_{x^*} + V\overline{u}_Y = -k''(t) + \overline{u}_{YY}, \tag{4.16}$$

$$\overline{u}_{x^*} + V_Y = 0, \tag{4.17}$$

together with the boundary conditions

$$\overline{u} = 0, V = 0 \text{ at } Y = 0, \tag{4.18}$$

$$\overline{u} \to -k'(t), \text{ as } Y \to -\infty, \tag{4.19}$$

and the initial condition

$$\overline{u} = -k'(0) \text{ at } t = 0. \tag{4.20}$$

Here we observe that the final set of equations given above, i.e. (4.16)-(4.20), apply for the interval $0 < x^* < x^*_{LE}$ where $x^*_{LE}$ denotes the constant leading edge value of $x^*$.

Next, we return to region 1 and make the same transformation as was made for region 2. The following equations are thus obtained for region 1:

$$\overline{u}_t + \overline{u}\overline{u}_{x^*} + V\overline{u}_Y = -k''(t) + \hat{g} + \overline{u}_{YY}, \tag{4.21}$$

$$\overline{u}_{x^*} + V_Y = 0, \tag{4.22}$$

from (4.2a,b), along with the boundary conditions, from (4.3), (4.4a,b),

$$\overline{u} \to -k'(t) + [u - edge] \text{ as } Y \to -\infty. \tag{4.23}$$

and $$\overline{u}_Y = 0, \overline{u} + k' = F_t + VF_Y - k'Fx^* \text{ at } x^* = F - k, \tag{4.24}$$

i.e. $$\overline{u}_Y = 0, \overline{u} + k' = \overline{F}_t + k' + V\overline{F}_Y - k'\overline{F}_{x^*} \text{ at } x^* = \overline{F}, \tag{4.24a},$$

where $\overline{F} = F - k$,

i.e. $$\overline{u}_Y = 0, \overline{u} = \overline{F}_t + V\overline{F}_Y \text{ at } x^* = \overline{F}. \tag{4.24b}$$

The above equations (4.21-4.24) for region 1 apply for $-k(t) < x^* < 0$ (or $0 < x < k(t)$), but $-\infty < y \leq \bar{f}(x^*,t)$ say, where $\bar{f}$ is negative.

The final equation set (4.16-4.20) of region 2 which is to be solved is exactly the same as the equation set of chapter 2 that describes the external boundary layer flow past an aligned flat plate (i.e. the Blasius-Rayleigh form), for any $\hat{g}$ value. Moreover, the equations (4.21)-(4.24b) will be shown in the next section to correspond to those of an external aligned (i.e. Goldstein type) wake, if $\hat{g}$ is zero. The assumption of effectively zero gravity in the analysis will be discussed more later. Thus, region 1 corresponds to a wake region, with the contact point (at the region 1-region 2 interface) corresponding to the trailing edge. Region 2 corresponds to the main flat plate area. Further, the lower edge of the ship-side wall in region 2 represents the leading edge of the plate.

The direct correspondence between the present ship-side problem for zero $\hat{g}$ and the earlier flat plate problem means that the computational work required here is a natural extrapolation of the research performed in part A of the thesis. However, the differing boundary conditions involving $u_w(t)$ can yield a different flow pattern in general.

## 4.4 Initial application to the ship side [Regions 1-2]

This application to the ship-side motion is the well-known impulsive start problem. The problem is defined by the following conditions: $k(t) = \Gamma t$ and $u_w = \Gamma$, where $\Gamma$ is a positive constant.

In this problem $u_w$ is independent of $x^*$, which makes the whole flow problem of region 2 the same as for the flat-plate boundary layer problem of chapter 2. The equations (4.16)-(4.20) must now be solved, but for a different coordinate system and velocities, which are for this example $-x^*, -Y$ and $-\bar{u}, -V$, respectively.

The solution for region 2 then gives the starting profile ($\bar{u}$) for region 1. Therefore in the wake region 1, we have to solve equations (4.21)-(4.24b) for the interval $0 < (-x^*) < \Gamma t$, with the profile $\bar{u}$ defined as that at the trailing edge of the ship-side

at $x^* = 0$ (figures 4.3-4). For sufficiently small times, this value ($\overline{u}$) is given by the Rayleigh profile as noted in chapter 3.

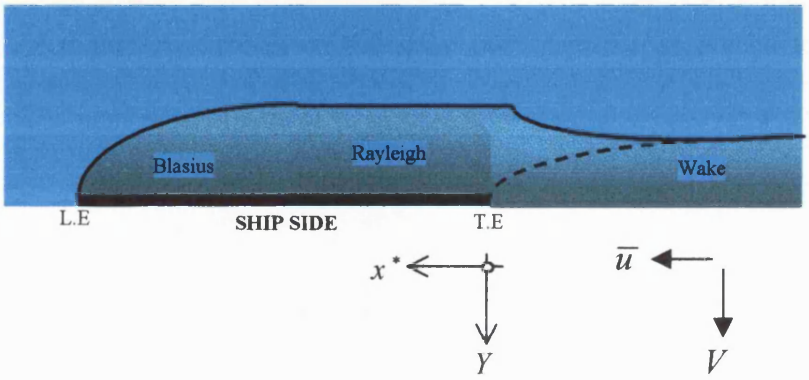


**Figure 4.3** **Forms of viscous boundary layer and wake regions**

The issue here is how we may now solve equations (4.21)-(4.24b) applied to this example, which are:

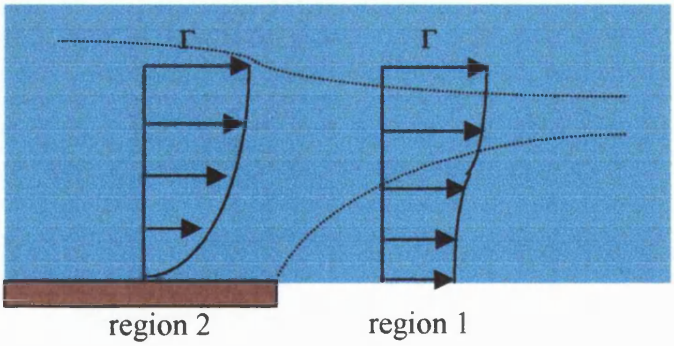


**Figure 4.4** **Velocity profiles for regions 1 and 2**

$$\overline{u}_t + \overline{u}\overline{u}_{x^*} + V\overline{u}_Y = \hat{g} + \overline{u}_{YY}, \tag{4.25}$$

$$\overline{u}_{x^*} + V_Y = 0, \tag{4.26}$$

with the associated boundary conditions

$$\overline{u} \to -\Gamma + [u - edge] \text{ as } Y \to -\infty, \tag{4.27}$$

$$\overline{u}_Y = 0, \tag{4.28}$$

and,

$$\overline{u} = \overline{F}_t + V\overline{F}_Y \text{ at } x^* = \overline{F}(Y,t). \tag{4.29}$$

The gravity term $\hat{g}$ here acts as a pressure gradient which is favourable in the $x^*$ (downward) direction, as expected both from physical consideration and from our comment just prior to (4.5), for the wake only (region 1), whereas it is effectively absent in the boundary layer of region 2. However, as indicated earlier, we will neglect the gravity contributions for now (we return to them in chapter 7). We introduce the Froude number,

$$Fr \equiv \frac{\hat{U}^2}{g\hat{L}}, \tag{4.30}$$

in line with the definition described in chapter 1.

Thus, in equations (4.25)-(4.29), neglecting the gravity effect is associated with $Fr$ (which is equal to $\hat{g}^{-1}$, according to (4.30) if $Fr$ is $\frac{\hat{U}^2}{g\hat{L}}$, and using page 115) being large. The neglect of gravity here also makes the boundary condition (4.27) become $\overline{u} \to -\Gamma$ at large negative $Y$, since [$u$-edge] is then zero, consistent with the governing equations.

We now transform the coordinates and velocity components by inverting the coordinate direction of $x^*$ with $\hat{x}$, which is negative downwards, so that

$$\left.\begin{aligned} \hat{V} &= -V, \\ \hat{Y} &= -Y, \\ \hat{\Psi} &= \overline{\Psi}, \\ \hat{u} &= -\overline{u}, \\ \hat{x} &= x^*_{LE} - x^* \end{aligned}\right\} \tag{4.31}$$

We know that at the edge of the boundary layer, the displacement in regions 1 and 2 may be written as $\hat{\Psi} \approx \hat{Y} - \delta$. In chapter 3 we have calculated the wake displacement δ. Thus using the coordinate transformation of (4.31) the displacement becomes $\overline{\Psi} \approx -Y - \delta$. So in equation (4.15b), we find that

$$\Psi \approx (-Y - \delta) + k'(t)Y . \tag{4.32}$$

Thus, due to the fact that $k' = \Gamma = 1$ here, we obtain from (4.32) the result

$$\Psi \to -\delta \tag{4.33}$$

at the outer edge of the viscous layers.

The equations now become

$$\hat{u}_t + \hat{u}\hat{u}_{\hat{x}} + \hat{V}\hat{u}_{\hat{y}} = 0 + \hat{u}_{\hat{y}\hat{y}}, \tag{4.34}$$

$$\hat{u}_{\hat{x}} + \hat{V}_{\hat{y}} = 0, \tag{4.35}$$

with the boundary conditions

$$\hat{u} \to \Gamma - [u - edge] \text{ as } \hat{Y} \to +\infty, \tag{4.36}$$

$$\hat{u}_{\hat{y}} = 0 \text{ at } \hat{Y} = \hat{f}(\hat{x},t), \tag{4.37}$$

and

$$\hat{V} = \hat{f}_t + \hat{u}\hat{f}_{\hat{x}} \text{ at } \hat{Y} = \hat{f}(\hat{x},t). \tag{4.38}$$

We note that almost all the negative signs cancel out here due to the $x^*$-axis inversion of equations (4.31).

Finally, we apply the Prandtl transposition (see Rosenhead 1963), and we introduce $\tilde{Y}$, $\tilde{V}$ as moving coordinates,

$$\hat{Y} - \hat{f} = \tilde{Y}, \tag{4.39a}$$

$$\hat{V} = (\hat{f}_t + \hat{u}\hat{f}_{\hat{x}}) + \tilde{V}. \tag{4.39b}$$

Under the transformation $(x^*, Y, t) \to (\hat{x}, \hat{Y}, t)$ we observe that

$$\left.\begin{aligned} \partial_{\hat{x}} &\to \left(\frac{\partial \tilde{Y}}{\partial \hat{x}}\right)(-\hat{f}_x)\partial_{\tilde{Y}} + \partial_{\hat{x}}, \\ \partial_{\hat{Y}} &\to \partial_{\tilde{Y}}, \\ \partial_t &\to \partial_t + \left(\frac{\partial \tilde{Y}}{\partial t}\right)(-\hat{f}_t)\partial_{\tilde{Y}}. \end{aligned}\right\} \tag{4.40}$$

So now the equations (4.34), (4.35) become

$$\hat{u}_t + \hat{u}\hat{u}_{\hat{x}} + \tilde{V}\hat{u}_{\tilde{Y}} = \hat{u}_{\tilde{Y}\tilde{Y}}, \tag{4.41a}$$

$$\hat{u}_{\hat{x}} + \tilde{V}_{\tilde{Y}} = 0, \tag{4.41b}$$

with the boundary conditions (neglecting $\hat{g}$ again)

$$\hat{u} \to \Gamma \text{ as } \tilde{Y} \to +\infty, \tag{4.42}$$

$$\hat{u}_{\tilde{Y}} = 0 \text{ at } \tilde{Y} = 0, \tag{4.43}$$

$$\tilde{V} = 0 \text{ at } \tilde{Y} = 0, \tag{4.44}$$

since (4.38) yields $\hat{f}_t + \hat{u}\hat{f}_{\hat{x}} + \tilde{V} = \hat{f}_t + \hat{u}\hat{f}_{\hat{x}}$ at $\tilde{Y} = 0$ and so the terms in $\hat{f}$ cancel out.

The positive constant $\Gamma$ can be normalized to unity without loss of generality. Hence we obtain precisely the earlier wake problem for an aligned flat plate, as applied to this example of an impulsively started ship-side.

Therefore the entire flow solution in regions 1 and 2 for negligible gravity is exactly that determined earlier in Part A for uniform flow past an aligned finite flat plate. It is interesting that the free-surface shape, $\hat{f}(\hat{x}, t)$, of the water-air interface is not

determined through this means, as it is removed from the problem through the Prandtl transposition described above. The boundary layer and wake displacement $(\mathrm{Re}^{-1/2})\cdot\delta(x,t)$ will be analysed in the next chapter.

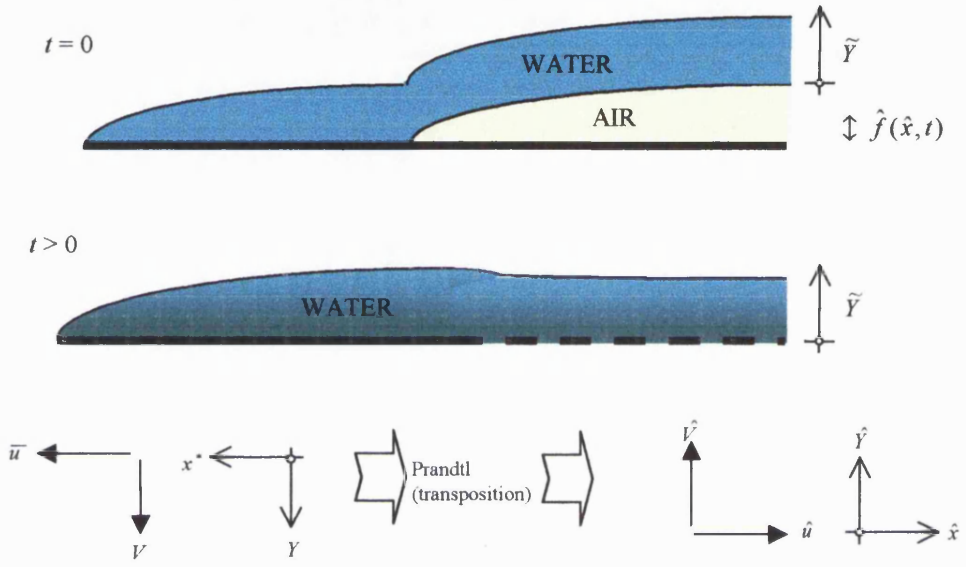


**Figure 4.5 Transposition for time t=0 and t>0**

# CHAPTER 5

# Modeling and analysis of downward vertical ship-side motion (continued)

## 5.1 Introduction

The flow problem of the ship-side described in section 4.4 was concluded to be equivalent to that for the wake behind a flat plate (or the Rayleigh solution for sufficiently early times), if the gravity effect is small. This is exactly as studied in chapters 2-3 (Part A of the thesis) and it means that, at least in the beginning, we effectively have the unsteady flow due to an impulsively started flat plate of finite length. The leading edge of the plate has a small Navier-Stokes region and the trailing edge has a small triple-deck region. The flow, as before, is near-Blasius in the neighbourhood of the leading edge and, further downstream, the flow on the plate essentially becomes of a Rayleigh form, followed by the unsteady wake. The viscous flow solution in the wake region 1 is unaffected by the shape of the side surface of the water, except in so far as the Prandtl transposition holds. The determination of the side free surface is really part of the outer inviscid problem of region 3, which is controlled by the small efflux conditions or small displacements that emerge from the solution in the viscous regions 1 and 2.

Our main aim in this chapter is to determine the flow field adjacent to the ship-side, consisting of the combined regions 1, 2 and the further outward region 3. This depends on a function of both the vertical spatial coordinate and of time, say $h(\hat{x},t)$, representing the small viscous displacement mentioned above.

## 5.2 Development of outer region problem

For conciseness, we denote the spatial fixed axes as $(\hat{x},\hat{y})$ and the velocity components as $Re^{-1/2}(\hat{u},\hat{V})$ as shown in figure 5.1. This is distinct from the notation in chapter 4 but the overlap between the inner and outer regions is relatively simple, as we will see.

In the region 3 (the "outer region") we obtain from (4.1a-c) the equations:

$$\hat{u}_{\hat{x}} + \hat{V}_{\hat{y}} = 0\,, \tag{5.1}$$

$$\hat{u}_{t} = -p_{\hat{x}}\,, \tag{5.2}$$

$$\hat{V}_{t} = -p_{\hat{y}}\,. \tag{5.3}$$

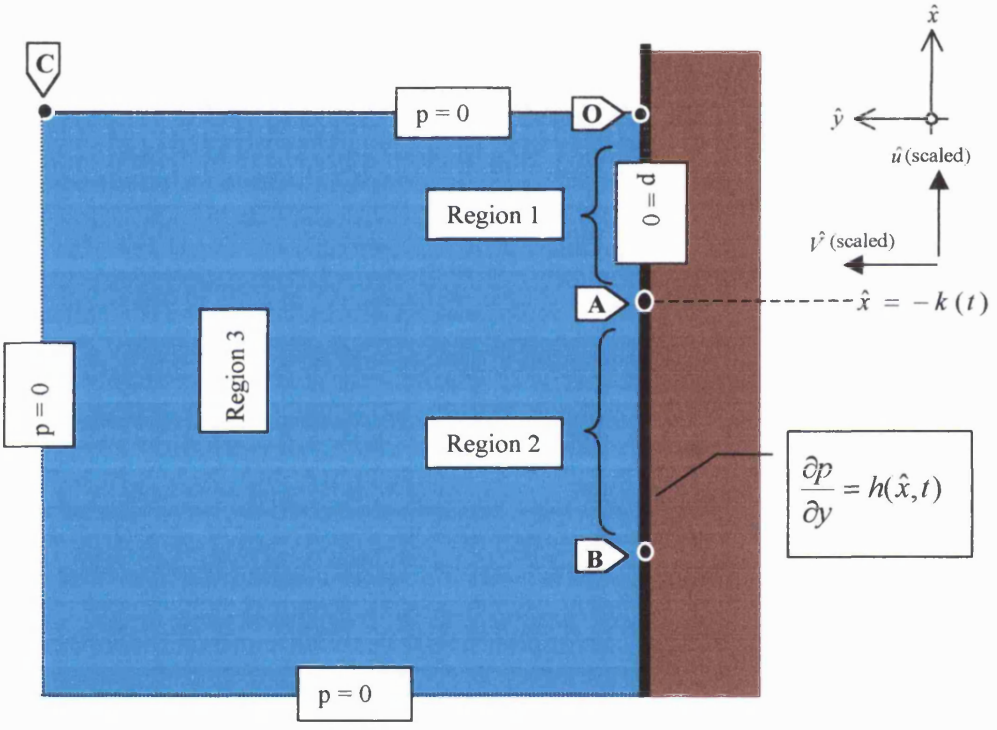


**Figure 5.1** **Domain of analysis showing regions**

The nonlinear advection terms are negligible here because the velocity components are small, and the viscous terms are negligible because of the order-one spatial scales, while $\hat{g}$ is omitted for now, based on the assumption of a sufficiently large Froude number. We note that $\hat{u}, \hat{V}, p$ are all typically of order unity.

Equations (5.1)-(5.3) in the water yield

$$-p_{\hat{y}\hat{y}} - p_{\hat{x}\hat{x}} = \hat{V}_{\hat{y}t} + \hat{u}_{\hat{x}t} = 0. \tag{5.4}$$

So the unknown pressure satisfies Laplace's equation in $\hat{x}$, $\hat{y}$,

$$\nabla^2 p = 0, \tag{5.5}$$

as expected in potential flow.

Also, from the continuity and $\hat{x}$-momentum balances we have

$$\hat{u}_{\hat{x}t} \equiv -p_{\hat{x}\hat{x}} \Rightarrow \hat{V}_{\hat{y}t} \equiv p_{\hat{x}\hat{x}}, \tag{5.6}$$

while from the $\hat{y}$-momentum balance

$$\hat{V}_{\hat{x}t} \equiv -p_{\hat{x}\hat{y}}. \tag{5.7}$$

Hence we have similarly $\hat{V}_t$ satisfying Laplace's equation $\nabla^2 \hat{V}_t \equiv 0$, as does $\hat{V}$ in view of the start from rest, and in addition

$$\partial_{\hat{x}}(p_{\hat{x}}) \equiv \partial_{\hat{y}}.(\hat{V}_t) \tag{5.8}$$

and

$$\partial_{\hat{y}}(p_{\hat{x}}) \equiv -\partial_{\hat{y}}.(\hat{V}_t). \tag{5.9}$$

Thus the Cauchy-Riemann equations hold between $p_{\hat{x}}$ and $\hat{V}_t$. So a complex potential function to control the problem may be defined as $p - i\Psi_t$, which is analytic in $\hat{z}(\equiv \hat{x} + i\hat{y})$, say $\Im(\hat{z})$, with the stream function $\Psi$ now satisfying $\hat{u} = \Psi_{\hat{y}}$ and $\hat{V} = -\Psi_{\hat{x}}$.

The boundary conditions, as shown by figure 5.1, are that the pressure $p$ is prescribed to be zero on side COA and $p_{\hat{y}} = -\hat{V}_t (= \Psi_{\hat{x}t})$ is prescribed as $h(\hat{x},t)$ on side AB, while the water is at rest in the far-field (condition 3). Thus $h = \Psi_{\hat{x}t}$ along AB.

To solve the flow problem we may now introduce a conformal transformation, which allows consideration of the problem in an upper ½-plane instead of the original ¼-plane. It should be noted that an alternative approach to the conformal mapping would be to perform a reflection about the $\hat{y}$-axis in an image system.

The mapping is

$$\bar{z} = -\hat{z}^2. \tag{5.10}$$

The mapped coordinate system is now defined by the polar coordinates $\bar{r}, \bar{\theta}$, so that

$$\bar{r}e^{i\bar{\theta}} = \hat{r}^2 e^{2i\hat{\theta}} e^{-i\pi}, \tag{5.11}$$

where $\hat{z} = \hat{r}e^{i\hat{\theta}}$, $\bar{z} = \bar{r}e^{i\bar{\theta}}$, and hence we have

$$\bar{r} = \hat{r}^2, \tag{5.12}$$

$$\bar{\theta} = 2\hat{\theta} - \pi \tag{5.13}$$

(see also Milne-Thompson 1968).

So on the BAO portion we obtain from (5.13)

$$\hat{\theta} = \pi \Rightarrow \bar{\theta} = \pi, \tag{5.14}$$

and on the OC portion we have

$$\hat{\theta} = \frac{\pi}{2} \Rightarrow \bar{\theta} = 0, \tag{5.15}$$

as shown in figure 5.2.

The new interval is $0 < \bar{\theta} < \pi$, with $0 < \bar{r} < \infty$, for the outer region water flow. The mapping into the $\bar{z}$-plane gives us again Laplace's equation, $\bar{\nabla}^2 p = 0$, in the ½-plane,

where $\bar{\nabla}^2$ denotes the operator $\frac{\partial^2}{\partial \bar{x}^2}+\frac{\partial^2}{\partial \bar{y}^2}$. Also, we require that the pressure $p$ is equal to zero on the $CO$ and $OA$ portions and at infinity (condition 3), while on the $AB$ portion of the axis the derivative $\frac{\partial p}{\partial \bar{y}} = \bar{h}(\bar{x},t)$ is analysed below; thus we have that the boundary conditions on the pressure are of mixed type.

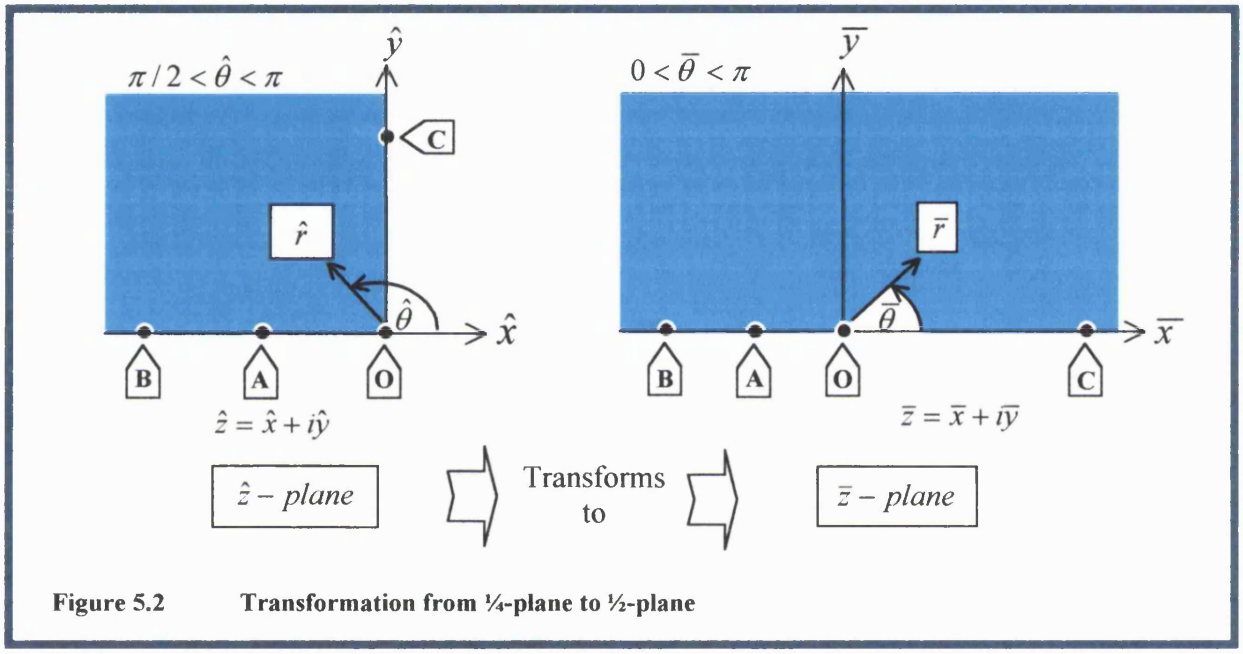


**Figure 5.2** **Transformation from ¼-plane to ½-plane**

We may now proceed using the function $p - i\Psi_t$, as mentioned before. So we have the complex function

$$p - i\Psi_t = \Im(\bar{z}) \tag{5.16}$$

where $\bar{z} = \bar{x} + i\bar{y}$.

In view of the mixed boundary conditions, with their crossover at the point $A$, we define

$$P + iQ = (\bar{z} - \bar{x}_A)^{-1/2}\left[\Im(\bar{z}) - \Im_0\right], \tag{5.17}$$

where

$$(\bar{z} - \bar{x}_A)^{-1/2} = (\bar{\bar{r}}e^{i\bar{\theta}})^{-1/2} \tag{5.18a}$$

$$= \bar{\bar{r}}^{-1/2} e^{-(i\bar{\theta})/2}, \tag{5.18b}$$

in terms of polar coordinates $\bar{\bar{r}},\bar{\bar{\theta}}$ with the origin shifted to $(\bar{x}_A,0)$. We have along the real axis

$$(\bar{z}-\bar{x}_A)^{-1/2} = \begin{cases} \bar{\bar{r}}^{-1/2} & \text{on the right: } \bar{\bar{\theta}}=0, \quad (5.19a) \\ \bar{\bar{r}}^{-1/2}e^{-i\pi/2} & \text{on the left: } \bar{\bar{\theta}}=\pi. \quad (5.19b) \end{cases}$$

We note that an alternative to (5.17) is to work with a ½ power instead of -½ and make allowance for possible non-decay in the far-field, but we choose to use the above method, which yields the same end results. Further, concerning (5.17), $\mathfrak{I}_0$ denotes the value of $\mathfrak{I}(\bar{z})$ at $\bar{z}=\bar{x}_A$. This is expected to be finite and in fact equal to $-i\Psi_t$ there, since $p$ is zero for $\bar{x}$ just above $\bar{x}_A$ and is assumed to be continuous at $\bar{x}_A$. In addition, $-\Psi$ along the ship side and wake can be anticipated to be $\delta$ (to match with regions 1,2 as in (4.33)), which is continuous at the trailing edge $\bar{x}=\bar{x}_A$ from the flow solutions in chapters 2,3 and has a non-zero value, say $\delta=\delta_0(t)$, at the trailing edge. So we allow for the $\delta_0$ factor by subtracting it off in (5.17), where $\mathfrak{I}_0 = i\delta_0'(t)$, leaving $(\mathfrak{I}-\mathfrak{I}_0)$ zero at $\bar{x}=\bar{x}_A$, which then keeps $(P+iQ)$ finite there despite the inverse square root term involved. The solution for $\Psi_t$ appears to be unique. Eigenfunctions associated with far-field circulation for instance, which can arise in aerodynamics, are ruled out here by the mixed boundary conditions on $p$, $\Psi_t$ along the edge of the ¼ plane. Again, $p$ and $\Psi$ are to decay in the far-field, and $\delta_0'$ is finite in general. Hence with the inverse square root in (5.17) the complex function $(P+iQ)$ also decays in the far-field. Continuing from the above we see that

$$(\bar{z}-\bar{x}_A)^{-1/2}[\mathfrak{I}(\bar{z})-\mathfrak{I}_0] = \begin{cases} (\bar{x}-\bar{x}_A)^{-1/2}(p-i\Psi_t+i\gamma_0) : \bar{x}>\bar{x}_A \quad (5.20a) \\ (\bar{x}_A-\bar{x})^{-1/2}(-ip-\Psi_t+\gamma_0) : \bar{x}<\bar{x}_A. \quad (5.20b) \end{cases}$$

where $\gamma_0 = -\delta_0'$. From these equations, we have along the $\bar{x}$-axis for $\bar{x}<\bar{x}_A$

$$P = -(\bar{x}_A - \bar{x})^{-1/2}(\Psi_t - \gamma_0), \tag{5.21}$$

and

$$Q = -(\bar{x}_A - \bar{x})^{-1/2} p. \tag{5.22}$$

Similarly along the $\bar{x}$-axis for $\bar{x} > \bar{x}_A$ we obtain

$$P = (\bar{x} - \bar{x}_A)^{-1/2} p, \tag{5.23}$$

and

$$Q = -(\bar{x} - \bar{x}_A)^{-1/2}(\Psi_t - \gamma_0). \tag{5.24}$$

The right-hand side of (5.23) is zero here, because of the zero pressure condition on COA in figure 5.1. In view of (5.21) and (5.23) we see that the quasi-pressure function $P(\bar{x},0)$ is known for all $\bar{x}$. Also it is assumed that the quasi-pressure variation $P$ tends suitably to zero in the far-field of the outer region 3.

## 5.3 The displacement derivative function $\Psi_t$

We derive as follows an expression for the displacement-like function $\Psi_t$ along the axes based on the aforementioned considerations. We may now employ directly the Cauchy-Hilbert relationship [Christ (1989) and Zayed(1996)],

$$Q(\bar{x}) = \frac{1}{\pi} \int_{-\infty}^{\infty} \frac{P(\bar{\xi})d\bar{\xi}}{(\bar{x} - \bar{\xi})}, \tag{5.25}$$

which gives us $Q$ along the $\bar{x}$-axis. The integral here and in succeeding formulae is the Cauchy principal value.

At this point, we make the problem more definite by introducing a constant $L$, which is the initial length of the submerged ship-side as shown in figure 5.3. The depth of the leading edge of the ship-side measured from the original water surface in the original coordinate system $\hat{x}, \hat{y}$ is given by the depth function $\tilde{L}(t)$, where

$\tilde{L} \equiv (L - \hat{x}_A)$. The location of the leading edge of the plate, that simulates the ship-side, is thus given on the $\hat{x}$-axis by the expression $\hat{x}_B = -\tilde{L}(t) = \hat{x}_A(t) - L$.

In the ½-plane analysis domain, for the region $\bar{x} > \bar{x}_A$ and substituting from equations (5.21) and (5.24), we obtain from equation (5.25) a form applied to the current problem,

$$-(\bar{x} - \bar{x}_A)^{-1/2}[\Psi_t - \gamma_0] = -\frac{1}{\pi}\int_{-\infty}^{\bar{x}_A}(\bar{x}_A - \bar{\xi})^{-1/2}[\Psi_t - \gamma_0]\frac{d\bar{\xi}}{\bar{x} - \bar{\xi}}. \qquad (5.26)$$

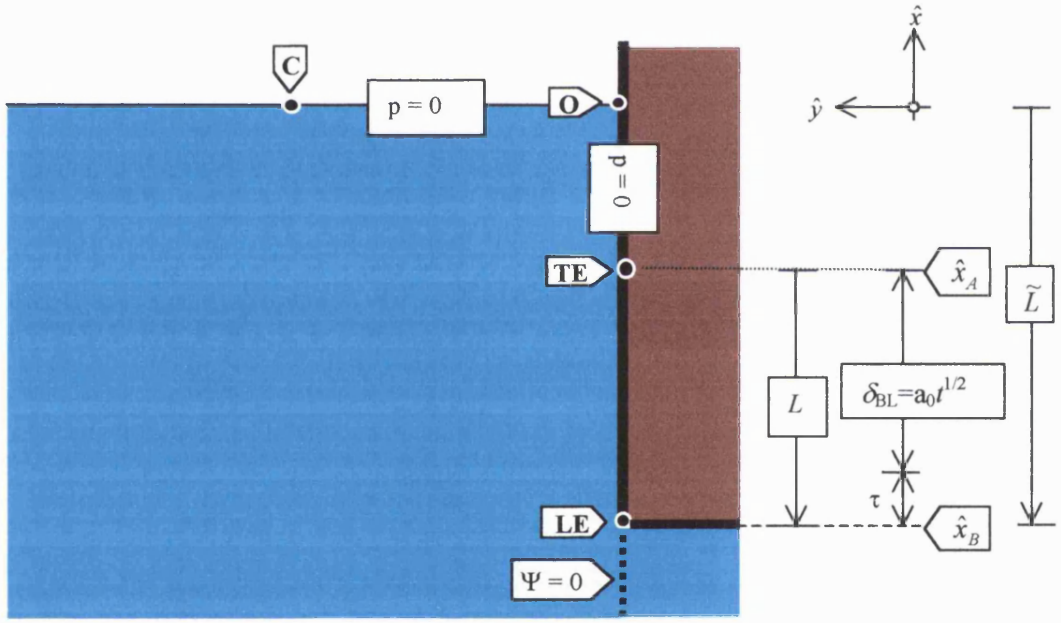


**Figure 5.3** **Domain of analysis for displacement derivative function**

The above expression for $\Psi_t$, the displacement-like function or the derivative of the negative displacement in effect, is thus valid along the ship side AB and the region $-\infty < \hat{x} < \hat{x}_B$. We next employ equation (5.3), which is valid for the outer region 3, along with matching to the viscous region solutions (see (4.33)), in order to obtain the associated function $\Psi_t$ on the right-hand side of (5.26), i.e. along entire region $-\infty < \hat{x} < \hat{x}_A$. Thus we have

$$\Psi_{\hat{x}t} \equiv -\hat{V}_t \equiv p_{\hat{y}} \equiv -\delta_{\hat{x}t}, \tag{5.27}$$

where $\delta$ is the scaled boundary layer and wake displacement function which was determined in chapters 2,3. Equation (5.27) corresponds to an 'injection' of fluid effect due to the positive relationship $\hat{V}_t = \delta_{\hat{x}t}$.

Thus $\Psi_t = -\delta_t$ with zero function of integration and

$$(\bar{x}-\bar{x}_A)^{-1/2}\left[\Psi_t + \delta_0{}'(t)\right] = -\frac{1}{\pi}\int_{-\infty}^{\bar{x}_A}(\bar{x}_A-\bar{\xi})^{-1/2}\left[\delta_t(\bar{\xi},t)-\delta_0{}'(t)\right]\frac{d\bar{\xi}}{\bar{x}-\bar{\xi}}, \tag{5.28}$$

in view of (5.26).

## 5.4 Model solutions

An approximate model for the displacement-like function is studied in Appendix A. However, a major shortcoming of that model lies in its treatment of the leading edge for the ship-side. In order to perform a more realistic analysis, as compared with that for the approximate model, it is necessary not only to define the leading edge as a moving coordinate with the length of the ship-side as constant, but also to treat the Rayleigh contribution satisfactorily. The accurate region 2 Blasius-Rayleigh solution influences the region 1 wake solution, thus simulating the problem of a downward moving ship-side more effectively. The present model and its analysis are pursued in order to obtain a smoother and more acceptable solution for the displacement derivative function $\Psi_t$.

We commence the analysis with the expression for $\Psi_t$ given in equation (5.28) which must be computed for $\bar{x} > \bar{x}_A$ (i.e. for both the edges of region 1 and region 2), but now taking into consideration a new model of the boundary layer displacement function $\delta$, in terms of $\bar{x}(=-\hat{x}^2)$ for $\hat{x} < 0$, using the map transformation equation (5.10). The problem has the leading edge of the plate being defined by $\hat{x}_B$ (see Figure 5.3) which is a function of time and is less than $\hat{x}_A$, as opposed to the approximate model which employs an alternative treatment of the leading edge (Appendix A).

Here as elsewhere the boundary condition has to be recognized as being applied to $\Psi$ or $\Psi_t$ (since the boundary layer gives $\Psi \approx -\delta(\hat{x},t)$ as $\hat{y} \to \infty$ at the boundary layer edge as in equation (4.33)) in terms of the fixed $\hat{x}, \hat{y}$ coordinates.

So equation (5.28) becomes now

$$\Psi_t = -\frac{(\bar{x}-\bar{x}_A)^{1/2}}{\pi}\int_{-\infty}^{\bar{x}_A} \frac{(\bar{x}_A-\bar{\xi})^{-1/2}}{(\bar{x}-\bar{\xi})}\left[\delta_t(\bar{\xi},t)-\delta_0'(t)\right]d\bar{\xi}-\delta_0'(t), \quad (5.29)$$

but in the integral here it must be recognised that $\delta$ and hence $\delta_t$ are zero for $\bar{\xi}$ less than $\bar{x}_B(=-\hat{x}_B^{\,2})$, whereas $\delta_0'$ of course is not, since it is independent of $\bar{\xi}$. With reference to Figure 5.3, we have the value $\hat{x}_A = -t$ and $\hat{x}_B = -t-L$, and so using transformation (5.10) we may conclude that $\bar{x}_A = -t^2$ and $\bar{x}_B = -(t+L)^2$, at time $t$, for the impulsively-started downward moving ship-side.

For typical times $t$ of order $O(1)$, we could evaluate (5.29) numerically using the numerical values of $\delta(\hat{x},t)$ from our previous boundary layer computations in chapters 2,3. However, a model for $\delta$ is more fruitful analytically in the form

$$\delta = \begin{cases} (\hat{x}-\hat{x}_B)^{1/2}\alpha_1 & \text{for } \hat{x}_B < \hat{x} < \hat{x}_B + t, \quad (5.30) \\ \alpha_0 t^{1/2} & \text{for } \hat{x}_B + t < \hat{x} < \hat{x}_A, \quad (5.31) \end{cases}$$

for times satisfying $0 \le t \le (\hat{x}_A - \hat{x}_B)$. Later times are incorporated subsequently, in section 5.7.

The coefficients $\alpha_0$ and $\alpha_1$ are real positive constants such that $\delta$ is continuous at the point $\hat{x} = \hat{x}_B + t$. Hence $\alpha_0 = \alpha_1$. Equation (5.30) in effect accounts for the Blasius component and equation (5.31) accounts for the Rayleigh component of the displacement function. The above model for $\delta$ now represents the numerical solution

fairly well, as shown in section 3.4, and in terms of the transformed coordinates $\bar{x} = -\hat{x}^2$ the model reads

$$\delta = \begin{cases} \left(t + L + (-\bar{x})^{1/2}\right)^{1/2} \alpha_1 & \text{for } \bar{x}_B < \bar{x} < -L^2, \quad (5.32) \\ \\ \alpha_0 t^{1/2} & \text{for } -L^2 < \bar{x} < \bar{x}_A, \quad (5.33) \end{cases}$$

in the new range $0 \le t \le L$. Also here, $\delta_0{}' = \dfrac{\alpha_0}{(2t^{1/2})}$, from the values at the trailing edge.

This leads to a new analytical expression for $\Psi_t$ (from equation (5.29)) using the "improved" model for $\delta$, namely

$$\begin{aligned} \Psi_t = & \frac{(\bar{x}-\bar{x}_A)^{1/2}}{\pi} \int_{-\infty}^{-L^2} \frac{(\bar{x}_A - \bar{\xi})^{-1/2}}{(\bar{x}-\bar{\xi})} \left(\delta_0{}'(t)\right) d\bar{\xi} \\ & - \frac{(\bar{x}-\bar{x}_A)^{1/2}}{\pi} \int_{\bar{x}_B}^{-L^2} \frac{(\bar{x}_A - \bar{\xi})^{-1/2}}{(\bar{x}-\bar{\xi})} \left[\partial_t \left(t + L + \left(-\bar{\xi}\right)^{1/2}\right)^{1/2} \alpha_1\right] d\bar{\xi} \\ & - \frac{(\bar{x}-\bar{x}_A)^{1/2}}{\pi} \int_{-L^2}^{\bar{x}_A} \frac{(\bar{x}_A - \bar{\xi})^{-1/2}}{(\bar{x}-\bar{\xi})} \left(\partial_t \left(t^{1/2}\alpha_0\right)\right) d\bar{\xi} \\ & - \delta_0{}'(t) \left[1 - \frac{(\bar{x}-\bar{x}_A)^{1/2}}{\pi} \int_{-L^2}^{\bar{x}_A} \frac{(\bar{x}_A - \bar{\xi})^{-1/2}}{(\bar{x}-\bar{\xi})} d\bar{\xi}\right], \end{aligned} \quad (5.34)$$

where the four constituent terms refer to the respective portions in the region $-\infty < \bar{x} < \bar{x}_A$. So we obtain, after differentiation, the final expression for the displacement derivative function in the concise form

$$\Psi_t = \frac{(\bar{x}-\bar{x}_A)^{1/2}}{\pi} \left(\delta_0' \Phi - \frac{\alpha_1}{2} \Omega\right) - \delta_0', \quad (5.35)$$

since the last two integrals shown in (5.34) cancel out due to $\delta_t = \delta_0{}'$ for the range $-L^2 < \bar{x} < \bar{x}_A$. Here the two remaining integrals are denoted as

$$\Phi = \int_{-\infty}^{-L^2} \frac{(\bar{x}_A - \bar{\xi})^{-1/2}}{(\bar{x} - \bar{\xi})} d\bar{\xi}, \tag{5.36a}$$

$$\Omega = \int_{\bar{x}_B}^{-L^2} \frac{(\bar{x}_A - \bar{\xi})^{-1/2}}{(\bar{x} - \bar{\xi})} \left(t + L + \left(-\bar{\xi}\right)^{1/2}\right)^{-1/2} d\bar{\xi}, \tag{5.36b}$$

which we will proceed to determine in the next section.

### 5.4.1 Evaluation of Φ and Ω integrals

To evaluate first the Ω integral, we make the substitution $m^2 = \bar{x}_A - \bar{\xi}$, with new limits for the integral [Evans (1989)]. Thus the integral becomes

$$\Omega = 2 \int_{(L^2 - t^2)^{1/2}}^{((t+L)^2 - t^2)^{1/2}} \frac{\left(t + L + \left(m^2 + t^2\right)^{1/2}\right)^{-1/2}}{(\bar{x} + t^2 + m^2)} dm. \tag{5.37a}$$

We note that here $0 \le t \le L$ and $\bar{x} > -t^2$, because $\bar{x}_A = -t^2$, so that the result is well defined. The form (5.37a) of the integral is suitable for computation using Simpson's rule.

In a similar manner, using the same substitution $m^2 = \bar{x}_A - \bar{\xi}$ and a table of integrals [Swokowski (1979)], we obtain

$$\Phi = \frac{\pi}{\rho} - \frac{2}{\rho} \tan^{-1}\left(\frac{(L^2 - t^2)^{1/2}}{\rho}\right), \tag{5.37b}$$

where $\rho = (\bar{x} - \bar{x}_A)^{1/2}$. The form (5.37b) is well defined, and substituting back into equation (5.35) we have

$$\Psi_t = -\frac{1}{\pi}\left\{\frac{\alpha_0}{t^{1/2}} \tan^{-1}\left(\frac{(L^2 - t^2)^{1/2}}{\rho}\right) + \frac{\alpha_1}{2} \rho\Omega\right\}, \tag{5.38}$$

which is the final form for the displacement derivative function.

### 5.4.1 Computational solution for the modeled $\Psi_t$

The computational solution for the present modeled $\Psi_t$ (equation 5.38) is described in this section, based on the evaluation of the $\Omega$ integral in section 5.4.1. The flow chart for the program is given below and the results are presented in the figures that follow the program (Program 5.1) at the end of the chapter.

The results for the variation of $\Psi_t$ with the $\bar{x}$-coordinate are presented in figures 5.4 for selected non-dimensional times not exceeding the non-dimensional length of the ship-side, which is unity. The times considered were for four equal intervals in the range 0.2-0.8. Larger times greater or equal to unity will be considered in section 5.8, since there is a restriction for the relatively small time analysis of $t<L$, from the limits implicit in (5.37a).

We recall that there exists a Blasius-like region in the initial portion of the plate near the leading edge followed by a Rayleigh region. For relatively small times, the contribution from the Rayleigh component is clearly the more significant. However, as time increases, the effect of Rayleigh profile is almost entirely eclipsed by that of the dominating Blasius type-flow that occupies an increasing proportion of the plate length. Thus the characteristic plateau in the $\Psi_t$ profile associated with the Rayleigh type tends to disappear as time increases, as observed in figure 5.4. Additionally, in region 1, there exists the Goldstein wake behaviour which is clearly distinguishable and exhibits a non-linear profile in which the gradient is largest at the trailing edge but flattens off with increasing distance from the trailing edge. This is further emphasised by the displacement derivative profiles of the wake region only, in figure 5.5. As time increases, the wake region profile flattens off, becoming almost perfectly flat for $t=1$, as shown by figure 5.6.

The model employed a higher degree of mesh refinement near the point of contact between regions 1 and 2, in order to ensure an accurate account of the discontinuity at this point.

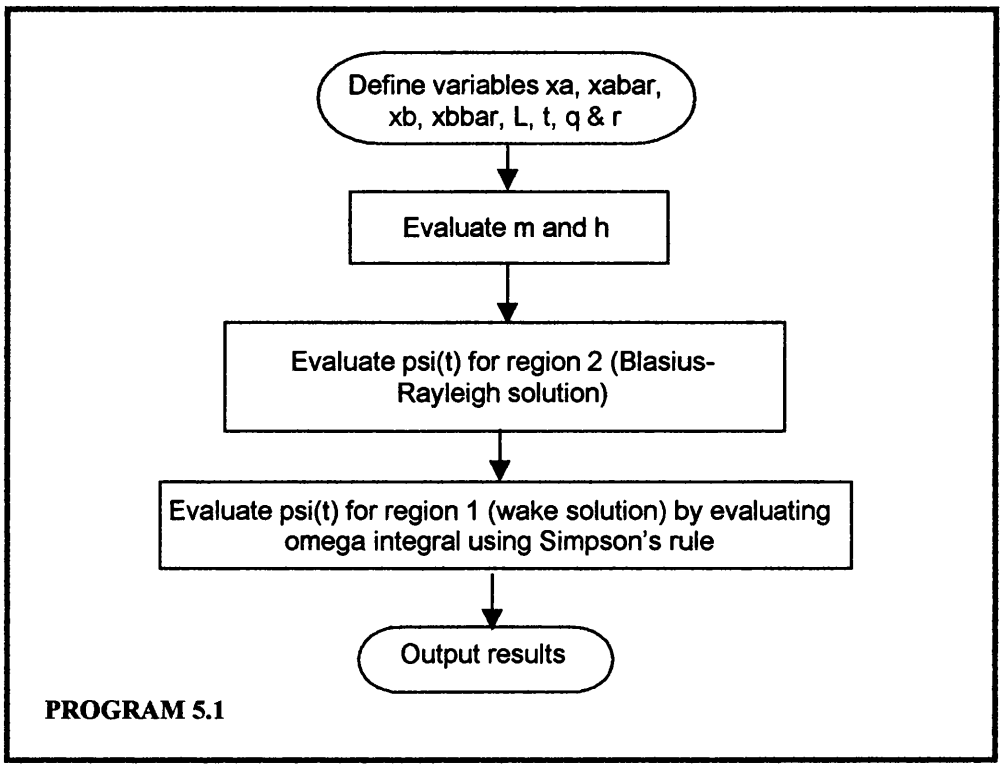


## 5.5 Analytical properties of the solution

We investigate the solution analytically below for two cases of interest.

### 5.5.1 At $\bar{x} = 0$.

For the $\Omega$ integral, we substitute in equation (5.37a) $\sigma^2 = -\bar{x}_A > 0$, and $\bar{x} = 0$ to find

$$\Omega = \int_{(L^2-\sigma^2)^{1/2}}^{(-\bar{x}_B-\sigma^2)^{1/2}} \frac{2\left(t + L + \left(m^2+\sigma^2\right)^{1/2}\right)^{-1/2}}{(\sigma^2+m^2)} dm, \qquad (5.39)$$

which is of $O(1)$.

### 5.5.2 As $\bar{x} \to \bar{x}_A^{+}$.

We write $\hat{x} = \hat{x}_A + \varepsilon$ and $\bar{x} = \bar{x}_A + \mu$ near the leading edge, where $\varepsilon, \mu$ are small increments. Using the fact that $\bar{x} = -\hat{x}^2$, we have $\bar{x}_A + \mu = -(\hat{x}_A{}^2 + 2\hat{x}_A\varepsilon + \varepsilon^2)$ which gives $\bar{x}_A + \mu = \bar{x}_A - 2\hat{x}_A\varepsilon - \varepsilon^2$. Thus $\mu \cong -2\hat{x}_A\varepsilon$, neglecting the higher order term.

Again for the $\Omega$ integral in equation (5.37a), we have

$$\Omega = 2\int_{(\bar{x}_A+L^2)^{1/2}}^{(\bar{x}_A-\bar{x}_B)^{1/2}} \left(t+L+\left(m^2-\bar{x}_A\right)^{1/2}\right)^{-1/2}\frac{dm}{m^2}, \qquad (5.40)$$

which is $O(1)$ generally.

## 5.6 Investigation for small times, $t \ll 1$

In this section, we consider evaluating equation (5.29) for small $t$, given the displacement function $\delta$ from the model of (5.32) and (5.33). There is now more than one length scale of interest for the small time analysis, given that $\hat{x}_A$, $\bar{x}_A$ are small. First, we have the general $|\bar{x}| \sim 1$ scale which allows the assumption of the trailing-edge depth $|\bar{x}_A|$ being negligible. We again consider a constant side speed of unity, imposed for $t > 0$.

In order to examine the problem on the main $|\bar{x}| \sim 1$ scale of concern, we simplify equation (5.29) to the form

$$\Psi_t = -\frac{\bar{x}^{1/2}}{\pi}\int_{-\infty}^{0}\frac{(-\bar{\xi})^{-1/2}}{(\bar{x}-\bar{\xi})}\left[\delta_t(\bar{\xi},t)-\delta_0'(t)\right]d\bar{\xi}-\delta_0'(t), \qquad (5.41a)$$

since $\bar{x}_A$ is small now.

After the examination of the integrals we have

$$\Psi_t = -\frac{\bar{x}^{1/2}}{\pi}\int_{-\infty}^{\bar{x}_B}\frac{(-\bar{\xi})^{-1/2}}{(\bar{x}-\bar{\xi})}(-\delta_0'(t))d\bar{\xi}-\delta_0'(t). \qquad (5.41b)$$

Using integration and the substitution $m^2 = -\bar{\xi}$, (5.41b) yields for small times

$$\Psi_t = -\frac{\alpha_0}{2t^{1/2}}\frac{2}{\pi}\tan^{-1}\left(\frac{L}{\bar{x}^{1/2}}\right) \qquad (5.41c)$$

for the model of (5.30), (5.31) but where the Blasius term is negligible compared with the Rayleigh term. If the distance from the origin $\bar{x}_A^{1/2}$ is taken to be small, we have $\Psi_t \to -\frac{\alpha_0}{2t^{1/2}} = -\delta_0'$ as we have assumed in the beginning of the analysis. In any case (5.41c) is valid for small times where $|\hat{x}|$ is of order unity. We have also assumed here that, from the mapping, $\bar{x}_B = -\hat{x}_B{}^2 = -L^2$ to leading order at small times.

## 5.7 Investigation for larger times

We now investigate the problem for non-dimensional times greater than the depth scale $L$ (the non-dimensional length of the ship's side). We re-introduce directly the displacement derivative function $\Psi_t$ for the problem from equation (5.29). We observe that for large times the second component of (5.31) now disappears. This is due to the fact that this term represents the Rayleigh component, which in a sense has been swept 'downstream' into the wake. Hence the flow adjacent to the ship-side has now developed into a purely Blasius type, for such larger times.

The ship-side parameters are clearly identified as $\hat{x}_A = -t$ and $\hat{x}_B = -t - L$, with the previous model of $\delta$ given by equation (5.30). Employing the transformation of (5.32), the displacement derivative function reduces to give

$$\Psi_t = -\frac{(\bar{x} - \bar{x}_A)^{1/2}}{\pi}\left(\frac{a_1}{2}\right)\cdot\Lambda, \tag{5.42}$$

where we now define the integral that is contained within the new $\Psi_t$ expression, valid for large times, as

$$\Lambda = \int_{\bar{x}_B}^{\bar{x}_A} \frac{(\bar{x}_A - \bar{\xi})^{-1/2}}{(\bar{x} - \bar{\xi})}\left[\left(t + L + \left(-\bar{\xi}\right)^{1/2}\right)^{-1/2}\right] d\bar{\xi}\,. \tag{5.43}$$

This clearly extends in time from the expression (5.36a) holding at earlier times. To evaluate $\Lambda$, we use the previous transformation $m^2 = \bar{x}_A - \bar{\xi}$ to obtain

$$\Lambda = 2\int_0^{((t+L)^2-t^2)^{1/2}} \frac{\left(t+L+\left(m^2+t^2\right)^{1/2}\right)^{-1/2}}{(\bar{x}+t^2+m^2)}\,dm, \qquad (5.44)$$

which may now be resolved computationally, for example by use of Simpson's rule.

## 5.8 Computational solution for larger times

The program for the solution of $\Psi_t$ which includes the $\Lambda$ integral is similar to that of section 5.4.2 and is given as Program 5.2 in this chapter. The length parameter is again taken to be unity and thus the times under consideration are now greater than or equal to 1.

The entire (figure 5.7) and wake region profiles (figure 5.8) of $\Psi_t$ with $\bar{x}$ are presented for equal time intervals in the range $t$=1 to $t$=24. We observe that the profiles follow a similar description to those of Program 5.1 in section 5.4.2, but with the fundamental differences that the Rayleigh effect is absent and the wake profile joins in a continuous manner with the Blasius-type portion.

## 5.9 A check for larger times

For an analytical check on the larger time case, we consider approaching the trailing edge $\bar{x}_A$ in both the negative and positive directions along the $\bar{x}$-coordinate axis.

### 5.9.1 As $\bar{x} \to \bar{x}_A^{+}$

We define $\varepsilon$ to be an infinitesimal positive constant such that $\bar{x} = \bar{x}_A + \varepsilon$, near the trailing edge. We then substitute $m = \varepsilon^{1/2} v$ in (5.44) to derive the expression

$$\Lambda \sim \frac{L^{-1/2}\pi}{\varepsilon^{1/2}}. \qquad (5.45)$$

Thus the displacement derivative function becomes, locally,

$$\Psi_t = -\frac{1}{2} L^{-1/2} \alpha_1. \qquad (5.46)$$

For the value of ship-side length $L$=1 we obtain the value –0.125 for $\Psi_t$ from (5.46) valid for larger times. It is concluded that near the trailing edge, $\bar{x} \approx \bar{x}_A$, the analytical and computational values are in exact agreement.

### 5.9.2 As $\bar{x} \to \bar{x}_A^-$

In order to see whether the above result is true for the other case, as $\bar{x} \to \bar{x}_A^-$, we perform the following investigation. We have that

$$\Psi_t = -\partial_t \delta = -\partial_t (t + L + (-\bar{x})^{1/2})^{1/2} \alpha_1 = -\frac{1}{2}(-t + t + L)^{-1/2} \alpha_1 \qquad (5.47)$$

from (5.32) and since $\bar{x} = \bar{x}_A = -t^2$. Thus

$$\Psi_t \sim -\frac{1}{2} L^{-1/2} \alpha_1 . \qquad (5.48)$$

This agrees exactly with equation (5.46), confirming that $\Psi_t$ is continuous across the trailing edge. Thus the same result for $\Psi_t$ is observed when approaching the trailing edge $\bar{x}_A$ from both the wake side and the plate (ship) side.

## 5.10 General form of the displacement derivative function $\Psi_t$

The general forms of the displacement derivative function valid for both small and large times are sketched in figure 5.9. The large time forms are predominantly Blasius-like forms and contain no Rayleigh effect, as compared with the smaller time forms. Figure 5.10 shows the computational $\Psi_t$ profiles for small and larger values of time in the range $0 < t \leq 3$. A smooth trend in the general form of the profiles may be observed as time increases. For small values of time the wake region profile is pronounced, but this flattens off with increasing time. For $t$>1 there is no distinguishable Goldstein near-wake region profile, in the sense that it is continuous with the Blasius-like displacement, whereas there exists a discontinuity for smaller times. Thus we observe a continuous trend of the $\Psi_t$ profiles with time and this appears to be physically sensible.

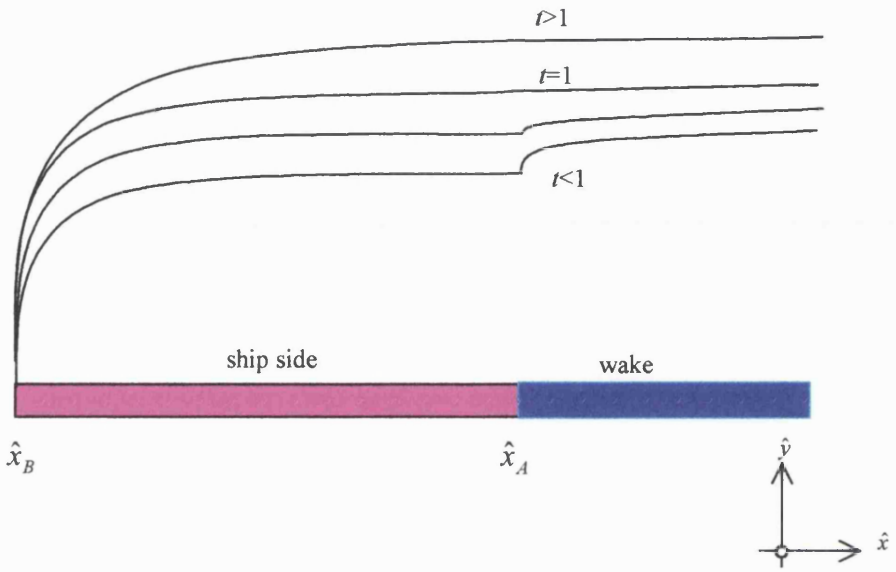


**Figure 5.9 Profiles for $\Psi_t$ for smaller and larger times**

The previous investigations were for a given value of $L$, which was taken as unity in order to coincide with the wake displacement solution of chapter 3. It will now be shown that the solution for large times is independent of the ship-side length parameter $L$. We will examine the displacement for ship-side lengths $L\sim 1$, at large times $t$. In considering equation (5.44), we see that the square of the upper limit of the $A$ integral is $(t+L)^2 - t^2 = 2tL + L^2$, and so typically $m = O(t^{1/2})$.

Employing the transformation $m = t^{1/2}\hat{m}$, expanding in a power series in (5.44), substituting $\bar{x} = t^2\bar{\bar{x}}$ and then putting $\hat{m} = (2L^{1/2})\sin\hat{\theta}$ say, yields

$$\Lambda \sim \frac{2^{1/2}\pi}{t^{3/2}(\bar{\bar{x}}+1)}. \qquad (5.49)$$

We then use this expression for the $\Lambda$ integral in the $\Psi_t$ equation (5.42) to obtain

$$\Psi_t \sim -\frac{\alpha_1}{2^{1/2}t^{1/2}(\bar{\bar{x}}+1)^{1/2}}, \qquad (5.50)$$

for large $t$. Thus we observe that $\Psi_t$ is independent of the ship-side length parameter $L$ then.

We now present the following tables to compare the large-time asymptotic prediction (5.50) with the computational results for two values of time, $t$=9 and $t$=48. Graphs of these results are presented in figures 5.11.

For $t$=9 we have

| $\bar{x}$ | $\Psi_t$ *(asymptotic)* | $\Psi_t$ *(computational)* |
|---|---|---|
| ***-81*** | Indeterminate | -0.124 |
| ***-64*** | -0.1288 | -0.092 |
| ***-49*** | -0.0939 | -0.077 |
| ***-36*** | -0.0791 | -0.066 |
| ***-24*** | -0.0703 | -0.062 |
| ***-16*** | -0.0659 | -0.059 |
| ***-9*** | -0.0626 | -0.057 |
| ***-4*** | -0.0605 | -0.055 |
| ***-1*** | -0.0594 | -0.054 |
| ***-0.24*** | -0.0591 | -0.054 |

*Table 5.1*

For $t$=48

| $\bar{x}$ | $\Psi_t$ *(asymptotic)* | $\Psi_t$ *(computational)* |
|---|---|---|
| ***-81*** | -0.0260 | -0.0252 |
| ***-64*** | -0.0259 | -0.0250 |
| ***-49*** | -0.0258 | -0.0249 |
| ***-36*** | -0.0257 | -0.0248 |
| ***-24*** | -0.0256 | -0.0247 |
| ***-16*** | -0.0256 | -0.0247 |
| ***-9*** | -0.0256 | -0.0247 |
| ***-4*** | -0.0255 | -0.0247 |

| | | |
|---|---|---|
| ***-1*** | -0.0255 | -0.0247 |
| ***-0.24*** | -0.0255 | -0.0247 |

*Table 5.2*

From the results, there is a small relative error between the asymptotic and computational results for both values of time. Referring to figure 5.11, the computational and analytical results are in very close agreement for the larger value of time, 48, which is expected given that the asymptotic solution is valid for large times. There is observed, however, a marginal error for the smaller value of time, as demonstrated by the computational and the analytical results.

## 5.11 Fortran 77 programs and figures

```
C       ********************************************************
C       January 1998            D.Papadopoulos
C       ********************************************************
C       Program to evaluate the Psi(t) variation with x-coordinate
C       and produce entire displacement function [y] valid for small times
C       ********************************************************
C       ********************************************************
C       Problem: Downward motion of ship in stationary fluid
C       ********************************************************

C       *** Definition of all variables, except y ***

        program psi

        REAL o(1000),res,h,L,t,sum
        REAL u,xbar,xabar,xbbar,xa,xb,x,pi,q,r,y,y1,y2,term,rho
        INTEGER i,j,mm,m

        mm = 360
        L = 1
        pi = 3.1415927

C       General loop to evaluate psi(t) for various times,
C       with constraint t<L

        do 3000 t=0.2,0.9,0.2

        xa = -t
        xb = xa-L
        xbbar = - ((xb)**2)
        xabar = - ((xa)**2)

C       q means a1  and r means a0
        q = 0.25
        r = 0.25

C       *** Determination of m and h
        m = (2 * mm) + 3
        h =  ((( - (t**2) + ((t+L)**2) )**0.5) - ( ( (L**2) -
 (t**2))**0.5))/((2*mm) + 2)

C       *** Evaluate Psi(t) for xb<x<xb+t, i.e. Blasius part

        do 5 x = xb,xb+t,0.01
        xbar = -((x)**2)
        y1=-q*0.5*((x-xb)**(-0.5))
        WRITE (6,*)  xbar,y1
5       continue

C       *** Evaluate Psi(t) for xb+t<x<xa, i.e. Rayleigh part

        do 10 x = xb+t,xa,0.01
        xbar = -((x)**2)
        y2=-r*0.5*(t**(-0.5))
        WRITE (6,*)  xbar, y2
10      continue

C       ***General loop to evaluate psi(t) (including constituent omega
C       integral) for values of the x-coordinate within initial range near
C       xa, having higher level of numerical refinement ***

        do 1000 x = (xa+0.001),(xa+0.101),0.005
```

5.1 Program to evaluate the $\Psi$, variation with $\bar{x}$, valid for small times.

```
          xbar = -((x)**2)

C         *** Evaluate o(j), also evaluating u(j) at each j ***

          do 24 j = 1,m-1
          u = ((j - 1) * h)+( ( (L**2) - (t**2) )**0.5)

24        o(j) = 2*((t+L+((u**2+t**2)**0.5))**(-0.5))/(xbar+t**2+u**2)


C         *** Evaluate first and final terms of omega integral ***

          sum = o(1)+ o(m) + (4*o(m-1))

C         *** Evaluate complete integral (i.e. including the intermediate terms)

          do 27 i = 1,mm
          j = 2 * i
27        sum = sum + (4.0 * o(j)) + (2.0 * o(j+1))

          res = (sum * (h/3.0))

C         *** Evaluate and output results for psi(t) [y] ***

          term=( ((   L **2) - (t**2)) / (xbar-xabar) )**0.5
          rho=r*(t**(-0.5))
          y = -((0.5/pi)*((xbar-xabar)**0.5)*(q*res))-
( rho*0.31831*atan(term) )
          WRITE (6,*)  xbar,y

1000      continue

C         ********************************************************************
C         *** General loop to evaluate psi(t) (including omega integral)
C         for values of the x-coordinate within secondary range having a lower
C         level of numerical refinement (i.e. larger x-coordinate interval)  ***

          do 2000 x = (xa+0.2),-0.05,0.1

          xbar = -((x)**2)

C         *** Evaluate o(j), also evaluating u(j) at each j ***

          do 1024 j = 1,m-1
          u = ((j - 1) * h)+( ( (L**2) - (t**2) )**0.5)

1024      o(j) = 2*((t+L+((u**2+t**2)**0.5))**(-0.5))/(xbar+t**2+u**2)


C         *** Evaluate first and final terms of omega integral ***

          sum = o(1)+ o(m) + (4*o(m-1))

C         *** Evaluate the complete integral (i.e. including the intermediate
C         terms) ***

          do 1027 i = 1,mm
          j = 2 * i
1027      sum = sum + (4.0 * o(j)) + (2.0 * o(j+1))

          res = (sum * (h/3.0))


C         *** Evaluate and output results psi(t) [y],
```

```
        term=( ((   L **2) - (t**2)) / (xbar-xabar) )**0.5
        rho=r*(t**(-0.5))
        y = -((0.5/pi)*((xbar-xabar)**0.5)*(q*res))-
( rho*0.31831*atan(term) )

        WRITE (6,*)  xbar,y

2000    continue

        WRITE (6,*)

3000    continue

        end
```

```
C       ************************************************************
C       JUNE 1998                    D.Papadopoulos
C       ************************************************************
C       Program to evaluate the Psi variation with x-coordinate
C         for LARGE TIMES
C       ************************************************************

C       Problem: Downward motion of ship in stationary fluid
C       ************************************************************

C       *** Definition of all variables, except y ***

        program simps
        REAL lam(10000),y,y1,res,h,L,t,sum
        REAL u,xbar,xabar,xbbar,xa,xb,x,pi,q,dt
        INTEGER i,j,mm,m
        mm =360
        L = 1
        pi = 3.1415927
        dt=1
C       q means α1
        q = 0.25

C       General loop to evaluate Psi(t) for various times

        do 3000 t=1,2,dt

        xa = -t
        xb = xa-L
        xbbar = -((xb)**2)
        xabar = -((xa)**2)

C       *** Determination of m and h ***
        m = (2 * mm) + 3
        h =  ( (- t**2 + (t+L)**2 )**0.5) / ((2*mm) + 2)

C       *** Evaluate Psi(t) for xb<x<xb+t, i.e. Blasius part

        do 500 x = xb,xa,0.01
        xbar = -((x)**2)
        y1=-q*0.5*((x-xb)**(-0.5))
        WRITE (6,*)  xbar,y1
500     continue


C       *** General loop to evaluate psi (including lamda integral) ***
C       *** for values of the x-coordinate ***

        do 2000 x = (xa+0.01),0.01,0.01

        xbar = - ((x)**2)

C       *** Evaluate lam(j), also evaluating u(j) at each j ***

        do 1024 j = 1,m-1
        u = ((j - 1) * h)
1024    lam(j) = 2*( (t+L+( (u**2+t**2)**0.5) )**(-0.5) )/(xbar+t**2+u**2)

C       *** Evaluate first and final terms of lamda integral ***

        sum = lam(1)+ lam(m) + (4*lam(m-1))

C       *** Evaluate the complete integrals (i.e. including the
```

5.2 Program to evaluate the $\Psi_t$ variation with $\bar{x}$, valid for larger times.

```
C       intermediate terms) ***

        do 1027 i = 1,mm
        j = 2 * i
1027    sum = sum + (4.0 * lam(j)) + (2.0 * lam(j+1))

        res = (sum * (h / 3.0))

C       *** Evaluate and output results for psi(t) [y],

        y = -((0.5)/pi) * ((xbar-xabar)**0.5) * q * res

        WRITE (6,*) xbar,y

2000    continue

        WRITE (6,*)

3000    continue

        end
```

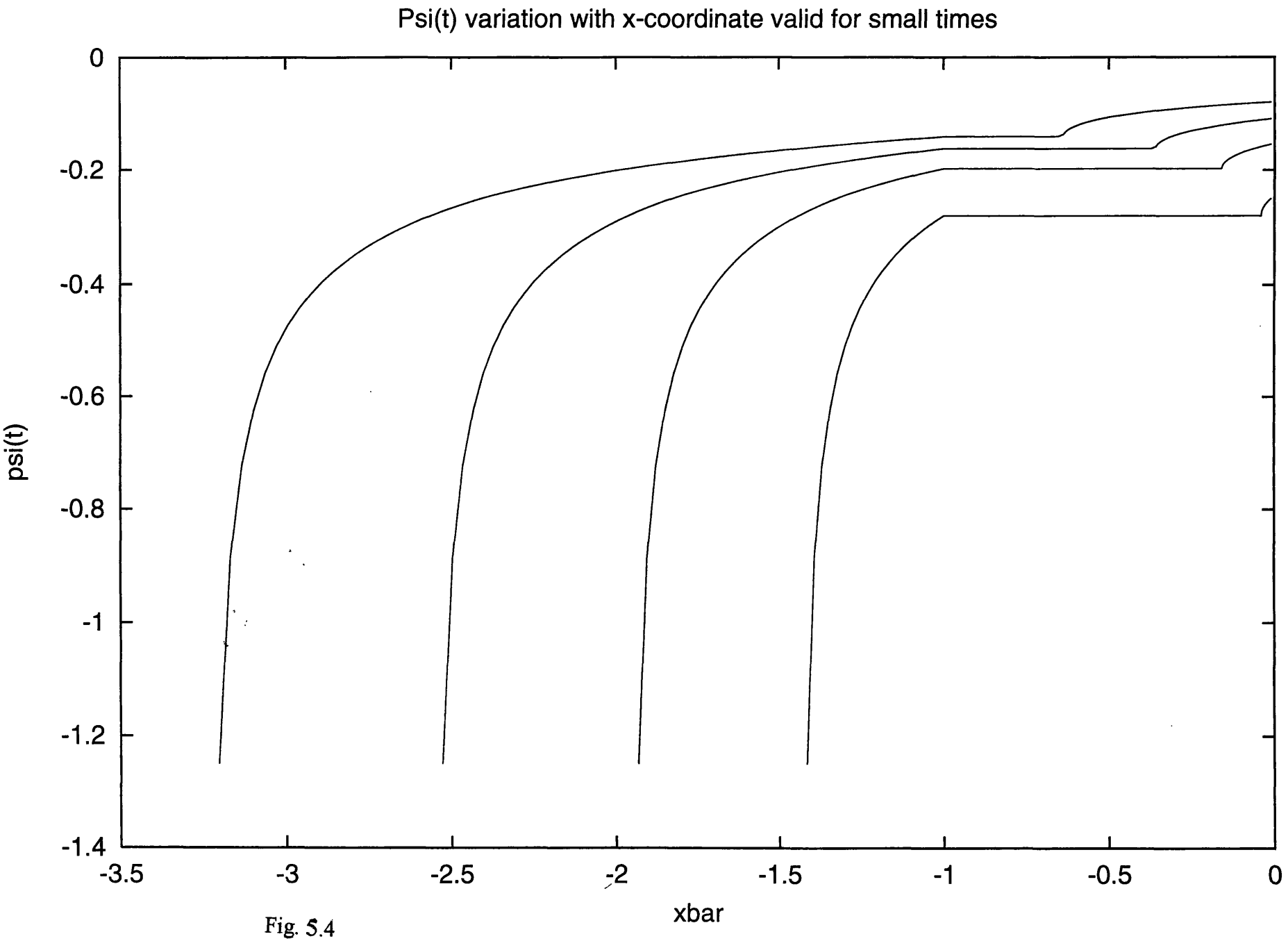
Psi(t) variation with x-coordinate valid for small times
psi(t)
xbar
0
-0.2
-0.4
-0.6
-0.8
-1
-1.2
-1.4
-3.5
-3
-2.5
-2
-1.5
-1
-0.5
0

Fig. 5.4

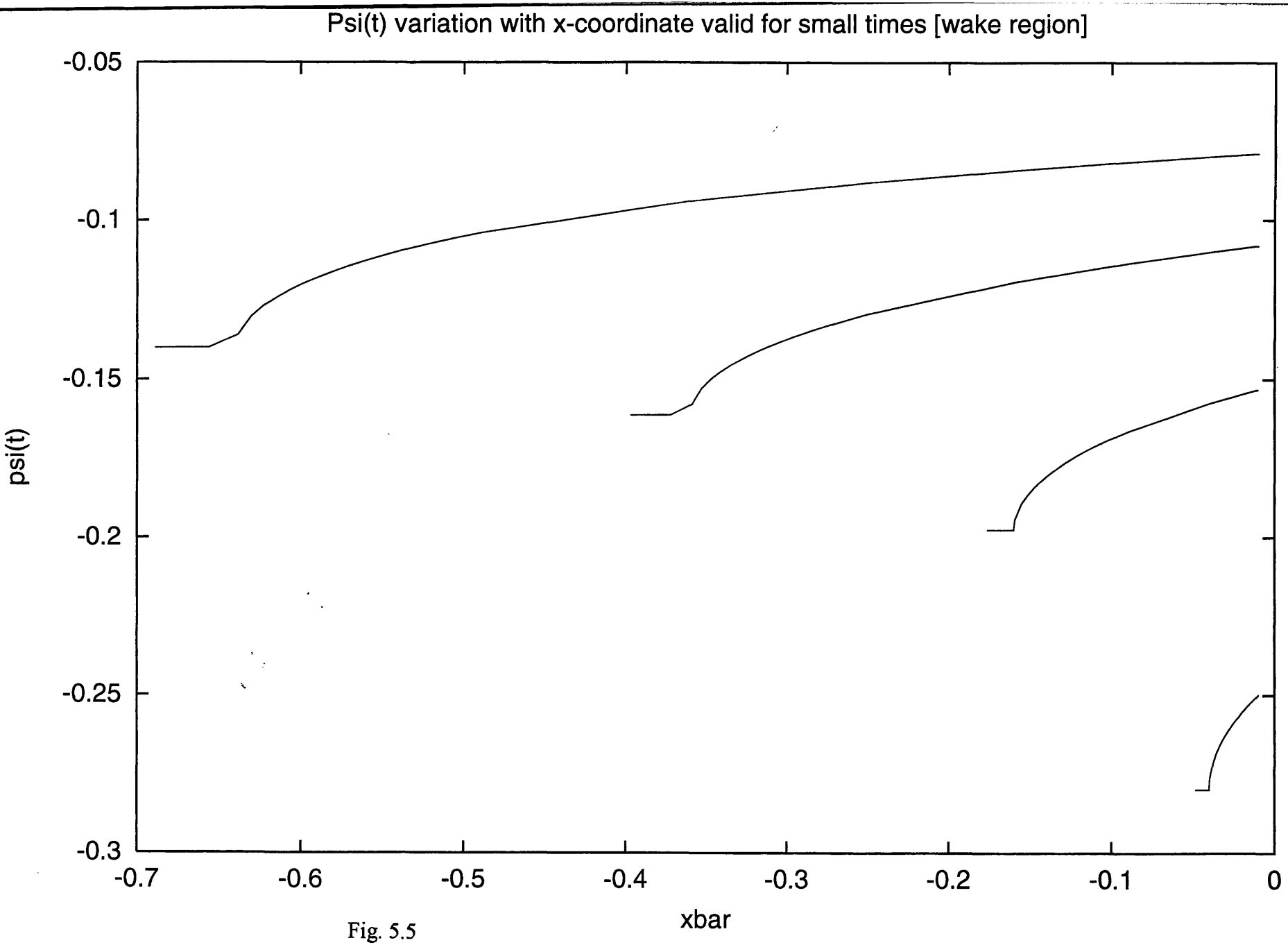
Psi(t) variation with x-coordinate valid for small times [wake region]
-0.05
-0.1
-0.15
-0.2
-0.25
-0.3
psi(t)
-0.7
-0.6
-0.5
-0.4
-0.3
-0.2
-0.1
0
xbar

Fig. 5.5

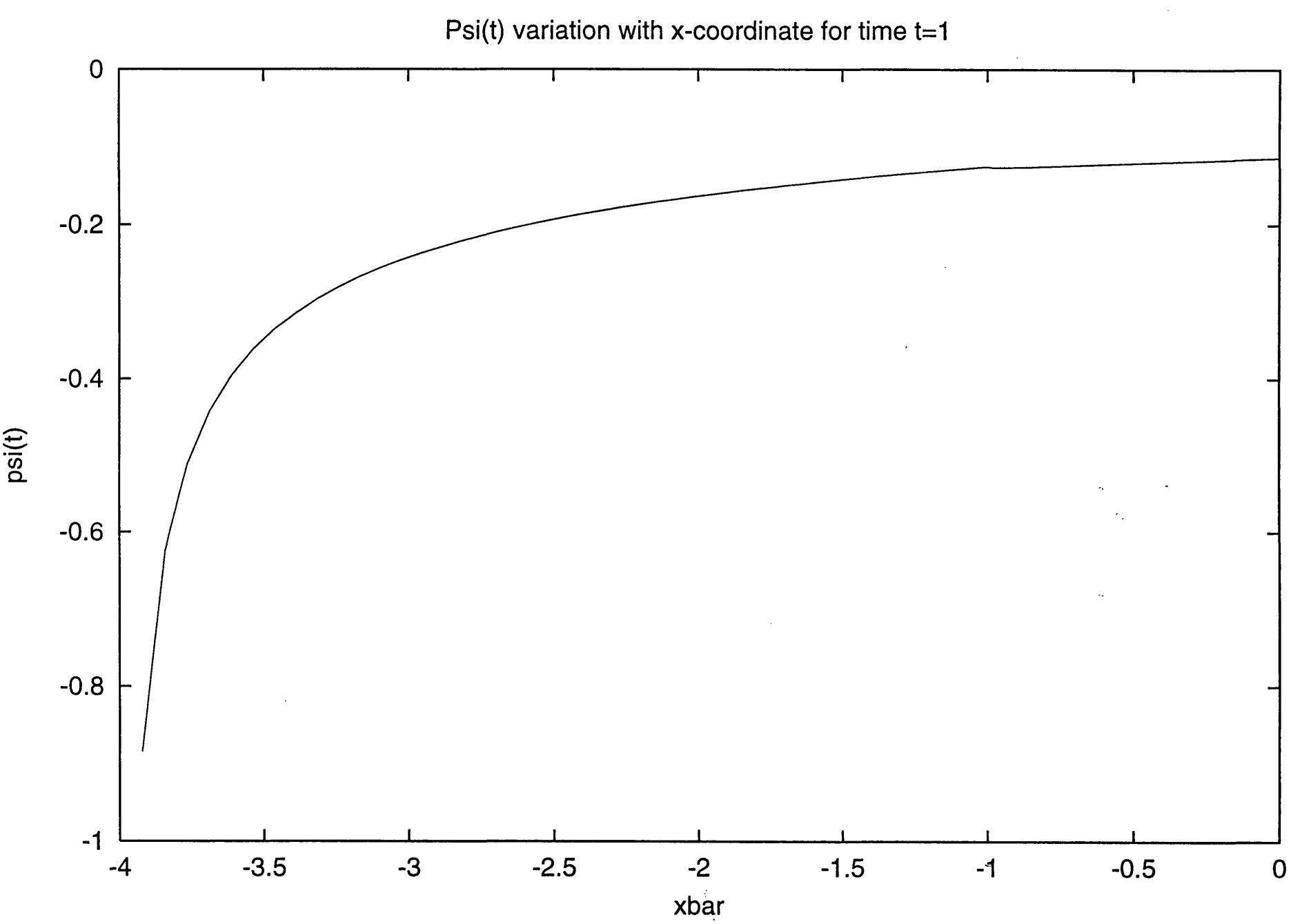
Psi(t) variation with x-coordinate for time t=1
0
-0.2
-0.4
-0.6
-0.8
-1
psi(t)
-4
-3.5
-3
-2.5
-2
-1.5
-1
-0.5
0
xbar

Fig. 5.6

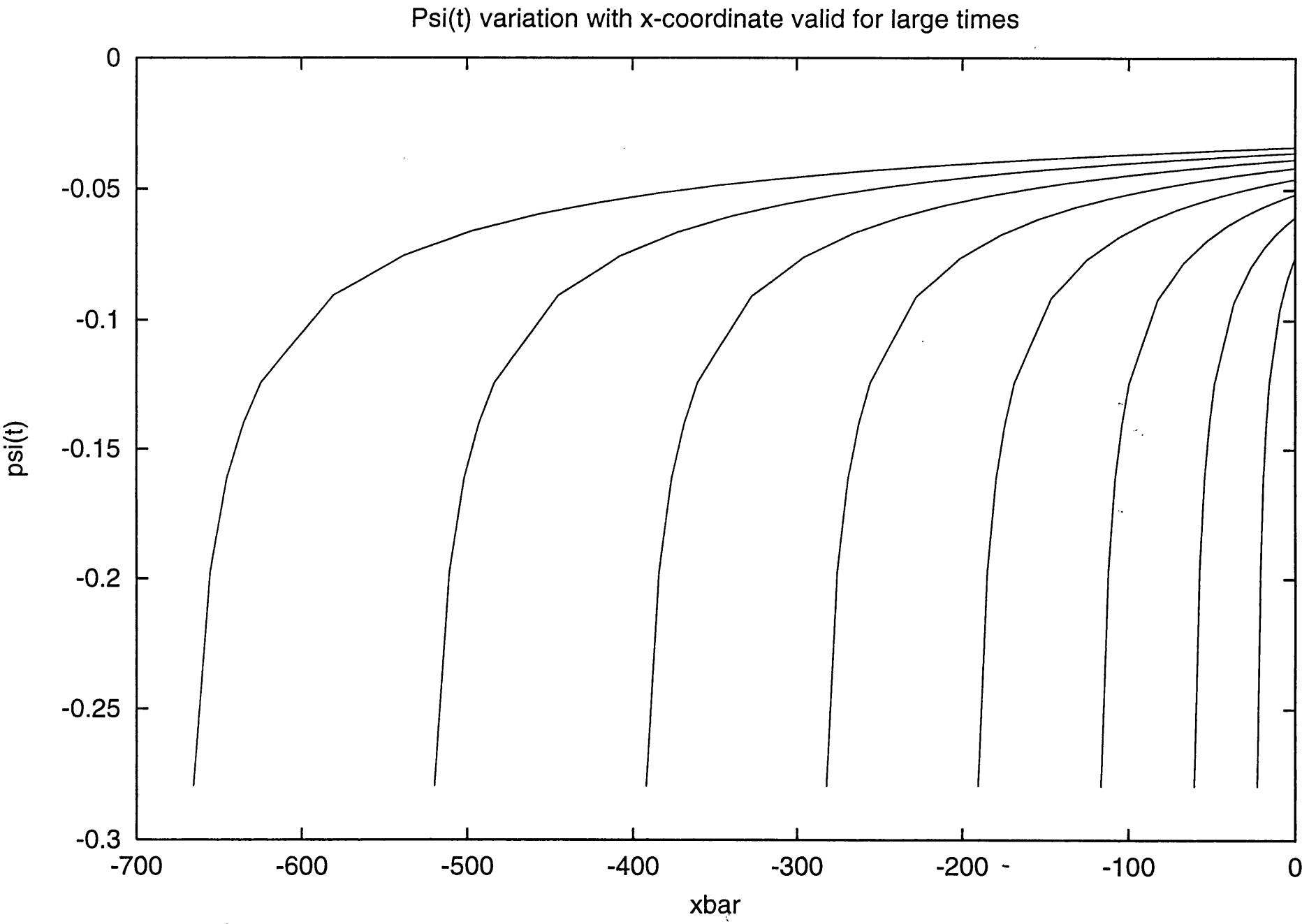
Psi(t) variation with x-coordinate valid for large times
0
-0.05
-0.1
-0.15
-0.2
-0.25
-0.3
psi(t)
-700
-600
-500
-400
-300
-200
-100
0
xbar

Fig. 5.7

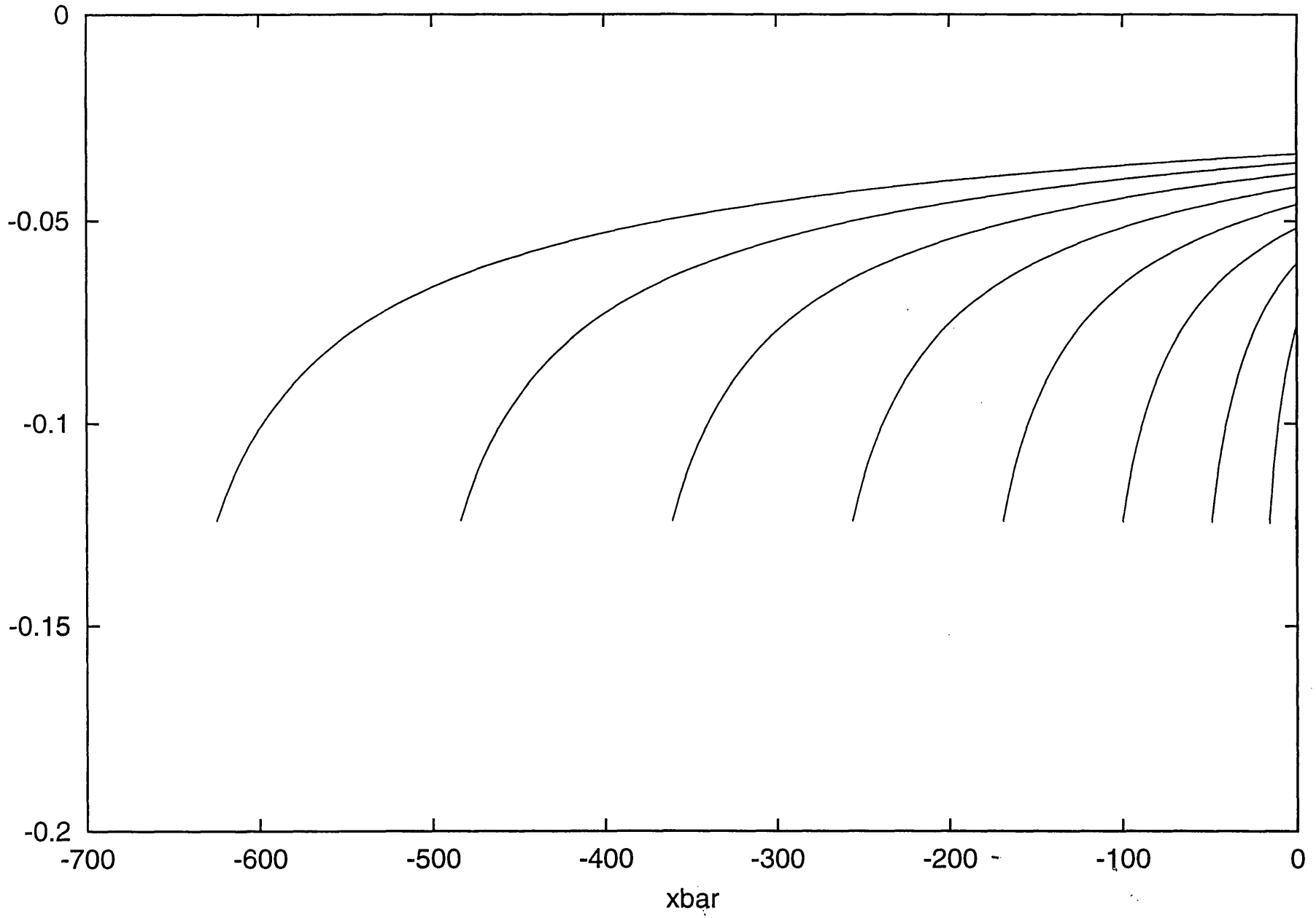
Psi(t) variation with x-coordinate valid for large times [wake region]
0
-0.05
-0.1
-0.15
-0.2
psi(t)
-700
-600
-500
-400
-300
-200
-100
0
xbar

Fig. 5.8

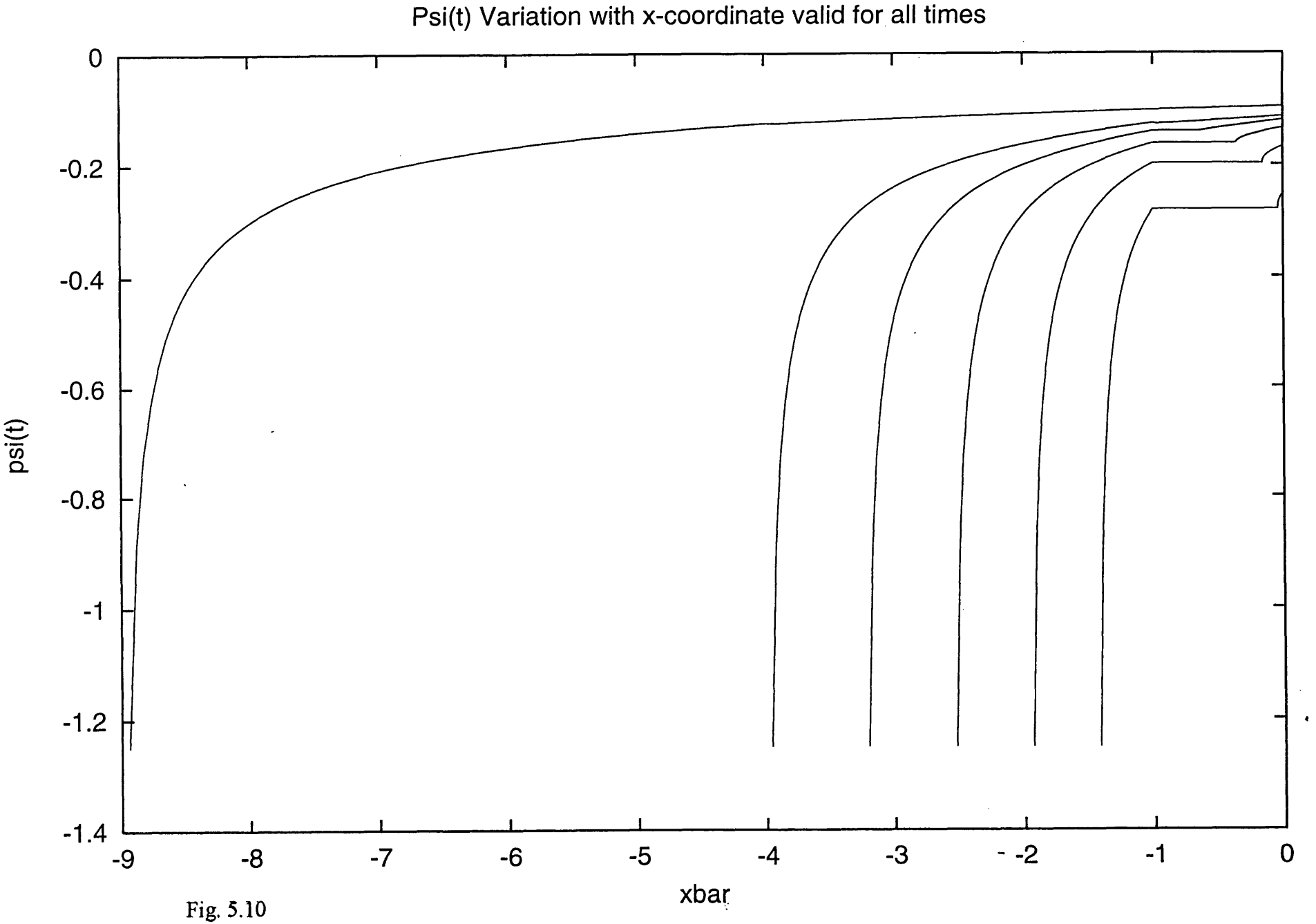
Psi(t) Variation with x-coordinate valid for all times
0
-0.2
-0.4
-0.6
-0.8
-1
-1.2
-1.4
psi(t)
-9
-8
-7
-6
-5
-4
-3
-2
-1
0
xbar

Fig. 5.10

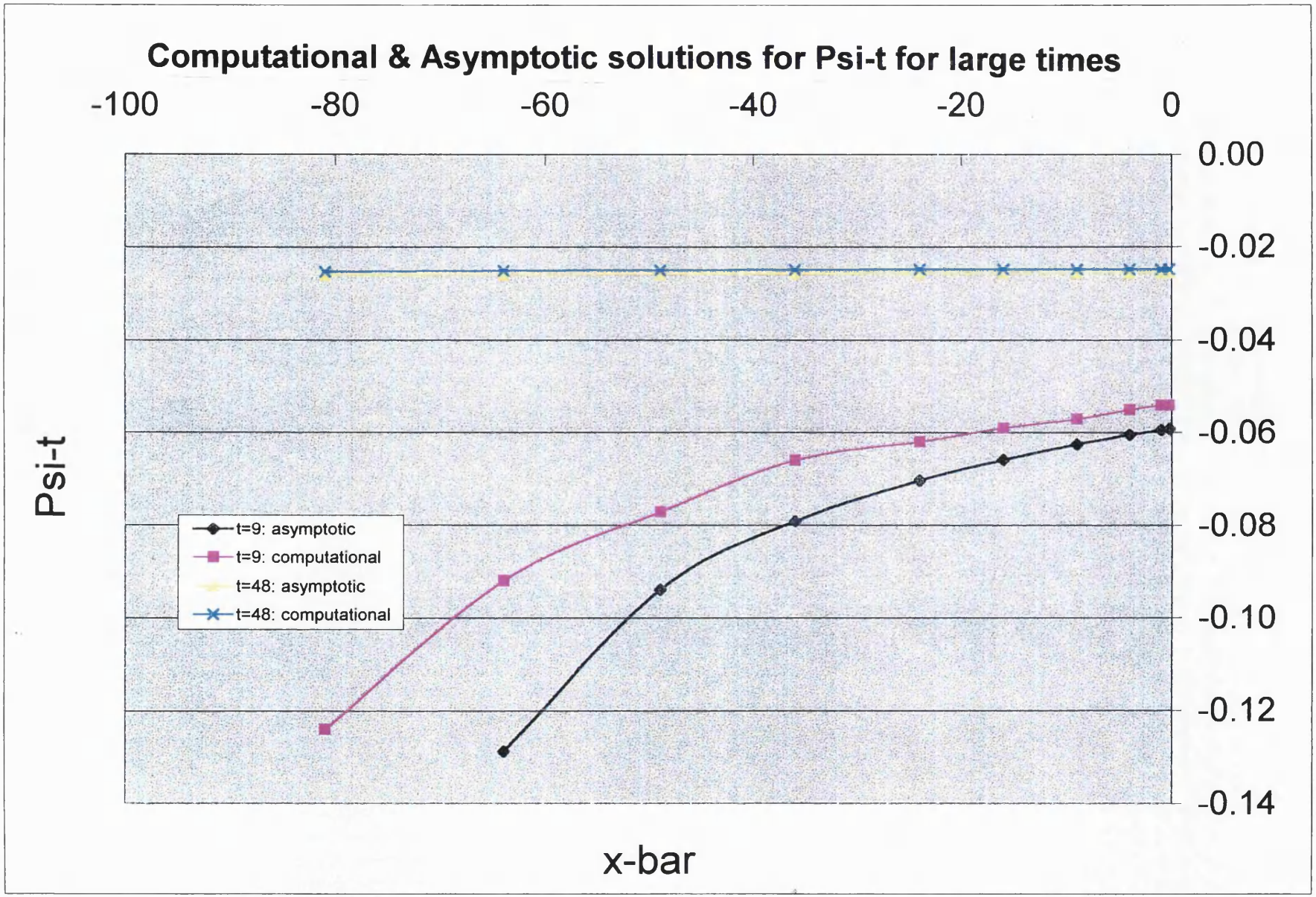
Computational & Asymptotic solutions for Psi-t for large times
-100
-80
-60
-40
-20
0
0.00
-0.02
-0.04
-0.06
-0.08
-0.10
-0.12
-0.14
Psi-t
x-bar
t=9: asymptotic
t=9: computational
t=48: asymptotic
t=48: computational

Fig. 5.11

# CHAPTER 6

# The shape of the upper and side free surfaces for vertical downward ship-side motion

## 6.1 Development of the upper free surface equations

In this chapter we determine the shapes of the water-air interfaces at the top free surface and the side free surface. In chapter 4, the solution for the viscous boundary layer and wake flow adjacent to the ship-side was ascertained. This is used next to determine the behaviour of the top air-water interface, which is present in the nearly-still outer region 3. This behaviour may be described by an "upper free surface" function $f_1$. In the governing equations of (5.1)-(5.3) which describe the flow, the unknown upper free surface position $\hat{x} = \mathrm{Re}^{-1/2} \cdot f_1(\hat{y},t)$ is controlled by $O = \frac{D}{Dt}(\hat{x} - \mathrm{Re}^{-1/2} \cdot f_1(\hat{y},t))$ i.e. by

$$\hat{u} = \frac{\partial f_1}{\partial t}, \qquad (6.1)$$

evaluated at $\hat{x} = 0$, from a Taylor expansion and using the property that the velocities $\mathrm{Re}^{-1/2}(\hat{u},\hat{V})$ are small. Here (6.1) is equivalent to condition 2c, as given at the beginning of chapter 4.

At high Reynolds numbers, which are of concern to us, the initial motion of the fluid is most pronounced in the inner regions (regions 1,2) where the unsteady boundary layer equations apply for some finite time interval. We now turn our attention to determine the scaled velocity $\hat{u}$, and hence the upper free surface function $f_1$, in the outer region. In order to evaluate $\hat{u}$, we begin the analysis in this chapter by reconsidering the outer region (region 3) of the system. There is also an extra zone, possibly of dimensions $O(Re^{-1/2})$ by $O(Re^{-1/2})$ and governed by the full Navier-Stokes or Euler equations, with radius of curvature of order unity, that joins the viscous wake area and the outer inviscid solution together.

The outer region 3 is described by

$$\left.\begin{aligned} \hat{u}_{\hat{x}} + \hat{V}_{\hat{y}} &= 0, \\ \hat{u}_t &= -p_{\hat{x}}, \\ \hat{V}_t &= -p_{\hat{y}}, \end{aligned}\right\} \tag{6.2}$$

as given by equations (5.1-5.3) in chapter 5, with zero pressure $p$ required along the upper free surface $\hat{x} = 0$ (for $\hat{y} > 0$) as well as along $\hat{y} = 0$ (for $0 > \hat{x} > \hat{x}_A$), and with given efflux conditions along $\hat{y} = 0$ (for $\hat{x}_B < \hat{x} < \hat{x}_A$).

A schematic diagram of the flow-field illustrates the domain of our investigation and is given in figure 6.1, where, in addition to the boundary-layer regions adjacent to the ship side, there exists the upper free surface whose shape is now to be determined.

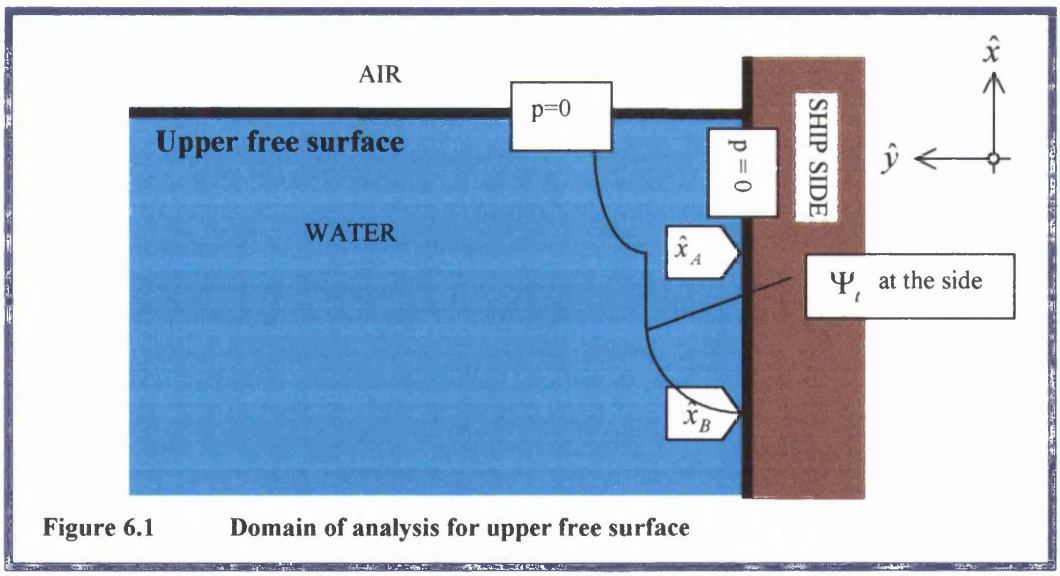


**Figure 6.1** **Domain of analysis for upper free surface**

We investigate the effect on the upper free surface, using the relation

$$\frac{\partial f_1}{\partial t} \equiv \left.\frac{\partial \Psi}{\partial \hat{y}}\right|_{\hat{x}=0} \tag{6.3}$$

from (6.1).To now determine $\frac{\partial f_1}{\partial t}$ we must first examine $\frac{\partial \Psi}{\partial \hat{y}}$ evaluated at $\hat{x} = 0$.

In chapter 5, we obtained the formula (5.35), which is the solution for $\Psi_t$ along $\bar{y} = 0$ for the transformed range $\bar{x} > \bar{x}_A$. Similarly, for the upper free surface solution at all points, we may use

$$\Psi_{\hat{y}} = \Psi_{\bar{y}} \bar{y}_{\hat{y}} + \Psi_{\bar{x}} \bar{x}_{\hat{y}}, \tag{6.4}$$

with the map transformation $\bar{z} = -\hat{z}^2$ giving

$$\bar{x} = \hat{y}^2 - \hat{x}^2, \tag{6.5}$$

and

$$\bar{y} = -2\hat{x}\hat{y}. \tag{6.6}$$

Thus

$$\bar{x}_{\hat{y}} = 2\hat{y}, \tag{6.7}$$

and

$$\bar{y}_{\hat{y}} = -2\hat{x}. \tag{6.8}$$

Thus (6.4) becomes, using equations (6.7) and (6.8),

$$\Psi_{\hat{y}} = \Psi_{\bar{y}}(-2\hat{x}) + \Psi_{\bar{x}}(2\hat{y}). \tag{6.9}$$

The area of investigation is along the positive $\bar{x}$-axis in the transformed $\bar{z}$-plane, in order to examine the upper free surface along which $\hat{x}$ is zero, as shown in figure 6.2.

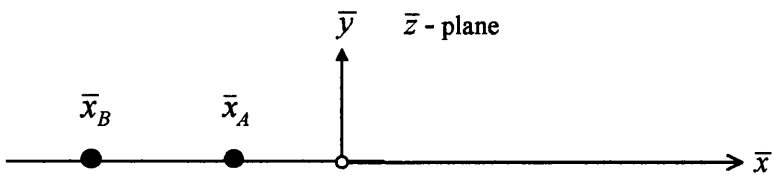


**Figure 6.2** **The $\bar{z}$-plane analysis**

Equations (6.5) and (6.6) are thus expressed then as

$$\bar{x} = \hat{y}^2, \tag{6.10}$$

and $\bar{y} = 0$. (6.11)

So equation (6.9) becomes

$$\Psi_{\hat{y}}\big|_{\hat{x}=0} = 2|\bar{x}|^{1/2}\Psi_{\bar{x}}\big|_{\bar{y}=0}. \tag{6.12}$$

Hence we may now obtain $f_1$ by substitution of equation (6.12) into (6.3) giving

$$\frac{\partial f_1}{\partial t} = 2|\bar{x}|^{1/2}\left(\frac{\partial \Psi}{\partial \bar{x}}\right)_{\bar{y}=0} \tag{6.13}$$

or, more conveniently,

$$\frac{\partial^2 f_1}{\partial t^2} = 2|\bar{x}|^{1/2}\frac{\partial}{\partial t}\left(\frac{\partial}{\partial \bar{x}}\Psi\right)_{\bar{y}=0}. \tag{6.14}$$

The next step in the analysis is to insert into equation (6.14) the formula for $\Psi_t\big|_{\bar{y}=0}$ which we have already developed in the previous chapter (equation 5.35 or 5.38) and which includes the displacement function $\delta$ for downward motion, giving

$$\Psi_t = -\frac{1}{\pi}\left\{\frac{\alpha_0}{t^{1/2}}\tan^{-1}\left(\frac{(L^2-t^2)^{1/2}}{\rho}\right)+\frac{\alpha_1}{2}\rho\Omega\right\}, \tag{6.15}$$

where $\Omega = \int_{\bar{x}_B}^{-L^2} \frac{(\bar{x}_A-\bar{\xi})^{-1/2}}{(\bar{x}-\bar{\xi})}\left(t+L+\left(-\bar{\xi}\right)^{1/2}\right)^{-1/2} d\bar{\xi}$.

Thus, substituting equation (6.15) into (6.14), we obtain

$$\frac{\partial^2 f_1}{\partial t^2} = -2|\bar{x}|^{1/2}\frac{\partial}{\partial \bar{x}}\left(\frac{1}{\pi}\left\{\frac{\alpha_0}{t^{1/2}}\tan^{-1}\left(\frac{(L^2-t^2)^{1/2}}{\rho}\right)+\frac{\alpha_1}{2}\rho\Omega\right\}\right). \tag{6.16}$$

At this stage it is worth noting that $\bar{x}$ is positive, since here on the upper free surface $\bar{x} \equiv \hat{y}^2$ from (6.10). As we have already computed the numerical solution for $\Psi_t$ along the $\bar{x}$ axis for all times in chapter 5, we may now proceed to determine directly the upper free surface function $f_1$ from equation (6.16).

In the subsequent sections, we shall consider the computational and analytical properties of the upper free surface for both small and large values of time, and subsequently for a general value of the time variable, respectively.

## 6.2 The upper free surface equation for small times

Based on the analytical solution for $\Psi_t$ from Chapter 5, section 5.6, we develop the solution for the upper free surface at small times for the $|\bar{x}| \sim 1$ scale.

The upper free surface is found below to rise for all scaled times, which is sensible physically since the ship-side boundary layer is contributing a positive mass flux, namely + $\delta Re^{-1/2}$ in scaled terms, into the outer-flow region 3. This is because fluid is being drawn or injected from the boundary layer as the ship-side moves downwards.

### 6.2.1 For the scale $|\bar{x}| \sim 1$

Near the origin, in preparation for matching there, we have the behaviour of $\Psi_t$ from consideration of equation (5.41c). Thus we expect that

$$\Psi_t \approx \left(-\frac{\alpha_0}{2t^{1/2}}\right)\left(1+O\left(\frac{\bar{x}^{1/2}}{L}\right)\right), \tag{6.17a}$$

which implies

$$\hat{u}_t = \Psi_{\hat{y}t} \approx \left(-\frac{\alpha_0}{2t^{1/2}}\right)\cdot O(1). \tag{6.17b}$$

So equation (6.1) for the upper free surface function gives upon substitution the estimate

$$(f_1)_{tt} \sim O(t^{-1/2}). \tag{6.18}$$

Hence the upper free surface requires, upon integration,

$$f_1 = O(t^{3/2}), \tag{6.19}$$

On the other hand, when $\bar{x} >> 1$, equation (5.41c) implies that

$$\Psi_t = O\left(t^{-1/2}\bar{x}^{-1/2}\right) \tag{6.20}$$

Thus equation (6.1) now gives the upper free surface satisfying

$$(f_1)_{tt} \sim t^{-1/2}\bar{x}^{-1}, \tag{6.21}$$

and thus

$$f_1 \sim t^{3/2}\bar{x}^{-1}. \tag{6.22}$$

The order estimates (6.19) and (6.22) together suggest an upper free surface effect as shown in Figure 6.3. This should be compared with the numerical profiles generated later.

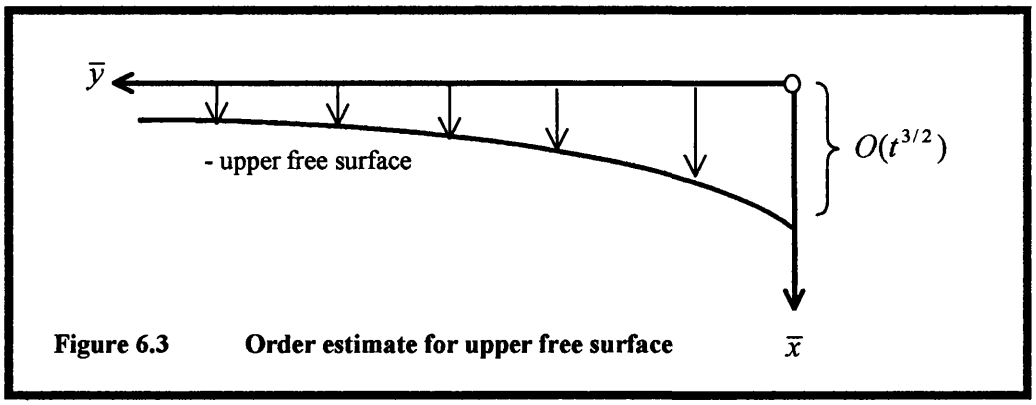


**Figure 6.3 Order estimate for upper free surface**

We now turn our attention to examining the upper free surface function $f_1$ in a more precise manner. We assume that equation (6.10) may be transformed as

$$\hat{y} = |\bar{x}|^{1/2} \Rightarrow d\hat{y} = \frac{1}{2|\bar{x}|^{1/2}} d\bar{x}. \tag{6.23}$$

Substituting equation (5.41c) for $\Psi_t$, with unit length $L$, into (6.14), yields

$$\frac{\partial^2 f_1}{\partial t^2} = -2|\bar{x}|^{1/2} \frac{a_0}{\pi t^{1/2}} \frac{\partial}{\partial \bar{x}} \left( \tan^{-1} \left( \frac{1}{|\bar{x}|^{1/2}} \right) \right), \tag{6.24}$$

where $a_0$ is a constant as defined in chapter 5. Equation (6.24) is a precise form for the leading order upper free surface function, valid for small times. This may differentiated to yield the expression

$$\frac{\partial^2 f_1}{\partial t^2} = \frac{a_0}{\pi t^{1/2}} \left( \frac{1}{\hat{y}^2 + 1} \right), \tag{6.25}$$

which gives upon successive integration the final form for the upper free surface function

$$f_1 = \frac{4}{3} \frac{a_0 t^{3/2}}{(\hat{y}^2 + 1)\pi}. \tag{6.26}$$

This may be used directly for calculations of the analytical results for various values of $\hat{y}$. The upper free surface asymptotic solution (6.26) is plotted against $\hat{y}$ for time values 0.2 and 0.8 and is presented in figure 6.4 at the end of the chapter. Without the inclusion of gravity, the response of the free surface given by (6.26) is somewhat theoretical, since it is unlikely that this shape would carry on infinitely with respect to time.

## 6.3 Computational Solution

Program 6.1 is for the evaluation of the upper free surface function $f_1$ from equation (6.16). This consists of evaluating the derivative of $f_1$ with respect to $\bar{x}$ and subsequently two successive numerical integrations with respect to $t$, for a fixed value

of $\hat{y}$, performed using the trapezoidal approximation. Figure 6.5 shows profiles of the upper free surface function, $f_1$, against the distance from the ship-side, $\hat{y}$, for a range of values of time from 0.2 to 1. As time marches on $f_1$ increases nonlinearly with time. The maximum value of $f_1$ occurs near the ship-side $\hat{y}$, which is in line with the expectation as seen in figure 6.3.

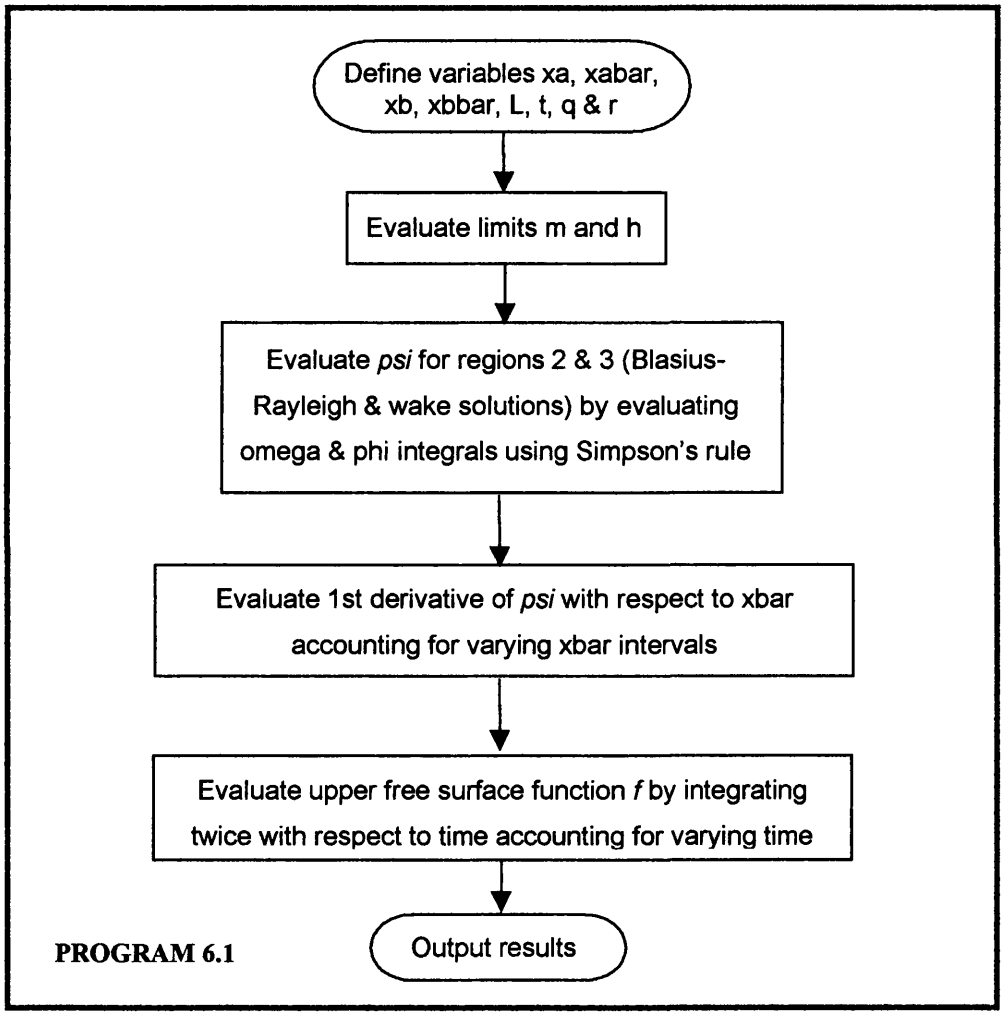


The profiles for $f_1$ versus time are presented in figure 6.6, for selected values of $\hat{y}$. As time marches on, $f_1$ exhibits a smooth downward trend as previously described.

The computational solution for the upper free surface together with the asymptotic solution of (6.26) for $t$=0.8 are presented in figure 6.7. Very good agreement is observed between the two profiles.

## 6.4 The upper free surface equation for large times

From previous analysis in chapter 5, we see that for large times $t$, the displacement derivative function given by equation (5.50) may be substituted into equation (6.14) to give the upper free surface function

$$\frac{\partial^2 f_1}{\partial t^2} = \frac{\bar{\bar{x}}^{1/2}\alpha_1}{\sqrt{2}t^{3/2}(\bar{\bar{x}}+1)^{3/2}}. \tag{6.27}$$

This gives upon successive integration the asymptotic form for the upper free surface function for large times $t>>1$, with $\bar{\bar{x}}$ remaining of order unity,

$$f_1 = \left(\frac{\alpha_1}{\sqrt{2}}\right)\bar{\bar{x}}^{1/2}t^{1/2}\int_0^1 \frac{Q^{1/2}(1-Q)dQ}{(\bar{\bar{x}}+Q^2)^{3/2}}. \tag{6.28}$$

To calculate (6.28) we compute the integral in (6.28) using Simpson's rule as given by program B1 of Appendix B.

When $\bar{x} \sim O(t^2)$, i.e. $\bar{\bar{x}}$ of $O(1)$ the function thus has the order of magnitude

$$f_1 \sim t^{1/2}. \tag{6.29}$$

Figure 6.8 shows the asymptotic form of $f_1$ for five values of large time in the range $10 \le t \le 50$ according to (6.28). (This gives, for small $\bar{\bar{x}}$, $f_1 \sim t^{1/2}\bar{\bar{x}}^{-1/4}$, i.e. $f_1 \sim t\bar{x}^{-1/4}$, implying that $f_1$ is of order $t$ at $O(1)$ distances $\bar{x}$; the linear growth in $t$ here agrees with the subsequent estimates for $f_1$ at large times). So we will now seek to obtain $f_1$ for all $t$, from a numerical treatment, to compare with the analytical form of (6.28).

## 6.5 Computational solution for larger times

In the same manner as with program 6.1, program 6.2 is concerned with the evaluation of the upper free surface function, but now for the larger times defined by $t>L$. As a result, program 6.2 is identical in structure as with program 6.1 except for

the only modification that the evaluation of $\Psi_t$ is via the integral $\Lambda$ in (5.44) as opposed to the integral $\Omega$ in (5.36b), which are identical in form but with different limits.

The profiles for $f_1$ versus time are presented in figure 6.9, for odd integer values of $\hat{y}$ in the range 1-20. As time marches on, $f_1$ exhibits a smooth almost linear trend downwards. The $f_1$ profiles against $\hat{y}$ for various time values in the range 1-40 are presented in figure 6.10, and show that as time increases, the upper free surface descends with a peak at $\hat{y}$=2.

## 6.6 The side free surface function

The evaluation of the scaled side free surface function $f_s$ may be made via the following equation, which employs the displacement function (5.38) and the wake displacement function (3.6). The shape function of the side free surface is given by

$$f_s(\bar{x},t) = -\Psi_t - \delta_w(\bar{x},t) \qquad (6.30)$$

for the region $\bar{x}_A \le \bar{x} \le 0$. This is effectively the function $f$ used in the wake study, in (4.4a). Here $\delta_w(\bar{x},t)$ is given by the boundary layer wake equation as derived computationally in chapter 3, while $\Psi_t$ is the displacement derivative function of chapter 5.

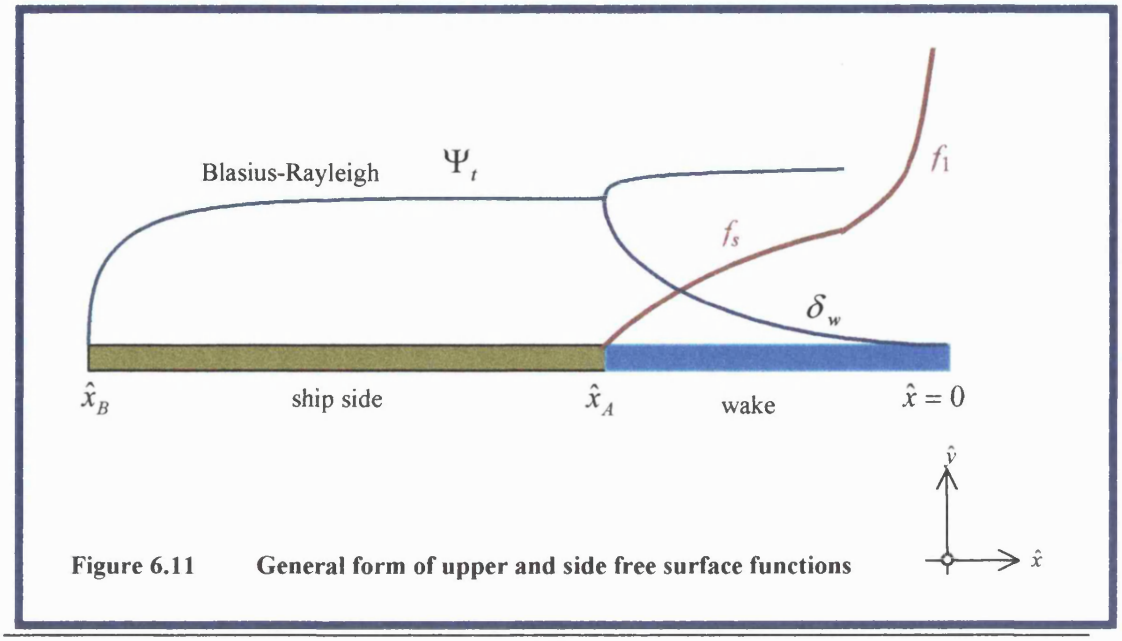


**Figure 6.11 General form of upper and side free surface functions**

The general shape of the side free surface profile may thus be ascertained from examination of figure 6.11, where the displacement and wake profiles are sketched.

The numerical evaluation of $f_s$ is generated by Program 6.3, which takes as inputs the numerical results for $\delta_w(\bar{x},t)$ and $\Psi_t$ generated by programs 3.1 and 5.1, respectively. The values of time considered first were from 0.2 to unity. The profiles for $f_s$ with $\bar{x}$ are given in figure 6.12. It is observed that as time increases, which corresponds to the ship-side submerging, there is a gradual rise in the side free surface function. The profiles produced compare well with the subsequent computational predictions of Li (2000) as shown in figure 6.13. Figure 6.14 shows that for large values of time in the range 3-7, the $f_s$ profiles converge to a limiting profile.

## 6.7 Fortran 77 programs and figures

```
C       ************************************************
C       February 1998   D.Papadopoulos
C       ************************************************
C       Program to evaluate the UPPER-FREE-SURFACE variation with
C       y-coordinate and time for SMALL TIMES
C       ************************************************
C       ************************************************

C       Problem: Downward motion of ship in stationary fluid
C       ************************************************

C       *** Definition of all variables, except y,t ***

        program smtop
        REAL o(1000),Psi(1000),gradPsi(1000)
        REAL res(1000),h,sum,term,rho
        REAL ystart,yprev,xbarprev,astart
        REAL dy,y,dt,t
        REAL u,xbar,xabar,xbbar,xa,xb,pi,q,r
        REAL ztt(1000,1000),zt(1000,1000),z(1000,1000)
        INTEGER i,j,mm,m,n,nn,L,a,aa

        mm =360
        L = 1
        pi = 3.1415927

C       q means a0 and r means a1
        q = 0.25
        r = 0.25

C       Valid for values of small times: t<1,thus (aa*dt)<1

        astart=0.05
        aa=19
        dt =0.05

C       Valid for integer values of ystart (unity) and fractional values of dy

        ystart=0.1
        nn=200
        dy=0.1

        do  7000 a=1,aa
        t=((a-1)*dt)+astart

C       *** Determination of m and h ***
        xa = -t
        xb = xa-L
        xbbar = -((xb)**2)
        xabar = -((xa)**2)

        m = (2 * mm) + 3
        h =  ((( - (t**2) + ((t+L)**2) )**0.5) - ( ( (L**2) - (t**2) )**0.5))
        ((2*mm) + 2)

C       ************************************************************

        do 2010 n=1,nn
        Psi(n)=0.
        gradPsi(n)=0.
2010    continue

C       General loop to evaluate Top shape (including omega
C       integral) for values of the xbar-coordinate
```

6.1 Program to evaluate the upper free surface variation with $\hat{y}$, valid for small times.

```
      do 3000 n=1,nn
      y=((n-1)*dy)+ystart
      xbar = y**2

C     *** Evaluate o(j), also evaluating u(j) at each j ***

      do 2024 j = 1,m-1
      u = ((j - 1) * h)+( ( (L**2) - (t**2) )**0.5)
2024  o(j) = 2*((t+L+((u**2+t**2)**0.5))**(-0.5))/ (xbar+t**2+u**2)


C     *** Evaluate first and final terms of the omega integral ***

      sum = o(1) + o(m) + (4*o(m-1))

C     Evaluate complete integral including the intermediate terms

      do 2027 i = 1,mm
      j = 2 * i
2027  sum = sum + (4.0 * o(j)) + (2.0 * o(j+1))

      res(n) = (sum * (h/3.0))

C     *** Evaluate Psi(n) ***

      term=( ((   L**2) - (t**2)) / (xbar-xabar) )**0.5
      rho=r*(t**(-0.5))
      Psi(n) = -((0.5/pi)*((xbar-xabar)**0.5)*(q*res(n)))-
      ( rho*0.31831*atan(term) )

3000  continue

C     ************************************************************

C     ** Evaluate gradient-Psi function accounting for varying intervals **

      do 4000 n=2,nn

      y=((n-1)*dy)+ystart
      xbar =  y**2
      yprev=((n-2)*dy)+ystart
      xbarprev=yprev**2

      gradPsi(n) = (Psi(n)-Psi(n-1)) / (xbar-xbarprev)
      ztt(n,a) = 2 * (xbar**0.5) * gradPsi(n)

4000  continue
7000  continue

C     ** Evaluate integral across time using trapezoidal approximation **

      do 9000 n=2,nn
      do 8000 a=1,(aa-1),1

      zt(n,1) = 0.0
      zt(n,a+1)=(dt*ztt(n,(a+1)))+zt(n,a)

8000  continue
9000  continue

C     **Evaluate and output results for f**

      do 9800 a=1,(aa-1),1
```

```
      do 9500  n=2,nn,1

      z(n,1)=0.0
      z(n,a+1)=(dt*zt(n,(a+1)))+z(n,a)

C     t=((a-1)*dt)+astart
C     WRITE (6,*) t,    z(n,a)

      y=((n-1)*dy)+ystart
      IF (y.GE.0.5)      THEN
      WRITE (6,*) y,    z(n,a)
      ENDIF

9500  continue

      WRITE (6,*) ''

9800  continue

      end
```

```
C       ***************************************************
C       ***************************************************
C       March  - October  1998          D.Papadopoulos
C       ***********************************************************
C       Program to evaluate the UPPER-FREE-SURFACE variation with
C       y-coordinate and time for LARGE TIMES
C       ***********************************************************
C       ***********************************************************

C       Problem: Downward motion of ship in stationary fluid
C       ***************************************************

C       *** Definition of all variables, except y,t ***

        program grtop
        REAL lam(1000),Psi(1000),gradPsi(1000)
        REAL res(1000),h,sum
        REAL yprev,xbarprev,ystart,astart
        REAL u,xbar,xabar,xbbar,xa,xb,pi,q,r
        REAL y,dy,t,dt
        REAL ftt(1000,1000),ft(1000,1000),f(1000,1000)
        INTEGER i,j,mm,m,n,nn,a,aa,L

        mm =360
        L = 1
        pi = 3.1415927

C       q means a0 and r means a1
        q = 0.25
        r = 0.25

C       astart must be 100 times smaller than the magnitude of dt.

        astart=0.01
        aa=41
        dt=1

        ystart=0.1
        nn=200
        dy = 0.1

C       *** General loop to evaluate ftt,ft and f functions over time domain *

        do  7000 a=1,aa

        t=((a-1)*dt)+astart

C       Determination of m and h
        xa = -t
        xb = xa-L
        xbbar = -((xb)**2)
        xabar = -((xa)**2)
        m = (2 * mm) + 3
        h =  ( (- t**2 + (t+L)**2 )**0.5) / ((2*mm) + 2)

C       Set all terms of arrays equal to zero

        do 2010 n=1,nn
        Psi(n)=0.
        gradPsi(n)=0.
2010    continue

        do 3000 n=1,nn
```

6.2 Program to evaluate the upper free surface variation with $\hat{y}$, valid for larger times.

```
        y=((n-1)*dy)+ystart
        xbar = y**2

C       *** Evaluate lam(j), also evaluating u(j) at each j ***

        do 2024 j = 1,m-1
        u = ((j - 1) * h)
2024    lam(j) = 2*((t+L+((u**2+t**2)**0.5))**(-0.5))/ (xbar+t**2+u**2)

C       Evaluate first and final terms of the phi and omega integrals

        sum = lam(1) + lam(m) + (4*lam(m-1))

C       Evaluate the complete integrals (i.e. including the intermediate
C       terms)

        do 2027 i = 1,mm
        j = 2 * i
2027    sum = sum + (4.0 * lam(j)) + (2.0 * lam(j+1))

        res(n) = (sum * (h/3.0))

C       *** Evaluate Psi(n) ***

        Psi(n) = -(0.5/pi)*((xbar-xabar)**0.5)*q*res(n)

3000    continue

C       ************************************************************
C       ** Evaluate gradient-Psi function accounting for varying intervals **

        do 5000 n=2,nn

        y=((n-1)*dy)+ystart
        xbar = y**2
        yprev=((n-2)*dy)+ystart
        xbarprev=yprev**2

        gradPsi(n) = (Psi(n)-Psi(n-1)) / (xbar-xbarprev)
        ftt(n,a) = 2 * (xbar**0.5) * gradPsi(n)

5000    continue
7000    continue

C       ** Evaluate integral across time using numerical approximation **

        do 9000 n=2,nn
        do 8000 a=1,(aa-1),1

        ft(n,1) = 0.0
        ft(n,a+1)=(dt*ftt(n,(a+1)))+ft(n,a)

8000    continue
9000    continue

C       **Evaluate and output results for f**

        do 9800  a=1,(aa-1),1

        do 9500  n=2,nn

        f(n,1)=0.0
        f(n,a+1)=(dt*ft(n,(a+1)))+f(n,a)
```

```
            t=((a-1)*dt)+astart
C           WRITE (6,*) t,    f(n,a)

            y=((n-1)*dy)+ystart
            IF (y.GE.0.5)      THEN
            WRITE (6,*) y,    f(n,a)
            ENDIF

9500        continue

            WRITE (6,*) ''

9800        continue

            end
```

```
C       Programs to evaluate side-free-surface function with x-coordinate,
C       for a given value of time

        PROGRAM SFS
        integer i,imax
        real x(1000),xx(1000),d(1000),w(1000),f(1000)

        open (1,file="ww.dat")
        open (2,file="dd.dat")
        open (9,file="f.dat")

        do 10   i=1,1000

        read (unit=1,fmt=*)   x(i),w(i)
        read (unit=2,fmt=*)   xx(i),d(i)

        if ((x(i).gt.100).or.(xx(i).gt.100)) then
        imax=i
        go to 11
        endif

10      continue

11      do 20   i=1,imax-1

        f(i)=d(i)-w(i)

        write (unit=9,fmt=*)   xx(i),f(i)

20      continue

        close (1)
        close (2)
        close (9)

30      end
```

6.3 Program to evaluate the side free surface function with $\bar{x}$, for a given value of time.

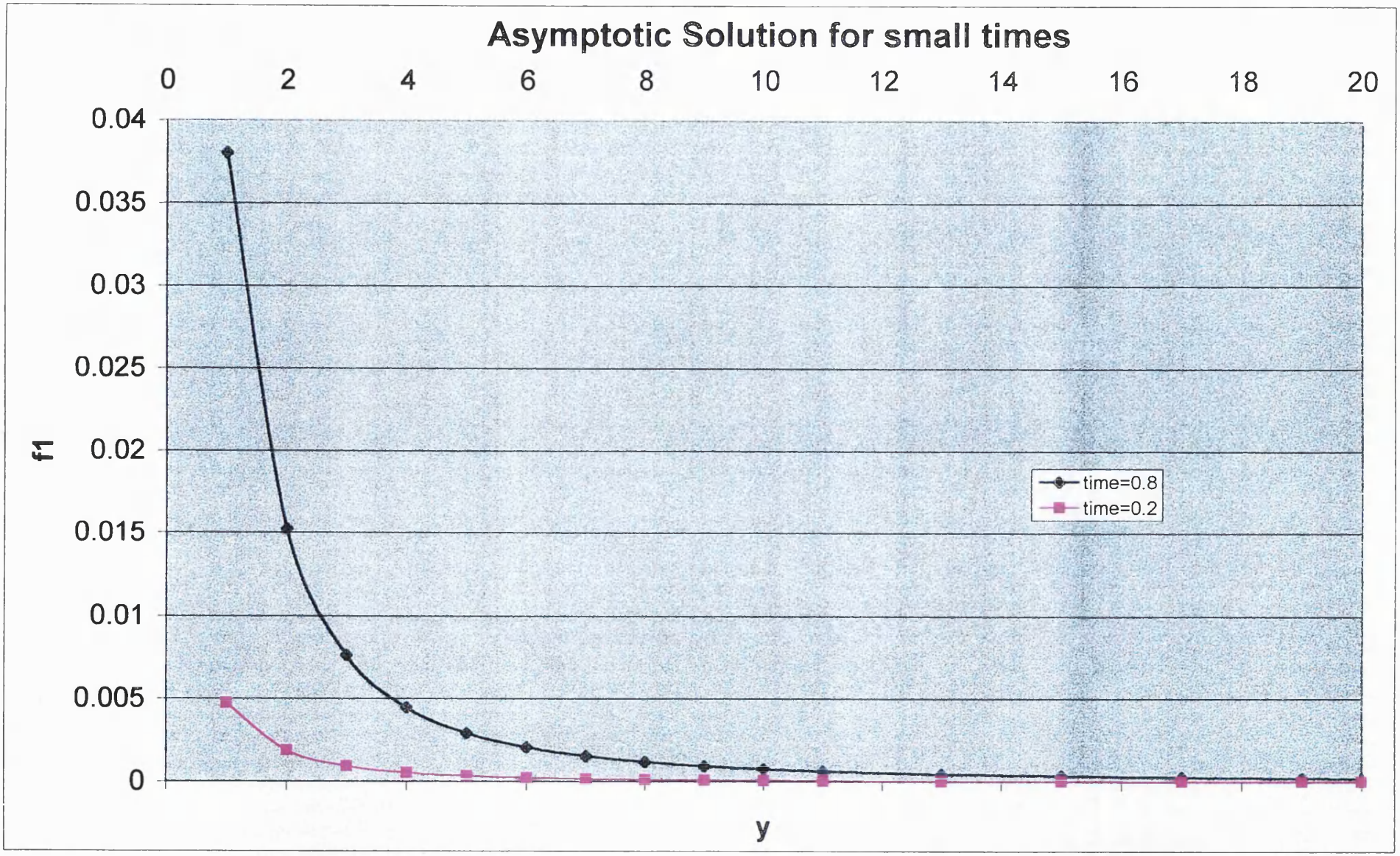
Asymptotic Solution for small times
0
2
4
6
8
10
12
14
16
18
20
0.04
0.035
0.03
0.025
0.02
0.015
0.01
0.005
0
f1
y
time=0.8
time=0.2

Fig. 6.4

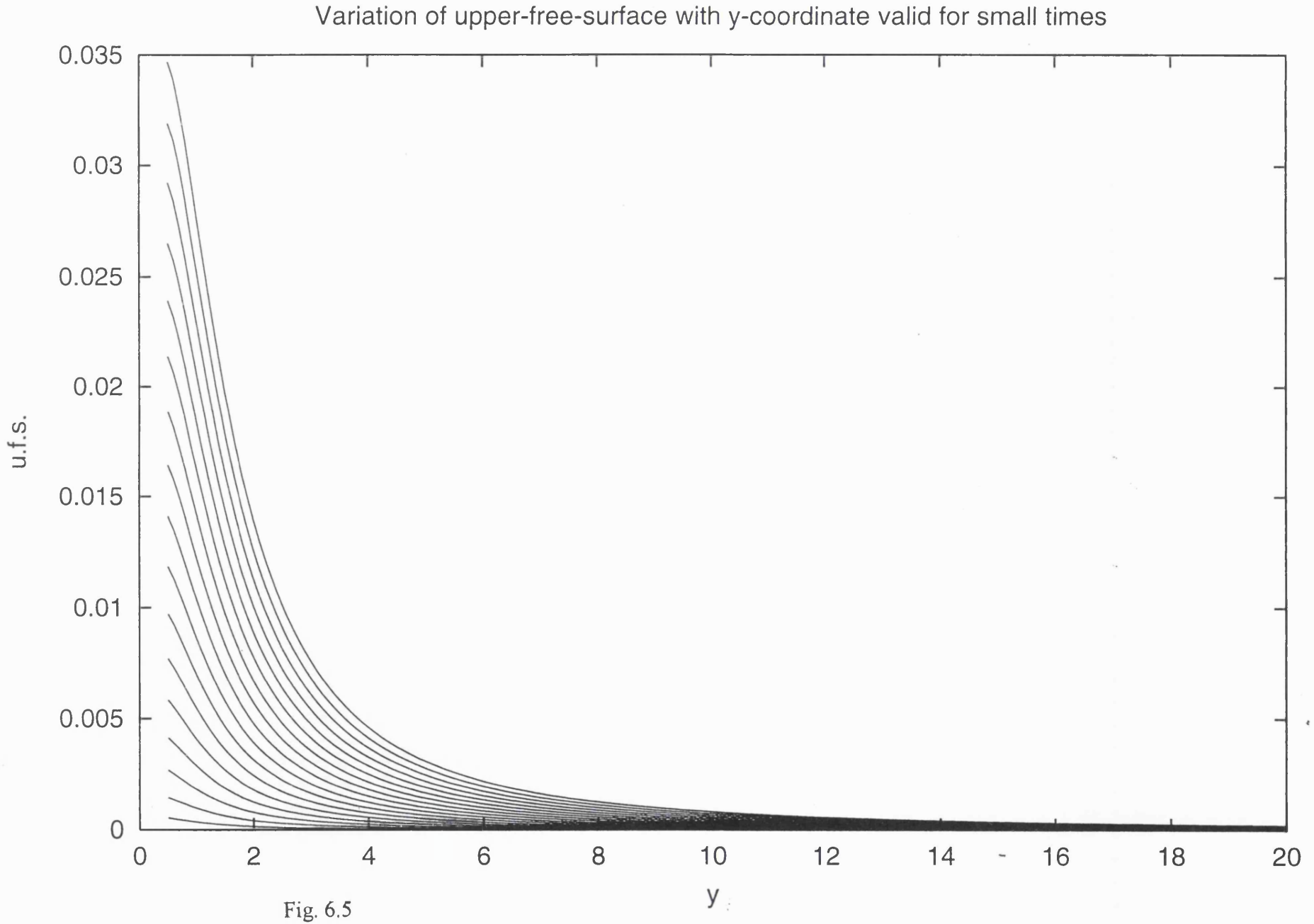
Variation of upper-free-surface with y-coordinate valid for small times
u.f.s.
y
0.035
0.03
0.025
0.02
0.015
0.01
0.005
0
0
2
4
6
8
10
12
14
16
18
20

Fig. 6.5

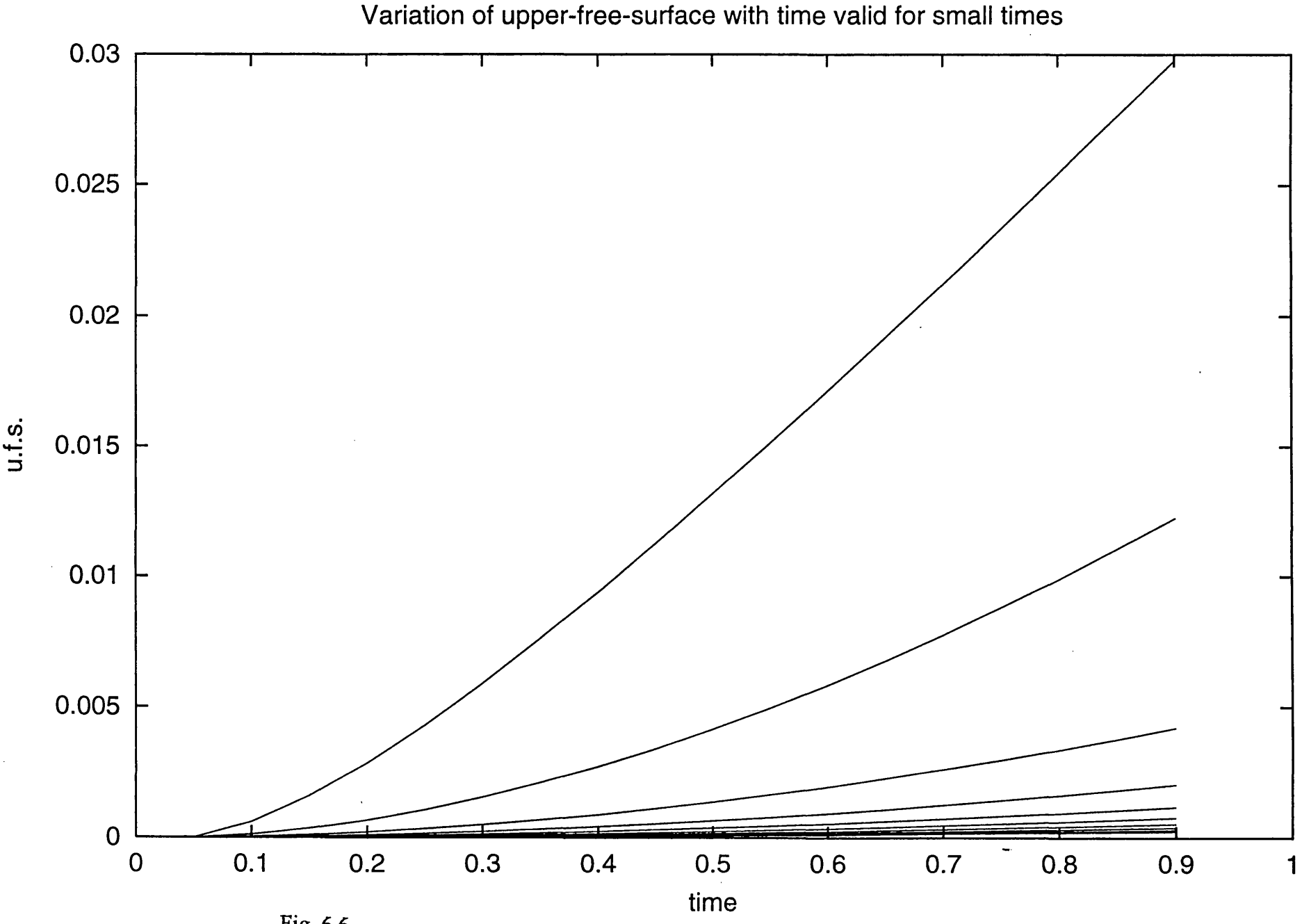
Variation of upper-free-surface with time valid for small times
0.03
0.025
0.02
0.015
0.01
0.005
0
u.f.s.
0
0.1
0.2
0.3
0.4
0.5
0.6
0.7
0.8
0.9
1
time

Fig. 6.6

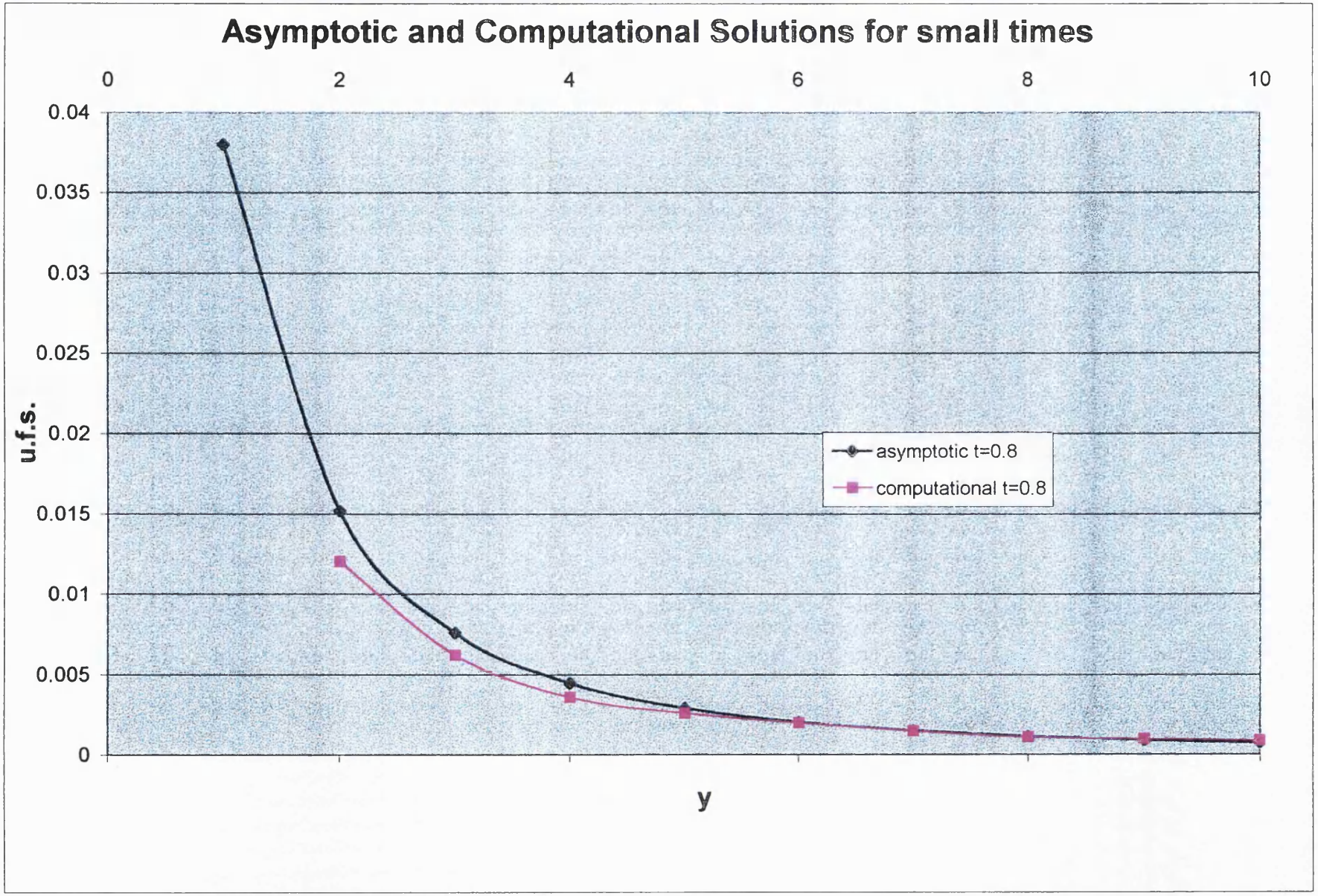
Asymptotic and Computational Solutions for small times
0
2
4
6
8
10
0.04
0.035
0.03
0.025
0.02
0.015
0.01
0.005
0
u.f.s.
y
asymptotic t=0.8
computational t=0.8

Fig. 6.7

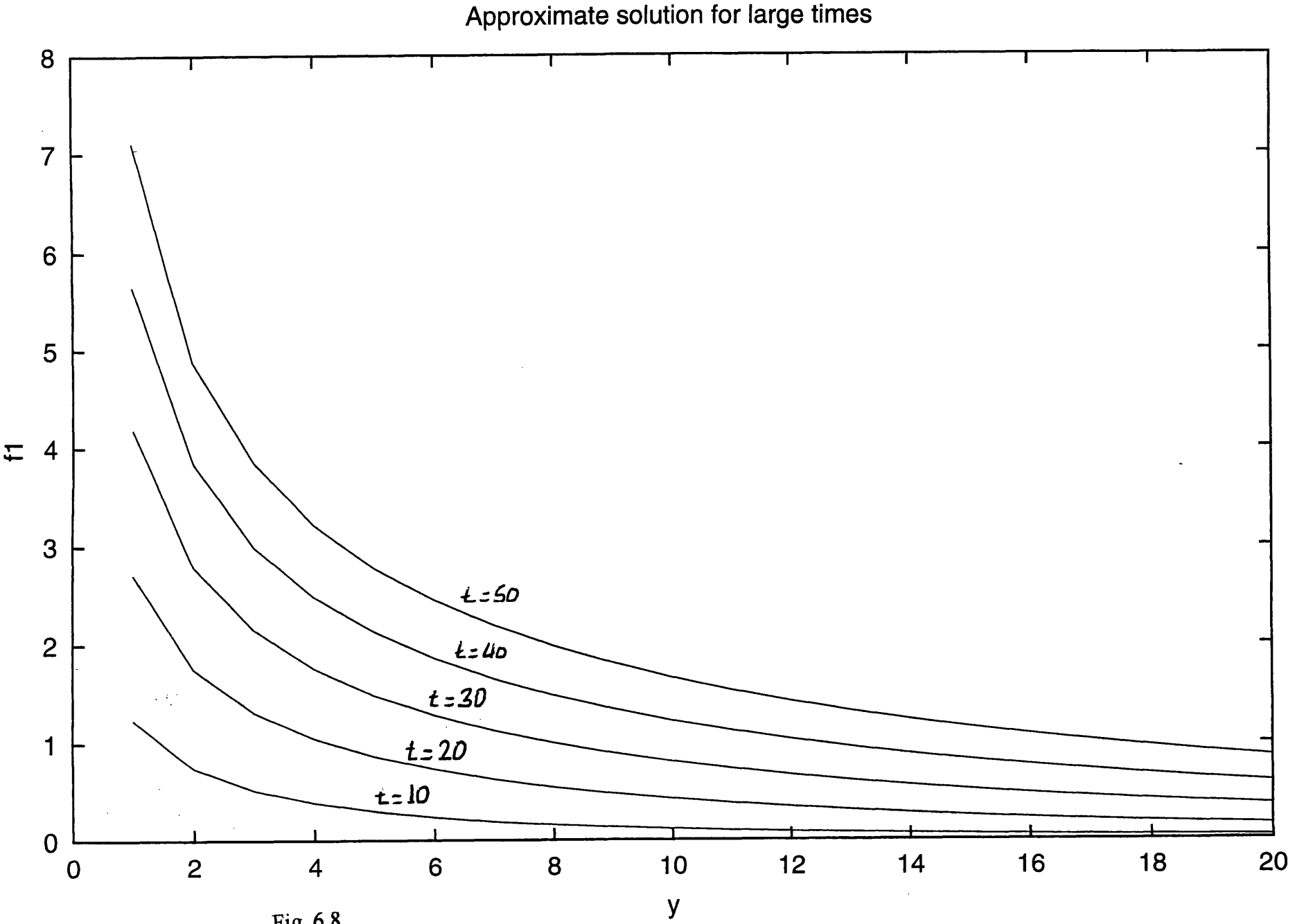
Approximate solution for large times
f1
y
t=50
t=40
t=30
t=20
t=10
0
1
2
3
4
5
6
7
8
0
2
4
6
8
10
12
14
16
18
20

Fig. 6.8

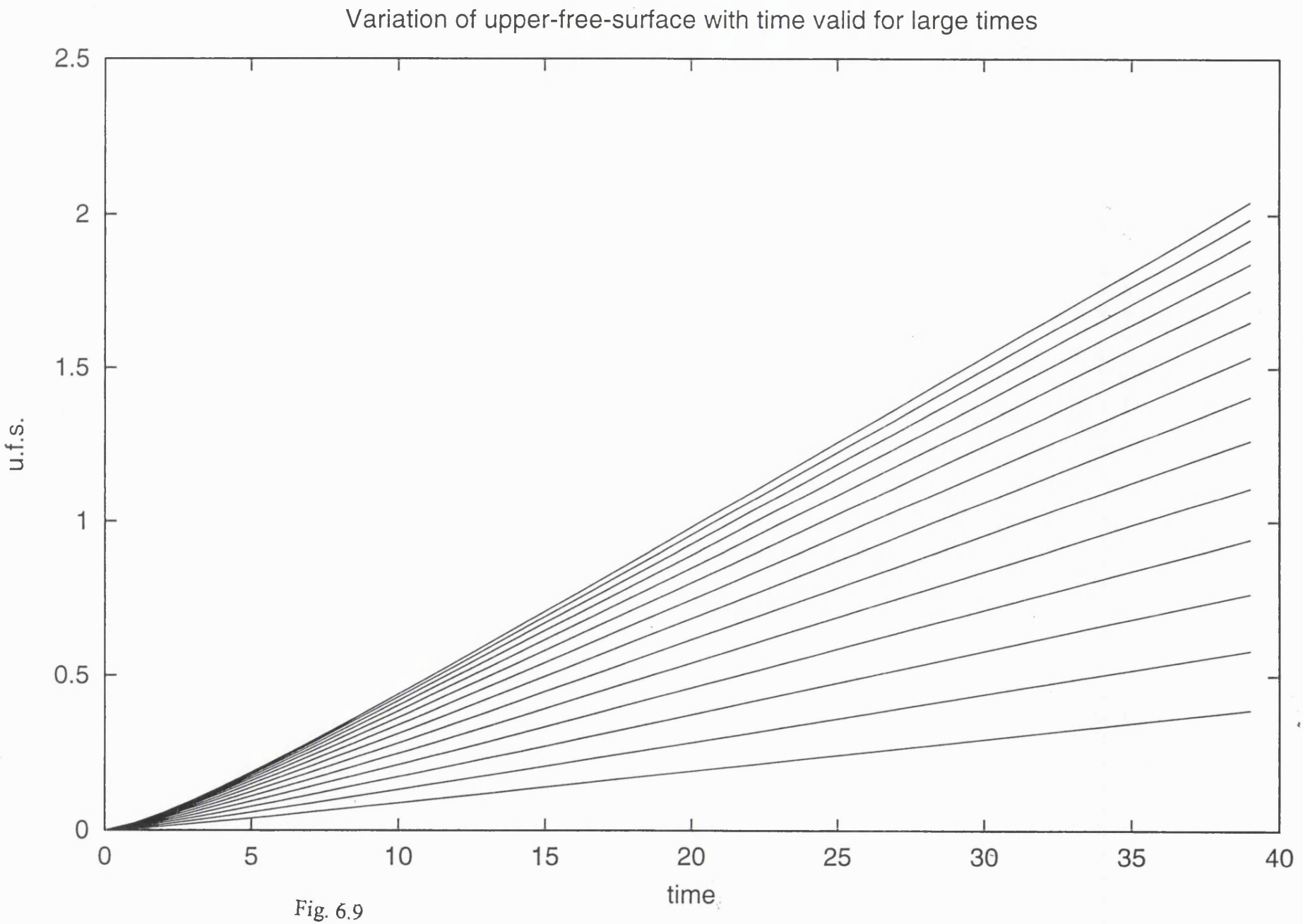
Variation of upper-free-surface with time valid for large times
u.f.s.
time
0
0.5
1
1.5
2
2.5
0
5
10
15
20
25
30
35
40

Fig. 6.9

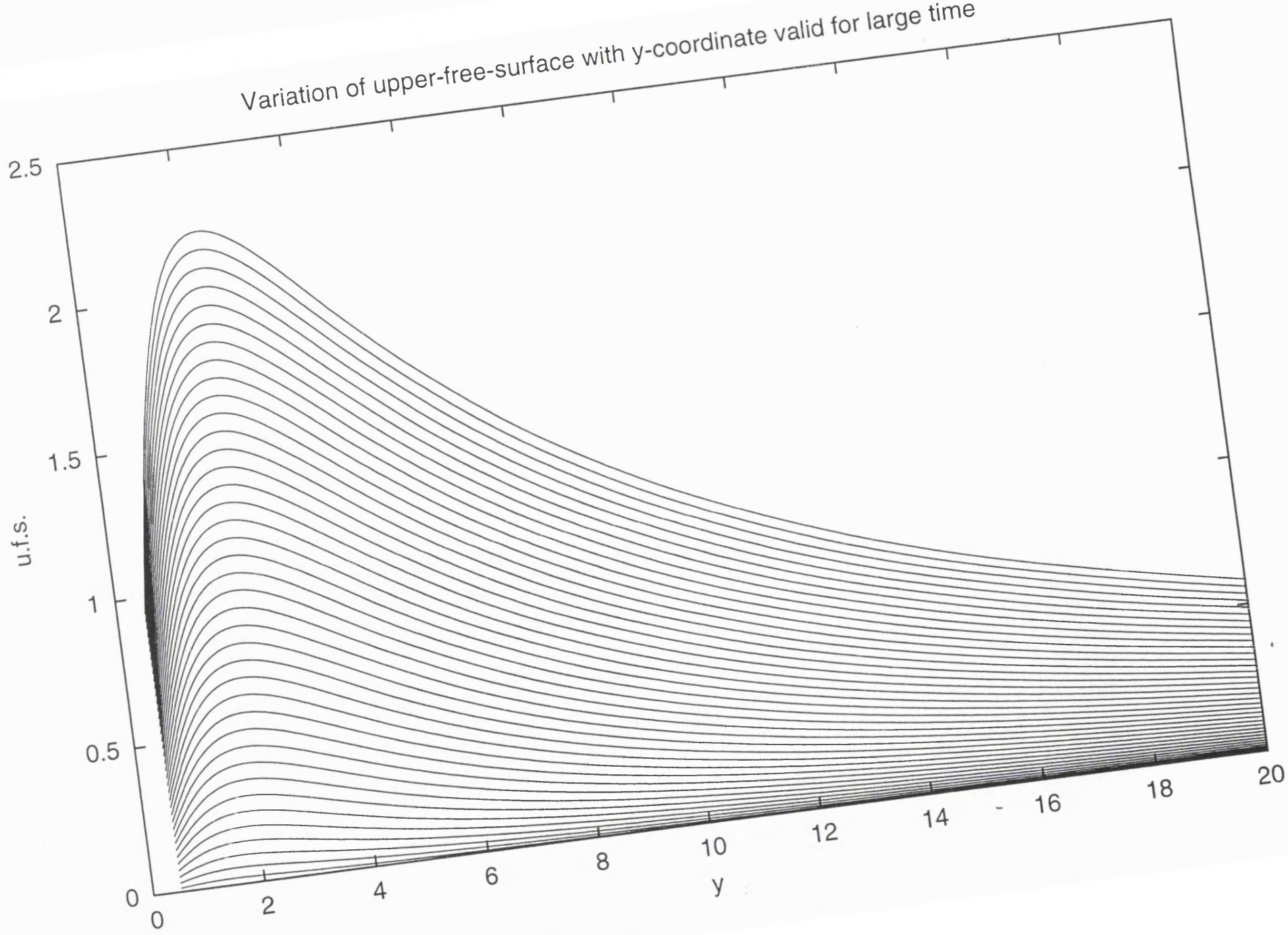
Variation of upper-free-surface with y-coordinate valid for large time
u.f.s.
2.5
2
1.5
1
0.5
0
0
2
4
6
8
10
12
14
16
18
20
y

Fig. 6.10

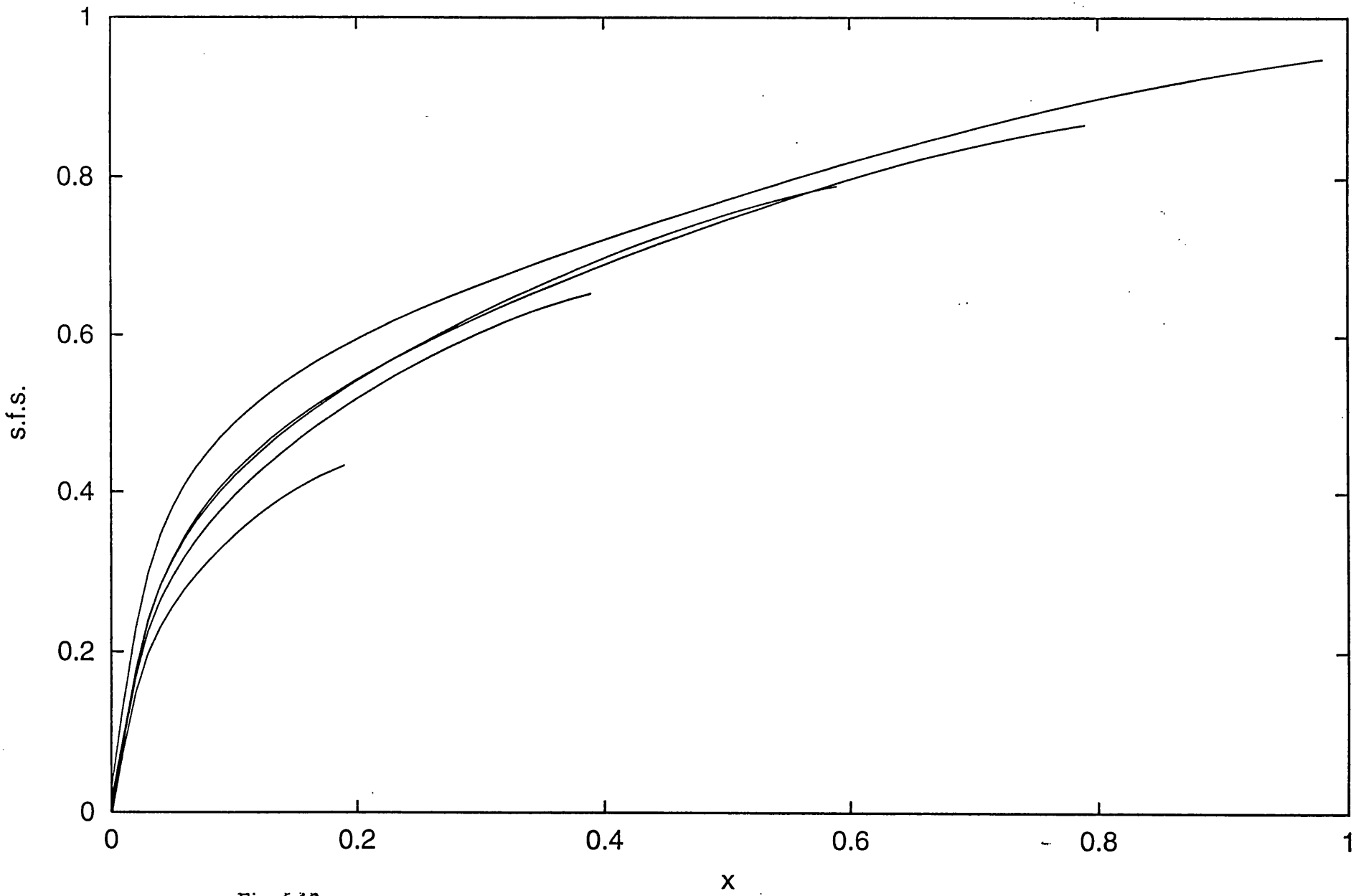
side-free-surface variation with x-coordinate valid for small times
s.f.s.
x
0
0.2
0.4
0.6
0.8
1

Fig. 6.12

# The shape of side free surface

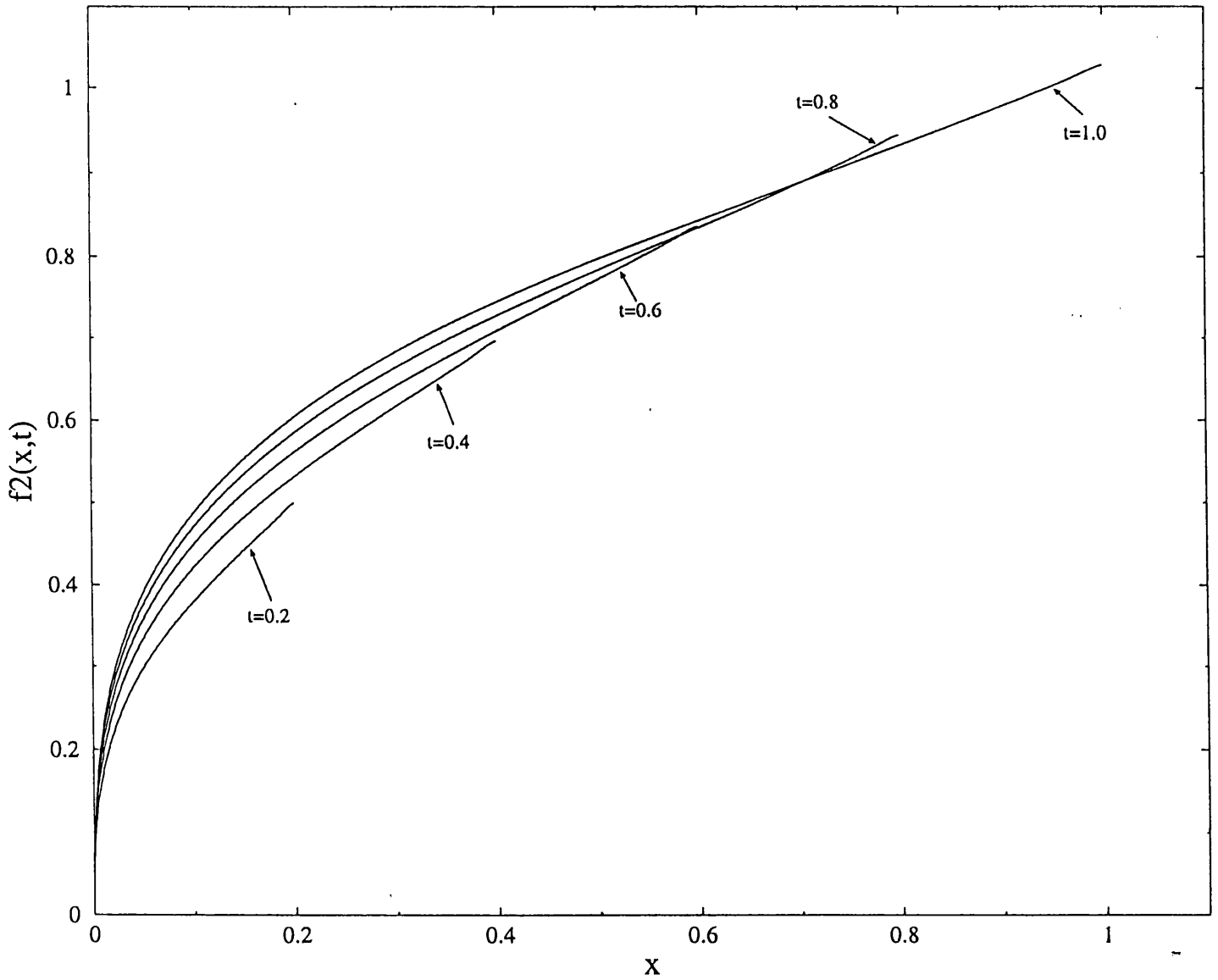


Fig. 6.13

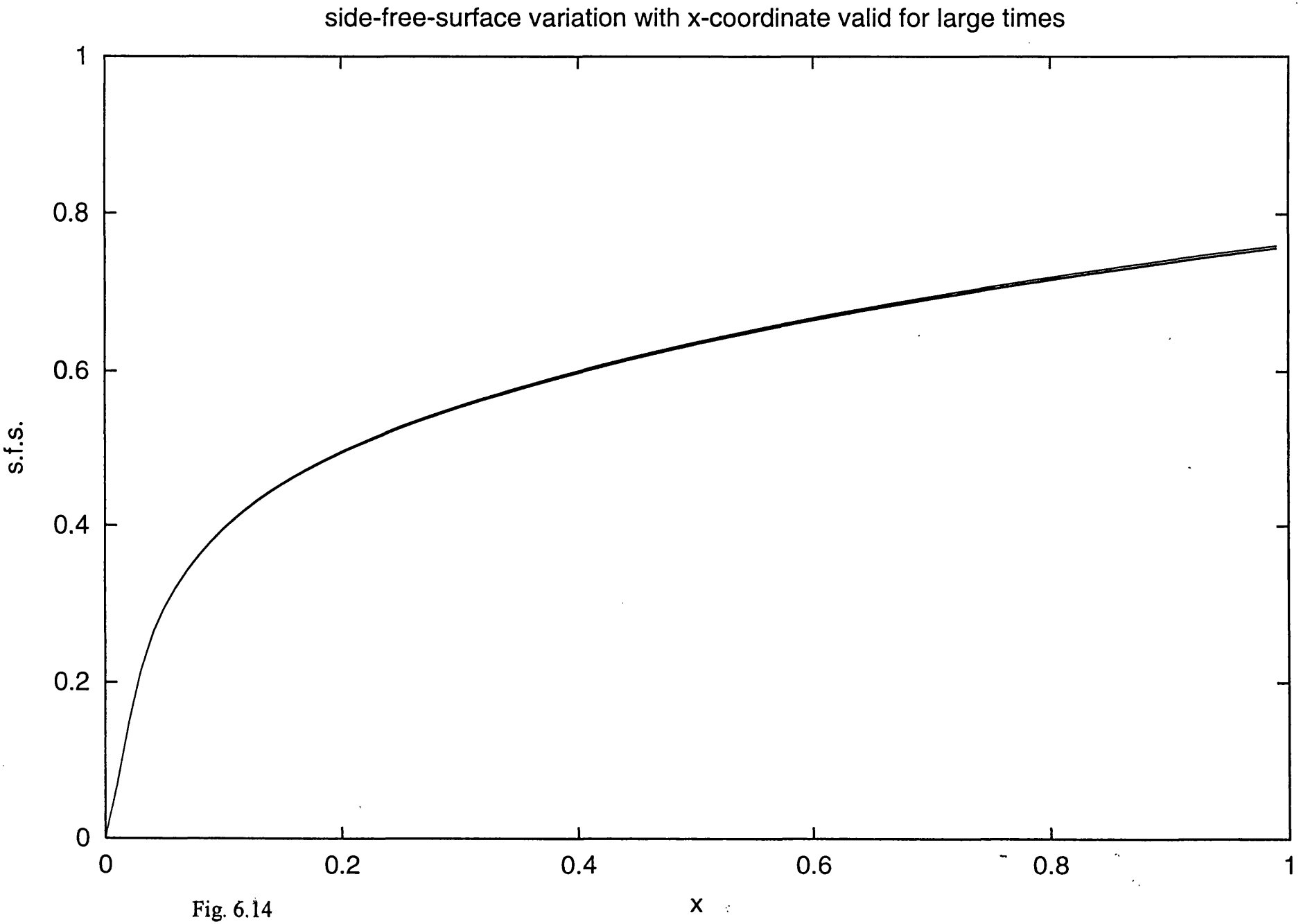
side-free-surface variation with x-coordinate valid for large times
s.f.s.
x
0
0.2
0.4
0.6
0.8
1

Fig. 6.14

# CHAPTER 7

## Investigation of the gravity effect

### 7.1 Introduction

The subject of this chapter is an examination into the influence of gravity on the downward motion of a vertical flat solid surface. Again, the solid surface or ship-side and the water are initially at rest, at time $t$=0. Gravity, which is again labeled $g$ here, alters the flow significantly when $g$ is still small, specifically when $g = \varepsilon \cdot \tilde{g}$ with $\tilde{g}$ of order unity and $\varepsilon \equiv \mathrm{Re}^{-1/2}$, where the Reynolds number is large. This corresponds to the Froude number $Fr$ being assumed to be comparable with $Re^{1/2}$, for mathematical convenience; chapter 1 suggests that in practice $Fr$ is about 0.005 to 4 whereas $\mathrm{Re}^{1/2}$ is about 224 to 3162. The alteration then to the work of the previous chapters is felt only in the outer inviscid region where $\hat{x} \sim 1$ and $\hat{y} \sim 1$, due to there being no effect at leading order in the inner region comprising the boundary layer and the wake.

The problem and its treatment are based on those of chapter 4 and 5, and in consequence the main aim here is to solve the Laplace equation subject to the influence of small values of gravity on the boundary conditions, in a fixed $\hat{x}$ and $\hat{y}$ coordinate system. So the unknown pressure is controlled by

$$\nabla^2 \tilde{p} = 0 \qquad (7.1)$$

in the quarter-plane $\hat{x} < 0$, $\hat{y} > 0$, as shown again in figure 7.1 below

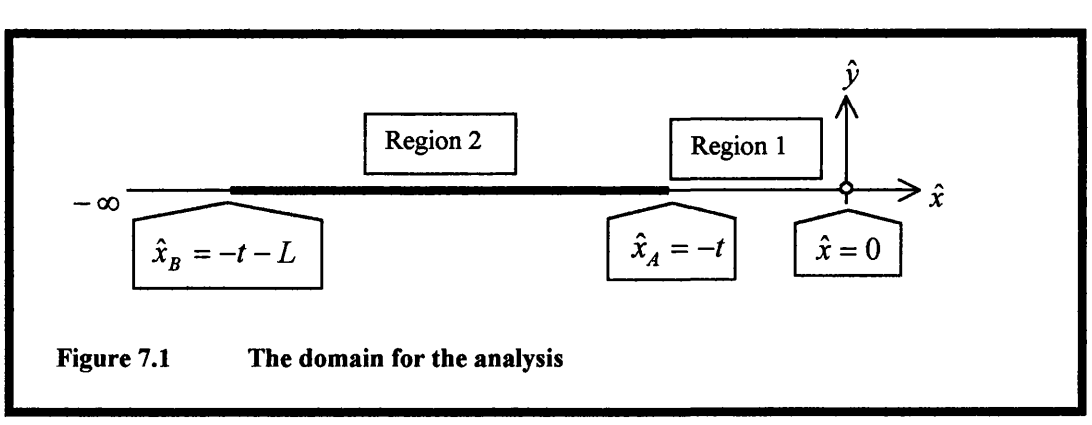


**Figure 7.1 The domain for the analysis**

## 7.2 Derivation of the problem

To derive the current problem we may consider the equations as follows. We start with the unsteady Navier-Stokes equations but are able to neglect the viscous terms since $\hat{x}$ and $\hat{y}$ are of order unity in the outer inviscid region. So we put

$$(u,v,p,\Psi) = (0,0,-g\hat{x},0) + \varepsilon(\tilde{u},\tilde{v},\tilde{p},\tilde{\Psi}) + \ldots, \tag{7.2}$$

where ε is small, $g = \varepsilon\tilde{g}$ and in similar manner to that in chapter 5, we obtain

$$\left.\begin{aligned} &\tilde{u}_{\hat{x}} + \tilde{v}_{\hat{y}} = 0, \\ &\tilde{u}_t = -\tilde{p}_{\hat{x}}, \\ &\tilde{v}_t = -\tilde{p}_{\hat{y}}, \end{aligned}\right\} \tag{7.3}$$

which yields equation (7.1) as expected.

To derive the altered boundary condition in the problem we use the atmospheric balance

$$p = -g\hat{f}_1 \tag{7.4}$$

at the unknown top surface $\hat{x} = \hat{f}_1(\hat{y},t)$. Applying now equation (7.2), which suggests that $\hat{f}_1$ is of order ε, we obtain in equation (7.4) the dominant balance $\varepsilon\tilde{p} = 0$, which is in essence a "modified pressure" effect; that leaves

$$\tilde{p} = 0 \text{ at } \hat{x} = 0. \tag{7.5}$$

For the condition in the wake region, i.e. region 1, we start with $p = 0$, i.e. atmospheric pressure, at the unknown surface

$$\hat{y} = \hat{f}_2(\hat{x},t). \tag{7.6}$$

The expectation here is that $\hat{f}_2 = \varepsilon\tilde{f}_2$ is also small, with $\hat{f}_2$ to tend to unity, and again we have $g = \varepsilon\tilde{g}$. So (7.6) gives $\varepsilon\tilde{p} - \varepsilon\tilde{g}\hat{x} = 0$ at $\hat{y} = 0$ from a Taylor expansion. Hence we obtain for the wake region

$$\tilde{p} = \tilde{g}\hat{x} \text{ at } \hat{y} = 0 \text{ (wake part).} \qquad (7.7)$$

Additionally, for the boundary layer condition we can continue to use $\varepsilon\tilde{\Psi}_{\hat{x}t} = -\varepsilon\tilde{v}_t = \varepsilon\tilde{p}_{\hat{y}} = -\varepsilon\delta_{\hat{x}t}$, to obtain

$$\frac{\partial\tilde{p}}{\partial\hat{y}} = -\frac{\partial^2\delta}{\partial\hat{x}\partial t} \text{ at } \hat{y} = 0 \text{ (boundary layer part).} \qquad (7.8)$$

Here $\delta$ is the given boundary layer (scaled) displacement along region 2, and in effect $\delta \equiv 0$ for $\hat{x} < -t - L$, where the ship-side length $L$ is unity; equation (7.8) means that $\tilde{\Psi} = -\delta$ along the edge of region 2 as in chapter 5. Finally, we assume again the condition in the far-field of $\tilde{\Psi} \to 0$. Hence the only change due to allowing for the scaled gravity force $\tilde{g}$ occurs in the boundary condition (7.7).

## 7.3 Solution for the gravity effect

The solution of the gravity effect problem is based on forming $\tilde{p} - i\tilde{\Psi}_t$, which is analytic in $\hat{z} = \hat{x} + i\hat{y}$, say $\Im(\hat{z})$, and is similar to the complex function examined in chapter 5. Again we introduce the same conformal transformation $\bar{z} = -\hat{z}^2$, which allows consideration of the problem in an upper ½-plane instead of the original ¼-plane. The mapped coordinate system is again defined by the polar coordinates $\bar{r}, \bar{\theta}$, in view of the mixed boundary condition similar to equation (5.17),

$$P + iQ = (\bar{z} - \bar{x}_A)^{-1/2}\left[\tilde{p} - i\tilde{\Psi}_t - \Im_0\right], \qquad (7.9)$$

with now the additional gravity effect term included such that $\Im_0 = \left[\tilde{p} - i\tilde{\Psi}_t\right] = (-\tilde{g}t + i\delta_0')$. Also we have as before $(\bar{z} - \bar{x}_A)^{-1/2} = \bar{\bar{r}}^{-1/2} e^{-(i\bar{\bar{\theta}})/2}$ in shifted polar coordinates.

Continuing from the above we see that for $\bar{x} < \bar{x}_A$, i.e. for $\bar{\theta} = \pi$,

$$P + iQ = \bar{r}^{-1/2} e^{-i\pi/2} (\tilde{p} - i\tilde{\Psi}_t + \tilde{g}t - i\delta_0'), \tag{7.10}$$

so that

$$P = \bar{r}^{-1/2} (-\tilde{\Psi}_t - \delta_0'), \tag{7.11a}$$

and

$$Q = \bar{r}^{-1/2} (-\tilde{p} - \tilde{g}t). \tag{7.11b}$$

In a similar way for $\bar{x} > \bar{x}_A$ i.e. for $\bar{\theta} = 0$, we have

$$P + iQ = \bar{r}^{-1/2} (\tilde{p} - i\tilde{\Psi}_t + \tilde{g}t - i\delta_0'), \tag{7.12}$$

so that

$$P = \bar{r}^{-1/2} (\tilde{p} + \tilde{g}t), \tag{7.13a}$$

and

$$Q = \bar{r}^{-1/2} (-\tilde{\Psi}_t - \delta_0'), \tag{7.13b}$$

where $\bar{r} = (\bar{x} - \bar{x}_A)$.

### 7.3.1 The displacement function $\tilde{\Psi}_t$

In a similar manner with chapter 5, we can derive an expression for the displacement-like function $\tilde{\Psi}_t$ along the axes based on the aforementioned considerations. We may again employ directly the Cauchy-Hilbert relationship, as in (5.25), $Q(\bar{x}) = \frac{1}{\pi} \int_{-\infty}^{\infty} \frac{P(\bar{\xi}) d\bar{\xi}}{(\bar{x} - \bar{\xi})}$, which gives us $Q$ along the $\bar{x}$-axis. The integral here and in succeeding formulae is again the Cauchy principal value.

Thus for region $\bar{x} > \bar{x}_A$ we find

$$(\bar{x}-\bar{x}_A)^{-1/2}\left[-\tilde{\Psi}_t-\delta_0{}'\right]=\frac{1}{\pi}\int_{-\infty}^{\bar{x}_A}(\bar{x}_A-\bar{\xi})^{-1/2}\left[\delta_t-\delta_0{}'\right]\frac{d\bar{\xi}}{\bar{x}-\bar{\xi}}$$

$$+\frac{1}{\pi}\int_{\bar{x}_A}^{0}(\bar{\xi}-\bar{x}_A)^{-1/2}(-\tilde{g}|\bar{\xi}|^{1/2}+\tilde{g}t)\frac{d\bar{\xi}}{\bar{x}-\bar{\xi}}+\frac{1}{\pi}\int_{0}^{\infty}(\bar{\xi}-\bar{x}_A)^{-1/2}(\tilde{g}t)\frac{d\bar{\xi}}{\bar{x}-\bar{\xi}} \qquad (7.14)$$

for the range $0>\hat{x}>-t$. Substituting (6.31) into (7.14) and using $\bar{x}_A=-t^2$, and $\bar{x}=-\hat{x}^2$, we have

$$(\bar{x}-\bar{x}_A)^{-1/2}\left[\tilde{f}_{2t}+\delta_{wt}-\delta_0{}'\right]=\frac{1}{\pi}\int_{-\infty}^{\bar{x}_A}(\bar{x}_A-\bar{\xi})^{-1/2}\left[\delta_t-\delta_0{}'\right]\frac{d\bar{\xi}}{\bar{x}-\bar{\xi}}$$

$$+\frac{\tilde{g}}{\pi}\int_{\bar{x}_A}^{0}(\bar{\xi}-\bar{x}_A)^{-1/2}(t-|\bar{\xi}|^{1/2})\frac{d\bar{\xi}}{\bar{x}-\bar{\xi}}$$

$$+\frac{\tilde{g}t}{\pi}\int_{0}^{\infty}(\bar{\xi}-\bar{x}_A)^{-1/2}\frac{d\bar{\xi}}{\bar{x}-\bar{\xi}}, \qquad (7.15)$$

where the first term of (7.15) on the right-hand side is calculated in a similar way as in chapter 5 in view of (5.28). The remaining two terms correspond to the gravity effect, and after integration and manipulation they simply leave $-\tilde{g}$.

Thus (7.15) reduces to

$$-(\tilde{f}_{2t}+\delta_{wt})=-\frac{(\bar{x}-\bar{x}_A)^{1/2}}{\pi}\int_{-\infty}^{\bar{x}_A}(\bar{x}_A-\bar{\xi})^{-1/2}[\delta_t-\delta_0']\frac{d\bar{\xi}}{\bar{x}-\bar{\xi}}-\delta_0'+\tilde{g}(\bar{x}-\bar{x}_A)^{1/2}. \qquad (7.16)$$

Following a procedure similar to that of section 5.4 we obtain again equation (5.38) but now with the additional gravity effect term, so that

$$\tilde{f}_{2t}=-\tilde{\Psi}_t-\delta_{wt}-\tilde{g}(\bar{x}-\bar{x}_A)^{1/2}. \qquad (7.17)$$

Thus substituting the solution for $\Psi_t$ from equation (5.38), we have

$$-(\tilde{f}_{2t}+\delta_{wt})=-\frac{1}{\pi}\left\{\frac{\alpha_0}{t^{1/2}}\tan^{-1}\left(\frac{(L^2-t^2)^{1/2}}{\rho}\right)+\frac{\alpha_1}{2}\rho\Omega\right\}+\tilde{g}(\bar{x}-\bar{x}_A)^{1/2}, \qquad (7.18)$$

where $\rho$, $\alpha_1$, $\alpha_0$ and $\Omega$ are defined in chapter 5.

To help to evaluate (7.18) we initially omit the $\delta$ terms. Then using the notations $\bar{x}=-\hat{x}^2$, $\bar{x}_A=-t^2$, we obtain the gravity effect as

$$\tilde{f}_{2t}\equiv-(t^2-\hat{x}^2)^{1/2}\tilde{g}. \qquad (7.19)$$

This gives

$$\tilde{f}_2=-\tilde{g}\int_{-\hat{x}}^{t}(t^2-\hat{x}^2)^{1/2}dt, \qquad (7.20)$$

where the limits of the integral in (7.20) are defined for $t>|\hat{x}|$. Hence upon integration, this yields

$$\tilde{f}_2=\left(-\frac{\tilde{g}}{2}\right)\left\{t(t^2-|\hat{x}|^2)^{1/2}-|\hat{x}|^2\cosh^{-1}\left(\frac{t}{|\hat{x}|}\right)\right\}. \qquad (7.21)$$

This effectively is for large $\tilde{g}$ values. The right-hand side of (7.21) may now be plotted to obtain the general trend of the side free surface function when it consists of only the gravity effect term. Fig. 7.4 shows this variation with $\hat{x}$ for $\tilde{g}$=0.2 for various values of time $t$. Also fig.7.5 shows the same variation but for various values of $\tilde{g}$ for a value of time $t$=1. The trends show that the function has a maximum at $\hat{x}$=0 and a value of zero at the trailing edge of the ship-side, as expected physically. Also the function apparently increases without bound in magnitude for larger time and/or larger gravity values; this is explained at the end of the next subsection.

However, in order to fully evaluate (7.18) at finite $\tilde{g}$, it is necessary add (7.21) into (7.18) and evaluate the resulting expression computationally.

### 7.3.2 Alternative derivation of the modified side free surface equation

In this sub-section we consider how the following alternative approach captures the $\tilde{g}$ gravity effect in a satisfactory manner. A proof of the boundary conditions of section 7.2 is also included in the analysis.

We first spot that (7.19) corresponds to the simple function

$$\left[\tilde{p} - i\tilde{\Psi}_t\right] = \tilde{g}\hat{z} + i(t^2 - \hat{x}^2)^{1/2}\tilde{g}\alpha. \tag{7.22}$$

Let us check that it satisfies all the required conditions. Using now the top surface condition along $\hat{z} = i\hat{y}$, we have

$$\left[\tilde{p} - i\tilde{\Psi}_t\right] = \tilde{g}\hat{z} + \alpha(\hat{z} - t)^{1/2}(\hat{z} + t)^{1/2} \tag{7.23a}$$

$$= \tilde{g}\hat{z} + \alpha(r_1, r_2)^{1/2} \exp\left(\frac{i}{2}(\theta_1 + \theta_2)\right), \tag{7.23b}$$

where $\alpha$ is an unknown real constant and the branch cut for the square root is such that $0 < \theta_1 < \pi$ and $0 < \theta_2 < \pi$ as shown in figure 7.2.

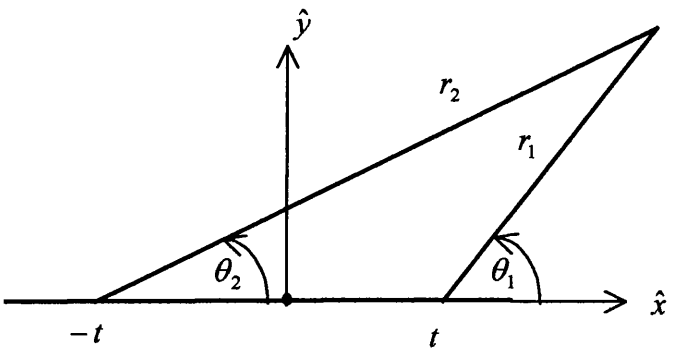


**Figure 7.2 Analysis of side free surface function**

However, along the $\hat{y}$-axis we have $\theta_1 = -\theta_2 + \pi$ and $r_1 = r_2$; so (7.23b) becomes

$$\left[\tilde{p} - i\tilde{\Psi}_t\right] = \tilde{g}iy + \alpha r_1 e^{i\pi/2}. \tag{7.24a}$$

Hence

$$\tilde{p} = 0 \tag{7.24b}$$

as required. The condition along the $\hat{x}$-axis for the wake region $-t < \hat{x} < 0$ gives $\theta_1 = \pi$, $\theta_2 = 0$, $r_1 = t - \hat{x}$ and $r_2 = \hat{x} + t$, and so we obtain

$$\left[\tilde{p} - i\tilde{\Psi}_t\right] = \tilde{g}\hat{x} + \alpha(t^2 - \hat{x}^2)^{1/2} e^{i\pi/2}. \tag{7.25a}$$

Thence

$$\tilde{p} = \tilde{g}\hat{x} \text{ and } \tilde{\Psi}_t = -\alpha(t^2 - \hat{x}^2)^{1/2}, \tag{7.25b}$$

which again agrees with equation (7.7). For the boundary layer region $\hat{x} < -t$, $\hat{y} = 0$, on the other hand, we have $\theta_1 = \pi$, $\theta_2 = \pi$, $r_1 = (t - \hat{x})$ and $r_2 = |\hat{x} + t|$, and so we have

$$\left[\tilde{p} - i\tilde{\Psi}_t\right] = \tilde{g}\hat{x} + ie^{i\pi/2}(\hat{x}^2 - t^2)^{1/2} e^{i\pi}. \tag{7.26a}$$

Hence here

$$\tilde{\Psi}_t = 0 \text{ and } \tilde{p} = \tilde{g}\hat{x} - \alpha\left|\hat{x}^2 - t^2\right|^{1/2}. \tag{7.26b}$$

This agrees with equation (7.8). Also, equation (7.26b) as $\hat{x}$ tends to $-\infty$ become $\tilde{p} \sim \tilde{g}\hat{x} + \alpha\hat{x}$ since $\tilde{x}$ is negative. So we require for the far-field decay that $\alpha = -\tilde{g}$. Thus equation (7.25b) for the wake part becomes now

$$(\tilde{\Psi}_t =)\tilde{g}(t^2 - \hat{x}^2)^{1/2} = -\tilde{f}_{2t}. \tag{7.27}$$

This is exactly (7.19), thus confirming the result there. Moreover at the top corner, at $\hat{x} = 0$, we see that $\tilde{f}_{2t} = -\tilde{g}t$, which leaves $\tilde{f}_2$ negative as time $t$ increases and also

shows that $|\tilde{f}_2|$ increases linearly with time, in keeping with the numerical results described in the previous subsection.

## 7.4 Computational analysis

The computational evaluation of the entire expression for the modified side free surface function including the gravity effect term is given by program 7.1, and consists of adding the solution from (7.21) to the results for $f_2$ from section 6.3. Figures 7.6-7.10 show the variation of the modified side free surface with $x$ for gravity values in the range $0.4 \le \tilde{g} \le 10$. The values of times considered were five equal steps in the range $0.2 \le t \le 3.0$. The results seem to make good physical sense. They also agree fairly well numerically with separate computations performed by Li (2000). As the value of gravity increases, the influence on the side free surface profiles becomes more pronounced. For the larger values of gravity, the effect on the side free surface is to draw it into the negative $\hat{y}$ region sooner. On the other hand it can be shown that the displacement contribution from $\delta$ always dominates just above but sufficiently near the trailing edge position $\hat{x} = -t$ as $\tilde{f}_2$ tends to zero, and that keeps $\tilde{f}_2$ always positive there. Indeed the $\delta$ term in $\tilde{f}_2$ gives rise to positive coefficient times $(\hat{x}+t)^{1/3}$ in $\tilde{f}_2$ locally, whereas the $\tilde{g}$ term gives rise to negative coefficient times $(\hat{x}+t)^{3/2}$, essentially, and since the former (1/3) behaviour is the greater it makes $\tilde{f}_2$ locally positive. A trend towards 'splashing' of the water onto the ship-side is clearly indicated for sufficiently large times with any positive gravity factor $\tilde{g}$.

## 7.5 Analysis near the top corner

This local analysis is of some interest, if rather an aside, on the local inviscid solution very near the top corner with the gravity effect $\tilde{g}$ present, although it also applies if $\tilde{g}$ is zero. In section 7.2 it is seen that equation (7.7) yields along region 2 the solution for $\tilde{f}_2$, at small or finite $|\hat{x}|$ for every time $t$. The aim here is to study locally both the side free surface at small $|\hat{x}|$ and the upper free surface shape, $f_1$ at small $|\hat{y}|$ for all time.

Thus locally we have to solve again equation (7.1) in the quarter-plane as shown in figure 7.3,

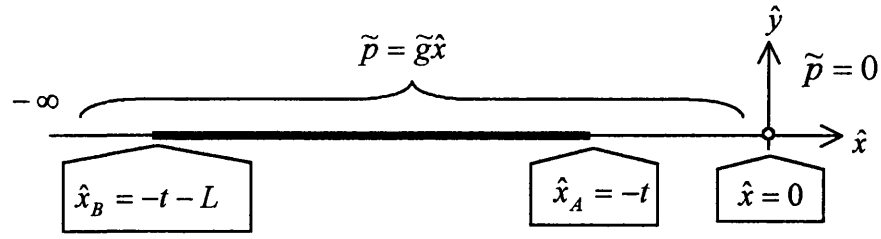


**Figure 7.3** **For the problem near the top corner**

with

$$\tilde{p} = 0 \text{ along } \hat{x} = 0, \text{ for all } \hat{y} > 0, \tag{7.28a}$$

and

$$\tilde{p} = \tilde{g}\hat{x} \text{ along } \hat{y} = 0, \text{ for all } \hat{x} < 0. \tag{7.28b}$$

The reason for (7.28b) is that the change in boundary conditions at $\hat{x}_A$ can be regarded as relatively far from the top corner.

We again construct the complex function $\tilde{p} - i\tilde{\Psi}_t$ of $\hat{z} = \hat{x} + i\hat{y}$, locally. The boundary conditions suggest that near the top $\hat{z} = i\hat{y}$ we must have

$$\left[\tilde{p} - i\tilde{\Psi}_t\right] = \tilde{g}i\hat{y} + iB_0 - iB_2\hat{y}^2 + iB_4\hat{y}^4 + \ldots\ldots, \tag{7.29}$$

with real constants $B_0, B_2, B_4, \ldots$. Then we obtain

$$\tilde{\Psi}_t = B_0 - \tilde{g}\hat{y} + B_2\hat{y}^2 - B_4\hat{y}^4 + \ldots\ldots \tag{7.30}$$

there. Thus

$$\tilde{\Psi}_{ty} = -\tilde{g} + 2B_2\hat{y}^2 - 4B_4\hat{y}^4 + \ldots\ldots, \tag{7.31}$$

giving $\frac{\partial \tilde{u}}{\partial t} \approx -\tilde{g}$ at the top surface.

So equation (7.29) simply extends in terms of $\hat{z}$ to

$$\left[\tilde{p} - i\tilde{\Psi}_t\right] = \tilde{g}\hat{z} + A_0 + A_1\hat{z} + A_2\hat{z}^2 + A_3\hat{z}^3 + A_4\hat{z}^4 + \ldots\ldots, \qquad (7.32)$$

with $A_1 = A_3 = A_5 = A_7 = \ldots = 0$ and $A_0, A_2 A_4, A_6, \ldots\ldots$ pure imaginary in order to satisfy equations (7.28a), (7.28b) along $\hat{z} = i\hat{y}$ and $\hat{z} = \hat{x}$. The constants $A_n$ and $B_n$ are determined by the global solution which takes into account the ship-side and not by the local solution. The relationship between the constants is given by

$$A_{0,2,4,6,\ldots} = iB_{0,2,4,6,\ldots}. \qquad (7.33)$$

Hence, along the side free surface we find

$$-i\tilde{\Psi}_t = iB_0 + iB_2\hat{x}^2 + iB_4\hat{x}^4 + \ldots\ldots \qquad (7.34)$$

so that

$$\tilde{\Psi}_t = -B_0 - B_2\hat{x}^2 - B_4\hat{x}^4 - \ldots\ldots \qquad (7.35)$$

But, considering the gravity effect alone, we require $\tilde{\Psi} = -f_2$ from equation (7.17). Thus we finally obtain the form

$$f_2 = \left(B_0 + B_2\hat{x}^2 + B_4\hat{x}^4 + \ldots\right) \cdot t. \qquad (7.36)$$

This is consistent with the findings in the previous sections and tends to confirm that the local solution near the top corner is regular in $\hat{z}$.

## 7.6 Fortran 77 programs and figures

```
C       Programs to evaluate side-free-surface function with x-coordinate,
C       for a given value of gravity

        PROGRAM GFS
        integer i,imax
        real x(1000),xhat(1000),sfs(1000),vv(1000),g,t,acosh(1000)

        g=10
        t=0.2

        open (1,file="plo")
        open (9,file="vv.dat")

        do 10   i=1,1000

        read (unit=1,fmt=*)   x(i),sfs(i)

C       Increment time value for small and large times

        if (x(i).ge.100) then

          write(9,*)''
          if (t.le.1)   then
          t=t+0.2
          else
          t=t+2.0
          endif

        else

C       Evaluate f2 with gravity effect term and write to file

        xhat(i) = x(i)
        acosh(i)=log(  (t/xhat(i)) + ( (((t/xhat(i))**2)-1)**0.5 ) )
        vv(i)=  sfs(i) + ((g/2)*((t*(((t**2)-(xhat(i)**2))**0.5))
-((xhat(i)**2)*acosh(i))))

          if (x(i).eq.0.01)  datum=vv(i)
          if (x(i).eq.0) then

          write (9,*)   '0      0'

          else

          write (9,*)   xhat(i)-0.01,vv(i)-datum

          endif

        endif

C       End program at end of input file
        if (x(i).ge.1000)  goto 20

10      continue

        close (1)
        close (9)

20      end
```

7.1 Program to evaluate the side free surface function with $\bar{x}$, for a given value of gravity.

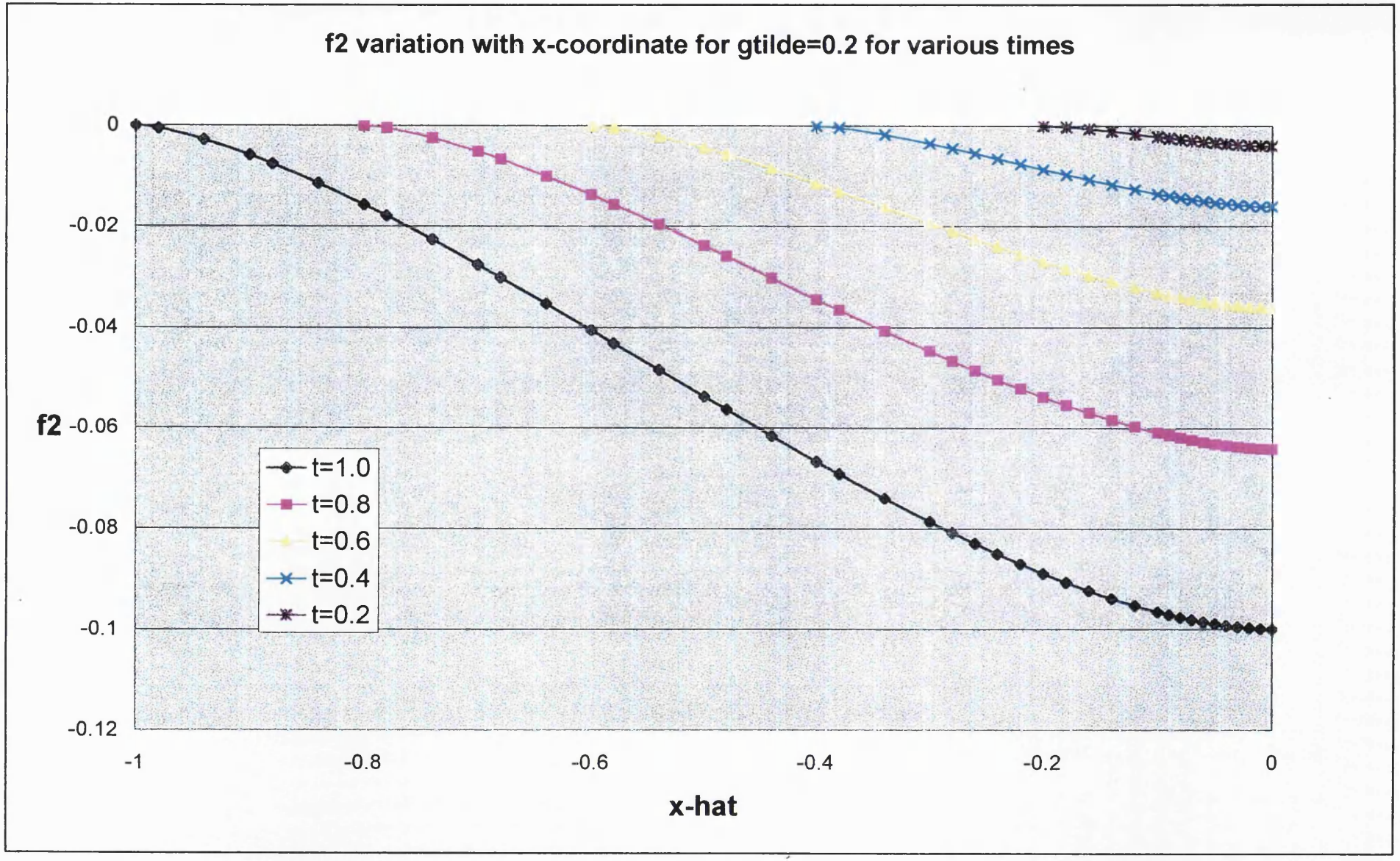
f2 variation with x-coordinate for gtilde=0.2 for various times
0
-0.02
-0.04
-0.06
-0.08
-0.1
-0.12
f2
-1
-0.8
-0.6
-0.4
-0.2
0
x-hat
t=1.0
t=0.8
t=0.6
t=0.4
t=0.2

Fig. 7.4

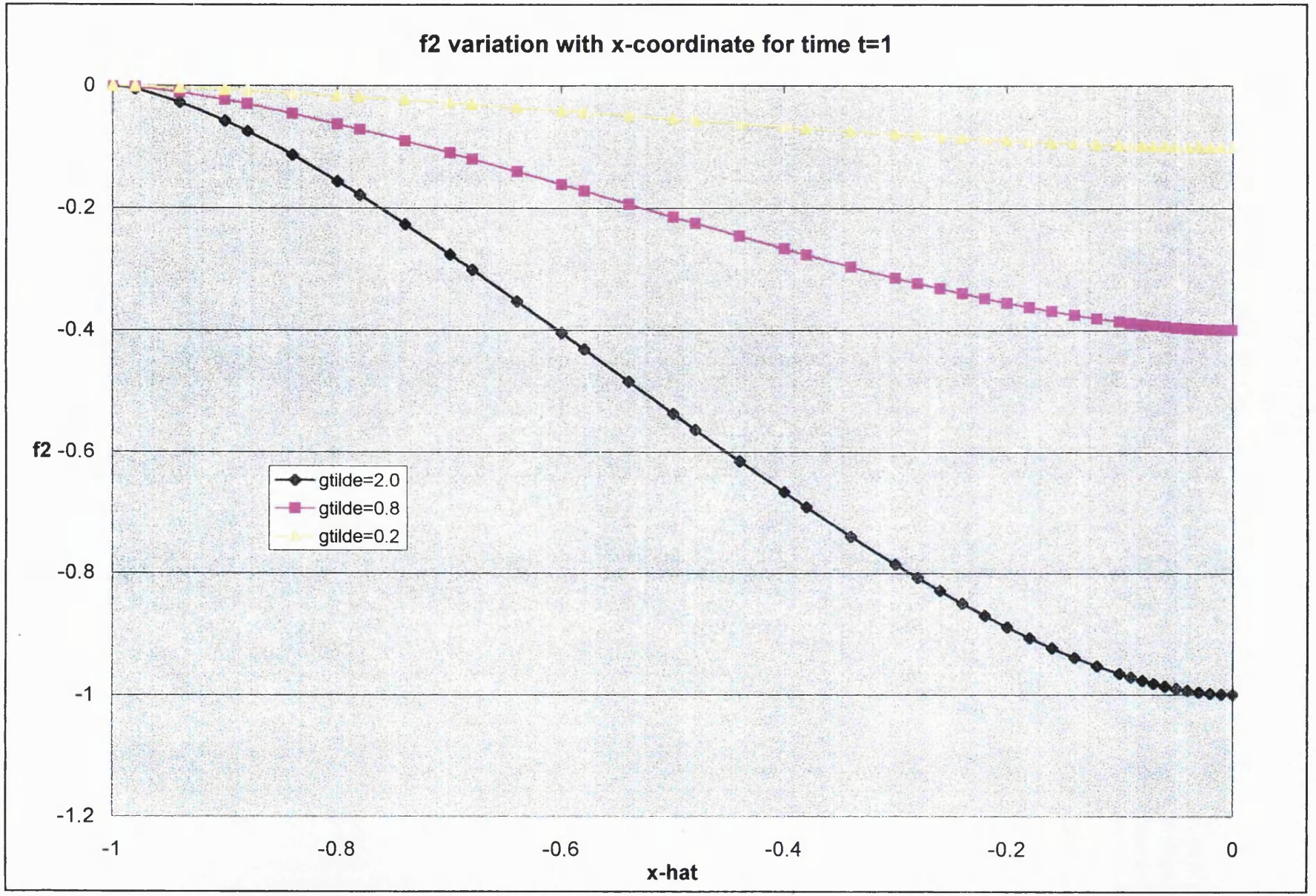
f2 variation with x-coordinate for time t=1
0
-0.2
-0.4
-0.6
-0.8
-1
-1.2
f2
-1
-0.8
-0.6
-0.4
-0.2
0
x-hat
gtilde=2.0
gtilde=0.8
gtilde=0.2

Fig. 7.5

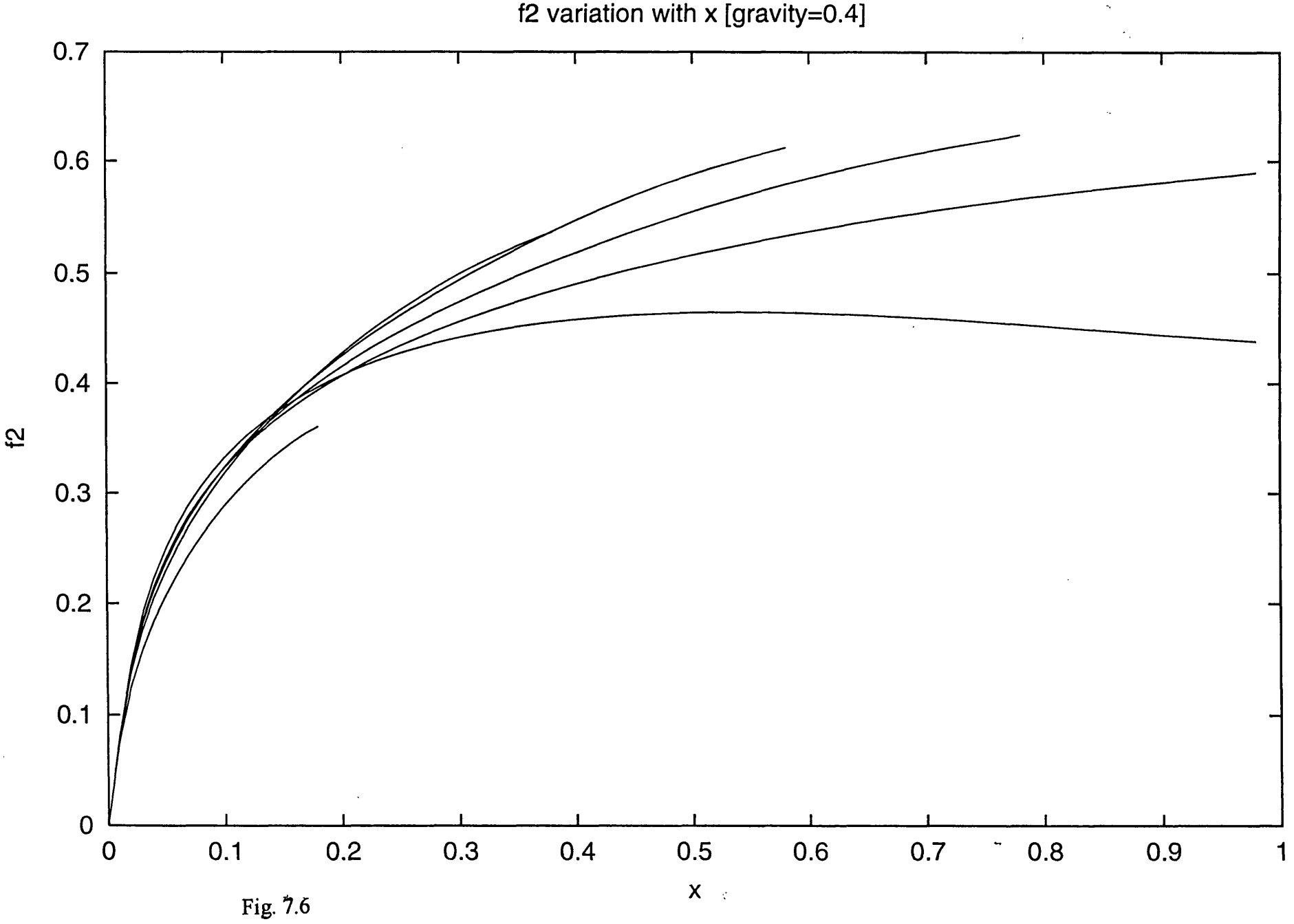


Fig. 7.6

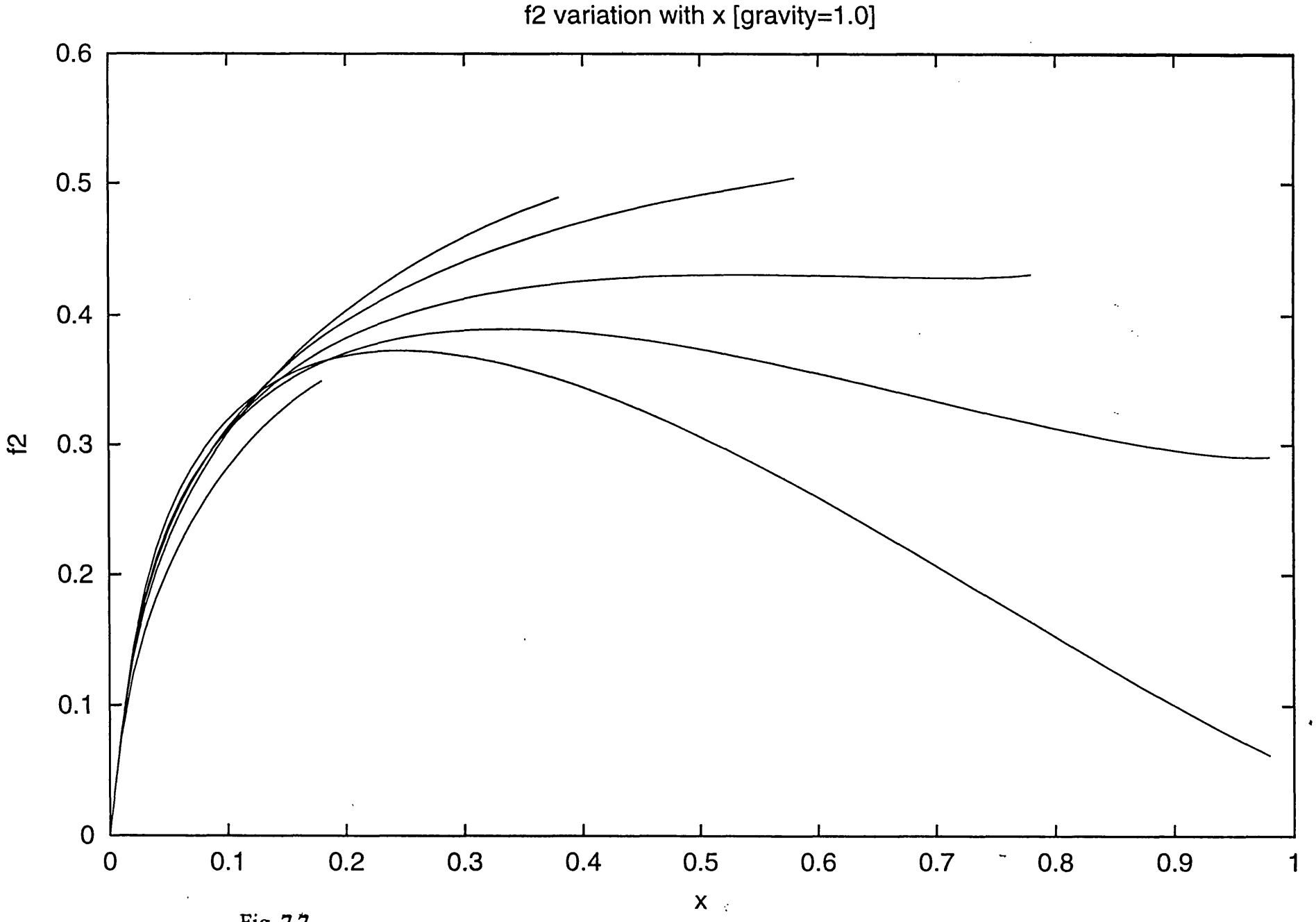


Fig. 7.7

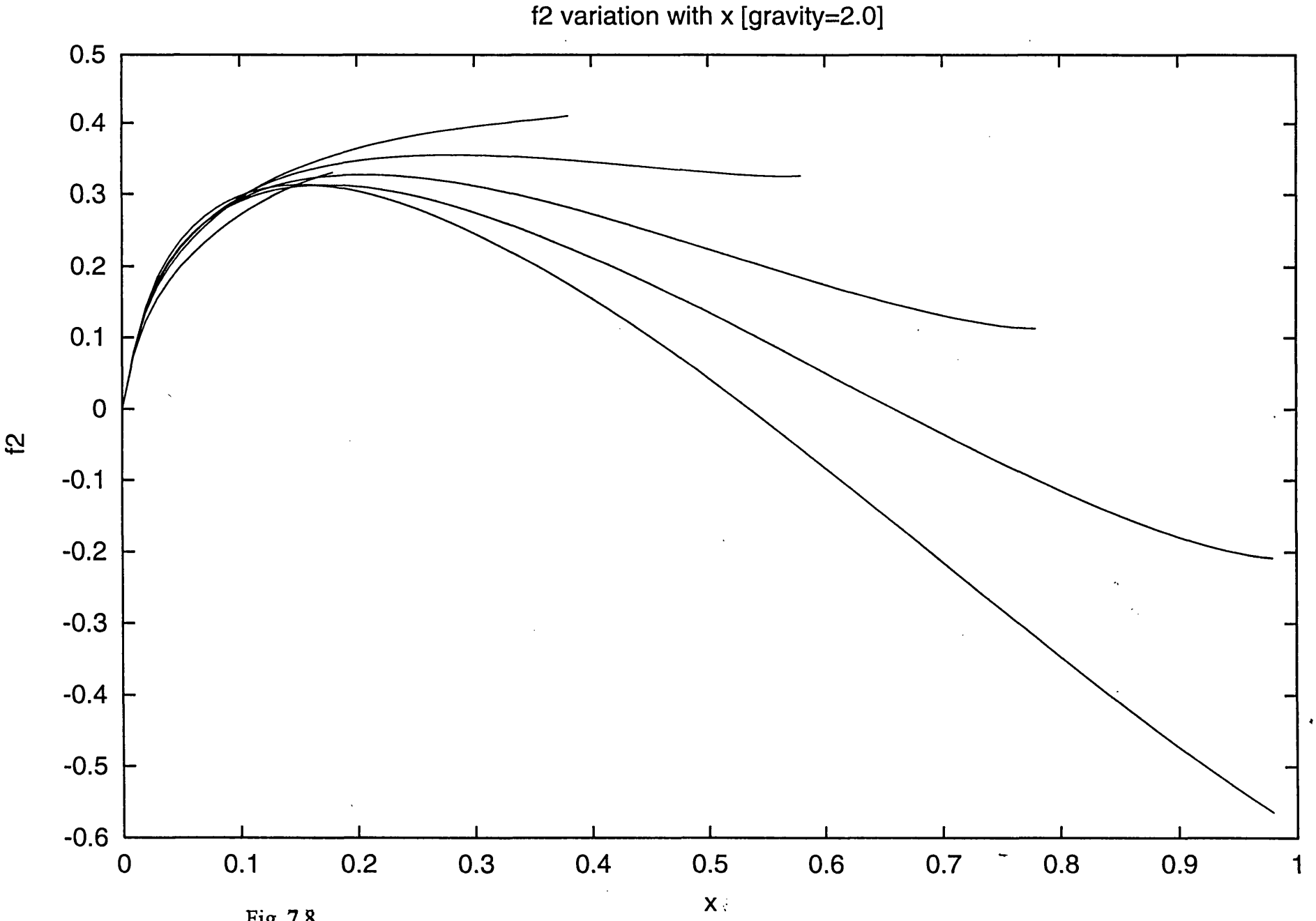
f2 variation with x [gravity=2.0]
f2
x
0.5
0.4
0.3
0.2
0.1
0
-0.1
-0.2
-0.3
-0.4
-0.5
-0.6
0
0.1
0.2
0.3
0.4
0.5
0.6
0.7
0.8
0.9
1

Fig. 7.8

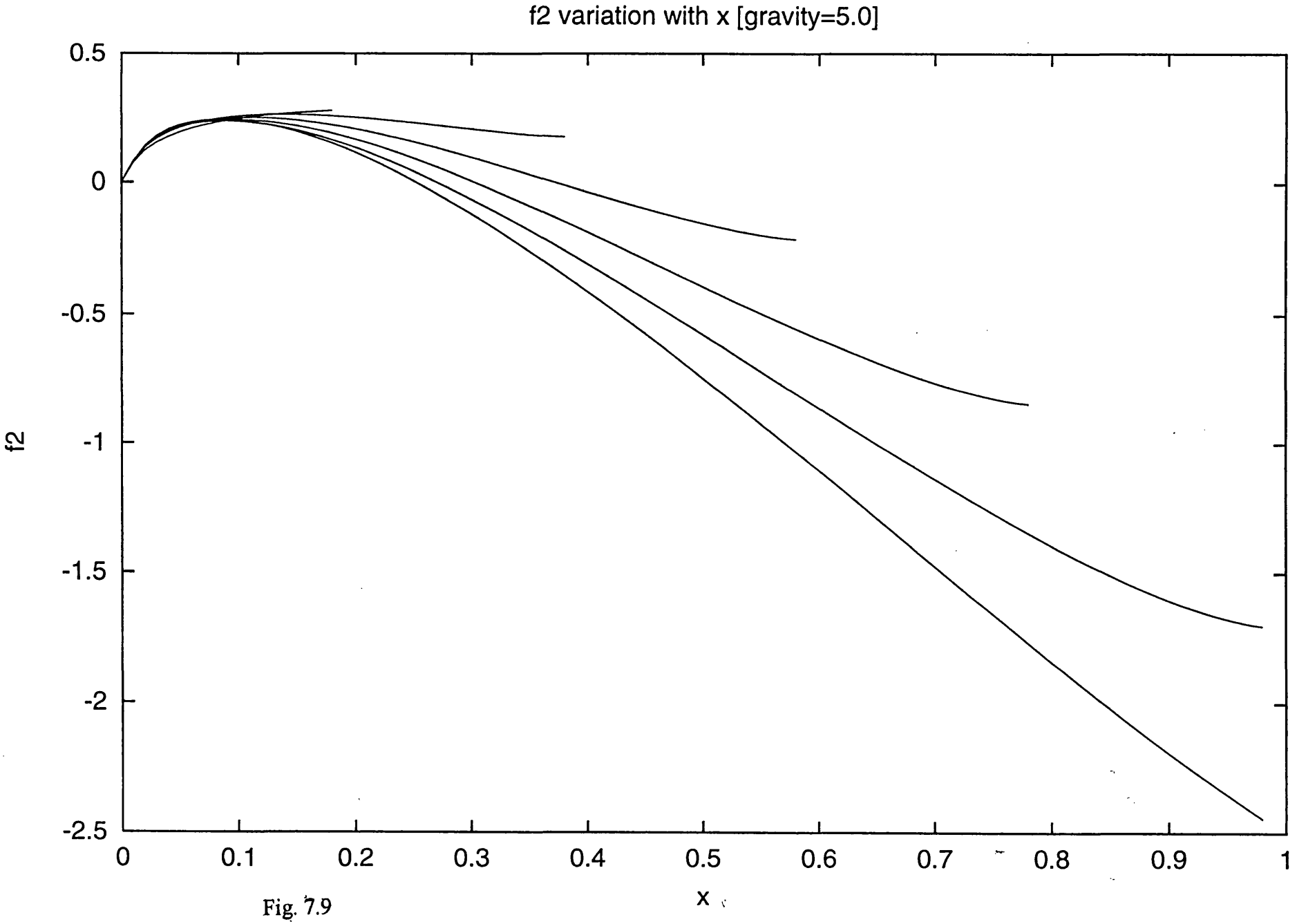
f2 variation with x [gravity=5.0]
0.5
0
-0.5
-1
-1.5
-2
-2.5
f2
0
0.1
0.2
0.3
0.4
0.5
0.6
0.7
0.8
0.9
1
x

Fig. 7.9

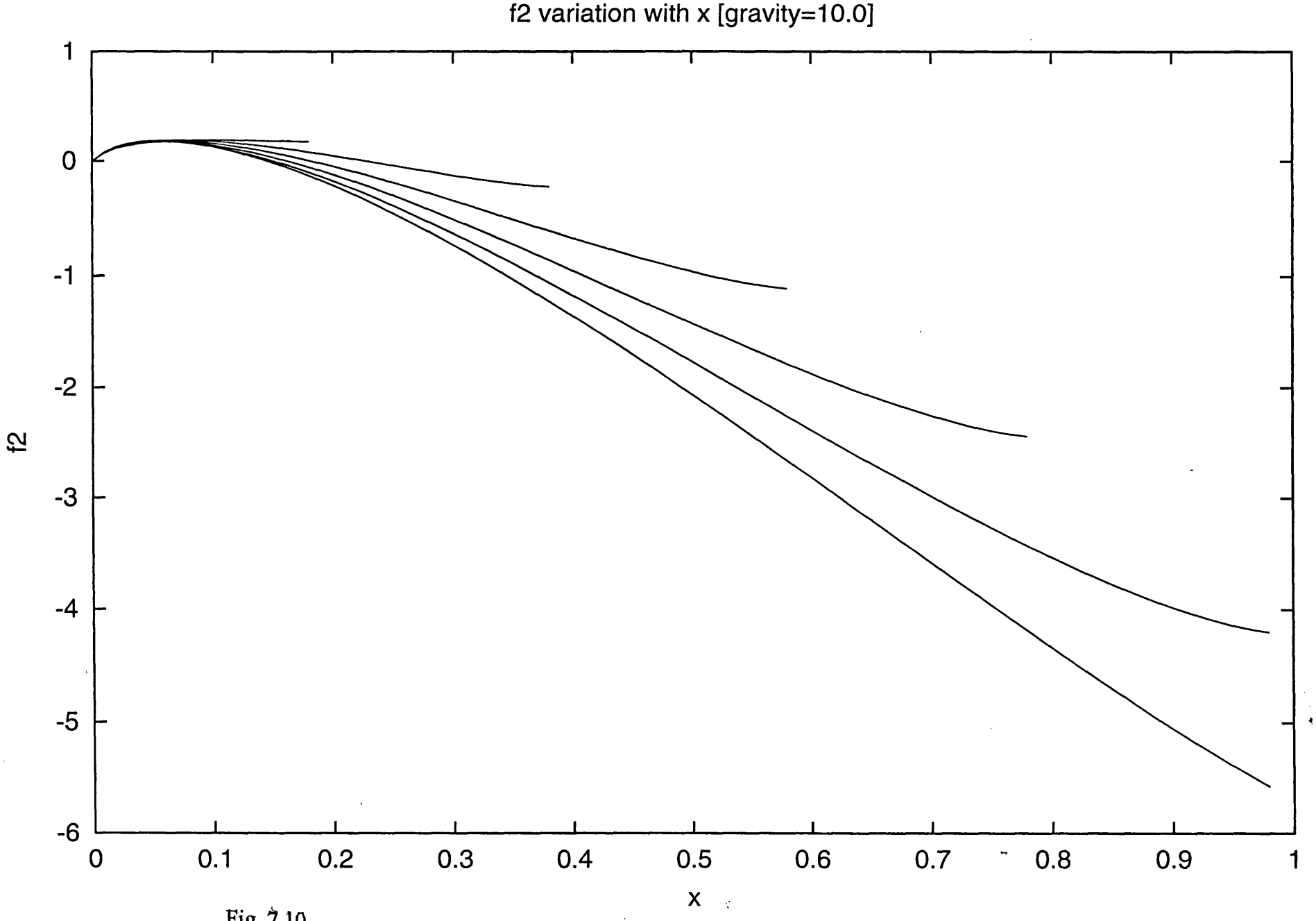
f2 variation with x [gravity=10.0]
f2
x
1
0
-1
-2
-3
-4
-5
-6
0
0.1
0.2
0.3
0.4
0.5
0.6
0.7
0.8
0.9
1

Fig. 7.10

# CHAPTER 8

## Water flow adjacent to an inclined ship-side moving downwards

### 8.1 Introduction

In this chapter a moving inclined ship-side will be investigated in brief for the case of downward motion. The ship-side is taken to be moving downward but in its own plane. Here the flow configuration and main flow structure appear at first sight to be similar to the earlier vertical case. This is for negligible gravity force. The diagram given below defines the domain of the problem in the Cartesian coordinate system consisting of $x_1$ (vertical), $y_1$ (horizontal), which are identical with $\hat{x}$, $\hat{y}$ used earlier but are in a more convenient notation here.

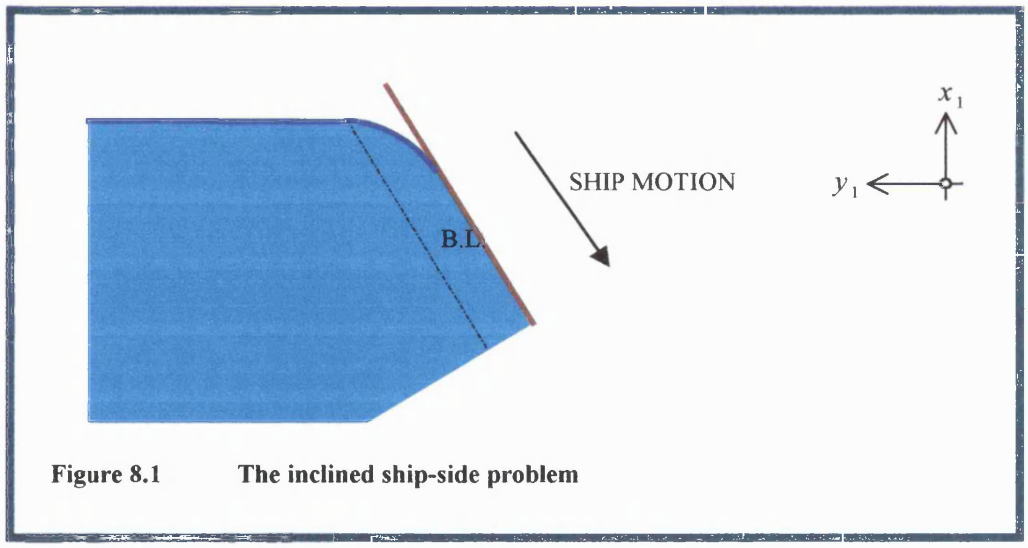


**Figure 8.1 The inclined ship-side problem**

For the inclined case, the only difference from the previous vertical case occurs in the outer inviscid problem where the Laplace equation must be solved with the following new conditions. With reference to the diagram below, the top CO has the same boundary conditions as for the vertical case, and similarly for the side portion OA. Side AB, however, must match to the boundary layer on the ship-side at an angle $\alpha$ (where $0 < \alpha < \pi$) below the horizontal. If $\alpha$ is equal to $\frac{\pi}{2}$ this corresponds to the earlier vertical case.

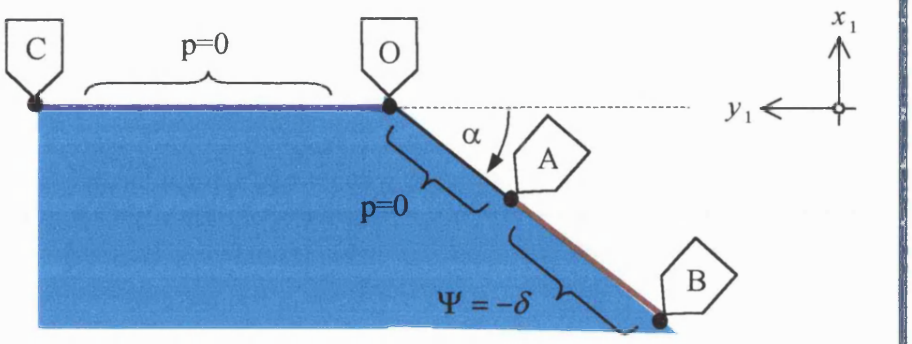


**Figure 8.2 The domain of the analysis**

We may solve this inclined ship-side problem by mapping the $x_1$, $y_1$ plane to the original ¼-plane of the vertical case for which the analysis has been performed in chapter 5.

## 8.2 Transformation to ¼-plane

The unknown scaled pressure satisfies Laplace's equation in $x_1, y_1$,

$$\nabla^2 p = 0, \tag{8.1}$$

as expected in potential flow. This is as in equation (5.5).

Also, as in chapter 5, the Cauchy-Riemann equations hold between $p_{x_1}$ and $\hat{V}_t$, where pressures and velocities are scaled as before. So a complex potential function to control the problem may be defined as $p - i\Psi_t$, which is analytic in $z_1 (\equiv x_1 + iy_1)$, say $\Im(z_1)$, with the stream function $\Psi$ again satisfying $\hat{u} = \Psi_{y_1}$ and $\hat{V} = -\Psi_{x_1}$.

The boundary conditions considered here are that: the pressure $p$ is prescribed to be zero on sides COA (from condition 2 of chapter 4); and $\Psi$ is prescribed in terms of the given boundary layer displacement as -$\delta$ (so the normal derivative $\frac{\partial p}{\partial n}$, or, in the

polar coordinates of figure 8.3, $r_1^{-1}\frac{\partial p}{\partial \theta_1}$, is prescribed) on the inclined side AB (from matching with the boundary layer); while the water is at rest in the far-field (condition 3). The precise form here of chapter five's function $h$ or $\frac{\partial p}{\partial n}$, from matching with the viscous boundary layer solution, can be determined subsequently. We need to remark however that the stated linearised boundary conditions on the side OA and implicitly on the inclined side below the leading edge point B are somewhat artificial, due to the non symmetry present for the latter and the off-vertical free surface for the former, in general. Instead the global effects may be expected to be nonlinear in reality. Nevertheless, the above formulation provides the beginnings of a generalisation from the original vertical side case of the earlier chapters.

To solve the inviscid flow problem we may again introduce a conformal transformation, which allows consideration of the problem in the original ¼-plane. The mapping is, say,

$$z_2 = z_1^{\,N}, \tag{8.2}$$

where $z_2$ is the complex coordinate for the ¼-plane of chapter 5, as shown now in fig. 8.3, and $N$ is defined below.

The $z_1$ coordinate system is now defined by the polar coordinates $r_1, \theta_1$, and $z_2$ by $r_2, \theta_2$ so that (8.2) reads

$$r_2 e^{i(\theta_2 - \pi/2)} = r_1^{\,N} e^{Ni(\theta_1 - \pi/2)}, \tag{8.3}$$

and hence we have

$$r_2 = r_1^{\,N}, \tag{8.4}$$

$$\theta_2 = N\left(\theta_1 - \frac{\pi}{2}\right) + \frac{\pi}{2}. \tag{8.5}$$

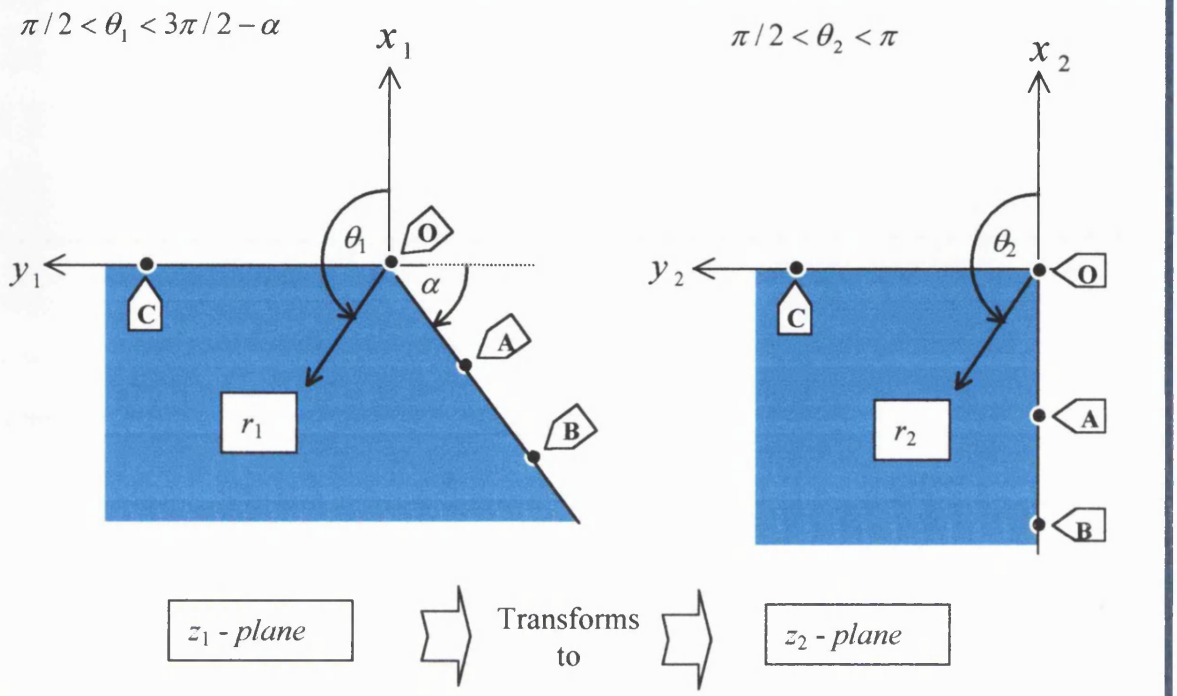


**Figure 8.3** **Mapping from inclined plane to ¼-plane**

So on the BAO 'side' portion we obtain from (8.5)

$$\theta_2 = \pi \Rightarrow \theta_1 = \frac{3\pi}{2} - \alpha \tag{8.6}$$

and on the OC 'top' portion we have also

$$\theta_2 = \frac{\pi}{2} \Rightarrow \theta_1 = \frac{\pi}{2}, \tag{8.7}$$

with the interval $\frac{\pi}{2} < \theta_1 < \frac{3\pi}{2} - \alpha$, and $0 < r_1 < \infty$ for the entire outer region of water flow. Here, to repeat, $\alpha$ is the angle between the inclined slope and the horizontal as indicated in figure 8.2. Also $N = \frac{\pi}{2(\pi - \alpha)}$ in view of (8.5), (8.6), and so $N$ is positive for the present range of $\alpha$ values.

The mapping into the $z_2$-plane gives us again Laplace's equation in terms of $x_2$, $y_2$, $\nabla_2^2 p = 0$ say, which can then be solved in exactly the same way as in chapter 5. The only difference is observed at the stage of the match with the boundary layer, where $\delta(r_2) = \delta(r_1^N)$. Here the boundary layer model is transformed according to the coordinate transformation (8.2) in a similar manner as with section 5.4. The boundary condition on the $AB$ portion of the axis is given by the derivative as $\Psi_t = -\delta(r_1,t)$; thus we have the boundary conditions on the pressure, which are of mixed type. We may now proceed using the function $p - i\Psi_t$ as explained in chapter 5.

## 8.3 The general displacement derivative function $\Psi_t$

We therefore derive as follows a general displacement-like function based on the aforementioned considerations. We may again employ directly the Cauchy-Hilbert relationship, similar to (5.25),

$$Q = \frac{1}{\pi}\int_{-\infty}^{\infty} \frac{P(\bar{\xi})d\bar{\xi}}{(\bar{x}-\bar{\xi})}. \tag{8.8}$$

where now $\bar{x} = -r_2^{\,2} = -r_1^{\,2N}$ from the transformation (8.4). So equation (8.8) using equations (5.21) and (5.24) with the new limits on the integral, in a manner similar to that in as with section 5.3, becomes

$$\Psi_t = -\frac{(r_{1A}^{\,2N} - r_1^{\,2N})^{1/2}}{\pi}\int_{-\infty}^{-r_{1A}^{\,2N}} \frac{(-r_{1A}^{\,2N} - \bar{\xi})^{-1/2}}{(-r_1^{\,2N} - \bar{\xi})}\left[\delta_t - \delta_0'\right]d\bar{\xi} - \delta_0'. \tag{8.9}$$

With reference to fig.8.3, we have the values $r_{1A} = t$ and $r_{1B} = (t+L)$, and so using (8.4) we conclude that the corresponding distances are $r_{2A} = t^N$ and $r_{2B} = (t+L)^N$, at time $t$; this is for the impulsively-started downward moving ship-side oriented at the inclination $\alpha$.

For general times $t$ of order $O(1)$ we could evaluate (8.9) numerically using the values of $\delta(r_1,t)$ from our previous boundary layer computations in chapters 2,3.

We prefer to use a modelled form as in the previous chapters. In terms of the transformed coordinates $r_1 = r_2^{1/N}$, the model reads

$$\delta = \begin{cases} \left(t + L - r_1^{N}\right)^{1/2} \alpha_1 & \text{for} \quad r_{1B}^{2N} > r_1^{2N} > L^2, \qquad (8.10) \\ \alpha_0 t^{1/2} & \text{for} \quad L^2 > r_1^{2N} > r_{1A}^{2N}, \qquad (8.11) \end{cases}$$

in the new range $0 \le t \le L$. Again, $\delta_t = \delta_0{}'$ for the range $L^2 > r_1^{2N} > r_{1A}^{2N}$. Also here $\delta_0{}' = \dfrac{\alpha_0}{(2t^{1/2})}$ from the values at the trailing edge. For the special vertical case of $\alpha = \dfrac{\pi}{2}$ and $N$=1, the displacement function equations (8.10-11) reduce to (5.30-31), as expected.

Thus, using the general model for $\delta$, we have

$$\begin{aligned} \Psi_t = & -\frac{(r_{1A}^{2N} - r_1^{2N})^{1/2}}{\pi} \int_{-\infty}^{-L^2} \frac{(-r_{1A}^{2N} - \bar{\xi})^{-1/2}}{(-r_1^{2N} - \bar{\xi})} \left(-\delta_0{}'(t)\right) d\bar{\xi} \\ & - \frac{(r_{1A}^{2N} - r_1^{2N})^{1/2}}{\pi} \int_{-r_{1B}^{2N}}^{-L^2} \frac{(-r_{1A}^{2N} - \bar{\xi})^{-1/2}}{(-r_1^{2N} - \bar{\xi})} \left(\partial_t \left((-\bar{\xi})^{1/2} + t + L\right)^{1/2} \alpha_1\right) d\bar{\xi} \\ & = \frac{(r_{1A}^{2N} - r_1^{2N})^{1/2}}{\pi} \int_{-L^2}^{-r_{1A}^{2N}} \frac{(-r_{1A}^{2N} - \bar{\xi})^{-1/2}}{(-r_1^{2N} - \bar{\xi})} \left[\partial_t (t^{1/2} \alpha_0)\right] d\bar{\xi} \\ & - \delta_0{}'(t) \left[1 - \frac{(r_{1A}^{2N} - r_1^{2N})^{1/2}}{\pi} \int_{-L^2}^{-r_{1A}^{2N}} \frac{(-r_{1A}^{2N} - \bar{\xi})^{-1/2}}{(-r_1^{2N} - \bar{\xi})} d\bar{\xi}\right], \qquad (8.12) \end{aligned}$$

where again the four constituent terms refer to the respective portions in the overall region $\infty > r_1^{2N} > r_{1A}^{2N}$. So we obtain, after differentiation, the final expression for the displacement derivative function in the concise form

$$\Psi_t = \frac{(r_{1A}^{2N} - r_1^{2N})^{1/2}}{\pi} \left(\delta_0' \Phi_1 - \frac{\alpha_1}{2} \Omega_1\right) - \delta_0', \qquad (8.13)$$

where the two integrals are defined as

$$\Phi_1 = \int_{-\infty}^{-L^2} \frac{(-r_{1A}{}^{2N} - \bar{\xi})^{-1/2}}{(-r_1{}^{2N} - \bar{\xi})} d\bar{\xi}, \tag{8.14}$$

$$\Omega_1 = \int_{-r_{1B}{}^{2N}}^{-L^2} \frac{(-r_{1A}{}^{2N} - \bar{\xi})^{-1/2}}{(-r_1{}^{2N} - \bar{\xi})} \left((-\bar{\xi})^{1/2} + t + L\right)^{-1/2} d\bar{\xi}, \tag{8.15}$$

which we will proceed to determine in the next section. For the special case of the ¼-plane analysis of chapter 5, $\alpha = \pi/2$ and $N = 1$, and equations (8.13-15) reduce to (5.34-6) as expected.

## 8.4 Evaluation of the $\Phi_1$ and $\Omega_1$ integrals

To evaluate the $\Phi_1$ and $\Omega_1$ integrals, we use the substitution $m^2 = -r_{1A}{}^{2N} - \bar{\xi}$. Thus we obtain for the $\Phi_1$ integral, in a similar manner to (5.37b),

$$\Phi_1 = (r_{1A}{}^{2N} - r_1{}^{2N})^{-1/2} \left[ \pi - 2\tan^{-1}\left( \frac{L^2 - r_{1A}{}^{2N}}{r_{1A}{}^{2N} - r_1{}^{2N}} \right)^{1/2} \right], \tag{8.16}$$

while for the $\Omega_1$ integral we have the form

$$\Omega_1 = 2 \int_{(L^2 - r_{1A}{}^{2N})^{1/2}}^{(r_{1B}{}^{2N} - r_{1A}{}^{2N})^{1/2}} \frac{\left(t + L + \left(m^2 + r_{1A}{}^{2N}\right)^{1/2}\right)^{-1/2}}{(m^2 + r_{1A}{}^{2N} - r_1{}^{2N})} dm. \tag{8.17}$$

The form (8.17) of the integral is again suitable for computation using Simpson's rule as given in the following section. Also the form (8.16) is well defined, and substituting back into equation (8.13) we have

$$\Psi_t = -\frac{1}{\pi} \left\{ \frac{\alpha_0}{t^{1/2}} \tan^{-1}\left( \frac{L^2 - r_{1A}{}^{2N}}{r_{1A}{}^{2N} - r_1{}^{2N}} \right)^{1/2} + \frac{\alpha_1}{2} (r_{1A}{}^{2N} - r_1{}^{2N})^{1/2} \Omega_1 \right\}, \tag{8.18}$$

which is the final form for the displacement derivative function of the inclined ship side.

## 8.5 Computational solution of general $\Psi_t$ function

The evaluation of the general displacement derivative function which includes the $\Omega_1$ integral is described in this section. The flow chart for the program is given below and the results are presented in the figures that follow the program (Program 8.1) at the end of the chapter. Program 8.1 now includes evaluation of the $\Omega_1$ integral which is a function of the angle of inclination, $\alpha$, of the ship-side. Computations were performed for five values of $\alpha$ in the range $0 < \alpha < \frac{3\pi}{4}$. Each run was for selected non-dimensional times not exceeding the non-dimensional length of the ship-side, which here is unity. The times considered were for four equal intervals in the range 0.2-0.8.

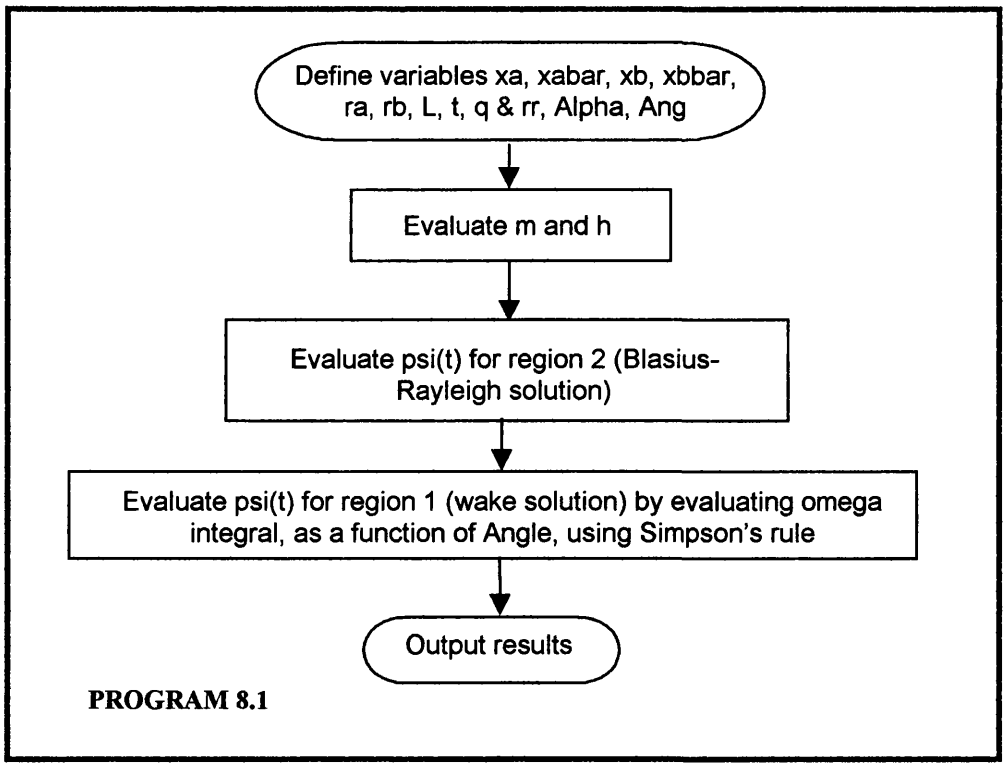


The $\Psi_t$ profiles (figures 8.4-8.8) are similar to those of section 5.4. For the case of $\alpha = \pi/2$, the profiles are identical since this corresponds to the special case of the vertical ship-side case. As the angle is increased, the wake regions became more

pronounced and elongated relative to the overall profiles. Further, the limiting cases of nearly horizontal side motion where $\alpha \to 0+$, $\alpha \to \pi-$ are clearly of much interest. The former case for instance resembles the so-called planing or gliding flow discussed in Milne-Thompson (1968, page 324) on purely inviscid grounds. It should be recalled however that the present boundary conditions imposed along the sides OA and below B are rather artificial, a feature which restricts the direct applicability to planing flows. It would be interesting to study this further.

## 8.6 Fortran 77 programs and figures

```
C       ********************************************
C       February 2000           D.Papadopoulos
C       ********************************************
C       INCLINED SHIP-SIDE PROBLEM
C       Program to evaluate the Psi(t) variation with general r-coordinate
C       and produce entire displacement function [y] valid for small times
C       ********************************************
C       ********************************************

C       *** Definition of all variables, except y ***

        program gpsi

        REAL o(2000),res,h,L,t,sum
        REAL u,ra,rb,r,pi,q,rr,y,y1,y2,term,rho,ALPHA,ANG
        INTEGER i,j,mm,m

        open (9,file="vv.dat")
        mm = 360
        L = 1
        pi = 3.1415927

        ALPHA=(pi)/2

        ANG=pi/(2*(pi-ALPHA))

C       General loop to evaluate psi(t) for various times,
C       with constraint t<L

        do 3000 t=0.2,0.9,0.2

C       ra means r1a, rb means r1b and r means r1 and rr means r2

        ra = t
        rb = t+L

C       q means a1  and a0
        q = 0.25

C       *** Determination of m and h
        m = (2 * mm) + 3
        h = ( (((rb**(2*ANG))-(ra**(2*ANG)) )**0.5)
              -(((L**2)-(ra**(2*ANG)) )**0.5)) /((2*mm) + 2)

C       *** Evaluate Psi(t) for rb-t<r<rb, i.e. Blasius part

        do 5 r = rb-0.01,rb-t,-0.01
        y1=-q*0.5*((rb-(r**ANG))**(-0.5))
        WRITE (unit=9,fmt=*)  r,y1
5       continue

C       *** Evaluate Psi(t) for rb-t<r<ra, i.e. Rayleigh part

        do 10 r = rb-t,ra,-0.01
        y2=-q*0.5*(t**(-0.5))
        WRITE (unit=9,fmt=*)  r, y2
10      continue

C       ***General loop to evaluate psi(t) (including constituent omega
C       integral) for values of the r-coordinate ***

        do 1000 r = (ra-0.001),0.01,-0.001
```

8.1 Program to evaluate the $\Psi$, variation with $\bar{x}$, valid for inclined problem.

```
C       *** Evaluate o(j), also evaluating u(j) at each j ***

        do 24 j = 1,m-1
        u = ((j - 1) * h)+( ( (L**2) - (ra**(2*ANG)) )**0.5)

        o(j) = 2*((rb+(((u**2)+(ra**(2*ANG)))**0.5))**(-0.5))
                /((ra**(2*ANG))+(u**2)-(r**(2*ANG)))

24      continue

C       *** Evaluate first and final terms of omega integral ***

        sum = o(1)+ o(m) + (4*o(m-1))

C       *** Evaluate complete integral (i.e. including the intermediate terms)

        do 27 i = 1,mm
        j = 2 * i
        sum = sum + (4.0 * o(j)) + (2.0 * o(j+1))
27      continue

        res = (sum * (h/3.0))

C       *** Evaluate and output results for psi(t) [y] ***

        term=(((rb**(2*ANG)) - (ra**(2*ANG)))
                /((ra**(2*ANG))-(r**(2*ANG))) )**0.5
        rho=q*(t**(-0.5))
        y =(-0.15915)*q*res*(((ra**(2*ANG))-(r**(2*ANG)))**0.5)
                -(rho*0.31831*atan(term))
        WRITE (unit=9,fmt=*)  r,y

1000    continue

        WRITE (unit=9,fmt=*)

3000    continue
        close (9)

        end
```

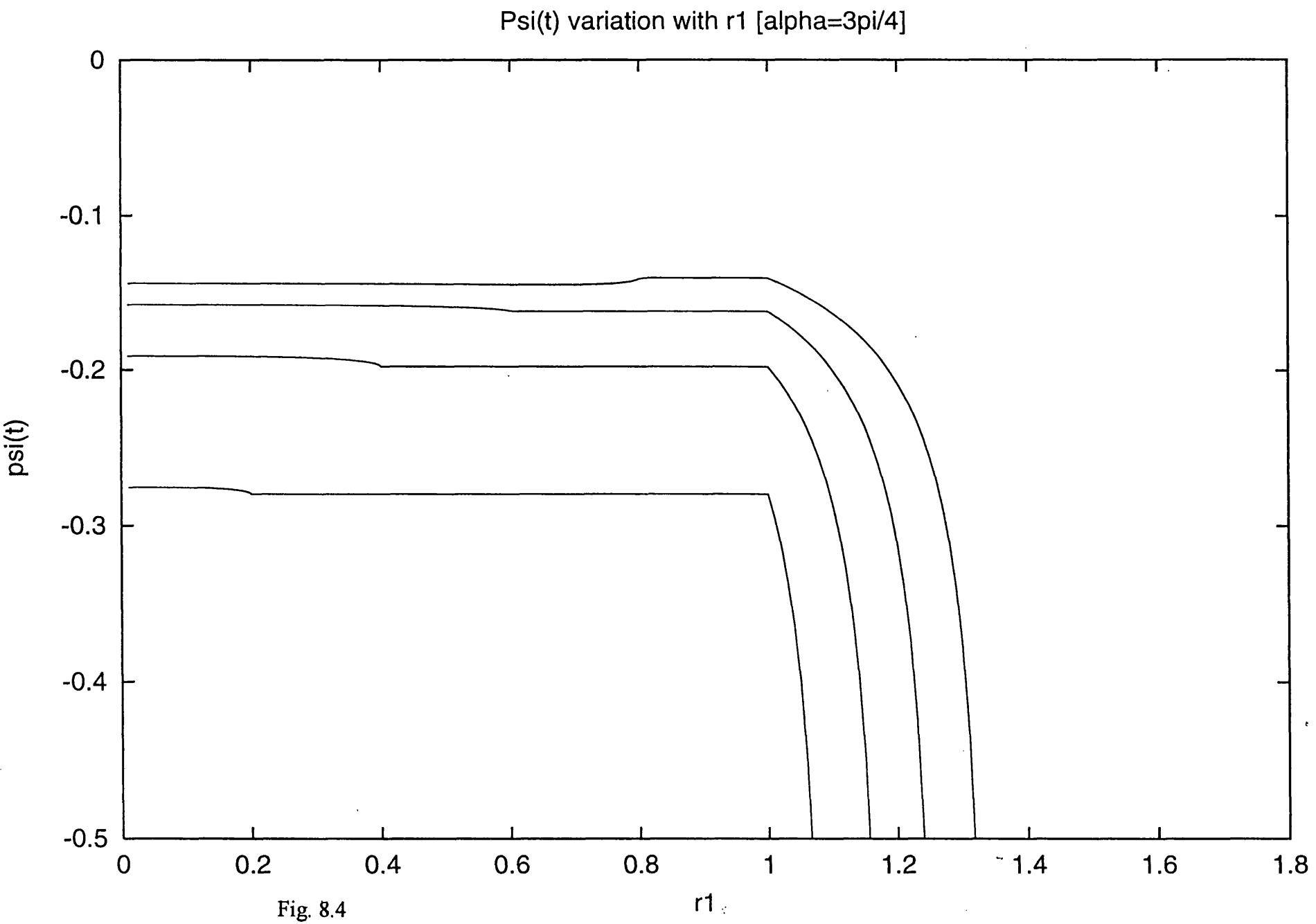
Psi(t) variation with r1 [alpha=3pi/4]
psi(t)
r1
0
-0.1
-0.2
-0.3
-0.4
-0.5
0
0.2
0.4
0.6
0.8
1
1.2
1.4
1.6
1.8

Fig. 8.4

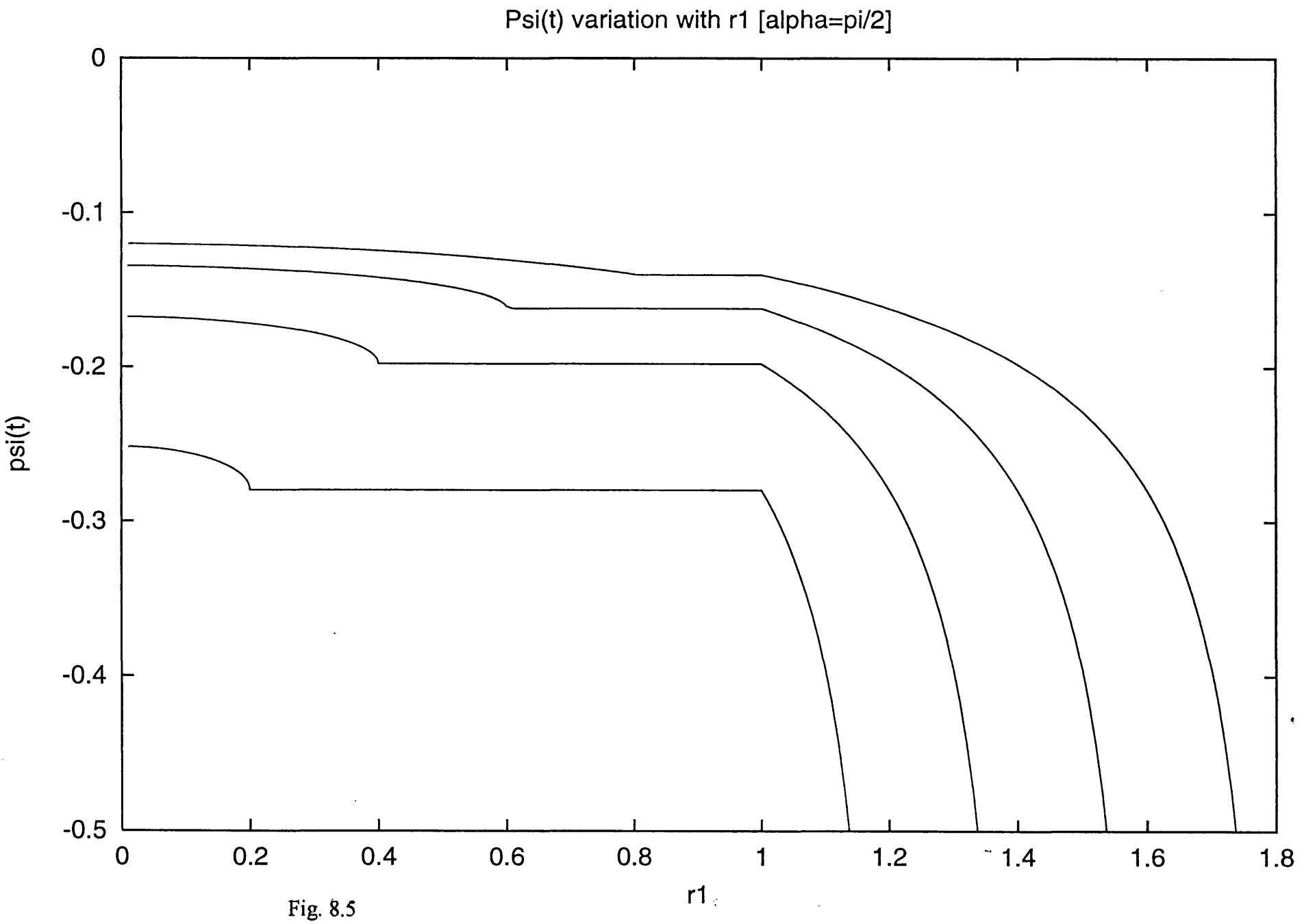
Psi(t) variation with r1 [alpha=pi/2]
psi(t)
r1
0
-0.1
-0.2
-0.3
-0.4
-0.5
0
0.2
0.4
0.6
0.8
1
1.2
1.4
1.6
1.8

Fig. 8.5

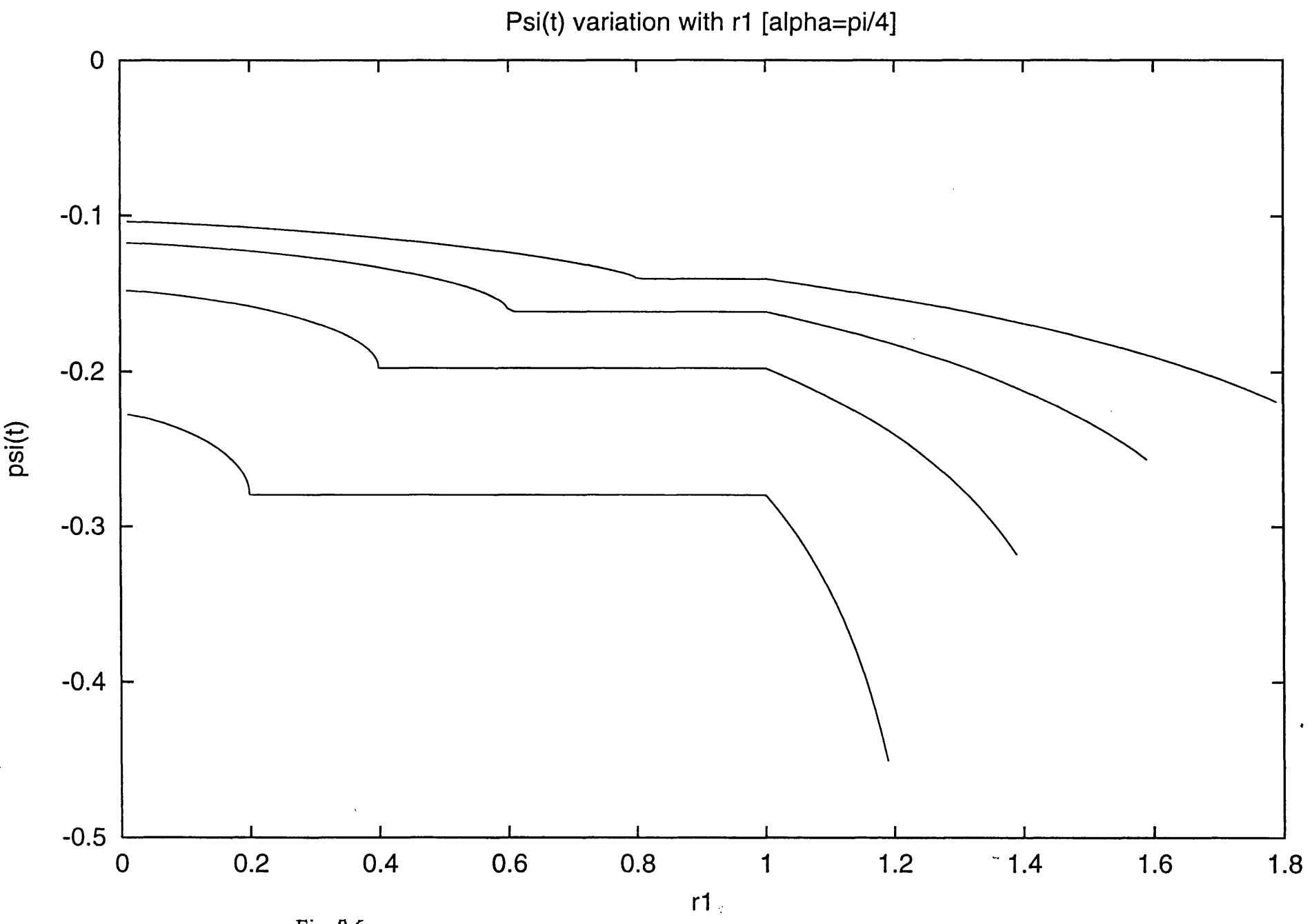
Psi(t) variation with r1 [alpha=pi/4]
psi(t)
r1
0
-0.1
-0.2
-0.3
-0.4
-0.5
0
0.2
0.4
0.6
0.8
1
1.2
1.4
1.6
1.8

Fig. 8.6

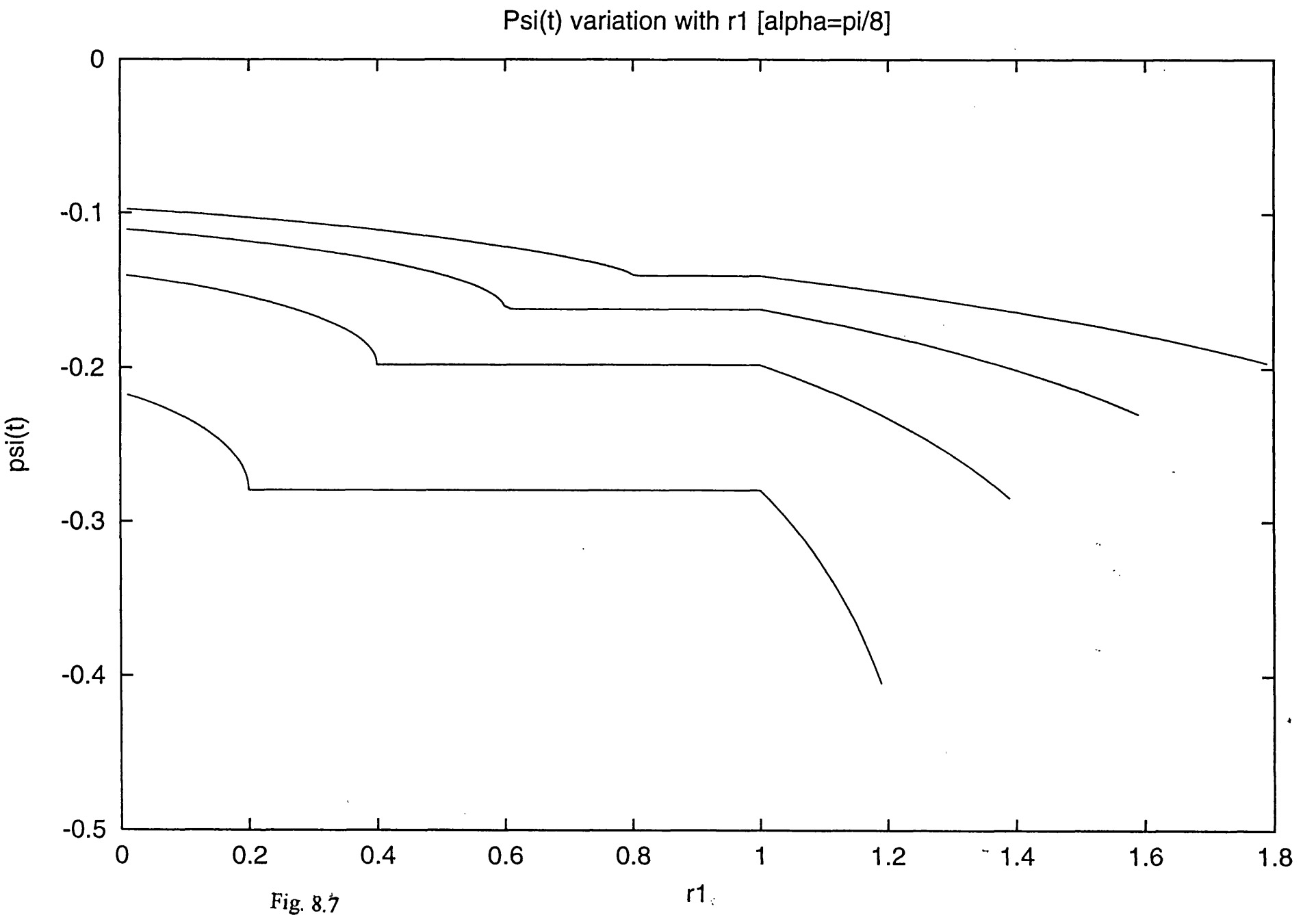
Psi(t) variation with r1 [alpha=pi/8]
psi(t)
r1
0
-0.1
-0.2
-0.3
-0.4
-0.5
0
0.2
0.4
0.6
0.8
1
1.2
1.4
1.6
1.8

Fig. 8.7

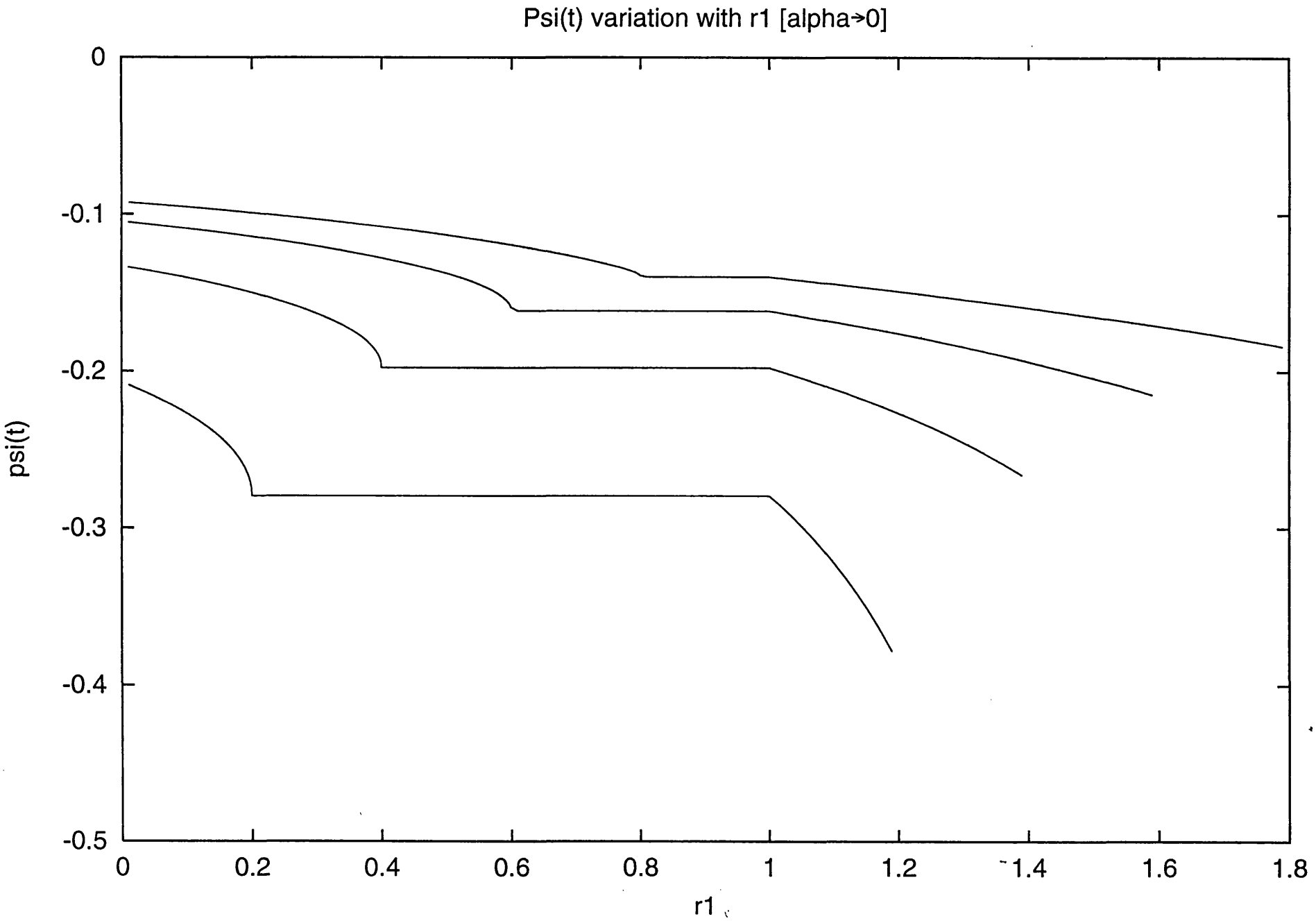
Psi(t) variation with r1 [alpha→0]
0
-0.1
-0.2
-0.3
-0.4
-0.5
psi(t)
0
0.2
0.4
0.6
0.8
1
1.2
1.4
1.6
1.8
r1

Fig. 8.8

# CHAPTER 9

## Other related flow configurations and comments

### 9.1 Introduction

In this chapter we consider briefly some related flow problems. These problems have been studied to some extent in the present project but remain to be completed in further research. One such problem is that of upward ship-side motion, where a short discussion is given in the following section.

Another problem that should be mentioned is the case of oscillating ship-side motion in which we expect the analysis to be harder, however, due to the difficulty of the appropriate boundary conditions. Such a problem is studied by Hocking (1987) where the vertical oscillation of a flat plate partially immersed in a non-wetting fluid produces a radiated wavetrain when the contact line between the plate and the free surface of the fluid cannot move freely along plate. He found that the generation of waves depends to a significant extent on the condition applied at the intersection of the free surface and the body.

On the other hand a more realistic configuration than that of chapter 8 is the wedge-shaped geometry of figure 9.1.

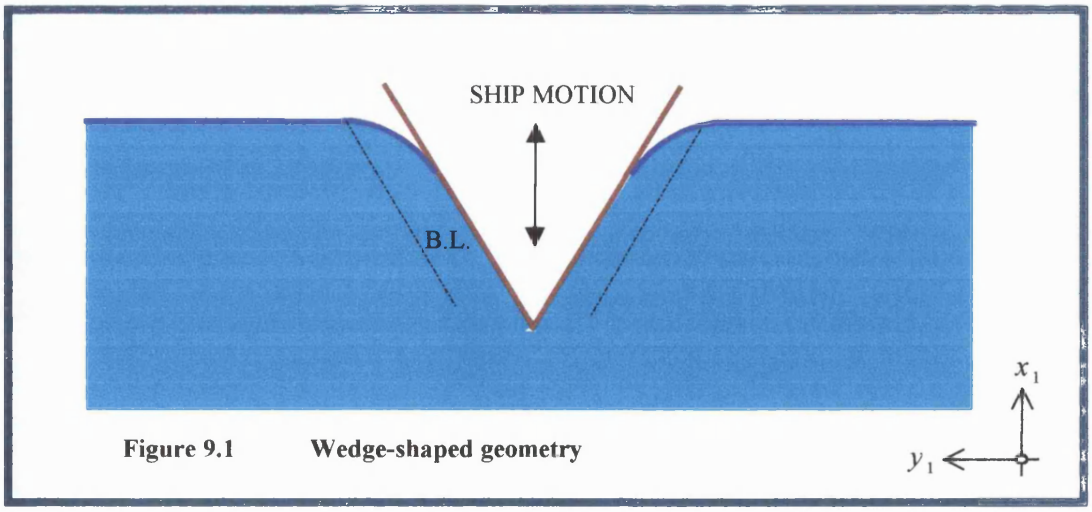


**Figure 9.1 Wedge-shaped geometry**

This is beyond the present scope of the thesis, except for $\alpha$ near $\pi/2$, ($\alpha$ being the angle of inclination to the horizontal), because the inviscid region becomes nonlinear.

Also the configuration for the inclined side for both upward and downward motions where the gravity effect is included needs further study. The target of such a study is to predict whether the water will have a 'splashing' effect as discussed in chapter 8.

Finally, concerning the square root behaviour defined in equation (5.17) near the contact point, the equivalent of the Kutta condition in the inviscid portion of the water motion remains not fully known for the present context of viscous-inviscid flows, where the inviscid part of the motion is only slightly disturbed compared with the viscous part. This suggests that further study should be made of viscous-inviscid properties close to a contact point, where in effect a free surface detaches at a trailing edge.

## 9.2 The upward ship-side motion

In this section we consider the basic construction for the upward ship-side motion problem. Again the unsteady viscous boundary layer equations are assumed to hold near the ship-side (for some time at least), while in the rest of the water flow the inviscid Euler equations apply, leading possibly to potential-flow properties as described in chapter 4 and 5.

The ship-side is moving upwards vertically, and so the velocity of the water for positive time ($t>0$) is expected to correspond to moving downwards relative to the ship-side. Here we note that the pressure $p$ is equal to zero in the air but is generally non-zero in the water, the atmospheric pressure level again being taken as zero for convenience. The development of the problem is thus straightforward and is similar to that of chapter 4. As before, we employ the unsteady Navier-Stokes equations and relevant boundary conditions for the flow. In a similar manner as in chapter 4, the Reynolds number is taken to be large and the scaled governing equations are defined again as

$$\bar{u}_t + \bar{u}\bar{u}_{\bar{x}} + v\bar{u}_y = -g + \bar{u}_{yy}, \tag{9.1}$$

$$\bar{u}_{\bar{x}} + v_y = 0, \tag{9.2}$$

where the constant gravity force is also included. The atmospheric pressure is taken to be zero without loss of generality, time $t>0$, $\bar{x}, y$ are the vertical and horizontal fixed spatial axes respectively, and $\bar{u}, v$ are the corresponding velocity components in a similar method as before. We now use a transformation to make the problem more definite for $\bar{x}<0$, $(\bar{x},y,t)\rightarrow(\bar{x},\eta,t)$, where $\eta = {}^{y}/_{f(\bar{x},t)}$. Here $f(\bar{x},t)$ is an unknown-scaled (shape) function of the vertical fixed spatial axis and time. The boundary conditions are now defined by

$$\bar{u} = \hat{v} = 0 \text{ at } \eta = 0 \text{ (at wall)}, \tag{9.3}$$

$$\bar{u}_{\eta} = 0,\ \hat{v} = 0 \text{ at } \eta = 1, \tag{9.4}$$

where the range of interest is $-k(t) < \bar{x} \leq 0$, and $k(t)$ is defined in section 4.3.2 since the ship-side is moving upwards $(\bar{x} < 0)$. In principle this final set of equations may be solved in almost exactly the same way as with the equation set of chapter 2, which describe the external boundary layer flow past an aligned flat, for a given value of the gravity term $g$.

# CHAPTER 10

## Conclusions

In the first part of the thesis (chapters 2,3) the unsteady incompressible boundary layer mainly over a flat plate that is started impulsively from rest with uniform velocity was considered. The two cases that were studied were those of the flow on the finite-length plate and the flow in the wake downstream of the plate. On the plate, the numerical solution was obtained using the Gaussian elimination method, where the previously obtained similarity results were found to be retrieved fairly well. A Blasius-Rayleigh-like flow regime was observed to exist over the plate. A major part of the convergence towards the Hall solution seemed to occur over the first five normalised time steps. A link with the double-stepping procedure of Smith and Timoshin (1996) was discussed and a comparison with a Blasius modified solution was also made and proved supportive.

For the trailing edge and the near wake Goldstein solution in the unsteady flow adjacent to the flat plate, in a similar manner as with the flat plate analysis, a Gaussian elimination of the discretized system of flow equations was undertaken with modified boundary conditions for the wake region. The numerical results observed were in close agreement with those of Papageorgiou and Smith (1989) in the steady state at large times. Grid refinement was performed for each of the coordinate directions and time for both the plate and wake problems. Numerically converging solutions were indicated.

Numerical investigations of the scaled displacement and skin friction quantities were also performed. The wake displacement results, which were later used for the side free surface solution, were found to be in very good agreement with the subsequent numerical predictions of Li (2000). Also the present numerical treatment for a modified boundary condition corresponding to an unsteady outer stream rather than a steady one was studied in order to make the problem and approach more widely applicable.

The second part (chapters 4-9) of the thesis consisted predominantly of the downward vertical and inclined ship-side motion problems. The flow problems were modeled and then investigated both analytically and numerically (chapters 4-6) using appropriate reductions from the Navier-Stokes equations. The solution compared favourably with those in previous work such as that of Li (2000). Further, the vertical problem was investigated in its outer inviscid region to deduce the shape of the upper and side free surfaces (chapter 6) generated by the downward motion of the ship-side. Close agreement between the analytical forms based on the development of a displacement derivative function and the computational results was observed. The results were found to make good sense from a physical perspective.

For the case of the downward vertical ship-side motion problem, the influence of relatively small gravity was also investigated (chapter 7). The results show a trend towards 'splashing' of the water onto the ship-side for sufficiently large times with any positive gravity factor $\tilde{g}$. For the case of the ship-side inclined at a general angle to the horizontal (chapter 8), the results showed agreement with the special vertical case of chapter 5. There was a trend in the displacement derivative function to become more elongated for smaller angles to the horizontal. Finally, other related cases were considered (chapter 9).

The principal results of this thesis are probably those for the unsteady flat plate flow itself, in chapters 2, 3, and for the predicted free surface shapes in chapters 6 and 7. Future research would be of interest on expanding the other related cases mentioned just above, as well as on the influences of allowing slip at or near the contact point (as opposed to the present assumption of no slip) and on the effects of increasing the relative gravity force. In particular the case of an oscillating ship-side is clearly one of practical significance also. Small oscillations or waves have been studied previously, most notably in the linear context, corresponding for instance to relatively large slipping of the moving contact point. It would be interesting to extend this case to the current setting, especially given that Elliott & Smith's (1998) work shows flow deceleration having an important influence on the solution structure near the trailing edge in the no-slipping configuration.

# APPENDICES

# APPENDIX A

## The approximate model for the displacement-like function

A slightly simpler model for the displacement-like function is presented in this appendix. It has the function $\delta_t$ given by

$$\delta_t = \partial_t (t^{1/2}\alpha_0)\left(\bar{x} + \tilde{L}\right), \tag{A.1}$$

satisfying the boundary condition $\Psi = 0$ at the leading edge $\bar{x} = -\tilde{L}$, as sketched in figure A.1.

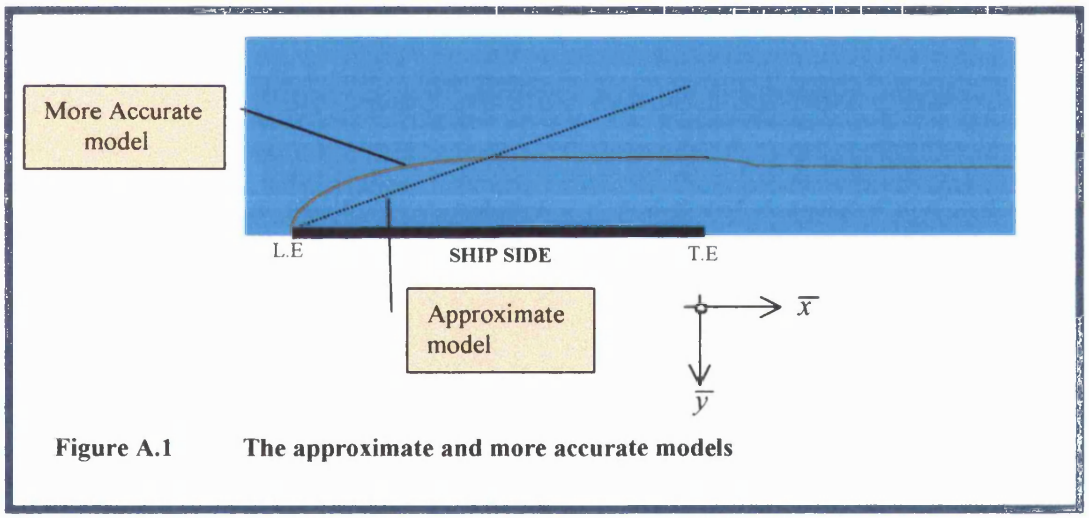


**Figure A.1** **The approximate and more accurate models**

The model captures some elements of both the approximate Rayleigh part of the efflux contribution (boundary layer displacement) in region 2 and the leading edge effect.

Substituting (A.1) into (5.28) leads to the following expression for the displacement function valid for A.1 the ship-side,

$$\Psi_t = \frac{(\bar{x} - \bar{x}_A)^{1/2}}{\pi}\left[\frac{\alpha_0}{2t^{1/2}}\right] \cdot \int_{-\tilde{L}^2}^{\bar{x}_A} \frac{(\bar{x}_A - \bar{\xi})^{-1/2}}{(\bar{x} - \bar{\xi})}\left(-\left|\bar{\xi}\right|^{1/2} + \tilde{L}\right) d\bar{\xi}\,. \tag{A.2}$$

To analyze the integral in equation (A.2), we use the substitution $q = \bar{x}_A - \bar{\xi}$, so that the integral becomes

$$I = -\int_{\bar{x}_A+\tilde{L}^2}^{0} \frac{q^{-1/2}}{(\bar{x}-\bar{x}_A+q)}((q-\bar{x}_A)^{1/2}+\tilde{L})dq. \qquad \text{(A.3)}$$

We further substitute $q = m^2$ to obtain the final integral

$$I(m) = \int_{0}^{(\bar{x}_A+\tilde{L}^2)^{1/2}} \frac{2}{(\bar{x}-\bar{x}_A+m^2)}((m^2-\bar{x}_A)^{1/2}+\tilde{L})dm \qquad \text{(A.4)}$$

for the interval $\bar{x}_A < \bar{x} < 0$.

To evaluate the integral in (A.4) and hence evaluate the displacement function $\Psi_t$ of (A.2), we employ Simpson's rule as given in for the Fortran 77 program at the end of the appendix, as program A.1.

The results are presented at the end of the chapter, and show the variation of the integral $I$ with velocity $\hat{u}$, for various $\bar{x}$-stations. We will now compare these results with the analytical solution for the integral $I$ given below.

Next, we investigate local analytical solutions for the present simplified ship-side model. We examine the solution for two cases of interest, near the origin as $\bar{x} \sim 0$, and as $\bar{x}$ approaches the trailing edge where $\bar{x} \to \bar{x}_A$. The question is whether we obtain results that correlate well with the computational results. We analyse the integral in (A.4) for both cases.

At $\bar{x} = 0$, first, if we first substitute $\Gamma^2 = -\bar{x}_A > 0$, the integral in equation (A.4) becomes

$$\frac{I}{2} = \left[\frac{\tilde{L}}{\Gamma}\tan^{-1}\left(\frac{A}{\Gamma}\right) - \sinh^{-1}\left(\frac{A}{\Gamma}\right)\right], \qquad \text{(A.5)}$$

where $A \equiv \sqrt{\tilde{L}^2 - \Gamma^2}$ . The selected values for the trailing edge are $\bar{x}_A = -t^2 = -6$, and for the length $L = 8$. Hence equation (A.5) using these values gives the value of the integral $I(m)$ as 7.124. This result is very close to the numerical result of 7.160 (generated by program A.1 evaluated near the origin at $\bar{x} = -0.05$, for $L$=8).

As $\bar{x} \to \bar{x}_A$, second, we substitute $\bar{x} - \bar{x}_A = \varepsilon^2 > 0$ near the leading edge, with $\varepsilon << 1$. We then expect the integral (A.4) to be dominated by the small $m$ contribution, where $m = \varepsilon\hat{m}$ is small and $\hat{m} \sim 1$. Thus the integral in (A.4) becomes

$$I = 2\int_{\hat{m}=0}^{\infty} \frac{(\tilde{L} - |\bar{x}_A|^{1/2})}{(\hat{m}^2 + 1)\varepsilon^2} \varepsilon d\hat{u} = \frac{(\tilde{L} - |\bar{x}_A|^{1/2})}{\varepsilon}\pi , \qquad \text{(A.6)}$$

leading to

$$I = \frac{5\pi}{\varepsilon}. \qquad \text{(A.7)}$$

Table A.1 represents analytical values calculated from equation (A.7) together with computational values for selected values of $\bar{x}$.

| $\bar{x}$ | $\varepsilon$ | *I (analytical)* | *I(computational)* | $\Psi_t$ |
|---|---|---|---|---|
| ***-5.8*** | 0.447 | 35.124 | 51.556 | ***0.5861*** |
| ***-5.5*** | 0.707 | 22.214 | 31.624 | ***0.5688*** |
| ***-5.2*** | 0.894 | 17.462 | 24.327 | ***0.5531*** |
| ***-5.0*** | 1.000 | 15.708 | 21.415 | ***0.5444*** |
| ***-4.0*** | 1.414 | 11.107 | 14.241 | ***0.5120*** |
| ***-3.0*** | 1.732 | 9.064 | 11.110 | ***0.4892*** |
| ***-2.0*** | 2.000 | 7.854 | 9.268 | ***0.4712*** |
| ***-1.0*** | 2.236 | 7.024 | 8.026 | ***0.4563*** |
| ***-0.05*** | 2.439 | 6.439 | 7.160 | ***0.4440*** |

*Table A.1*

The variation of the integral contained within the displacement function, as well as the displacement function itself, are plotted against $\bar{x}$ in figures A.2 and A.3, respectively. The results suggest that as $\bar{x}$ approaches $\bar{x}_A$ (which is -6), the analytical and computational results diverge marginally. This suggests that the approximate model for the displacement-like function is unsatisfactory. The evaluation of $\Psi_t$ from equation (A.2) is also shown.

In contrast to this approximate model, an accurate solution was developed which is described in section 5.4 of the thesis.

# AA. Fortran 77 programs and figures

```
C       Problem: Downward motion of ship in stationary fluid
C               Analysis of flow in the "nearly still" Region 3


        program simpsons rule

        REAL f(100),res,h,sum,u,xbar,xabar,L,LB,t,pi,r,y
        INTEGER i,j,mm,m

        xbar = - 5.8
        mm = 15
        L = 8
        t=(6**0.5)
        r=0.25
        pi=3.1415927
        xabar = -(t**2)

C       define f(j), j = 1, and m,        where (m = 2mm + 2)

        m = (2 * mm) +2

        LB = (L + ((-xabar)**0.5))

        h = (((xabar + (LB**2))**(0.5)) / (2 * mm - 1))

        WRITE (6,*) ''
        WRITE (6,*) ' Integral results for xabar =',xabar
        WRITE (6,*) '    and for xbar =',xbar
        WRITE (6,*) ''

C       Evaluate f(j) also evaluating u(j) at each j
        do 24 j = 1,m
        u = ((j - 1) * h)
        f(j) = (2*( LB-( ((u**2)-xabar)**0.5)) ) /  ( xbar -xabar+(u**2))

24      WRITE (6,*)' u=',u ,' f(j)=',f(j)

C       Evaluate first and final terms of the integral

        sum = f(1) + f(m)

        WRITE (6,*) ' sum{first term} = ' , sum

C       Evaluate the complete integral (including the intermediate terms)

        do 25 i = 1,mm
        j = 2 * i
25      sum = sum + (4.0 * f(j)) + (2.0 * f(j+1))

C       Output results
c       WRITE (6,*) ' sum{whole} = ' , sum

        res = (sum * (h / 3.0))
        WRITE (6,*) ' res = ' , res

        y=(((xbar-xabar)**0.5)*r*res)/(2*pi*(t**0.5))


        WRITE (6,*) y,xbar

        end
```

A.1 Program to evaluate $\Psi$, using the approximate model.

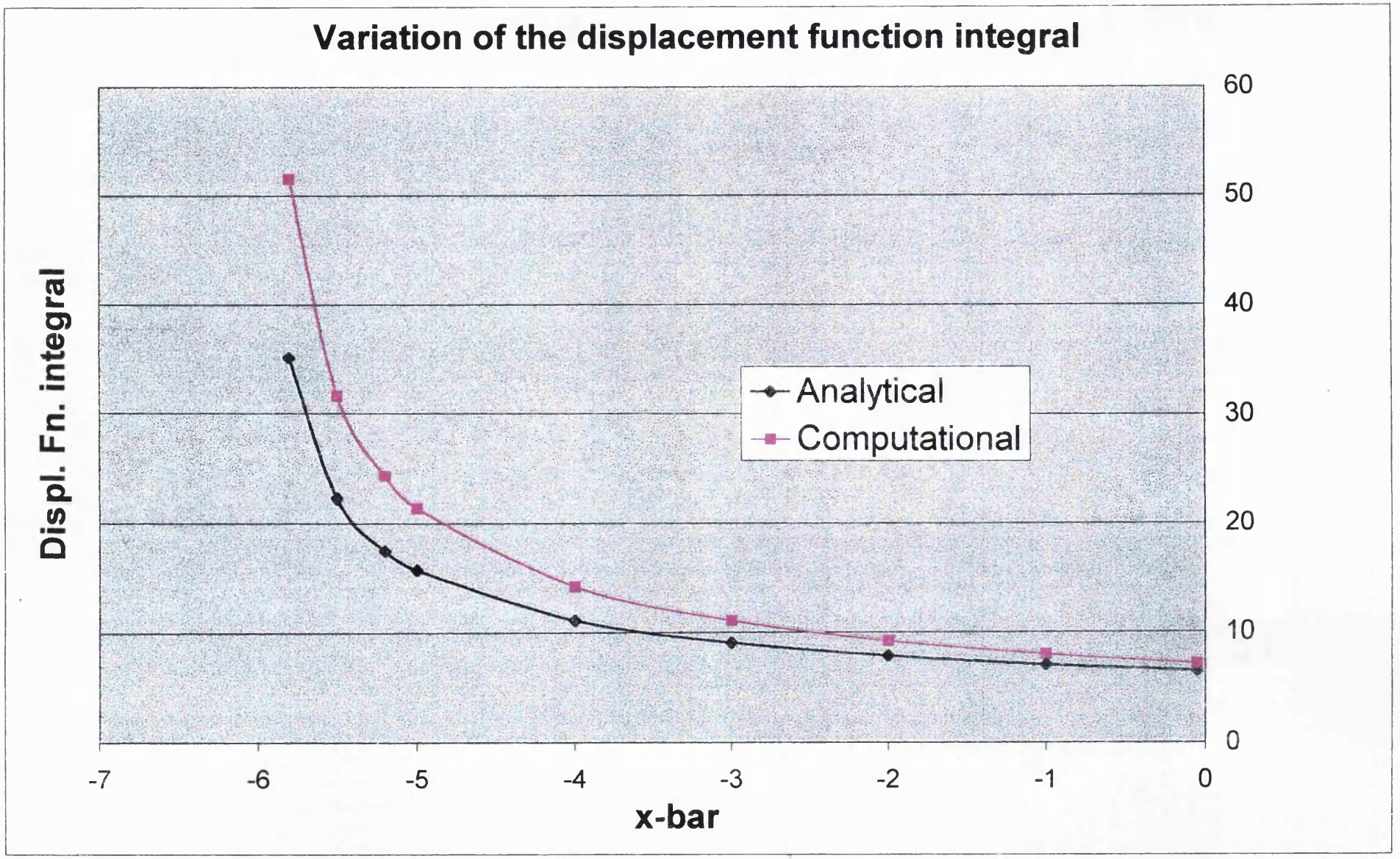
Variation of the displacement function integral
Displ. Fn. integral
x-bar
Analytical
Computational
60
50
40
30
20
10
0
-7
-6
-5
-4
-3
-2
-1
0

Fig. A.2

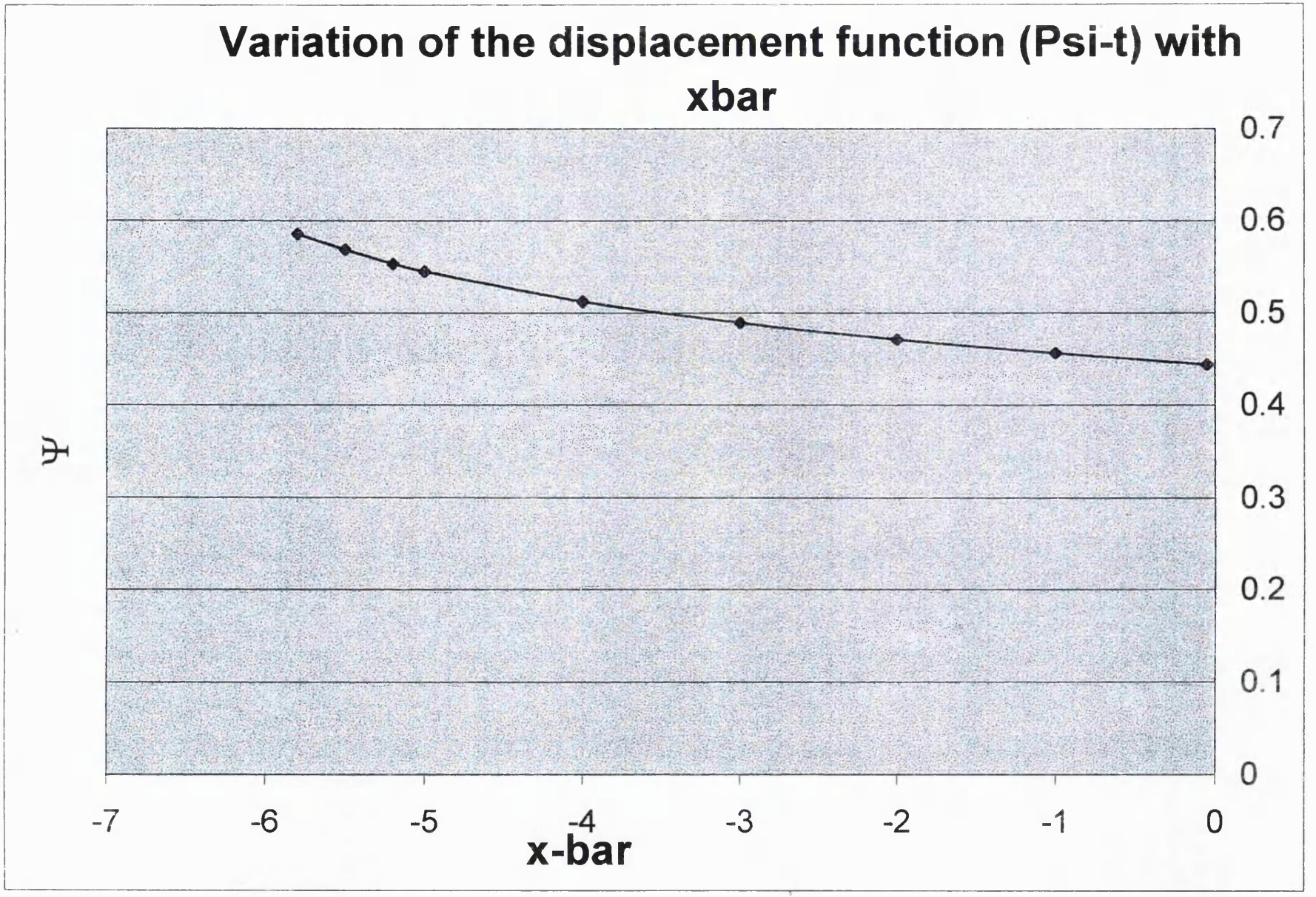
Variation of the displacement function (Psi-t) with xbar
0.7
0.6
0.5
0.4
0.3
0.2
0.1
0
-7
-6
-5
-4
-3
-2
-1
0
x-bar

Fig. A.3

# APPENDIX B

```
C       Problem: To evaluate f1 integral for approximate solution for large ti

        program s

        REAL o(1000),res,sum,t,ybar,Q,h,f1,xdbar,mm,m
        INTEGER i,j

C       Definition of constants
        mm=100
        m=(2*mm)+2
        h=1/m

C       General loop for value of large time

        do 2000 t=10,50,10

C       Loop for values of y-coordinate

        do 1000 ybar=1,20,1

        xdbar = (ybar**2) / (t**2)

C       Evaluate function o(Q) for whole interval
        do 24 j = 1,m
        Q= ((j-1)*h)
24      o(j) = ((Q**0.5)*(1-Q))/ ((xdbar+(Q**2))**1.5)

C       Evaluate first and final terms of the integral
        sum = o(1) + o(m)+ (4* o(m-1))

C       Evaluate the complete integral (including intermediate terms)
        do 25 i = 1,mm
        j = 2*i
25      sum = sum + (4.0 * o(j)) + (2.0*o(j+1))

        res = (sum * (h / 3.0))
        f1 = 0.17678 * (t**0.5) * (xdbar**0.5) * res

C       Output Results for f1 versus y-coordinate
        WRITE (6,*) ybar,f1

1000    continue

        WRITE (6,*) ''

2000    continue

        end
```

B.1 Program to evaluate the approximate solution for $f_1$ valid for large times

# References


1. Abramowitz, M. & Stegun, I. 1972 *Handbook of Mathematical Functions*. New York: Dover.
2. Batchelor, G.K. 1967 *An Introduction to Fluid Dynamics*. Cambridge University Press.
3. Billingham, J. & King, A.C. 1995 The interaction of a moving fluid/fluid interface with a flat plate. *J. Fluid Mech.* **296**, 325.
4. Blasius, H. 1908 *Z. Math. Phys.* **56**, 1 (Engl. Transl. Boundary layers in fluids with little friction *Tech. Memo. Nat. Adv. Comm. Aero., Wash.* no. 1256).
5. Brotherton-Ratcliffe, R.V. & Smith, F.T. 1989 Viscous effects can destabilize linear and nonlinear water waves. *Theoret. Comput. Fluid Dynam.* **1**, 21.
6. Chang, H., Liu, Y. & Miao, G. 1994 Free-surface effects on ship frictional resistance. *J. Kansai Soc.* **222**, 65.
7. Christ, M. 1989 *Lectures on Singular Operators*. American Mathematical Society, No.77.
8. Daboussy, D., Dias, F. & Vanden-Broeck, J.-M. 1997 On explicit of the free-surface Euler equation in the presence of gravity. *Phys. Fluids* **9**, 2828.
9. Daboussy, D., Dias, F. & Vanden-Broeck, J.-M. 1998 Gravity flows with a free surface of finite extent. *Eur J. Mech., B/Fluids*, **17**, 19.
10. Degani, A.T., Walker, J.D.A. & Smith, F.T. 1998 Unsteady separation past moving surface. *J. Fluid Mech.* **375**, 1.
11. Dennis, S.C.R. 1972 The motion of a viscous fluid past an impulsively started semi-infinite flat plate. *J. Inst. Maths Applics.* **10**, 105.
12. Dimitriou, I.D. 1993 *Michaniki Refston.* Foundas Publishers.
13. Drazin, P.G. & Howard, L.N. 1966 Hydrodynamic stability of parallel flow of inviscid fluid. *Adv. Appl. Mech.* **9**, 1.
14. Elliott, J.W. & Smith, F.T. 1998 The effect of smooth deceleration of the external stream on an aligned flat-plate boundary layer. *Quart. J. Mech. Appl. Math.* **51**, 3.
15. Evans, C.W. 1989 *Engineering mathematics, a programmed approach.* Chapman & Hall.

16. Foda, M. & Cox, R.G. 1980 The spreading of thin liquid films on a water-air interface. *J. Fluid Mech.* **101**, 33.

17. Fraenkel, L.E. & McLeod, J.B. 1997 Some results for the entry of a blunt wedge into water. *Phil. Trans. R. Soc. Lond.* **A, 355**, 523.

18. Gerald, C.F. & Wheatley, P.O. 1989 *Applied numerical analysis*, 4th edn. Addison-Wesley publishing company.

19. Goldstein, S. 1930 Concerning some solutions of the boundary layer equations in hydrodynamics. *Proc. Camb. Phil. Soc.* **26**, 1.

20. Goldstein, S. 1965 *Modern Developments in Fluid Mechanics*, volume I. Dover.

21. Hall, M.G. 1969 The boundary layer over an impulsively started flat plate. *Proc. R. Soc. London.* **A310**, 401.

22. Hocking, L.M. 1987 Waves produced by a vertically oscillating plate. *J. Fluid Mech.* **179**, 267.

23. Howison, S.D., Ockendon, J.R. & Wilson, S.K. 1991 Incompressible water-entry problems at small deadrise angles. *J. Fluid Mech.* **222**, 215.

24. James, M.L., Smith, G.M. & Wolford, J.C. 1985 *Applied numerical methods for digital computation with Fortran*, 3rd edn. New York: Harper & Row Publishers.

25. Jones, C.W. & Watson, E.J. 1963 *Laminar boundary layers*, (edited by Rosenhead), Oxford University Press.

26. Kang, Y. & Vanden-Broeck, J.-M. 2000 Gravity-capillary waves in the presence of constant vorticity. *Eur. J. Mech. B-Fluids.* **19**, 253.

27. Kaufmann, W. 1963 *Technische Hydro- und Aeromechanik.* Springer-Verlag.

28. King, A.C. 1991 Moving contact lines in slender fluid wedges. *Quart. J. Mech. Appl. Math.* **44**, 173.

29. King, A.C., Billingham, J. & Popple, D.F. 1998 The interaction between an advected fluid/fluid interface and a flat plate. *Proc. of FEDSM.*

30. Lam, S.H. & Crocco, L. 1959 Notes on the shock-induced unsteady laminar boundary layer on a semi-infinite flat plate. *J. Aero Sci.* **26**, 54.

31. Lamb, H. 1932 *Hydrodynamics*. Cambridge University Press.

32. Landau, L.D. & Lifshitz, M.E. 1987 *Fluid Mechanics*. Pergamon Press.

33. Li, L. 2000. Private communications.

34. Markatos, N.C. & Assimacopoulos, D. 1995 *Ypologistiki Refsto-dynamiki.* Papasotiriou Publishers.

35. Mattingly, G.E. & Criminale, W.O. 1972 The stability of an icompressible two-dimensional wake. *J. Fluid Mech.* **51**, 233.

36. Milne-Thompson, L.M. 1968 *Theoretical Hydrodynamics.* Mcmillan & Co Ltd.

37. Papageorgiou, D.T. & Smith, F.T. 1989 Linear instability of the wake behind a flat plate placed parallel to a uniform stream. *J. Fluid Mech.* **208**, 67.

38. Peridier, V.J., Smith, F.T. & Walker, J.D.A. 1991 Vortex-induced boundary-layer separation. Part 1. The unsteady limit problem $\mathrm{Re} \rightarrow \infty$. *J. Fluid Mech.* **232**, 99.

39. Peridier, V.J., Smith, F.T. & Walker, J.D.A. 1991 Vortex-induced boundary-layer separation. Part 2. Unsteady interacting boundary-layer theory. *J. Fluid Mech.* **232**, 133.

40. Prandtl, L. 1963 *The Essentials of Fluid Dynamics.* Blackie & Sons Ltd.

41. Phillips, W.R.C. 1996 On a class of unsteady boundary layers of finite extent. *J. Fluid Mech.* **319**, 151.

42. Rayleigh, Lord. 1911 On the motion of solid bodies through viscous liquid. *Phil. Mag.* **21**, 697.

43. Roache, P. 1976 *Computational Fluid Dynamics.* Hermosa Publishers.

44. Rosenhead, L. 1963 *Laminar boundary layers.* Oxford University Press.

45. Sato, H. & Kuriki, K. 1961 The mechanism of transition in the wake of a thin flat plate placed parallel to a uniform flow. *J. Fluid Mech.* **11**, 321.

46. Schlichting, H. 1970 *Boundary Layer Theory.* McGraw-Hill.

47. Smith, F.T. 1982 On the high Reynolds number theory of laminar flows. *IMA J. Appl. Maths.* **28**, 207.

48. Smith, F.T., Bowles, R.G.A. & Li, L. 2000 Nonlinear effects in absolute and convective instabilities of a near-wake. *Eur. J. Mech. B-Fluids.* **19**, 173.

49. Smith, F.T. & Timoshin, S.N. 1996 Blade-wake interactions and rotary boundary layers. *Proc. R. Soc. Lond.* A**452**, 1301.

50. Smith, F.T. & Timoshin, S.N. 1996 Planar flows past thin multi-blade configurations. *J. Fluid Mech.* **324**, 355.

51. Somalinga, S. & Bose, A. 2000 Numerical investigation of boundary conditions for moving contact line problems. *Phys. Fluids.* **12**, 499.

52. Stewartson, K. 1951 On the impulsive motion of a flat plate in a viscous fluid. Part I. *Quart. J. Mech. Appl. Math.* **4**, 182.

53. Stewartson, K. 1973 On the impulsive motion of a flat plate in a viscous fluid. Part II. *Quart. J. Mech. Appl. Math.* **26**, 143.

54. Swokowski, E.W. 1979 *Calculus with analytic geometry*, 2nd edn. Boston: Prindle, Weber and Schmidt.

55. Telionis, D.T. 1981 *Unsteady viscous flows*. Springer-Verlag, New York Inc.

56. Vanden-Broeck, J.-M. 1989 Bow flows in water of finite depth. *Phys. Fluids* **A1**, 1328.

57. Vanden-Broeck, J.-M. & Dias, F. 1996 Free-surface flows with several stagnation points. *J. Fluid Mech.* **324**, 393.

58. Vanden-Broeck, J.-M. & Tuck, E.O. 1994 Flow near the intersection of a free surface with a vertical wall. *SIAM J. Appl. Math.* **54**, 1.

59. Van Dommelen, L.L. 1981 Unsteady boundary layer separation. PhD Thesis, Cornell University, Ithaca, NY.

60. White, F. 1991 *Viscous Fluid Flow*, McGraw-Hill.

61. Williams, J.C. 1982 Flow development in the vicinity of the sharp trailing edge on bodies impulsively set into motion. *J. Fluid Mech.* **115**, 27.

62. Williams, J.C. & Stewartson, K. 1983 Flow development in the vicinity of the sharp trailing edge on bodies impulsively set into motion. Part 2. *J. Fluid Mech.* **131**, 177.

63. Zayed, A.I. 1996 *Handbook of Function and Generalized function Transformations*. CRC Press.